9/1+ -

ZfK-324

Technical University Dresden
Section of Physics

Proceedings of the V^th International Symposium on the Interactions of Fast Neutrons with Nuclei

November 17-21, 1975 in Gaussig (GDR)

Edited by
D. Seeliger

July 1976

Postanschrift: Akademie der Wissenschaften der DDR
Zentralinstitut für Kernforschung Rossendorf
8051 Dresden
Postfach 19 Deutsche Demokratische Republik

Diese Publikation wurde in der Abteilung Information des Zentralinstitutes für Kernforschung hergestellt

AKADEMIE DER WISSENSCHAFTEN DER DDR

ZENTRALINSTITUT FÜR KERNFORSCHUNG
ROSSENDORF BEI DRESDEN

ZfK - 324

Proceedings
of the Vth International Symposium on the Interactions of Fast Neutrons with Nuclei

organized by

the Technical University of Dresden

November 17–21, 1975 in Gaussig (GDR)

edited by

D. Seeliger

Материалы
V Международного симпозиума по вопросам взаимодействия быстрых нейтронов с ядрами

организованного

Техническим Университетом г. Дрезден

17 по 21 ноября 1975 г., Гаусснг (ГДР)

Издатель

Д. Зеллгер

July 1976

Organizing Committee

D. Seeliger
P. Müller
H. Ludwig
W. Wagner

Technical University Dresden
Section of Physics
Nuclear Physics Group

Materials of the preceding events have been published in:

- Wissenschaftl. Zeitschrift TU Dresden 21 (1972) 691
- ZfK-Report, ZfK-261 (1973)
- ZfK-Report, ZfK-271 (1974)
- Wissenschaftl. Zeitschrift TU Dresden 24 (1975) 1351

CONTENTS

PREFACE

This report contains review lectures and original representations of the "7-th International Symposium on the Interactions of Fast Neutrons with Nuclei" organyzed by the Nuclear Physics Group of the Technical University Dresden.

The organized annual Seminars and Symposiums have traditionally the following scientific programme:

- experimental investigations of fast neutron induced nuclear reactions;
- theories of nuclear reaction mechanisms, especially of precompound processes;
- nuclear level density;
- neutron data evaluation;
- experimental techniques and data processing.

The limited number of participants as well as the excellent conditions in the recreation center of the Technical University Dresden in the Gaussig-castle permited much useful discussions between scientists stimulating further research work.

We would like to thank all participants, especially our lectures for their active work during the Sessions, panel discussions, personal consultations and Sociable events. They made it a great pleasure for the organizing Committee to perform this 1975 meeting of the "Gaussig Neutron and Preequilibrium Club". Further we want to thank the Rector and the International Department of the Technical University Dresden for the valuable support of this Symposium. A special thanks is due to the staff of the Gaussig recreation center. We would like to thank the Central Institute for Nuclear Research of the Academy of Science for making possible the publication of this report.

And finally, we are much indepted to Ch. Gerlach, B. Krause, H. Ludwig, R.Krause, R. Prengel, U. Kaiser and R. Richter for technical assistance.

Prof. Dr. sc. nat. D. Seeliger

LIST OF PARTICIPANTS

BULGARIA
E. Dermendjiev

CZECHOSLOVAKIA
E. Betak

EGYPT
M. Mohamed
M. Youssouff

FRANCE
J. Prehaut
M. Cindro

GERMAN DEMOCRATIC REPUBLIK

- Central Institute of Nuclear Research Rossendorf
  - D. Albert
  - L. Funke
  - E. Hentschel
  - B. Kühn
  - I. Rotter
  - E. Seifert
- Karl-Marx-University Leipzig
  - G. Otto
- Technical University Dresden
  - R.D. Arlt
  - D. Hermsdorf
  - W. Hirsch
  - D. Hoffmann
  - J. Höhn
  - M. Josch
  - J. Kayser
  - G. Kloß
  - P. Mädler
  - W. Meiling
  - A. Meister
  - G. Musiol
  - G. Ortlepp
  - W. Pilz
  - R. Reif
  - B. Richter
  - S. Sassonov
  - D. Schmidt
  - Th. Schweitzer
  - J. Schöne
  - D. Seeliger
  - K. Seidel
  - H.U. Siebert
  - Th. Streil
  - R. Teichner
  - S. Unholzer
  - W. Wagner
  - F. Weidhase
  - B. Weißbach
  - G. Zschornack

HUNGARY
G. Pető
T. Sztaricskai

ITALY
L. Colli
E. Gadioli

MEXICO
H. Arriola

MONGOLIA
B. Bassaragtscha

POLAND
J.S. Brzosko
E. Herrmann
Lewandowski
I. Turkiewicz

UNION OF SOVIET SOCIALIST REPUBLICS
M.V. Blinov
A. Ermjakov
V.N. Nevedov
V.D. Toneev
A. Tufubalin

YUGOSLAVIA
E. Holub

SCIENTIFIC PROGRAMME **Page**

MONDAY Nov., 17, 1975

TUESDAY, Nov. 18, 1975

THURSDAY, Nov. 20., 1975

SESSION I

Current Problems in (n,2n)-Reactions

N. Cindro [x] and J. Prehaut
Service Physique Nucléaire Centre d'Etudes de Bruyères-le-Châtel
B.P. 61-92120 Montrouge-France

Predominant around 14 MeV where most measurements of the total reaction cross sections have been performed, (the n,2n) reaction has been a long standing favourite source of inspiration for experimenters, evaluators and systematizers. Every aspect of these reactions was thoroughly analyzed and effects like shell closure, isotopic and isotonic effects were repeatedly examined. It would thus appear that after twenty years of intensive studies, there would be little room for further investigation of this reaction. We shall, consequently, sketch in this paper only very few problems that still carry some interest. Fortunately for physicists, these are not minor ones, since they comprise:

- the understanding of the mechanism of (n,2n) reactions,
- the Csikai-Petö effect, viz., generally speaking, the isotopic and isotonic effects in the systematics of (n,2n) cross sections.

Other problems, marginal for the global understanding of (n,2n) reactions but still carrying some interest, will be discussed at the end of this paper.

1. THE MECHANISM OF (n,2n) REACTIONS

It was known for many years that even the simplest closed form evaporation formulas can account for the total (n,2n) cross sections in a wide range of energies and nuclei within better than 20 to 30 % of the experiment.

We are, thus, at present, interested in the difference, which, in the light of recent investigations (1,2) appears to be negative (that is the compound nucleus evaporation formulas appear to overestimate the experimental values). Several mechanisms are proposed to account for this difference, some remaining in the frame of the statistical model such as reestimating the relative values of Γ_γ and Γ_n in the region of $U_{ex} \approx S(n)$, some adding new mechanisms, such as direct or preequilibrium contributions. The two kinds of mechanisms act in different stages of the (n,2n) process and thus modify different components of the (n,2n) cross section. The former ($\Gamma_\gamma \approx \Gamma_n$ around $U_{ex} \approx S(n)$) means essentially the abbandon of the Weisskopf assumption. The latter mechanism, on the other hand, acts on the primary spectrum by hardening it; thus it reduces the fraction of neutrons capable of giving rise to the emission of secondary neutrons.

We shall examine both of these mechanisms with respect to the simple compound nucleus evaporation model as a basis. In this sense we should first define our basis, i.e. the compound nucleus model to be used in the calculation.

x) Permanent address: Institut "Rudjer Boskovic", Zagreb, Yugoslavia

1.1. Compound Nucleus Model Calculations

Every nuclear physics student is familiar with the fact that under the assumptions that:

a) we neglect the emission of charged particles
b) the emission of a second neutron takes place whenever it is energetically possible (the Weisskopf assumption) and
c) the logarithm of the nuclear level density ω (U) at a given excitation energy U,

$$S(U) = \log \omega (U)$$

can be satisfactorily expressed in terms of a Taylor expansion by keeping only the zero and first order terms, i.e. that:

$$S(U) = S(U_{max}) - (U_{max} - U)\frac{dS}{dU} \quad U = U_{max}$$

then the cross section for the emission of one single (and no more than one) neutron after the nucleus is bombarded with a neutron of energy E_n is given by (3)

$$\sigma(n,n') \approx \sigma_{ne}\left\{1 + \frac{E_n - S(n)}{\theta}\right\} \exp\left\{-\frac{E_n - S(n)}{\theta}\right\} \qquad (1.1)$$

Here θ is defined as:

$$\frac{1}{\theta(U)} = \frac{dS(U)}{dU} \qquad (1.2)$$

which is the well known thermodynamic relationship between the entropy and the temperature; hence the denomination of θ as nuclear temperature (we note that here θ has the dimensions of energy, while kT rather than the temperature T, has the dimensions of energy in thermodynamics). The quantity σ_{ne} stands for the reaction cross section of the nucleus with a neutron of energy E_n. It is visible that when the energy difference $E_n - S(n)$ becomes much larger than θ, $\sigma(n,n')$ will represent only a small fraction of σ_{ne}. The rest is then (n,2n), the cross section for the emission of two consecutive neutrons given by the obvious expression:

$$\sigma(n,2n) = \sigma_{ne}\left\{1 - \left(1 + \frac{U_R}{\theta}\right) \exp\left(\frac{-U_R}{\theta}\right)\right\} \qquad (1.3)$$

where $U_R = E_n - S(n)$.

Stringent as they may seem at first sight, the above three assumptions appear to be quite well satisfied for neutron energies E_n several MeV above the (n,2n) threshold $Q(n,2n) = S(n)$ and below the threshold of three particle emission. This means that for a wide range of nuclei (heavier nuclei in particular) the simple closed form expression (1.3) gives the general trend of the (n,2n) cross sections quite well. An obvious consequence, for instance, is that the essential parameter governing $\sigma(n,2n)$ is the excess energy U_R (see insert fig. 1) and that meaningful comparisons of cross sections can be done only at comparable values of U_R. It has taken about 15 years to nuclear physicists to realize this trivial point.

1.2. Departures from Simple Compound Nucleus Evaporation Predictions

In order to systematically study the departures from compound nucleus model evaporation predictions, we present here the cross sections calculated systematically for about 80 nuclei in the excess energy range U_R = 5-7 MeV [4]. The reasons for this choice of U_R are twofold:

1) Q(n,2n) = S(n) being, in general, 8-9 MeV, the region of $U_R \approx 6$ corresponds roughly to 14-15 MeV incident energy, where a large number of experimental data exist;
2) It can be shown that the compound nucleus evaporation calculations of the type described below are rather independent of the choice of two crucial parameters: the density parameter a and the neutron inverse cross sections $\sigma_{inv}(n)$; this "flatness" (in a two parameter plane) of the calculated (n,2n) cross sections makes them very suitable for a systematic comparison.

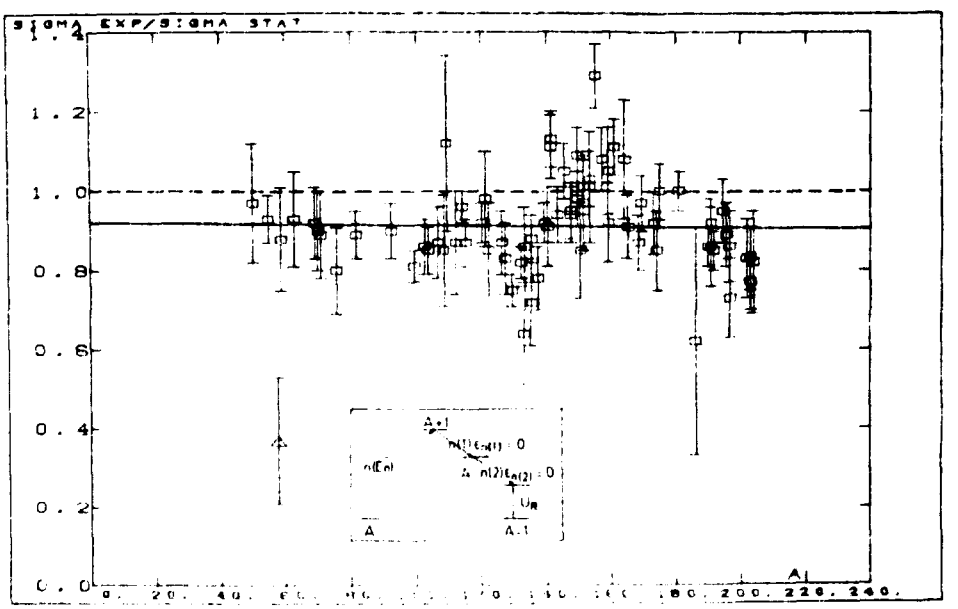

Fig. 1 Ratio of experimental and simple evaporation (n,2n) cross sections (ref. [4]) for values of the excess energy U_R centered around 6 MeV ($\Delta U_R = \pm 1$ MeV). Dotted is the unity line; the full line is a least square fit of the form $a\Delta + b$.

Figure 1 gives the results of the systematic calculation which is presented in more detail in the contribution by Holub et al. to this Conference [4]. We find the above results rather gratifying, as they show that in this most frequently encountered energy region ($U_R = 6 \pm 1$ MeV) a simple a priori compound nucleus calculation renders the experimental values at least as well as any of the ad hoc empirical, semiempirical and quasiphenomenological formulas. The distribution of the relative differences between experimental and evaluated cross sections as given by the formulas of Pearlstein [5], Adam and Jeki [6] and Chatterjee and Chatterjee [7] respectively and the calculation of Holub et al. is given in fig. 2. Although the sample of experimental results is somewhat limited, one would be tempted to seriously question the usefulness of empirical expressions

in view of the global success of simple a priori (that is without adjustable parameters) compound nucleus calculation. It is clear, however, that this conclusion is limited to the above convenient region of U_R. We shall see that right above the (n,2n) threshold the discrepancy with experiment becomes more severe.

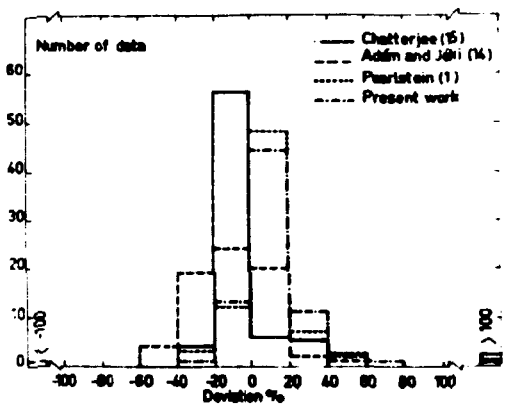

Fig. 2 Distribution of relative differences between experimental and evaluated (n,2n) cross sections as given by the calculations of Pearlstein [5] Adam and Jeki [6], Chatterjee and Chatterjee [7] and Holub et al [4] respectively.

A more thorough examination of fig. 1 reveals that the bulk of the data lies below the unity line. This means that, except for the region around A = 150 (which, let it be noted en passant, is the region of deformed nuclei) the simple statistical model evaporation calculations of ref. [4] overestimate systematically the experiment. This fact was observed earlier by Holub and Cindro [2] for the ratio points of experimental data vs. the Pearlstein estimates [5]

A least square fit analysis of the data points in fig. 1 gives a straight line:

$$\sigma_{exp} / \sigma_{stat} = -0.000061\ A + 0.92$$

(the very low point for A = 58 corresponding to ^{58}Ni was arbitrarily omitted). A χ^2-analysis gives a similar results. The pertinent question to be asked is whether the above discrepancy between the experimental and calculated data is significant. In other words, could a suitable change of parameters bring the calculated values in accordance with the experiment or does one need an extension of the model.

The first possibility is discussed in the contribution by Holub et al. [4] While it is likely that drastic and erratic changes of input parameters for each individual nucleus could bring the ratio points to or close to unity, the

overall conclusion of ref. [4] is that no systematic variation of the parameters applied in a smooth way to all the nuclei could shift the least square line up to unity. The only exception, i.e. the only parameter capable of moving up the bulk of the data points would be the reaction cross section σ_{ne} around 14 MeV, which was taken from Mani et al. [8]. Although a systematic uncertainty in the optical model cross sections of ref. [8] is not unconceivable, there is no other independent evidence for the need of, say, a decrease of σ_{ne} by 10 %. Besides, this decrease would even worsen the disagreement around A = 150, and, moreover, its effect on the calculated cross sections may be more complex: a consequent decrease of $\sigma_{inv}(n)$ values used at neighbouring energies would soften the primary neutron emission spectrum and thus tend to increase the total (n,2n) cross sections. Thus explanations calling for an extension of the model appear to be more likely.

1.3. Extensions of the Simple Evaporation Model

Straightforward extensions of the simple evaporation model can be obtained by dropping some of the simplifications used in the calculation. A commonly employed extension consists in dropping the Weisskopf assumption, i.e. making Γ_γ competitive with Γ_n in the region of $U_{ex} \approx S(n)$ by, e.g. treating explicitly the effects of the angular momentum in the model.

1.3.1. Competitivity of Γ_γ : the decay of states near the neutron emission threshold

In the evaporation calculation of ref. [4] the assumption that a neutron is emitted whenever energetically possible was not strictly applied. Γ_γ was calculated from the Weisskopf single particle formula [9]:

$$\Gamma_\gamma = C \frac{1}{\omega(U - E_n)} \int_0^{E_n} E_\gamma^3 \, \omega(E_n - E_\gamma) \, dE_\gamma \qquad (1.4)$$

The symbols in the expression (1.4) are self-explanatory. The normalizing coefficient C_γ is calculated from the experimentally estimated width at the excitation energy U = S(n).

It appears, however, that the above estimate of Γ_γ is unsufficient to account for the gamma decay of unbound states near the neutron emission threshold. Now an underestimate of this probability would mean an overestimate of the very low energy part of secondary emission spectrum and, consecutively, an increase of the (n,2n) cross section. It should, at the same time, produce a decrease in the corresponding total (n,n') cross section. Hence, the same compound nucleus theory which overestimates the (n,2n) process should, when applied to inelastic scattering, give (n,n') cross sections smaller than the experimental ones. This fact was checked by Abboud et al. [10] who found that experimental (n,n') cross sections for several nuclei measured above the neutron emission threshold were actually larger than the ones calculated by the compound nucleus evaporation model.

In order to account for the discrepancy Decowski et al. [11] performed a complete compound nucleus calculation including the effects of angular momentum. The recent investigation of the spin distribution of states populated in a nuclear reaction at high excitation energies and the introduction of the concept of yrast levels made this approach possible. The underlying idea was that the states where the gamma decay competes successfully with the particle emission are states of relatively high angular momentum.

Let the incoming neutron, which brings in several units of angular momentum (up to about 5-6 for a 14 MeV neutron on an A = 100 target) excite a state of high angular momentum. As the first emitted neutron carries away little angular momentum on the average (low energy), the residual state is likely to be a high spin state. Its spin cannot be carried away by the (again low energy) second neutron; hence the possibility of the gamma decay competition. For excitation energies much above the neutron emission threshold this effect will be smaller, since the second neutron will have more energy available.

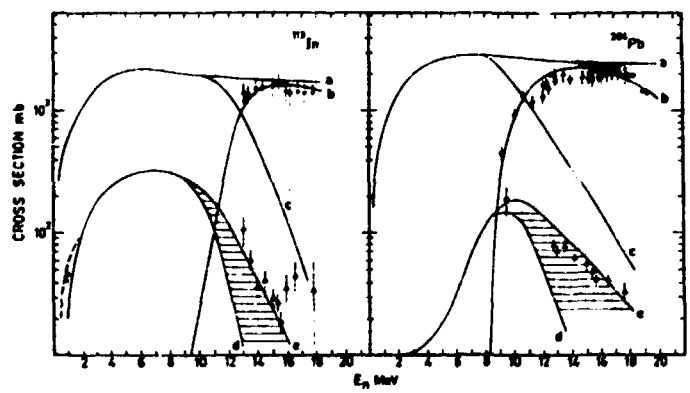

Fig. 3 Comparison of the experimental cross sections for the $^{113}In(n,n')$ and $^{204}Pb(n,n')$ cross sections to isomeric states of these nuclei (triangles) and the $^{113}In(n,2n)$ and $^{204}Pb(n,2n)$ cross sections (circles) with calculations, (a): compound nucleus formation cross sections; (b): (n,2n) cross sections; (c): neutron total inelastic cross sections; (e) and (d) cross sections for the formation of an isomeric state with and without the gamma decay of unbound states, respectively. The shaded areas thus correspond to the integrated cross sections originating from the gamma decay of unbound states (ref. [11]).

The results of the calculations of ref. [11] for ^{113}In and ^{204}Pb are shown in fig. 3. It appears that e.g. the inelastic scattering to a given isomeric state is considerably increased. It is not possible however, to estimate the contribution of the gamma decay of unbound states to the total inelastic cross section from the curves on fig. 3. In an earlier calculation Decowski et al. [12] estimate this contribution to 260 and 120 mb, for, respectively, ^{89}Y and ^{115}In target nuclei at 16 MeV neutron energy. These values are larger than the overestimates of the experimental values by the simple evaporation calculations of ref. [4]

It is clear that crucial to the above interpretation is the behaviour of (n,n') and (n,2n) cross sections around the (n,2n) threshold ($E_n \approx S(n)$). A point in favour of the assumed competitivity of Γ_γ and Γ_n is the experimental observation that (n,2n) reactions appear at bombarding energies by 0.5-1 MeV higher than the (n,2n) threshold [14, 15, 16]. The same is true for (n,3n) reactions, which may explain the failure of simple evaporation calculations of (n,2n) cross sections just above the (n,3n) threshold. These observations would then delimit the range where the Γ_γ vs. Γ_n competitivity is effective to 0.5-1 MeV above the particle emission threshold.

1.4. The presence of nonequilibrium processes

As mentioned in the introduction nonequilibrium processes may contribute to the emission of primary and secondary neutrons in the (n,2n) reactions. Their influence will be felt as a reduction in the value of the cross section as compared to the one calculated from the simple evaporation model.

There are two formally different ways to treat the nonequilibrium processes: the inclusion of direct transitions to collective states of the nucleus and the inclusion of preequilibrium processes using one of the existing models. We shall discuss now some results obtained by the two above approaches.

1.4.1. The role of direct emission

It is natural to include direct processes in the calculation of (n,2n) cross sections, since we know that they are present in the inelastic scattering of medium energy neutrons. Enhance direct transitions to low lying levels of the residual nuclei will partially deplete the low energy part of the evaporation spectra and thus reduce the fraction of primary neutrons capable of giving rise to the emission of secondary neutrons. Typical values of angle integrated cross sections for the inelastic scattering of medium energy neutrons on the first 2^+ levels of some Se, Nd and Sm isotopes are shown in Table 1 [15]. The analysis shows that the scattering is largely due to direct processes, Hauser-Feshbach type calculations for the above processes giving typically values of a few millibarns. It appears thus that direct (non evaporative) scattering of, say, 14 MeV neutrons to only the low lying collective states amounts to a few hundred millibarns. This number is by itself sufficient to account for the difference between simple evaporation and experimental (n,2n) cross sections at this energy.

Table 1: Angle integrated cross sections for the inelastic scattering of medium energy neutrons to the first 2^+ state

Nucleus	^{76}Se		^{82}Se		^{142}Nd		^{148}Nd		^{148}Sm		^{152}Sm	
Energy (MeV)	6	8	6	8	7		7			14	7	14
(2^+) mb	204	184	254	209	65		224		178	76(a)	286	182(a)

(a) Estimate based on parameters used to fit absolute angular distributions at 7 MeV (Ch. Lagrange, Priv. Comm.)

A schematic model for inelastic scattering based on direct transitions was developed recently by Lukjanov et al. [16]. The direct transition amplitude was calculated under the simplifying assumption that its main contributions come from the external region of nuclei. Using plane waves for the elastic scattering wave function and a simple asymptotic form for the radial dependence of the bound state nuclear wave functions, they obtained the direct part of the angle integrated neutron emission spectrum under the parametrized form:

$$\sigma^D(\varepsilon, E_n) = \gamma \cdot \frac{\varepsilon}{E_n} \cdot (E_n - \varepsilon) \qquad (1.5)$$

where E_n and ε stand for incident and outgoing neutron energies, respectively. It was found that this expression fits well the forward peaked part of the spectrum. The isotropic part of the spectrum was fitted by a Maxwellian shape:

$$\sigma^M(\varepsilon, E_n) = \alpha\ \varepsilon \exp(-\varepsilon/\theta) \qquad (1.6)$$

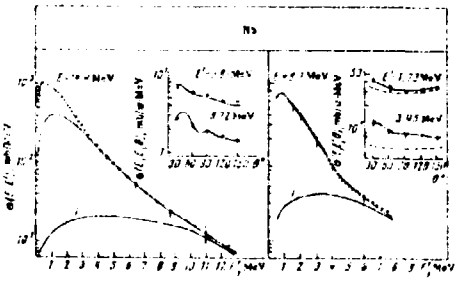

Fig. 4 The angle integrated total neutron spectrum and selected angular distributions from 14.4 MeV neutrons + ^{93}Nb: experimental points, result of the calculation (solid line), contribution of direct processes (curve 1). (from ref. [17]).

The above decomposition of the spectra is shown on fig. 4 for the neutron spectra of n + ^{93}Nb at incident energies of 14.4 and 9.1 MeV respectively. Table 2 shows the numerical results of ref. [16] for a number of nuclei at 14.4 MeV. The fraction n of direct inelastic emissions (col. 6) is given as:

$$n = \frac{\langle \sigma^D \rangle}{\langle \sigma^D \rangle + \langle \sigma^M \rangle}$$

The cross section $\sigma(n,2n)$ in column 7 of table 2 is the (n,2n) cross section calculated in ref. [16] as one half of the integrated experimental cross section for the emission of all neutrons (dots in fig. 4) and the value of the energy integrated inelastic cross sections ($\langle \sigma^D \rangle + \langle \sigma^M \rangle$). σ(all neutron emission) = $\sigma(n,n_1) + \sigma(n,n_2) \approx (n,n') + 2\sigma(n,2n)$, where $\sigma(n,n')$ stands for purely inelastic (no second neutron) emission. It would thus appear that the above value of ($\langle \sigma^D \rangle + \langle \sigma^M \rangle$) is equal to $\sigma(n,n')$, which does not come out clearly from ref. [16]. The comparison with experiment (col. 8) is rather unsatisfactory. Column 9 gives the simple evaporation results of ref. [4].

Table 2: Direct + compound analysis of angle integrated spectra (refs. [16] and [14]) at 14.4 MeV

Nucl.	a mb/MeV^2	θ MeV	γ mb/MeV^2	$\langle \sigma^D \rangle$ mb	$\langle \sigma^M \rangle$ mb	f %	Calc. σ(n,2n)(16) mb	Calc. σ(n,2n)exp. mb	Calc. σ(n,2n)(4) mb
^{89}Y	72	1.17	0.34	235	1240	16	1120	860 (a)	995
^{93}Nb	84	1.18	0.28	193	1470	12	1040	1380 (b)	1596
^{52}Cr	51	1.21	0.49	338	940	26	110	350 (c)	585
^{56}Fe	31	1.43	0.50	345	790	30	480	440 (d)	837
^{59}Co	52	1.25	0.39	270	1010	21	480	790 (e)	814

(a) Ref. [14].
(b) Ref. [13].
(c) M. Bormann et al., Nucl. Phys. A115 (1968) 309
(d) Neutron Cross Sections, BNL-325 (1966)
(e) Average taken from values reported in Z. Bödy, INDC(Hun)-10 (1973)

The crudity of the calculation of ref. [16] and the absence of experimental inelastic spectra does not permit to conclude whether or not the inclusion of the direct component distributed over the whole range of the spectrum corresponds to reality. Thus we shall now discuss the other method of including nonequilibrium processes, that is the use of existing preequilibrium models.

1.4.2. Preequilibrium processes in (n,2n) reactions

It is not our aim to discuss the preequilibrium processes in any detail since they will be treated separately. We shall only show the role they may play in multiple nucleon emission at medium incident energies ($E_n \sim 10$-20 MeV).

Let us illustrate this role by the results on 14 MeV neutron bombardment of ^{93}Nb where both experimental data and calculations exist [17]. The underlying idea is to assume that in the primary emission of nucleons both preequilibrium and equilibrium processes are present; the secondary emission is also influenced but in different way. A decomposition of the total neutron spectrum from 14.6MeV neutron bombardment of ^{93}Nb i.e. neutrons from (n,n'γ), (n,2n), (n,pn) and (n,np) is shown in fig. 5. The summed theoretical spectrum was obtained by adding a preequilibrium term to the usual Weisskopf-Ewing evaporation. This term was obtained using the method described by Cline and Blann [18] and with the nucleon collision rate parameters $\lambda^+ = \lambda^{NN}/5$ where λ^{NN} were given by the free nucleon-nucleon collision rates of Kikuchi and Kawai [19]. This choice is equivalent to scaling the preequilibrium contribution; it is significant that it agrees with independent estimates from the analysis of proton spectra [18].

An important point stemming from the analysis of ref. [17] is that the role of preequilibrium in the secondary emission is quite negligible (at least for medium energy incident particles. Thus its effect should be examined in the primary emission spectrum only.

A simple way of obtaining a rough idea of the preequilibrium part in the total emission of neutrons is to fit the emission spectrum with an ansatz of the form:

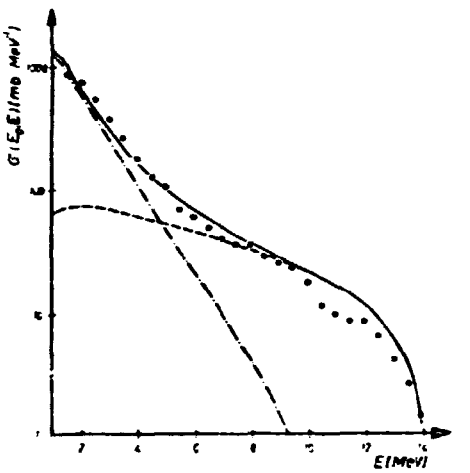

Fig. 5 Computed neutron emission spectrum from ^{93}Nb + n (14.6 MeV) compared with the experiment (dots); dashed line: preequilibrium, dashed-dotted line: equilibrium and full line: total spectrum, respectively (from ref. [17]).

$$\sigma(\varepsilon) = K_1(E_n)\,\varepsilon\cdot\sigma_{inv}(\varepsilon)\cdot\exp\left\{U/T\right\} + K_2(E_n)\,\varepsilon\,\sigma_{inv}(\varepsilon)\sum_{m=1}^{m=\infty}\left[\frac{U}{E_n + S(n)}\right]^{m-1}\cdot m(m-1) \qquad (1.7)$$

where U and E_n + S(n) stand for the excitation energies of the residual and compound system, respectively. The fitting using the above ansatz is performed for neutron energies ε higher than a given energy $\varepsilon_{fit} < \varepsilon_{th} = E_n - S(n)$ (emission of secondary neutrons impossible). The variable parameters in the fit are K_1, K_2 and T; the range of T was nevertheless restricted to values compatible with existing evaporation analyses.

Thus the physical quantity obtained by adjusting T, K_1 and K_2 to fit the higher energy part of the emission spectrum is the spectrum of the primary emitted neutrons, $\sigma(n,n_1;\varepsilon)$. Let it be kept in mind that this quantity should not be identified with the experimental angle integrated spectra shown in figs. 5 and 7, where all emitted neutrons (primary and secondary) are present. The values of T, K_1 and K_2 obtained from the neutron spectra of ^{48}Ti at E_n = 14 MeV and ^{93}Nb at E_n = 14.6 MeV by using the ansatz (1.7) are shown on table 3 [20]. A comparison with values for ^{93}Nb obtained in an earlier analysis [21] (same experimental data, same ansatz) shows that the determination of T, K_1 and K_2 is far from being unambiguous. Thus the above described method of obtaining the preequilibrium contribution has to be taken with more than a grain of salt.

A byproduct of the above analysis are the values of the matrix element $|M|^2$ extracted by the comparison of the energy integrated preequilibrium part of (1.7) with the complete Griffin formula [24]. These values are compared in table 3 with values suggested from independent analyses of Gadioli [22] and Kalbach [23]. As well as the values of T and K, the values of $|M|^2$ obtained in ref. [20] should also be taken as indicative.

Starting from the above numbers it is possible, under certain assumptions, to

calculate the (n,2n) cross sections. We take the calculated integrated cross section for the emission of primary neutrons:

$$\sigma(n,n_1) = \sigma(n,n') + \sigma(n,2n) + \sigma(n,np) + \sigma(n,n\alpha) + \ldots$$

and the experiment cross section for the total neutron emission:

$$\sigma(n,n_t) = \sigma(n,n') + 2\sigma(n,2n) + \sigma(n,np) + \sigma(n,pn) + \sigma(n,n\alpha) + \sigma(n,\alpha n) + \ldots$$

the latter obtained from, e.g. integrating the experimental neutron spectra (17, 25). Their difference:

$$\sigma(n,n_t) - \sigma(n,n_1) = \sigma(n,2n)$$

gives $\sigma(n,2n)$ assuming that $\sigma(n,pn)$ and $\sigma(n,\alpha n)$ are negligible. The values of $\sigma(n,2n)$ for ^{48}Ti and ^{93}Nb calculated using the above method and with fitted values of T, K_1 and K_2 obtained from table 3, are shown in table 4. The calculated value for ^{93}Nb at 14.6 MeV (1265 mb) somewhat underestimates the experiment (1444 ± 104 mb). We remember that simple evaporation calculations of ref. [4] (1610 mb) overestimated the experiment. The part of preequilibrium vs. compound emission is estimated in ref. [20] to 10 % vs. 90 % for ^{93}Nb and to 8 % vs. 92 % for ^{48}Ti. These numbers refer, of course, to primary emission; as, however, the secondary emission proceeds essentially by evaporation only, these numbers give an indication of the preequilibrium contribution to (n,2n) cross sections also.

A somewhat different approach in establishing the preequilibrium contribution in the (n,2n) cross sections was adopted by Bayhurst et al. [14].

These authors have fitted excitation functions of (n,2n) reactions from threshold to 28 MeV for several nuclei by adding a preequilibrium term to the evaporation formula. Their evaporation calculation differ from the one in ref. [4] in the values of $\sigma_{inv}(n)$ and a different estimate of Γ_γ. Moreover, a different set of level densities was adopted and the effects of angular momentum were explicitly taken into account for outgoing (primary) neutrons leaving the (first) residual nucleus with an excitation U 2 MeV. A sample of the results of ref. [14] is shown in fig. 6. Table 5 compares the values for the compound nucleus (n,2n) cross sections given in ref. [14] with those of refs. [4] and [5] for ^{169}Tm at E_n = 10-18 MeV. Even when taking into account the above mentioned differences in the calculations, the comparison is surprising, since the low values of $\sigma^c(n,2n)$ quoted in ref. [14] are obtained without an apparent scaling factor.

The absolute value of the preequilibrium contribution was calculated in ref. [14] by using decay rates λ reduced by a factor of 4 as compared to the values of λ^{NN} obtained from the free nucleon interaction matrix element of Kikuchi and Kawai [19]; the corresponding factor was 5 in the calculations of Hermann et al. (ref. [17]). The calculations of ref. [14] show, in general, an increasing contribution of preequilibrium processes at higher incident energies. For ^{169}Tm the contributions of equilibrium and preequilibrium emissions become equal at $E_n \approx$ 19 MeV (Fig. 5).

Table 3: Values of T, K_1 and K_2 and $|M|^2$ obtained from fitting the expression (1.7) to neutron emission spectra (ref. [20*])

Nucl.	ℓ_{th} E_n-S(n)	ℓ_{fit} MeV	T MeV	K_1 MeV^{-2}	K_2 MeV^{-2}	χ^2	$\|M\|^2$ Calc.	M^2 Gad.(a)	M^2 Kal. (a)
^{49}Ti	2.4	3.4	1.6	$0.17\cdot10^{-4}$	$0.35\cdot10^{-3}$	13.5	$4.3\cdot10^{-5}$	$6.8\cdot10^{-5}$	$6.3\cdot10^{-5}$
^{93}Nb	5.9	8.2	1.24	$0.045\cdot10^{-4}$	$0.34\cdot10^{-3}$		$1.1\cdot10^{-5}$	$0.96\cdot10^{-5}$	$1.05\cdot10^{-5}$
^{93}Nb	5.8	6.	1.3	$0.054\cdot10^{-4}$	$0.38\cdot10^{-3}$	3.1	$1.2\cdot10^{-5}$	$0.96\cdot10^{-5}$	$1.05\cdot10^{-5}$
^{93}Nb(b)	5.9	5.8	1.24	$0.03\cdot10^{-3}$	$0.62\cdot10^{-3}$				

*) Incident neutron energies for ^{49}Ti and ^{93}Nb, E_n = 14 and 14.6 MeV respectiv.
(a) $|M|^2$ Gad = $8/A^3$ MeV^2 (ref. [22]), $|M|^2$ Kal = $190/A^3E$ MeV^2 (ref. [23])
(b) result from ref. [21]

Table 4: Values of $\sigma(n,n_1)$, $\sigma(n,n')$ and $\sigma(n,2n)$ deduced from the fitted values of K_1, K_2 and T from table 3 (ref. [20])

Nucleus, E_n	$\sigma(n,n_1)$ exp.	$\sigma(n,n_1)$ calc.	$\sigma(n,n')$ calc.	$\sigma(n,2n)$ calc.	$\sigma(n,2n)$ exp.
^{49}Ti, 14	1576 (a)	1259	955	304	
^{93}Nb, 14.6	2910 (a)	1655	412	1265	1444 ± 104 (b)

(a) obtained from the angle integrated spectra of refs. [17] and [25]
(b) ref. [13]

Table 5: Compound nucleus cross sections $\sigma^c(n,2n)$ for ^{169}Tm calculated from refs. [14], [4] and [5].

E_n (MeV	$\sigma^c(n,2n)$ mb		
	Ref (14)	Ref (4)	Ref (5)
10	1250	1523	1308
12	1650	2100	2006
14	1650	2200	2186
16	1500	2157	1385
18	1000	1336	813

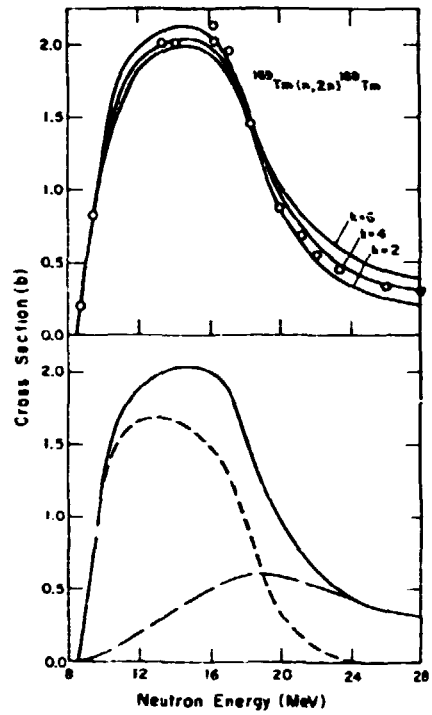

Fig. 6 Calculated and experimental cross sections for $^{169}Tm(n,2n)^{168}Tm$. The upper part of the figure shows the fits of an equilibrium plus preequilibrium component for three different values of k, the scaling factor for the transition rate λ_{n+2} in the preequilibrium model. The lower part of the figure shows the decomposition of the fit (full-curve) into the equilibrium (short dashed curve) and the preequilibrium component with k = 4 (long dashed curve) (ref. [14]).

Ab ovo preequilibrium calculations

While ordinarily the analysis of spectra and excitation functions is performed by comparing an incoherent sum of equilibrium and preequilibrium components to the relevant physical quantities, it is tempting to undertake a complete preequilibrium calculation equivalent to stating that the equilibrium is the end of a long equilibration process. A complete calculation based on, say, the exciton model should thus be able to account for both preequilibrium and equilibrium features of a reaction. Without discussing in detail the possible difficulties of such an approach, we present here some preliminary results obtained by Bersillon and Faugère [27].

The crucial point of such calculations is the representation of the time evolution of the particle emission rate. In the exciton model, this quantity can be obtained by solving the set of coupled equations known as "master equations" [24]. We can, conveniently, represent these equations by a flow diagram, where each considered configuration (n_o = (2p,1h) = 3 to $\bar{n} = \sqrt{2gE_{exc}}$) is represented by a box. W (p,h) represent the energy integrals of the particle emission probabilities $w(p,h,\mathcal{E})$ for each particular box. The time evolution of a reaction corresponds in this schematic model to the time evolution of the population of the different boxes leading to emission rates characteristic of each given instant. At the time the emission of the particle(s) has taken place the population of the boxes should be zero (100 % emission).

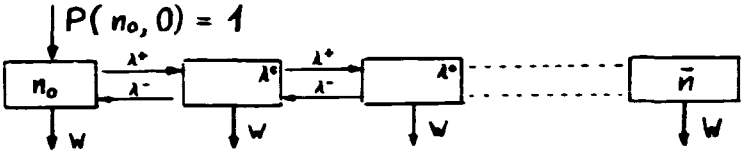

This problem could be treated in two ways. The master equations can be solved numerically by taking finite time intervals Δt. This was done, for instance, by Cline [28] and by Cline and Blann [18] by taking time intervals Δt of the order of one percent of the man transition time. The temporal evolution of a typical reaction shows a gradual shift from the harder preequilibrium to softer "Maxwelian with a tail" emission spectra.

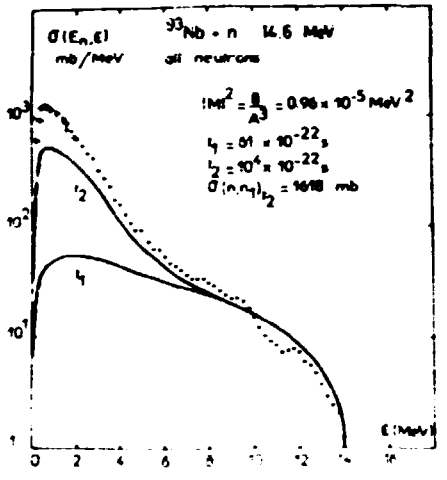

Fig. 7 The result of an ab ovo calculation obtained by solving the master equations of ref. [24]. The points and crosses represent the angle integrated total neutron spectra from the interaction of 14.6 MeV neutrons with ^{93}Nb. The two lines (t_1 and t_2) represent calculated primary emission spectra at instants of time corresponding to 61 · 10^{-22}s and 10000 · 10^{-22}s, respectively (ref.[20]).

Recently Bersillon and Faugère [27] have attempted to solve analytically the master equations. The example shown in Fig. 7 is the emission of primary neutrons following the 14.6 MeV neutron bombardment of ^{93}Nb. The initial configuration contained $n_0 = 3$ excitons, $P(n_0,0) = 1$, the decay rates λ where those of Williams [29] with $|M|^2 = 9/A^3$ MeV^2 [22] and the single particle level density parameter $g = A/11.8$ MeV^{-1}.

The spectrum of the primary emitted neutrons is shown at two instants: $t_1 = 61.10^{-22}$s and $t_2 = 10\,000.10^{-22}$s corresponding, respectively, to roughly 24 % and 100 % emission. The evolution of the spectrum towards a "Maxwellian with a tail" shape is quite visible (notice the log scale!).

It is instructive to compare, even partially, these results with experiment. The points and crosses on fig. 7 represent the experimental total emission spectrum (all neutrons). Only primary neutrons are, however, present for energies $\mathcal{E} > 5.8$ MeV. The curve t_2 fits this part of the spectrum quite well. The equilibration time $t_2 = 10^{-16}$s is not unreasonable either. A more extended set of analyses is, however, needed before a definite judgement could be rendered.

2. THE CSIKAI-PETŐ EFFECT REVISITED

In 1966 Csikai and Pető [30] made the observation that a regularity exists in the (N-Z) dependency of (n,2n) cross sections at a given excess energy U_R. Taking the existing data for $U_R = 3$ MeV and using the simple Weisskopf formula (1.3) to adjust some other data to $U_R = 3$ MeV, Csikai and Pető observed that for constant values of the neutron number N the (n,2n) cross sections for $U_R = 3$ MeV plotted against N-Z lie on straight lines approximately parallel to each other (except for N = 28) and this irrespectively of Z being even or odd. Thus a simple empirical formula was deduced giving:

$$\sigma(Z \pm \Delta Z, N) = \sigma(Z,N) \mp m(U_R)\Delta Z \qquad (2.1)$$

with $m = 231$ for $U_R = 3$ MeV and all values in millibarns. This so called Csikai-Pető effect was extensively used by evaluators and recommended values of (n,2n) cross sections were given on the basis of the above expression.

The newly obtained values of (n,2n) cross sections for a wide range of incident energies and in particular the measurements on series of isotopes like the ones presented at this Conference [13] permit, at present, a critical revaluation of the original observations which led to the expression (2.1).

Let us first say that simple evaporation formulas like the Weisskopf one (e.g. 1.3) are unable to reproduce the Csikai-Pető trend, as they give the (n,2n) cross section essentially as a function of only one parameter, the excess energy U_R. It is nevertheless plausible that at residual excess energies U_R midway between the (n,2n) threshold and saturation (the latter roughly coinciding with the (n,3n) threshold) there should be a rising effect on (n,2n) cross sections as (N-Z) increases: neutrons are more likely emitted when their relative fraction in the nucleus increases. Trends in cross sections for series of isotopes shown in ref. [13] exhibit this fact rather clearly.

Figures 8 and 9 show what would be the Csikai-Pető effect for a number of isotones around N = 50 and 82 respectively and for a set of values of the residual excitation U_R. The (n,3n) threshold lies normally 7-8 MeV above the (n,2n) threshold; $U_R = 3$ MeV is thus midway between the two. It appears that the cross sections for given values of N and U_R have a mounting tendency, but the latter is rather irregular, the slopes varying with both U_R and N. Besides, the scatter of experimental points is such that substantial variations of the slope of the lines passing through data points are permitted.

The data shown in the figures 8 and 9 are from recent compilations of Bödy [31] and Kondaiah [32] and from a few recent measurements of (n,2n) cross sections. We have not included in the data any adjusted values, i.e. we have not scaled

the (n,2n) cross sections at different values of U_R by the use of the Weisskopf formula (1,3).

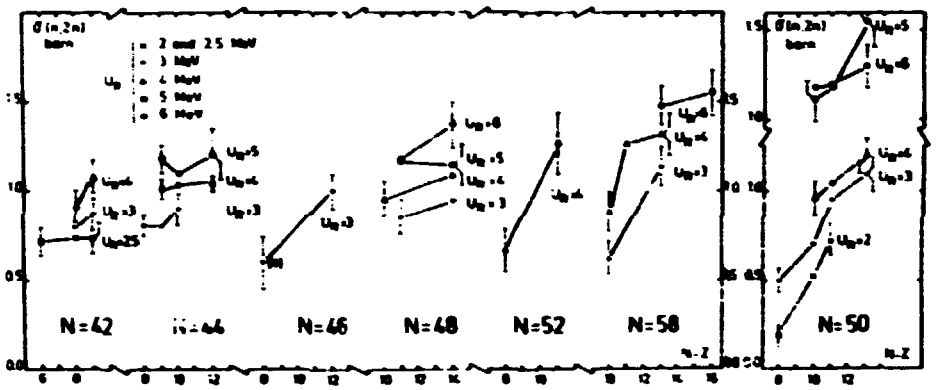

Fig. 8 The (N-Z) dependency of the (n,2n) cross sections at various values of the excess energy U_R for several isotones around N = 50. Notice the changes in the vertical scale.

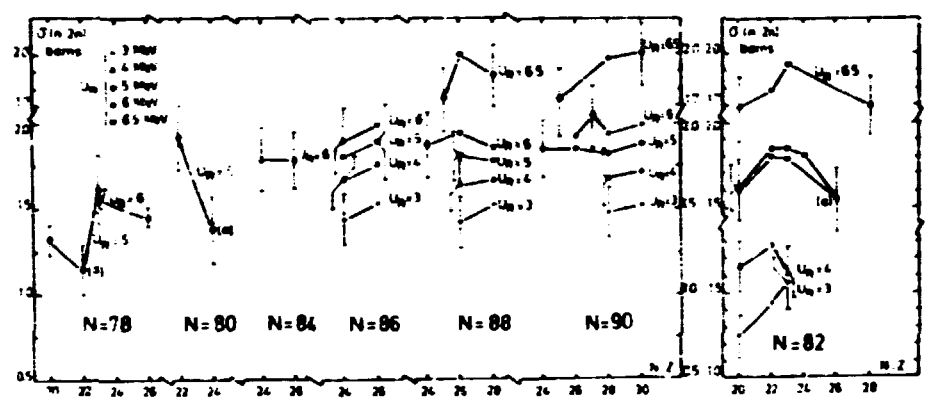

Fig. 9 The (N-Z) dependency of the (n,2n) cross sections at various values of the excess energy U_R for several isotones around N = 82. Notice the changes in the vertical scale.

Thus, 10 years later and with a large number of experimental data available, we can say that while the original observation of Csikai and Petö still stands in the sense that (n,2n) cross sections for U_R = 3 MeV rise when plotted vs. (N-Z) the regularity of the rise and the generality of this statement (hence its applicability for evaluation purposes at $U_R \neq 3$ MeV) is certainly not borne out by experiment.

3. CONCLUSIONS

We have briefly discussed two kinds of problems related to (n,2n) reactions. The first one relates to the reaction mechanism. We have seen that the (n,2n) cross sections are reproduced to within about 20 % by a simple evaporation formula, at least for energies well above the (n,2n) but still below the (n,3n) thresholds. The difference can be accounted for either by making the model more

sophisticated (effects of $\Gamma_\downarrow$ and T_ℓ) or by adding nonequilibrium contributions. It is possible that, e.g. near the (n,2n) threshold, both of these mechanisms are present and necessary. It is our feeling, however, that the inclusion of preequilibrium processes has the advantage of giving a unified view of the process.

As to the observed (N-Z) regularities in (n,2n) cross sections known as the Csikai-Petö effect, it appears that a more extensive analysis of data do not bear out their generality.

The authors are indebted to G. Mosinski for a number of numerical calculations and constant assistance in writing this paper.

REFERENCES

[1] K. Seidel, D. Seeliger and A. Meister, Contrib. to 3rd Soviet Nat. Conf. on Neutron Physics, Kiev 1975.

[2] E. Holub and N. Cindro, Phys. Letters 56B (1975) 143.

[3] J. Blatt and V.F. Weisskopf, Theoretical Nuclear Physics, J. Wiley and Sons, N. York (1963), p. 374.

[4] E. Holub, O. Bersillon, N. Cindro and J. Jary, Contribution fo this Conference.

[5] S. Pearlstein, Nucl. Data A3 (1967) 327.

[6] A. Adam and L. Jeki, Acta Phys. Ac. Sc. Hungariae 26 (1969) 335.

[7] A. Chatterjee and S. Chatterjee, Nucl. Phys. A125 (1969) 593.

[8] G.S. Mani, M.A. Melkanoff and I. Iori, Rep. CEA 2380 (1963).

[9] Ref.[3], p. 623.

[10] A. Abboud, P. Decowski, W. Grochulski, A. Marcinkowski, K. Siwek, J. Turkiewicz and Z. Wilhelmi, Acta Phys. Pol. B2 (1971) 527.

[11] P. Decowski, W. Grochulski, J. Karolyi, A. Marcinkowski, J. Piotrowski, E. Saad and Z. Wilhelmi, Nucl. Phys. A204 (1973) 121.

[12] P. Decowski, W. Grochulski and A. Marcinkowski, Nucl. Phys. A194 (1972) 380.

[13] J. Frehaut and G. Mosinski, Contr. to 3rd Soviet Nat. Conf. on Neutron Physics, Kiev 1975 and this Conference.

[14] B.P. Bayhurst, J.S. Gilmore, J.R. Prestwood, J.B. Wilhelmy, N. Jarmie, B.H. Erkkila and R.A. Hardekopf, Phys. Rev. C12 (1975) 451.

[15] G. Haouat, J. Lachkar, M.T. McEllistrem, Y. Patin, J. Sigaud and F. Cocu, to be published and private communication.

[16] A.A. Lukyanov, O.A. Salnikov and E.M. Saprykin, Sov. J. Nucl. Phys. 21 (1975) 35.

[17] U. Herrmann, D. Seeliger and K. Seidel, Report ZfK-271 (1974) p. 50.

[18] C.K. Cline and M. Blann, Nucl. Phys. A172 (1971) 225.

[19] K. Kikuchi and M. Kawai, Nuclear Matter and Nuclear Reactions, North Holland, Amsterdam, 1966, p. 36.

[20] L. Faugère, Private communication.

[21] D.H. Hermsdorf, S. Sassonov, D. Seeliger and K. Seidel, J. Nucl. Energy 27 (1973) 747.

[22] E. Gadioli and L. Milazzo-Colli, Lecture Notes in Physics 22 Ed. by N. Cindro et al., Springer Verlag (1973), p. 84.

[23] C. Kalbach, Acta Phys. Slovaca 25 (1975) 100.

[24] J.J. Griffin, Phys. Rev. Lett. 17 (1966) 488.

[25] D. Seeliger, K. Seidel, D. Hermsdorf, S. Sassonov and V.D. Toneev, Contr. to the 3rd Soviet Nat Conf. on Neutron Physics, Kiev 1975.

[26] M. Blann and A. Mignerey, Nucl. Phys. A186 (1972) 245.
[27] O. Bersillon and L. Paugère, Private communication.
[28] C.K. Cline, Thesis, Univ. of Rochester, 1971.
[29] F.C. Williams, Phys. Letters 31B (1970) 184.
[30] J. Csikai and G. Petö, Phys. Letters 20 (1966) 52.
[31] Z. Bödy, INDC (Hun) - 10 (1973).
[32] E. Kondaiah, J. Phys. A7 (1974) 1457.

MEASUREMENT OF (n,2n) AND (n,3n) CROSS SECTIONS AT INCIDENT ENERGIES BETWEEN 8 AND 15 MeV

J. FREHAUT - G. M. MOSINSKI

Service Physique Nucléaire Centre d'Etudes de Bruyères-le-Chatel
B.P. 61-92120-Montrouge-France

ABSTRACT

Cross sections of (n,2n) and (n,3n) reactions were measured for several nuclides between 8 and 15 MeV using a large liquid scintillator to count the neutrons directly. Measurements were made relative to the fission cross section of ^{238}U for the Nd isotopes 142-144-146-148-150, for the Sm isotopes 148-150-152-154 and for the natural elements Ti, V, Cr, Cu, Zr, Mo and Pb.

The relative accuracy of the measurements was generally of the order of 5 to 10 %.

INTRODUCTION

The activation technique generally used to measure (n,2n) and (n,3n) cross sections is based on the determination of the activity produced in a sample after neutron bombardment, and is therefore limited to nuclides which leave a suitably active residual isotope. The large liquid scintillator method used in the present experiment is based on the detection of the emitted neutrons and thus can be used for any nuclide, provided that several grams of material are available. This method is of particular interest for providing (n,2n) cross sections for natural elements and for the different isotopes of a given element

EXPERIMENTAL METHOD

A description of the principle of the method and details of the experimental set up and of corrections are given elsewhere [1, 2]. The experiment relies on two properties of the neutron detector, a large Gd-loaded liquid scintillator: its high neutron efficiency and the relatively long lifetime in the scintillator for neutrons before capture. This gives identification of an (n,2n) event by two separate pulses in the scintillator within the 30 μs following the event.

Detection of (n,2n) and (n,3n) events

About 10 to 15 grams of the sample to be measured are placed at the center of the scintillator and irradiated by a collimated neutron beam. Neutrons are produced by the $D(d,n)^3He$ reaction, using a gaseous target and the 14 MeV tandem Van de Graaff accelerator pulsed at a frequency of 2.5 MHz (pulse width $\sim$ 2 ns). An electrostatic beam sweeper is used to keep only three bursts within each 60 μs interval.

After each group of three bursts, a 30 μs counting gate is opened at the output of the liquid scintillator. The number of gates containing 0, 1, 2, ... pulses are recorded during a run. These data are corrected for the two sources of background in the scintillator:

- The natural background, measured for the same number of counting gates with the accelerator beam off.
- The accelerator dependent background, measured with the beam on and the sample out for the same number of incident neutrons.

The data are also corrected for the detection dead time (120 ns), for the detector efficiency ($\sim$ 75 %), and for the possibility of two (n,n') or (n,n) events occuring in the same counting gate, being then indistinguishable from a (n,2n) event.

These corrections give the number of gates containing 2 or 3 neutrons, i.e. the number of (n,2n) and (n,3n) events, for non fissionable materials.

In the case of fissionable materials, it is necessary to subtract the fission events of neutron multiplicity 2 or 3. The total number of fissions can be calculated from the higher measured multiplicities (>4) using fission multiplicity distributions previously determined with a fission chamber [3]. These distributions and the calculated number of fission thus enable one to deduce the number of fission events of multiplicity 2 or 3.

(n,2n) and (n,3n) cross section determinations

A relative incident neutron flux measurement allows the (n,2n) and (n,3n) cross sections to be normalized on a reference cross section.

In the case of fissionable materials, (n,2n) and (n,3n) cross sections can be directly obtained relative to their fission cross section, since the number of fission events occuring during the measurement is also determined. Because of the lack of accurately determined (n,2n) cross sections, a fission cross section was also choosen as reference for non fissionable materials, the fission cross section of ^{238}U.

Relative flux measurement

The flux monitor consists of a small liquid scintillator located 1,5 meter behind the sample, in the collimated neutron beam. Monoenergetic incidnet neutrons in the energy range 6-15 MeV are produced using the $D(d,n)^3He$ reaction. With the pulsing system adopted, it is possible, by the time-of-flight technique, to separate the monoenergetic neutrons, the only neutrons which induce (n,2n) or (n,3n) reactions, from deuteron break-up neutrons as well as from neutrons induced by (d,n) reactions on the target materials. This technique provides very precise relative flux measurement for (n,2n) and (n,3n) reactions.

A relative determination of the efficiency of the monitor versus neutron energy, using the results of a Monte-Carlo calculation, allows, in the case of ^{238}U, an accurate determination of the apparent fission cross section and of the fission neutron multiplities. This calibration is necessary since, in contrast to (n,2n) or (n,3n) events, fission events may be induced by the secondary neutrons.

RESULTS

The large liquid scintillator efficiency was determined using a ^{252}Cf source and assuming a value of $\bar{\nu}$ = 3.732 ± 0.000 for the average number of prompt neutrons emitted per spontaneous fission.

The standard fission cross section of ^{238}U used for the normalization of the results was taken from the evaluation of SOWERBY et al. [4].

Error derivation

The errors quoted are standard errors derived by quadratic addition of the statistical errors of the experimental data and the errors of the corrections. The uncertainties of the standards, $\bar{\nu}$ for ^{252}Cf and the fission cross section of ^{238}U, have not been included.

(n,2n) and (n,3n) cross sections

The cross sections for 7 natural elements and for the measured Nd and Sm isotopes are given in table 1 and 2 respectively together with the ^{238}U fission cross section used as a standard.

Enriched isotopes were used for the measurements on Neodymium and Samarium. The contribution of the non measured isotopes present in small quantities in the samples was subtracted using the respective calculated cross sections given by PEARLSTEIN [5].

Earlier measurements using the same technique for 16 other nuclei and 3 natural elements have been reported elsewhere [6, 7].

DISCUSSION

The results for the seven measured natural elements are plotted in figures 1 and 2. Plots for Ti, Cr and Zr show an elbow in the rising slope of the (n,2n) cross section at an energy just above the threshold for the most abundant isotope: 12 MeV for Ti (^{48}Ti, 73,9 %), 12.5 MeV for Cr (^{52}Cr, 83,7 %) and 12.5 MeV for Zr (^{90}Zr, 51,5 %).

In the case of vanadium, the contribution of the 0.24 % abundant ^{50}V is negligibleand the measured cross section is in fact that of the ^{51}V isotope.

Results obtained for the Cu sample are in agreement with the values obtained from the measurements published for the ^{63}Cu and ^{65}Cu isotopes [8].

The large liquid scintillator method was also used by MATHER et al. for (n,2n) cross section measurements on natural elements 9 . Their results for Mo at 12.4 and 14.3 MeV are consistent with the values obtained in the present experiment; their results for Cu at 14.06 MeV and for Pb at 12.4 and 14.06 MeV are however 10 % lower.

Figure 3 presents the measured cross sections for Sm and Nd plotted versus the mass number A for different values of the excess energy U_R above threshold, which corresponds to the total kinetic energy available for the two emitted neutrons.

Table 1:

Experimental results for the (n,2n) cross section of Ti, V, Cr, Cu, Zr, Mo and Pb. Cross sections are normalized on the fission cross section of ^{238}U as evaluated by Sowerby et al. [4]

$E_n \pm \Delta E_n$ MeV	σF, mb	$\sigma(n,2n)$, mb						
	^{238}U	Ti	V	Cr	Cu	Zr	Mo	Pb
9,44±0,120	960					199±14	199±10	934± 44
9,93±0,110	952					290±14	366±17	1162± 54
10,19±0,100	949	13± 1		30± 2	10± 2	320±15	458±21	1275± 59
11,44±0,090	957	41± 3	18± 2	57± 3	88± 5	482±24	799±39	1722± 83
11,88±0,090	965	53± 3	80± 6	70± 4	160± 9	516±26	895±44	1780± 88
12,36±0,080	978	103± 7	173±12	75± 6	260±18	600±40	1026±68	1945±129
12,85±0,080	999	190±13	288±19	143±10	379±19	705±47	1115±74	2033±136
13,33±0,080	1031	279±19	405±28	226±16	487±33	848±58	1166±79	2111±143
13,80±0,070	1086	386±26	527±36	323±22	582±40	992±68	1245±85	2260±154
14,76±0,076	1216	501±35	629±44	451±32	677±48	1058±74	1252±88	2235±156

TABLE II

Experimental results for the (n, 2 n) and (n, 3 n) cross sections of Neodymium and Samarium isotopes. Cross sections are normalized on the fission cross section of ^{238}U as evaluated by Sowerby et al. [4]

$E_n \pm \Delta E_n$ MeV	^{238}U	^{142}Nd	^{144}Nd	^{146}Nd	^{148}Nd	^{150}Nd	^{148}Sm	^{150}Sm	^{152}Sm	^{154}Sm
	σ_f, mb	σ (n, 2 n), mb								
8,03 ± 0,150	953			174 ± 14	346 ± 20	241 ± 17				
8,18 ± 0,150	957		145 ± 14							
8,44 ± 0,110	962			478 ± 24	673 ± 32	606 ± 30				140 ± 14
8,59 ± 0,140	963		332 ± 21				163 ± 14	182 ± 15	36 ± 14	
8,94 ± 0,120	964		645 ± 31	858 ± 41	1119 ± 50	989 ± 47	361 ± 20	429 ± 24	316 ± 17	565 ± 29
9,44 ± 0,120	960		893 ± 43	1150 ± 54	1288 ± 59	1261 ± 59	679 ± 34	731 ± 37	641 ± 31	965 ± 46
9,93 ± 0,110	952		1186 ± 56	1365 ± 65	1474 ± 68	1384 ± 69	1032 ± 49	1131 ± 57	1049 ± 49	1219 ± 61
10,42 ± 0,100	948	222 ± 17	1276 ± 61	1469 ± 70	1525 ± 71	1545 ± 73	1179 ± 57	1233 ± 60	1221 ± 58	1426 ± 68
10,91 ± 0,100	952	470 ± 26	1414 ± 68	1639 ± 80	1635 ± 78	1640 ± 79	1379 ± 67	1408 ± 69	1415 ± 68	1596 ± 78
11,88 ± 0,090	965	978 ± 66	1565 ± 102	1787 ± 116	1713 ± 111	1817 ± 118	1669 ± 110	1594 ± 104	1614 ± 101	1814 ± 118
12,85 ± 0,080	999	1473 ± 98	1727 ± 120	1920 ± 128	1809 ± 121	1950 ± 130	1732 ± 116	1776 ± 119	1764 ± 118	1942 ± 129
13,80 ± 0,070	1086	1725 ± 118	1727 ± 121	2006 ± 137	1906 ± 131	2012 ± 139	1835 ± 128	1933 ± 134	1902 ± 132	2071 ± 143
14,28 ± 0,070	1136		1755 ± 127		1804 ± 133					
14,76 ± 0,070	1216	2077 ± 146	1850 ± 137	2040 ± 153	1834 ± 142	1774 ± 138	1912 ± 149	2049 ± 148	1985 ± 143	2131 ± 156
		σ (n, 3 n), mb								
12,85 ± 0,080	999					10 ± 2				
13,80 ± 0,070	1086				28 ± 4	51 ± 5				
14,28 ± 0,070	1136				69 ± 6					
14,76 ± 0,070	1216			32 ± 5	143 ± 11	267 ± 18			10 ± 4	16 ± 5

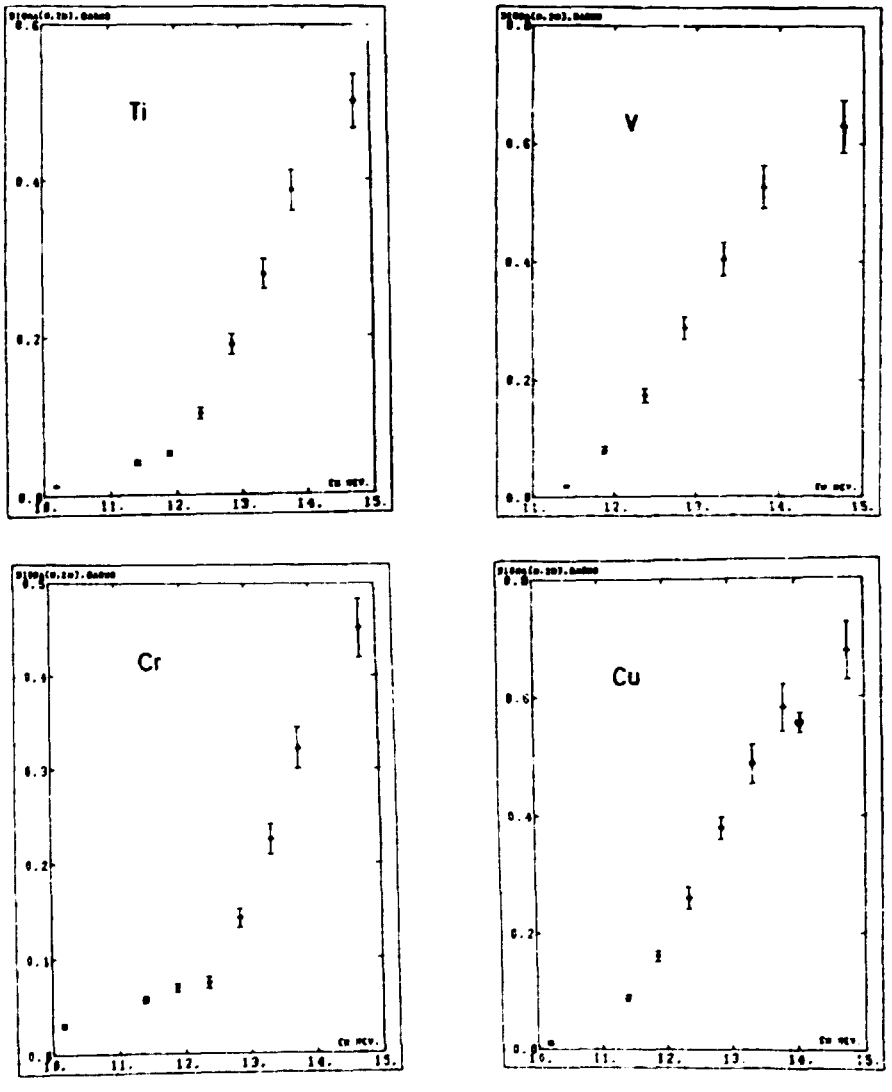

Fig. 1 Experimental (n,2n) cross sections for Ti, V, Cr and Cu in the neutron energy range 8-15 MeV: + Present experiment, Ref. [9]

CSIKAI and PETÖ [10] have assumed a linear dependency of the (n,2n) cross section versus A at constant excess energy U_R and for Z constant. Straight lines can in fact be drawn through our experimental points, but the slope of the observed dependency on A seems to vary with U_R. Moreover, the slopes predicted by ref. [10] are larger than the presently observed ones.

The ADAM-JEKI phenomenological formula [11] derived for U_R = 3 MeV also exhibits a too large dependency of $\sigma(n,2n)$ versus A.

The values given by PEARLSTEIN's semi-empirical calculations are 10 to 15 % larger than the results of the present measurement, except for ^{142}Nd, where they are about 10 % lower. Nevertheless, the general shape of the dependency of $\sigma(n,2n)$ versus A for a given Z is fairly well reproduced in both cases, except

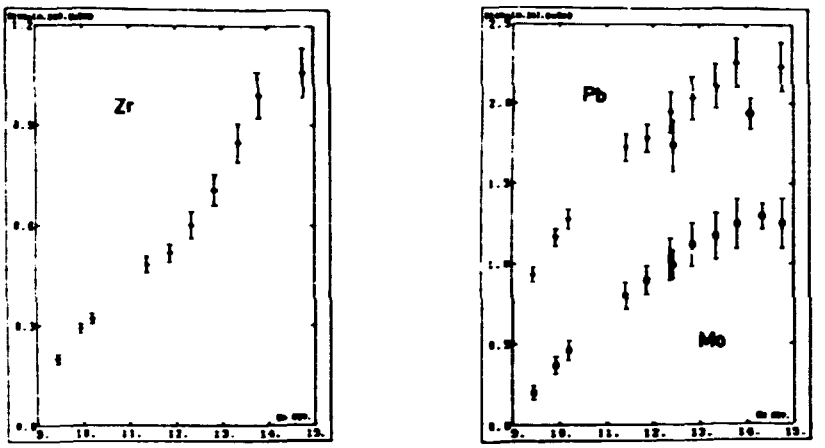

Fig. 2 Experimental (n,2n) cross sections for Zr, Mo and Pb in the neutron energy range 8–15 MeV: +, ▪ Present experiment, ● Ref. [9]

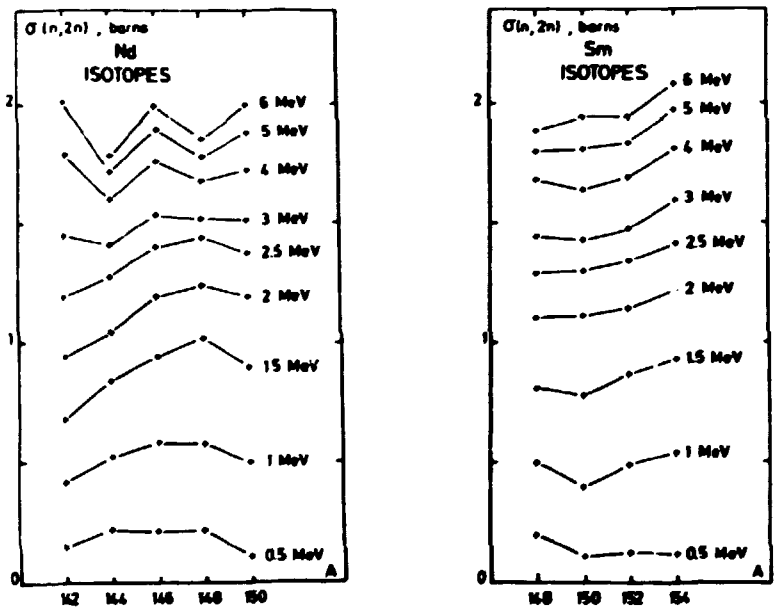

Fig. 3 Experimental cross sections for Sm and Nd isotopes plotted versus the mass number A for different values of the excess energy U_R

for ^{142}Nd above U_R = 3 MeV.

CONCLUSION

(n,2n) cross sections for structure materials are needed for the design of fusion reactors. The present results are to date the only ones to cover the entire energy range from threshold to 15 MeV for several such materials.

Measurements of (n,2n) cross sections for series of isotopes give more fundamental information on the process itself and should help for a better understanding of the mechanism of multiple neutron emission.

REFERENCES

[1] J. FREHAUT, G. MOSINSKI, Rapport CEA-R-4627 (1974).

[2] J. FREHAUT, G. MOSINSKI, Acta Physica Slovaca 25 (1975) 195.

[3] M. SOLEILHAC et al., J. Nucl. Energy 23 (1969) 257.

[4] M.G. SOWERBY et al., AERE Report R 7273 (1973).

[5] S. PEARLSTEIN , Nuclear Data B, Section A, 3 (1967) 3.

[6] J. FREHAUT, G. MOSINSKI, to be published in the preceedings of the Confrence on Nuclear Cross Sections and Technology, Washington (1975).

[7] J. FREHAUT, G. MOSINSKI, to be published in the proceedings of the National Soviet Conference on Neutron Physics, Kiev (1975).

[8] Z.T. BÖDY, INDC (HUN) - 10 (1973) 30.

[9] D.S. MATHER et al., AWRE Report 047/69 (1969).
AWRE Report 072/72 (1972).

[10] J. CSIKAI, G. PETÖ, Phys. Letters 20 (1966) 52.

[11] A. ADAM, L. JEKI, Acta Phys. Hungarica 26 (1969) 335.

SESSION II

THE ROLE OF PRECOMPOUND PROCESSES IN NUCLEAR REACTIONS WITH MULTIPLE NUCLEON EMISSION

A. Meister, D. Seeliger, K. Seidel
Technische Universität Dresden, Sektion Physik, DDR 8027 Dresden,
Mommsenstraße 13, GDR

Abstract

The knowledge, that precompound processes play an increasing role in (n,n') and (n,p)-reactions with incident energies $\gtrsim$ 10 MeV and can well described with preequilibrium models, is used to evaluate their influence on the following nucleon emissions. Especially the (n,2n), (n,pn) and (n,np) reactions are studied around 14 MeV incidence energy. Always cross sections, calculated with inclusion of preequilibrium emissions, are compared with such, where the same parameters are used, but precompound emissions are neglected and so the reactions are described only as successive compound nucleus evaporations - the usually used procedure in the past. The influence of precompound processes on the reaction cross sections is found to be in dependence on the mass number ($50 \leq A \leq 180$) and incidence energy ($8 \leq \epsilon_0 \leq 30$ MeV) in the range of a few percent up to some orders of magnitude.
After studies of the systematics of this effect evaluations for several nuclei are carried out.

1. Introduction

The spectra of the (n,n') and (n,p) reactions after 14 MeV neutron bombardment of nuclei show an appreciable contribution of precompound emissions [1,2]. The relations are illuminated in fig. 1, where for a mean nuclear system with mass number A = 100 calculated spectra are given, which represent the experimental values. For comparision spectra calculated with the same parameters but with neglect of precompound processes are inserted. Nucleons emitted in the energy range ϵ = 0 ... 7 MeV may leave residual nuclei with excitation energies to be able to emit further nucleons. The number of these residual nuclei, their excitation energy distribution and consequently

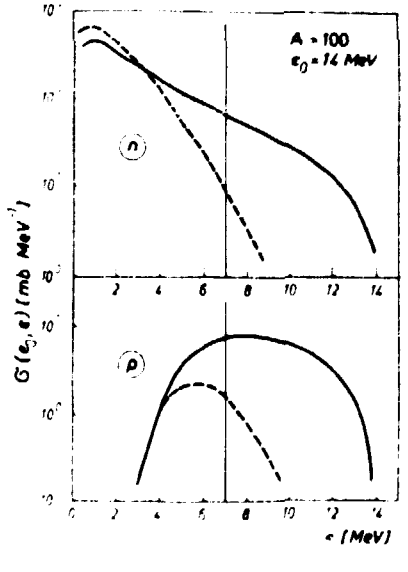

Fig. 1: Neutron and proton spectra from an nuclear system (A = 100)+n at an excitation energy E=21 MeV, taking into account precompound emissions (——) and not taking into account (- - -)

the cross sections of reactions like (n,2n), (n,pn), (n,np), ... are influenced by precompound processes, as can be seen from fig. 1.

It can be assumed, that precompound processes in (n,n') and (n,p) reactions are described by preequilibrium models with an accuracy [1, 2], allowing an quantitative estimate of their role in reactions with multiple nucleon emissions.

The used formalism contains up to four possible successive neutron and/or proton emissions from all exciton steps of the preequilibrium stage and as well as of the equilibrium stage. The preequilibrium transitions are described with Blann's Hybrid model [3], the compound nucleus emissions with the Weisskopf-Ewing formula [4].

2. Systematic influence of precompound processes on the reactions (n,2n),(n,pn) and (n,np)

In this chapter model systems with mean parameters and clear relations among them are studied to isolate the dominant systematic trends. By this way system formation cross sections and inverse cross sections are taken from a generalized optical potential [5]. Single particle level densities follow from $g = a \cdot \frac{6}{\pi^2} \cdot 2$ with $a = A/7{,}5 \cdot MeV^{-1}$ [6], the mean behaviour of the level density parameter in the Fermi gas model. Mostly, equal binding energies of neutrons and protons of all deexcitation steps of the system are used and pairing energy shifts are neglected. The used intranuclear transition rates between preequilibrium states are for all calculations $^1/k = {}^1/10$ times the collision rates in nuclear matter, the extracted mean behaviour from the interpretation of 14 (n,n') precompound spectra [7].

2.1. Nucleus with mass number A = 100

Fig. 2 shows the deexcitation of this system, consisting of Z protons and N neutrons and formated with a cross section of 1720 mb, by successive neutron and proton emissions. The transition strengths of the decay are given in mb as sum of preequilibrium plus equilibrium decay. The corresponding values in the case, if precompound processes are not taken into account are quotet in parenthesis.

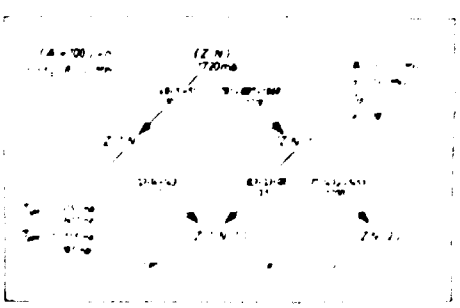

Fig. 2: Deexcitation of a system with Z protons and N neutrons (Z+N=100) at an excitation energy of 21 MeV by neutron and proton emissions. Further explanations in the text.

It's to see, that precompound emissions, caused by the hardening of the spectra and especially the changed sharing between proton and neutron deexcitation, lower the (n,2n) cross section by about 15 % and enhance the (n,np) and (n,pn) cross section by about 20 % and 100 % respectively. Also the total neutron and proton emission cross sections are influenced remarkable. The lowering of (n,2n) cross sections is shown in Ref. [8] by a systematic compilation of experimental values.

The portion of second neutrons emitted still in the preequilibrium stage of the

system is in the case of the (n,2n) and the (n,pn) reaction in the order of 2 %, so that the spectra of these neutrons can be parameterized as evaporation spectra.

2.2. Excitation energy dependence

At the same model nucleus the neutron incidence energy is varied in the range from 8 to 30 MeV. Fig. 3 shows the results. The (n,2n) cross section increases above the reaction threshold very rapidly and drops down at higher energies to such a degree as the (n,3n) channel is opened. The hard precompound spectrum causes in contrast to assumed multiple compound nucleus evaporations a typical high energy tail. The occurence of such high energy tails was instructively demonstrated with experimental (p,n),(n,p) and (n,n') excitation functions in Refs. [9] and with experimental (p,xn) and (,xn) excitation functions x = 3,4 and 5, ... in Refs. [9, 10]. So one has a situation, that precompound emissions lower the (n,2n) cross section in the region of the resonance like maximum, whereas, beginning 2 ... 3 MeV above the (n,3n) threshold, an appreciable increased cross section is obtained.

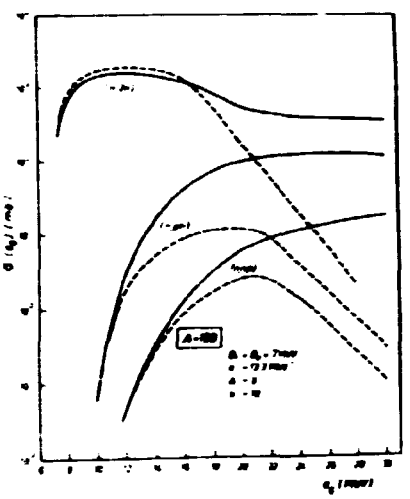

Pig. 3: Excitation functions, taking into account precompound processes (——) and not taking into account (- - -).

Because of the coulomb wall, which hinders the emission of charged particles, the (n,pn) and (n,np) cross sections rise only some MeV above the threshold and precompound processes enhance in medium mass nuclei the cross sections increasingly with higher excitation energies. The influence on the (n,np) reaction is smaller than on the (n,pn) reaction because of the lower mean excitation energy of the system before the proton emission.

2.3. Mass number dependence

To see the main trend of the influence of precompound processes in dependence on the mass number, the mass number trends of the nucleon binding energies, of the level density parameter and of the optical model absorption cross section are taken into account. Values are indicated in fig. 4 together with the results.

The (n,2n) cross section behaviour can be understood by the help of the excitation function (fig. 3). The smaller nucleon binding energy with increasing mass number causes a compression of the resonance like function and a shift to lower excitation energies. In the case of constant incidence energy ϵ_0 = 14 MeV

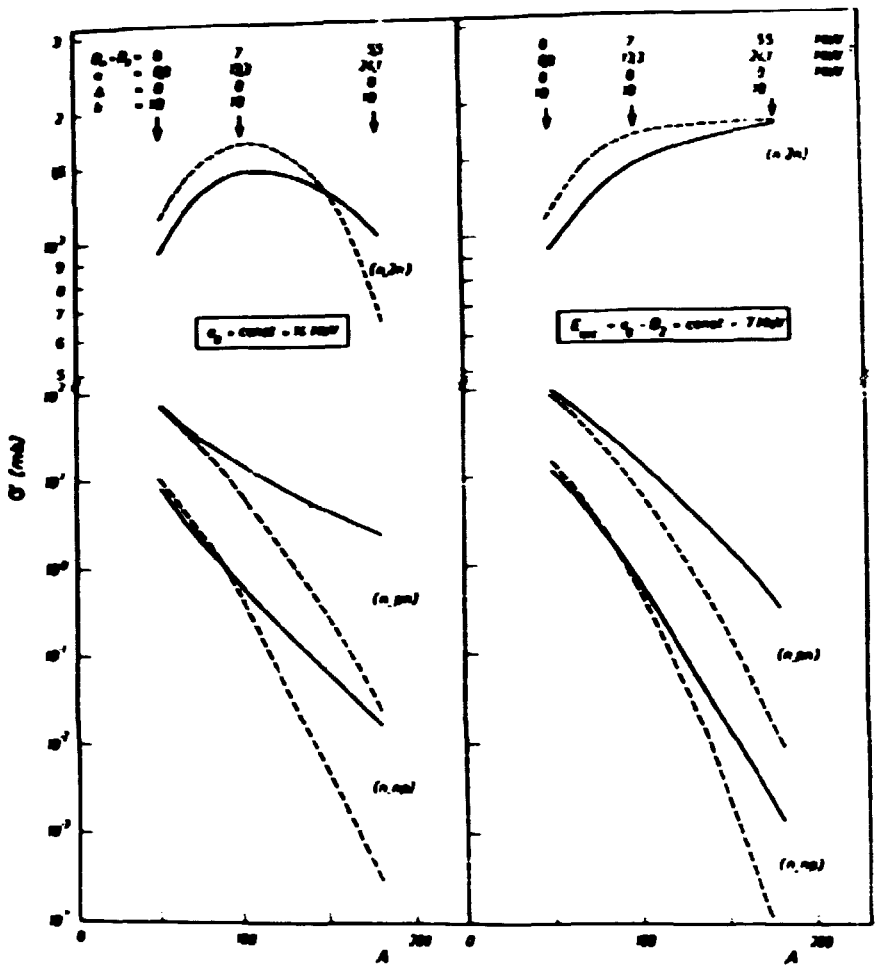

Fig. 4: Mass number dependence of the cross section, taking into account precompound processes (——) and not taking into account (- - -).

(fig. 4, left hand) one observed at heavy nuclei that the high energy tail acts already and precompound processes enhance the cross section, whereas at medium mass and light nuclei one has relations, as discussed for the A = 100 system.

In the case of constant excess energy $E_{exc.}$ - a parameter, which is often used in systematic compilations, to exclude binding energy effects - one can see in fig. 4, right hand, that the influence of precompound processes decreases with higher mass number. This occurs, because the compound nucleus contribution to the (n,n') cross section increases $\sim A$, but the precompound contribution only $\sim A^{1/3}$ [1], or in other words more and more low energy neutrons are emitted, because the level density parameter increases $a \sim A$.

The (n,pn) and (n,np) cross sections decrease rapidly with A because of the coulomb wall. But the higher the coulomb barrier is, the more important is the

influence of precompound emissions with hard spectra, so that at A = 180 by two orders of magnitude enhanced cross sections are obtained.
Ar heavy nuclei the cross sections, calculated with ϵ_0 = const. are larger than the corresponding with E_{exc} = const. = ϵ_0 - B, because B and therefore also E_{exc} decrease with A. That is also the reason, why at ϵ_0 = const. a larger influence by the precompound emission is observed.
At A$\leq$90 precompound processes diminish the (r,np) cross section, because compound nucleus proton emissions are not too strong suppressed by the coulomb wall, and therefore like the (n,2n) reactions, the high energetic precompound neutron emission reduces the proton emission probability, compared to two successive evaporations.

3. The influence of precompound processes on the (n,2n), (n,pn) and (n,np) reaction cross sections for several concrete nuclei

Calculations were carried out for nuclei in the mass range 58$\leq$A$\leq$209, for which neutron emission spectra were interpreted. Again cross sections, computed taking into account preequilibrium emissions are directly compared with the corresponding values, where precompound processes are neglected, to see the influence of the precompound mechanism.
Besides individual binding energies (taken from [11]) of all possible residual nuclei and level density parameters (taken from [12]) also the pairing effect is taken into account as well as in the compound nucleus and the precompound stage.
The superconductivity model of nuclei showed, that for heavy nuclei a pairing energy shift Δ in the preequilibrium state density does not depend on the complexity of the states, that means the exciton number [13]. Therefore Δ-values extracted from nuclear masses [14] are used for the preequilibrium and the equilibrium state densities. It may only be mentioned, that also a study of the systematic trends of shell and pairing effects on the influence of precompound processes was undertaken [15].

The role of all the mentioned values, effects and their interference find its expression in fig. 5.
In the case of the (n,2n) reaction the expected main mass number trend is confirmed. The cross sections are lowered between 14 % and 29 %. The influence of precompound processes is smaller for heavy nuclei than for light and medium mass nuclei. An entire inverted behaviour is observed at ^{58}Ni, where precompound emissions enhance the (n,2n) cross section by a factor of two (from 0.67 to 1.55 mb in the frame of the used formalism). The origin is the very high (n,p) cross section compared to the neutron emission probability.

The (n,np) cross sections are generally enhanced by precompound processes, and especially at high mass numbers a strong influence is indicated. These nuclei emit also the second nucleon, the proton, still from preequilibrium states: the compound nucleus emission is almost completely suppressed.
Also in the case of the (n,pn) reaction the expected trend of an enhancing influence of precompound processes at heavy nuclei is to see. The prime nucleon in the emission, the proton, is to a very high percentage a preequilibrium proton. At lighter nuclei the compound nucleus proton emission plays a role and

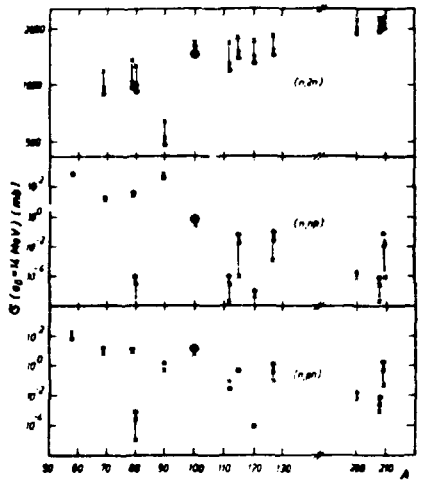

one has a competition between the reduction of the compound nucleus formation probability by precompound emissions and relatively large low energy precompound emissions in the neutron channel.

Fig. 5: Cross sections of several concrete nuclei, taking into account precompound processes (x) and not taking into account (•). Larger symbols: A= 100 model system.

4. Conclusion

The presented evaluation show, that precompound processes must be taken into account not only for improved interpretations of neutron emission spectra at 14 MeV incidence energy, but also for the interpretation of the cross sections of the (n,2n), (n,pn) and (n,np) reactions. The main mass number and excitation energy trends can be isolated, but the need of a careful consideration at each individual nucleus is indicated.

References

[1] D. Seeliger, K. Seidel and D. Wohlfarth,
Conf. on Neutron Physics, Kiew (UdSSR) 1971, Proc. p. 243;

D. Hermsdorf, S. Sassonov, D. Seeliger and K. Seidel,
Conf. on Nuclear Structure Study with Neutrons, Budapest (Hungary) 1972;

[2] G.M. Braga-Marcazzan, E. Gadioli-Erba, L. Milazzo-Colli and P.G. Sona,
Phys. Rev. C6 (1972) 1398;

G.M. Braga-Marcazzan and L. Milazzo-Colli,
Intern. Sem. on Interactions of Fast Neutrons with Nuclei,
Gaussig (GDR) 1973, Proc. p. 39;

[3] M. Blann, Phys. Rev. Lett. 27 (1971) 337;

[4] V.D. Weisskopf and D.H. Ewing, Phys. Rev. 57 (1940) 472;

[5] F.G. Perey, Phys. Rev. 131 (1963) 745;
A. Lindner, IPK-17, EANDC 73 "U" (1966);

[6] U. Fasoini and E. Saetta-Menichella, Energia Nucleare 15 (1968) 54

[7] A. Meister, D. Seeliger and K. Seidel,
Wiss. Zeitschr. d. TU Dresden 24 (1975) H. 5;

[8] E. Holub and W. Gindro, Phys. Lett. 56B (1975) 143;

[9] E. Gadioli, E. Gadioli-Erba and P.G. Sona, Nucl. Phys. A217 (1973) 589;

C. Birattera, F. Gadioli, E. Gadioli-Erba, A.M. Grassi-Strini, A. Strini and G. Tagliaferri, Nucl. Phys. A201 (1973) 579;

P. Decowski, W. Grochulski and A. Marcinkowski, Int. Sem. on Interactions of Fast Neutrons with Nuclei, Gaussig (GDR) 1973, Proc. p. 71;

[10] C. Birattari, E. Gadioli, A.M. Grassi-Strini, G. Strini, G. Tagliaferri and L. Zetta, Nucl. Phys. A166 (1971) 605;

J. Bisplinghoff, J. Ernst, A. Hardt, R. Löhr, H. Machner, T. Mayer-Kuckuk and R. Schanz, Int. Conf. on Nuclear Physics, Munich (FRG) 1973, Proc. p. 516;

K. Miyano, H. Sekikawa, T. Kaneko and M. Nomoto, Nucl. Phys. A230 (1974) 98;

[11] G. Maples, G.W. Goth and J. Cerny, Nucl. Data A2 (1966) 429;

[12] U. Paccini and E. Saetta-Menichella, Energia Nucleare 15 (1968) 54; interpolations with: D. Seeliger and K. Seidel, Wiss. Zeitschrift TU Dresden 21 (1972) 714;

[13] A.V. Ignatjuk and Ju. V.Sokolov, Jadernaja Fisika 17 (1973) 723;

A.V. Ignatjuk and Ju. V.Sokolov, Int. Sem. on Interactions of Fast Neutrons with Nuclei, Gaussig (GDR) 1973), Proc. ZfK-271, p. 7;

[14] P.E. Nemirowsky and Yu. V. Adamchuk, Nucl. Phys. 39 (1962) 551;

[15] K. Seidel, D. Seeliger and A. Meister, 3rd Conf. on Neutron Physics, Kiev (USSR) 1975, Preprint TU Dresden 05-26-75.

ANALYSIS OF DIFFERENTIAL ELASTIC AND INELASTIC SCATTERING CROSS SECTIONS BY HAUSER-FESHBACH-THEORIE

A.H. Mohamed, T. Schweitzer, D. Seeliger, K. Seidel, S. Unholzer
Technische Universität Dresden, Sektion Physik,
DDR 8027 Dresden, Mommsenstraße 13, GDR

Abstract:

The differential elastic and inelastic scattering cross sections of 3.4 MeV neutrons for the elements Na, Mg, Al, Si, P, V, Mn, Fe, Co, Pb and Bi have been determined experimentelly. Obtained angular distributions are compared with optical model and Hauser-Feshbach theory calculations by the program ELISA.

1. Introduction

We have measured the angular distribution of the scattering of 3.4 MeV neutrons for 11 elements (Na, Mg, Al, Si, P, Mn, Fe, Co, V, Pb, Bi) for investigations of the reaction mechanism in the middle range of excitation energy, to proof the validity of the statistical theory in this energy region and not last to find a consistent and absolut description of the neutron scattering data over a wide range of nuclear masses. Systematical measurements are also important for the evaluation of more accurate neutron data.
The experimental distributions are compared with the results of optical model calculations and predictions of the statistical theory with inclusion of level width fluctuations for ^{24}Mg, ^{28}Si, ^{56}Fe, ^{209}Bi.

2. Experimental method and data preparation

The measurements were carried out at the 500-keV pulsed beam DD-neutron generator of the Technical University. Scattered neutrons were measured with the time-of-flight method in the energy range from 1 - 3.4 MeV between 15° and 150°. A more detailed discription of the experimental method is given elsewhere [1].
The main part of data handling and analysis was carried out with computer techniques at the BESM-6 computer.
Corrections for the measured cross sections were carried out with the computer code KOREKT.

ALGOL PROCEDURES:

KOREKT - main program
GEORK - corrections for geometrical effects, computation of integrated cross sections, χ^2-fitting of the angular distribution in a Legendre Polynom representation
AMEISE - corrections for flux attenuation and multiple scattering effects for integrated and differential cross sections
ZEICHN - graphical representation

For unfolding of the neutron time of flight spectra, computation of cross sections, estimation of the neutron energies we have written the program system

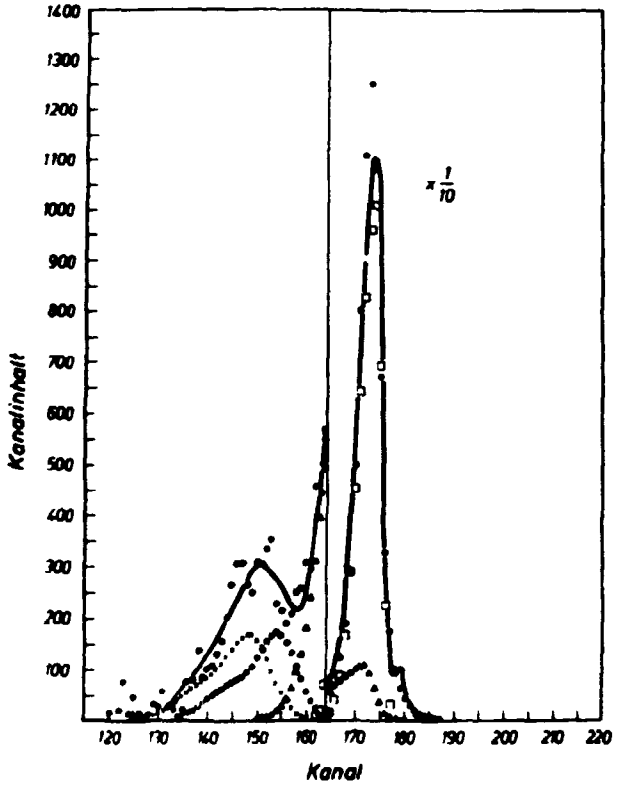

Fig. 1:

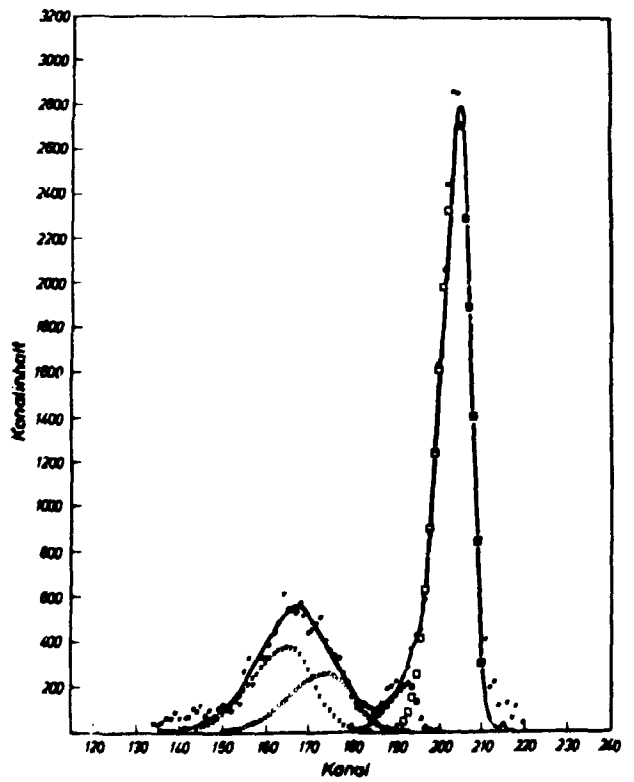

Fig. 2:

FIRM, which consists of a row of self contained ALGOL-PROCEDURES and FORTRAN-SUBROUTINES.

PROCEDURES:

FIRM - main program
FITGS - for χ^2-fitting of discrete time-of-flight spectra with analytical or experimental reference peaks
GAUSS - for computation of analytical and transformation (in position and amplitude) of experimental reference peaks
GRAPH - for graphical representation

SUBROUTINES:

SIGMA - for estimation of cross sections and neutron energies
FITFEL-INVERS- for computation of the experimental errors

The main problem in data preparation is to reduce strong overlapping neutron peaks. The overlap is naturally caused by the final energetical resolution of the experimental system. The problem is enlarged with strong distinctions in the amplitudes and also because of the dependence in the shape of the time-of-flight peaks from parameters of the pulsing system. It is here not possible to give any general resolution function, which can act steadily on the experimental distributions.
What we can do in this principal matter from an physical point of view?

1. All the parameters of overlapping peaks are independent from each other. We have in an analytical representation a lot of fitting parameters (number of overlapping peaks $\times^n$ in the case of nonsymmetrical Gauss curves). This gives mostly a bad adaption to experiments
2. Partition in analytical groups (the shape of the curves is set parameter). That gives a better representation of the experimental distribution in the case of comparable amplitudes (even if we cannot see any structure)
3. Partition in groups of experimental reference peaks, which contain the special structure of the equipment. The last gives most possibilities to get a best fit of the overlapping time-of-flight peaks even in cases of large distinctions in amplitudes. These facts are shown in fig. 1 and fig. 2. We have used analytical functions of the nonsymmetrical Gaussean type, which give a sufficient representation of the time-of-flight peaks.

EXPERIMENTAL ERRORS

Statistical errors of the peak arreas have been estimated to be less than 1 % for elastic scattering and better than 5 % for inelastic scattering. Systematical errors within the angular distributions are mostly affected by geometrical uncertainties in the distance between target and scattering sample and by uncertainties in the unfolding of time-of-flight peaks (between 1 and 30 %) which in some cases overlapp strongly.
Such errors are stated in figures 3-6.

3. Theoretical analysis

The experimental cross sections have been compared with theoretical predictions, which consist of calculations of the shape elastic scattering cross sections by the optical model and of the compound reaction components by Hauser-Feshbach theory with Moldauer fluctuation corrections. Both type of calculations were carried out by the computer program ELISA [2], which includes the following possibilities:

- calculations in the framework of a usual spherical optical potential;
- calculations of compound nuclear processes in the framework of Hauser-Feshbach statistical theory, eighter with or without Moldauer fluctuation corrections. In this calculations besides the discrete levels of final nuclei a continuous part of final states, with definite level density parameter a and spin cut-off factor σ, may be included.
- Calculations are possible for spins 0, 1/2 and 1 of incoming or outgoing particles.

In the present work optical potential parameters from Holmqvist [3] were used for all calculations, so that no fitting procedure was needed. In the statistical theory calculations the open proton and alpha channels have been taken into account.

4. Results and discussion

On figs. 1-4 comparison between experiment and theory is shown for some typical representatives of light, medium and heavy nuclei.

Altogether, the computed elastic differential cross sections are in good accordance with experimental results. In all cases besides the shape elastic reaction a considerable sompound elastic part of the cross section must be added. In the case of ^{28}Si the compound elastic part seems to be overestimated by the statistical theory (see fig. 4).

The calculated inelastic cross section is in good agreement with the experimental results for the first 2^+ -state of ^{24}Mg (see fig. 3). It seems, that no essential contributions of other reaction mechanisms in this case are evident.

For ^{28}Si (see fig. 4) there are striking deviations between calculations and experiment for both elastic and inelastic (2^+ level at 1.77 MeV) cross sections. If we assume, that the compound nucleus formation cross section is overestimated by an factor 2, than we get a satisfactory description of elastic scattering. But in this case the existing discrepancies for inelastic scattering are increased, leading to the assumption, that for the excitation of the 2^+ state an other (direct) reaction mechanism is responsible. A reason for this behaviour is probably due to the considerable deformation of the ^{28}Si ground state. Further investigations of this point are needed.

The differential elastic scattering cross section for ^{56}Fe (see. fig. 5) is in a good agreement with calculations, whereas the experimental inelastic cross section for the first 2^+ state at 0.84 MeV is considerably higher than the results of calculations by the statistical theory. We assume that this is due-to

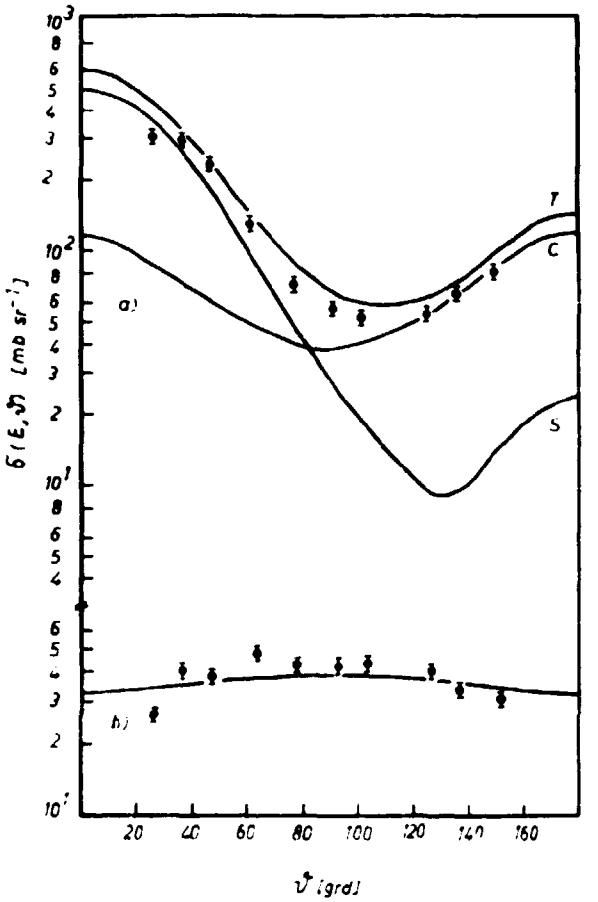

Fig. 3: Differential elastic and inelastic scattering cross sections in the center of mass system for ^{24}Mg at 3,4 MeV incident energy.
Theoretical curves (full lines) are calculated with the program ELISA 2 including optical model and statistical Hauser-Feshbach calculations with Holmqvist's optical model parameter set 3 .
a) elastic scattering; T - total elastic, S - shape elastic and C - compound elastic contributions,
b) inelastic scattering with excitation of the 1-st state.

direct excitation processes.

Also for the heavy nucleus ^{209}Bi (fig. 6) elastic scattering is well described by the program employed. In the case of inelastic scattering the situation is different for the two excited levels: For the first excited $7/2^-$ state at 0,91 MeV both shape and magnitude of statistical theory calculation are in satisfactory agreement with experiment. A small, probably direct, contribution is evident. The calculations, corresponding to the second state at 1,61 MeV are based on the spin-parity assigument $J^\pi = 13/2^+$ [4]. Theoretical predictions only in this one case are higher than experimental cross sections, and the shape of angular distributions is also different. Further calculations are needed, especially with other J^π -assignment.

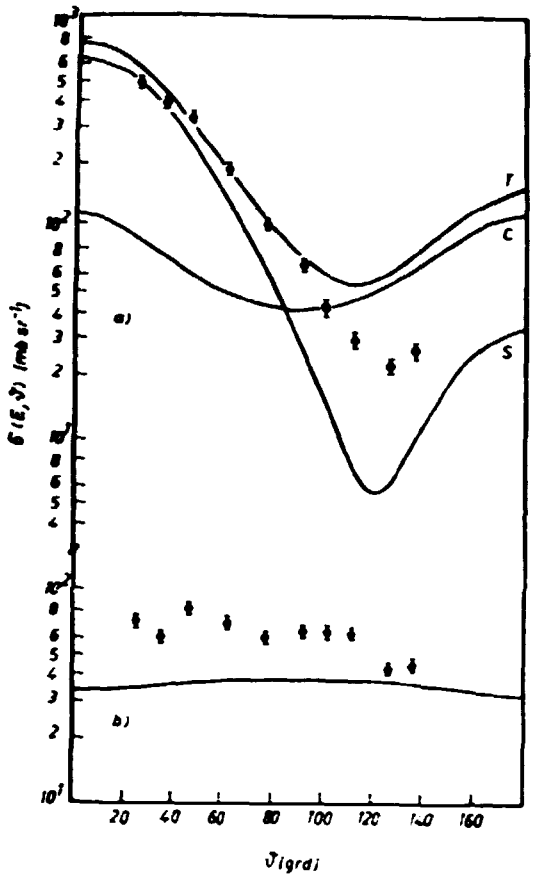

Fig. 4: The same as on Fig. 3, but for ^{28}Si

5. Summary

- It was shown by some examples, that the differential elastic scattering cross section at 3,4 MeV neutron energy may be well described by the computer program ELISA, including both shape elastic and compound elastic contributions. The Holmqvist's optical parameters have been found as a very useful parameter set for this purpose.
- The experimental differential inelastic scattering cross sections in general are not completely reproduced by the statistical Hauser-Feshbach theory including Moldauer fluctuation corrections. We assume, that additional direct contributions must be taken into account, even in this comparatively low energy region around 3 MeV. Further theoretical investigations are needed to confirm this assumption.

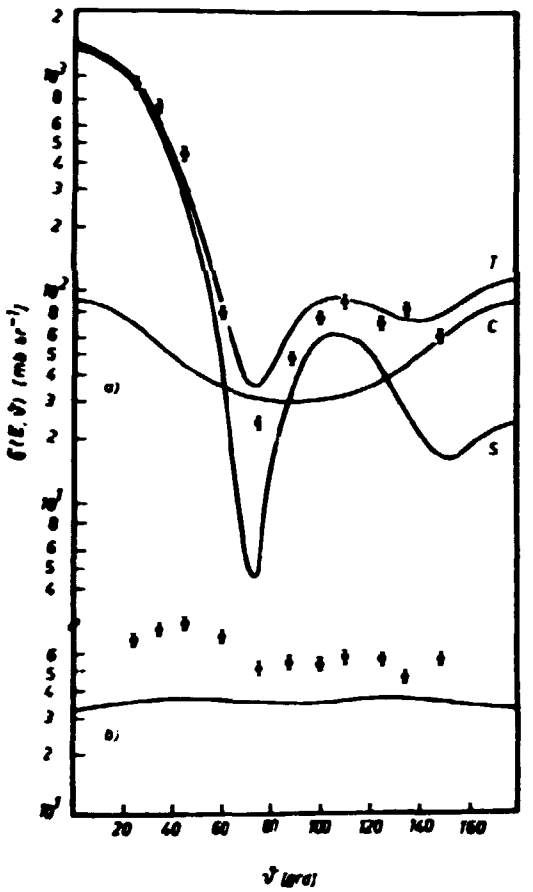

Fig. 5: The same as on Fig. 3 but for ^{56}Fe

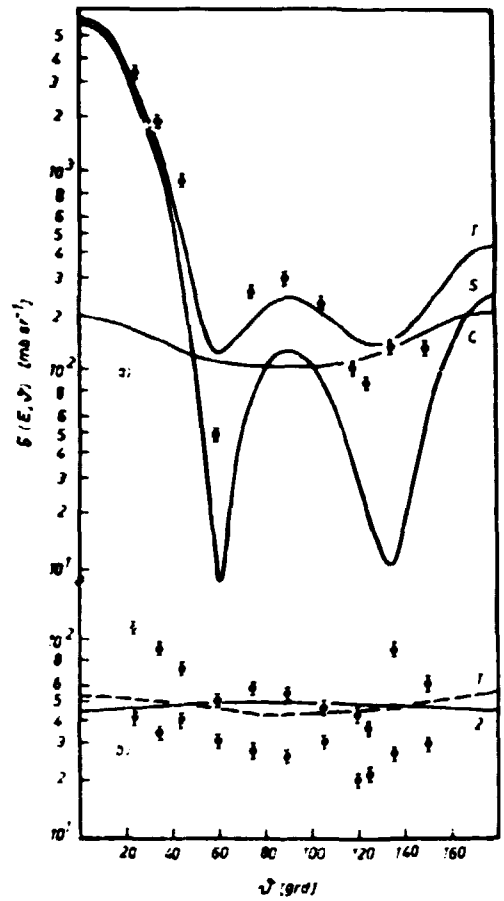

Fig. 6: The same as on Fig. 3, but for ^{209}Bi; in this case the first (open circles) and second (full points) excited states have been measured and calculated (broken line and full line, respectively).

References

[1] Schweitzer, T. et al., ZfK Report, ZfK-283 (1974) 7
Schweitzer, T. et al., Mat. IV. Symposium on Interactions of Fast Neutrons with Nuclei,
Gaussig, Nov. 1974 (to be publ. in Wiss. Zeitschr. TU Dresden, 1975)
Kaiser, U. et al., TU Dresdan Report, TU-Informationen 05-40-75, 1975

[2] Kiessig, G., Dissertation TU Dresden 1975

[3] Holmqvist, B. and Wiedling, T., Journal of Nuclear Energy vol 27 pp. 543 (1973)

[4] Tanaka, S. et al., Nucl. Phys. A179 513-523 (1972)

IMPROVED CORRECTIONS FOR THE IMPROVED ACTIVATION TECHNIQUE OF 14 MeV NEUTRON CAPTURE CROSS SECTION MEASUREMENTS

G. Pető, Institute of Experimental Physics, Kossuth University,
H - 4001 Debrecen POB. 105, Hungary

Abstract

A new way of corrections is described for the 14 MeV neutron capture cross section determination by activation technique. The method is tested experimentally by the $^{115}In/n,\gamma/^{116m}In$ reaction.

To explain the disagreement between the capture cross sections obtained by the spectrum method [1], [2] and by the activation technique [3] , [4] some [5-8] more accurate activation measurements have been performed. These work using proper and improper, overlapping or contradicting corrections were able to produce capture cross sections as low as the result of the spectrum method. Using, only the more realistic correcting method of the above papers: target backing thickness dependence, sample thickness dependence and assuming a constant background it was not possible [9] to get such low cross section for In and Au. These high cross sections may arise [10] from the emission the distance dependence of scattered neutron background. The aim of the present work is to investigate this effect.

According to the calculations of Bödy et al. [11] the target backing can produce a distant dependent scattered neutron background. In order to find this background experimentally we have constructed a sample holder for irratiations at different distances. The sample holder with the earlier [9] target head is shown in Fig. 1. The sample is fixed by air pressure difference to a tube con-

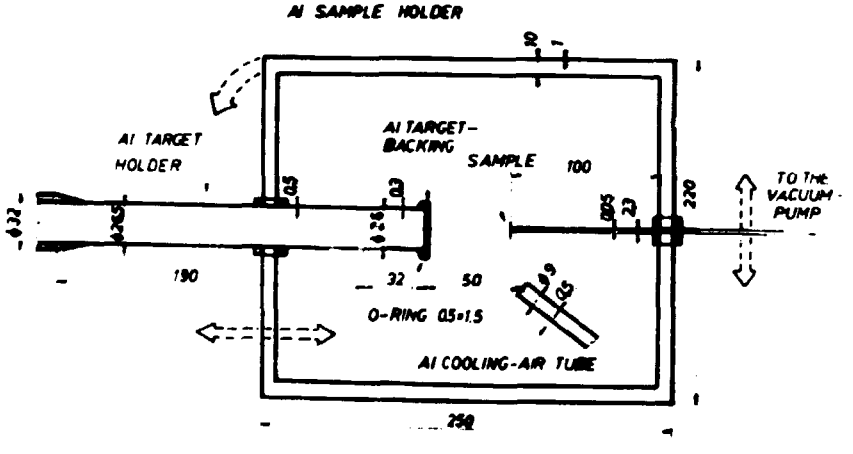

Fig. 1: The target-sample arrangement. The sample is fixed to the Al tube by the pressure difference produced by a vacuum-pump.

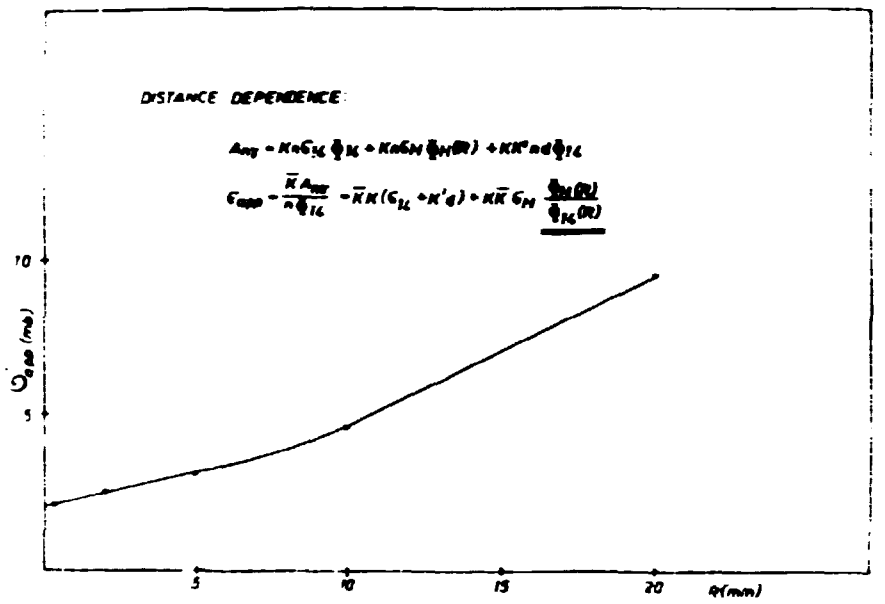

Fig. 2: The apparent activation cross section for the $^{115}In/n,\gamma\ /^{116m}In$ reaction in the function of distance from the target. The formula shows that the extrapolated value to the zero thickness still contains the contribution from the scattered neutron background.

nected to a vacuum-pump. The cross section measured with - and without the sample holder have not shown any effect from the holder. A tritium target on an Al backing [12] was used for neutron production. The other details of the experimental technique agree with the earlier work [9].

The Fig. 2 shows the obtained distance dependence. As we have remarqued before [11] we do not think to get any reasonable correction by extrapolation of this curve to the zero distance. It was even impossible to fit the calculated dependence [11] to the measured one because of their completly different shape. However this effect still might be important in case of a copper target backing.

To determine the origin of the obtained distance dependence the possible simplest model was assumed:

1. A scattered neutron background exists around the target producing activity in the sample according to the following formula:

$$K.\ n_2\ .\sigma_M\ .\ \bar{\Phi}_M\ /R?/$$

where K is a constant depending on the irradiation time and so on, n_2 the number of the target atoms, "?" indicates: it is not sure that the activity is proportional with n because of the self-shielding in the sample, $\bar{\Phi}_M$ /R?/ is the scattered neutron flux. It is also not sure that it depends on the distance /R/.

2. In the sample the 14 MeV neutron flux / $\bar{\Phi}_{14}$/ produce a scattered neutron flux proportional with the sample thickness d, so the contribution to the activity is $K.K'.n.d.\ \bar{\Phi}_{14}$.

3. Adding to these the activity produced by the 14 MeV neutron beam, the total activity of the sample /$A_{n\gamma}$/ can be given in the following form:

$$A_{n\gamma} = K_n \left(\sigma_{n\gamma} + K'd\right) \bar{\Phi}_{n\gamma} + K_n \sigma_N \bar{\Phi}_N(R) \qquad (1)$$

In the present case the 14 MeV neutron flux is measured by the ^{115}In/n,n'/ ^{115m}In inner monitor reaction so

$$\bar{\Phi}_{n\gamma} = \bar{K} \frac{A_{nn'}}{n}$$

where $A_{nn'}$ is the activity produced in the above reaction. So we have

$$A_{n\gamma} = K\bar{K}\left(\sigma_{n\gamma} + K'd\right) A_{nn'} + K_n \sigma_N \bar{\Phi}_N(R) \qquad (2)$$

Plotting the measured $A_{n\gamma}$ activities at a given thickness /d/ in the function of $A_{nn'}$ a straight lines has been obtained independently from the place of irradiation. Samples were irradiated in forward direction at a distance of 0.3, 2, 5, 10 and 20 mm, at 8 different positions on the target backing and backward directions, too. The result is shown in Fig. 3

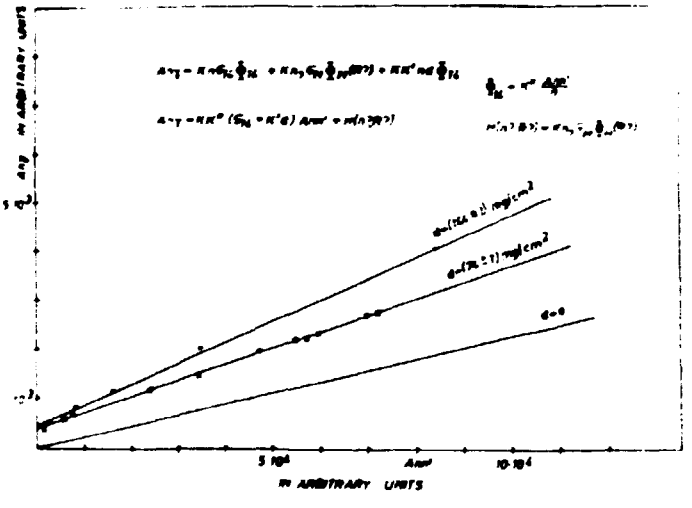

Fig. 3: The new correction method. The linear dependence of the $A_{n\gamma}$ activities on the $A_{nn'}$ activities obtained by irradiation of the samples at different directions proves that the scattered neutron background is constant and one can obtain it from the $A_{nn'} = 0$ / $\bar{\Phi}_{14} = 0$/ extrapolation. The thickness dependence can be determined from the slope difference of the lines.

The linear dependence, at least in first approximation, proves the validity of the assumption that the scattered neutron background does not depend on the distance from the target. It also shows the negligiblebility of the scattered neutrons from the Al target backing. The two different thicknesses render it possible to determine the d = 0 corrected line. In such a way, taking into account only the constant background and the thickness dependence one can get a cross

section of 1 mb. This value would be in good agreement with other results but it might also be an accidental agreement because of the different way of corrections.

Our further plan to investigate the details of the thickness dependence, the DD neutron background and so on, but now we think that the above simple correction method can advantageously applied for the determination of the fast neutron capture cross section.

References

[1] Rigoud, F., Irigaray, J.L., Petit, G.Y., Longo, G.L., Sapporetti, F., Nuclear Physics A173, 551 (1971)

[2] Cvelbar, F., Budnar, M., Hodgson, E., Potokar, M., Contributions to the conference on Nuclear Structure Study with Neutrons, D-21, p. 252, Budapest (1972)

[3] Csikai, J., Bacsó, J., Daróczy, A., Nuclear Physics 41, 316 (1963)

[4] Menlove, H.O., Coop, K.L., Grench, A.H., Sher, R., Phys. Rev. 16 3, 1299 (1967)

[5] Valkonen, M., Kantele, J., Nucl. Instr. Meth. 103, 549 (1972)

[6] Ponnert, K., Magnusson, G., Bergqvist, I., Physica Scripta 10, 35 (1974)

[7] Rigaud, F., Desthuillers, M.G., Petit, G.Y., Irigaray, J.L., Longo, G., Saporetti, F., Nucl. Sci. and Engineering 55, 17 (1974)

[8] Valetin, J., Kulisic, P., Cinfro, N., Lett. Nuovo Cim. 10. 1 (1974)

[9] Pető, G., Csikai, J., Long, V., Mukherjee, S., Bánhalmi, J., Miligy, Z., Acta Phys. Slovaca 25, 185 (1975)

[10] Magnusson, G., Bergqvist, I., private communication

[11] Bödy, Z.T., Pető, G., Csikai, J., Remarks on the 14 MeV neutron capture cross sections, Contribution delivered at the Symposium on fast neutron interactions and on the problems of high current neutron generators, 127-30 August Debrecen, Hungary, 1975 To be published in ATOMKI Közlemények

[12] The tritium target has been produced in Institute of Nuclear Research, Swierk near Otwock, Poland

NONSTATISTICAL EFFECTS IN THE $^{115}In(n,\gamma)^{116}In$ REACTION INDUCED BY NEUTRONS IN THE 0 - 2 MeV ENERGY RANGE

J. S. Brzosko, Institute of Experimental Physics, Warsaw University, 69 Hoza street, Warsaw

E. Zukowski, Department of Physics, Bialystok Division of the Warsaw University, 41 Lipowa street, Bialystok, Poland

S. Zaremba, Institute of Nuclear Research, Swierk, Otwock, Poland

Abstract

The problem is discussed of the intermediate structure existing within the framework of the compound nucleus including a resonance in the γ-ray strength function for $E_\gamma \cong 7$ MeV. The analysis is based on new experimental data as well as on our earlier data so far not explored which are subjected to a new treatment. The thermal and resonance data are take into account. The present authors propose explanation of the anomalous maximum in the (n,γ) excitation function for $E_n \cong 1$ MeV by the existence of the particle-core configurations.

1. Introduction

In the recent years the radiative capture in the ^{115}In nuclei was investigated by many authors. The analysis of nonstatistical effects based in the neutron resonance region [1] reveals no deviations from the statistical model. A similar conclusion results from Corvi and Stefanson's experimental data [2] concerning the population of the low-energy states in the (n,γ) process. On the other hand the same data reveal important correlations $(\Gamma^{\circ}_{n_j}, \Gamma_{\lambda\gamma_j})$ and $(\Gamma_{\lambda\gamma_j}, \Gamma_{\lambda\gamma_i})$ for γ - transitions which do not play a significant role in the (n,γ) reaction.

For fast neutrons, E_n = 0-2 MeV, fluctuation of the low-energy states population was observed [3].

Especially interesting is the abnormal maximum observed in the excitation function see (fig. 2). It appears near the neutron energy of E_n = 1 MeV and for this value it accounts for 30 % of the reaction cross section. When analysing the nature of the mentioned maximum of the cross section for low-energy state population against neutron energy account was taken of:

- part of the earlier experimental data not explored as yet by our group (population intensity of low-energy states measured in coincidency with gammas $E_\gamma \geq 3.5$ MeV [3]),
- emission intensity of the high energy γ -rays against neutron energy [4],
- intensity of the direct γ -transitions to low-energy states and its depopulation intensity for resonance [3] and thermal [5] neutrons.

2. Experimental

The measurements of γ -ray spectra were carried out in an enclosed neutron source geometry (fig. 1 [6]). It deserves emphasis that less than 15 % the to-

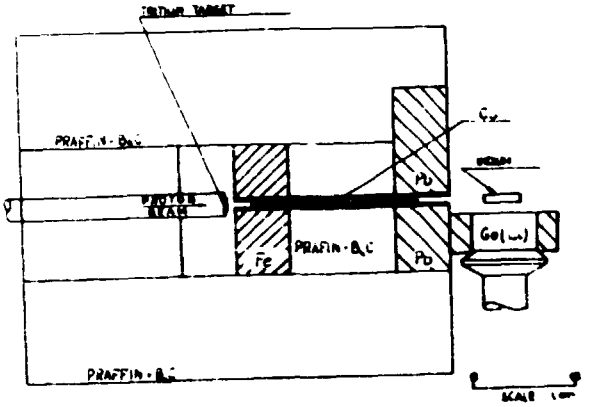

Fig. 1: The enclosed neutron source geometry for measurements of the γ -ray spectra from (n,γ) reactions.

tal number of the $^{115}In(n,\gamma)$ ^{116}In reactions were initiated by slowing-down neutrons, and this contribution was controlled in every run by comparing the induced activities of ^{116}In and ^{115}In [6].

The low-energy part of the γ -spectrum, determining the population of low-energy states, was measured using a 17 cm^3 Ge-Li detector.

The earlier data come from measurements in a coincidence regime. The γ -rays, $E_\gamma \geq 3.5$ MeV, were registered using the NaI(Tl) counter. These counters were operated in a fast-slow coincidence system. The γ -spectra were analysed by the SAMPO computer procedure, the statistical and peak extraction errors were of the order of 5-50 %. The coincidence experiment eliminates the statistical part of the γ -spectrum ($E_\gamma^{max} \cong 2$ MeV), and makes it possible to observe the nonstatistical effects.

3. Analysis of the data in terms of the compound nucleus model

Calculations of the total and partial excitation functions and γ -ray spectra were performed basing of the modified method proposed by Starfeld [7] and continuated by our group [8], [4], [9]. In this method the probability of γ -ray emission has the form:

$$P_\gamma \propto E_\gamma^2 \, \sigma_\gamma(E_\gamma) \, \rho(E^*, J) \qquad (1)$$

where: σ_γ is the absorption cross section and ρ is the density of the final nucleus levels. The σ_γ includes alongside the giant E1 resonance also the resonance-like amplification (ER) at energies 6-8 MeV. The following analytical form has been adopted:

$$\sigma_\gamma(E_\gamma) = 0.0133 \frac{NZ}{A} E_\gamma \left\{ \frac{\Gamma_{E1} \exp[-d|E_\gamma - E_{E1}|]}{E_{E1}[(E_\gamma - E_{E1})^2 + \frac{1}{4}\Gamma_{E1}]} (1-b) + \frac{\Gamma_{ER} \exp[-d|E_\gamma - E_{ER}|]}{E_{ER}[(E_{ER} - E_\gamma)^2 + \frac{1}{4}\Gamma_{ER}]} b \right\} \qquad (2)$$

where: E_{E1}, Γ_{E1}, E_{ER}, Γ_{ER} are the characteristics of the giant E1 and ER-resonances, b is a parameter defining the relative contribution of the ER-resonance with regard to the giant one, and d is the resonance shape-factor parameter. In the calculations we assumed $E_{ER} \cong 7$ MeV and $\Gamma_{ER} \cong 1$ MeV. The predictions were performed using the DRABINKA programme quoted in refs. [4] and [9].

The ER-resonance parameters were fitted to obtain agreement of the theoretical predictions with the experimental data. In the calculations the level density

parameters [10] and E1 giant resonance parameters were fixed. The transmission coefficients were taken from ref. [11]. It was found that the calculations are strongly dependent on the b-parameter. Resonable changes in the normally fixed parameters do not effect drastically the b-value when analysed against excitation energy, and do not destroy the concistency between experiment and theory. In result we obtain a fairly good agreement for the (n,γ) and $(n,n'\gamma)$ reactions, i.e. of excitation curves, high-energy parts of γ-spectrum and its neutron energy dependences (fig. 2), isomeric cross sections for the (n,γ) processes, and of the partial excitation curves for the $(n,n'\gamma)$ process. The b-parameter determined in this way was used to predict the population intensity of the states $E^* = 273$ keV ($E_\gamma = 273$ keV) and $E^* = 313$ keV ($E_\gamma = 186$ keV) (fig.3), as well as the spin distribution of the low-energy states obtained via a γ-ray cascade from the compound nucleus (fig. 4).

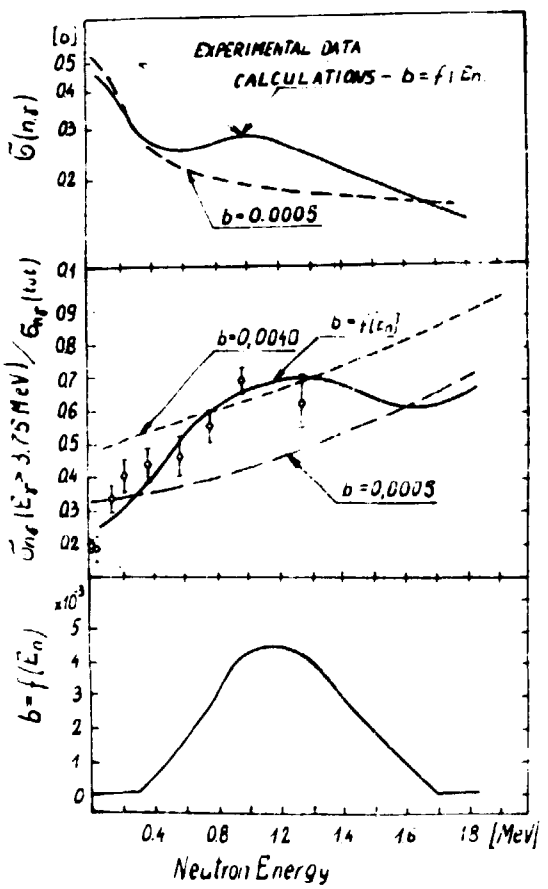

Fig. 2: Comparison of the experimental data and the predicted values based on formulas (1) and (2). The lower part of the figure presents the energy dependence of the b-parameter.

4. Population of the low-energy states of ^{115}In and its relation to the nonstatistical effects

Existence of the resonance-like structure in the γ-ray strength function is a well known experimental fact fairly well theoretically explained [12]. The ER-resonance may be treated as a general property of nuclei. It is the reason of the bump appearance in the γ-spectra emitted from highly excited nuclei. This fact cannot be treated as a nonstatistical effect and is in agreement with the statistical theory of the compound nucleus [13].

The dependence of the b-parameter on energy discussed in Section 3 violates evidently the Brink hypothesis [14] (it is assumed that the nuclear photoeffect is independent of the detailed structure of the initial state, so that if it were possible to perform the photoeffect on an excited state, σ_γ would have the same energy dependence as for the ground state) and cannot be explained by the ER-resonance, but may be ascribed to the existence of the intermediate configuration strongly coupled to the exit channel. In the case discussed above we exclude the possibility of the directlike process appearing because the general properties of the compound nucleus are realized (see Section 1), and this phenomenon accounts for nearly

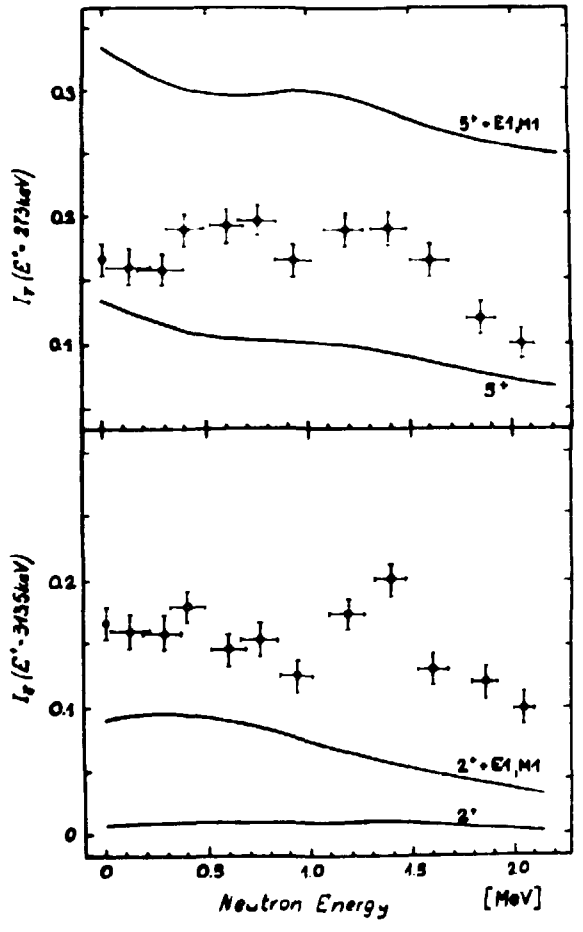

Fig. 3: Population intensity of the levels $E^* = 273$ keV ($E_\gamma = 273$ keV) and $E^* = 313$ keV ($E_\gamma = 186$ keV) measured when the coincidence regime is switched off. The solid lines refer to predictions obtained as a result of the partial calculations shown in fig. 2. The notation E1, M1 informs us that the population of the low-energy states whose spins differ by unity with respect to the measured ones, has been added.

30 % of total reaction cross section.

To investigate the nature of the intermediate configurations close to the excitation energy $E = 7{,}8$ MeV ($E_n \cong 1$ MeV) of the ^{116}In nucleus we have analysed the population intensity of the low-energy states. Fig.5 gives a comparison of the two measurements. In the ratio of the two strongest γ -transitions between low-energy states is measured for all γ -cascades of the compound nucleus, in the other the same quantity is measured in coincidency with high-energy, $E_\gamma \geq 3$ MeV, γ -transitions. The data differ both quantitatively and qualitatively. Fig. 5 additionaly shows the difference between the above mentioned data and those obtained for thermal and resonance neutrons [5], [2]. The structure observed in fig. 5 and 3 does not provide sufficient explanation of the b-parameter phenomenon.

Let us try to compare the coincidence experiment results for many lines with the experiment performed for thermal and resonance neutrons. The data are compared in fig. 6 and in Table I for neutron energies of $E_n = 230 \pm 150$, 1060 ± 100, 1950 ± 130 keV. These neutron energies lie below, in and above the phenomenon energy range. Fig. 6 and 4 show that the main portions of the population intensities and spin distributions have the same character for all energies under study. Since our first energy point of $E_n = 230$ and the thermal one are close to the same excitation energy of the compound nucleus, it is possible to compare the results for the coincidence regime switched on. As a result we find (see Table I) that the population intensity decreases to $\eta \cong 0{,}3$, which is in a good agreement with the role of the high-energy transition in the total (n,γ) cross section (for $E_n = 230$ keV we have $\eta \cong 0{,}4$).

Let us consider the low-energy states or the γ -transitions which fulfil simul-

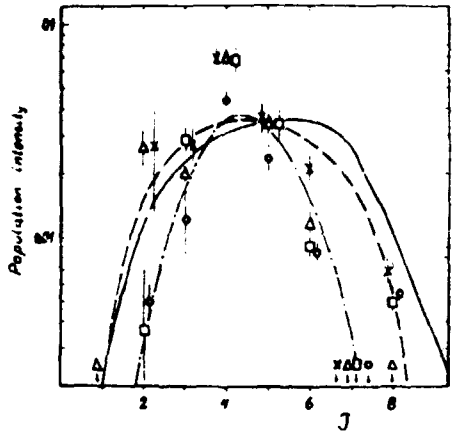

Fig. 4: The spin distribution of the low-energy state fed via a γ -ray cascade from the compound nucleus. X-thermal data [5], Δ - E_n=230 keV, $\square$ -E_n=1060 keV, O-E_n=1950 keV. The latter three data come from coincidence measurements. The solid curves present the predictions for the coincidence regime at $E^* = 0$-2 MeV ——— . ——— simple measurements at E_n = th, and — — at E_n = 2 MeV.

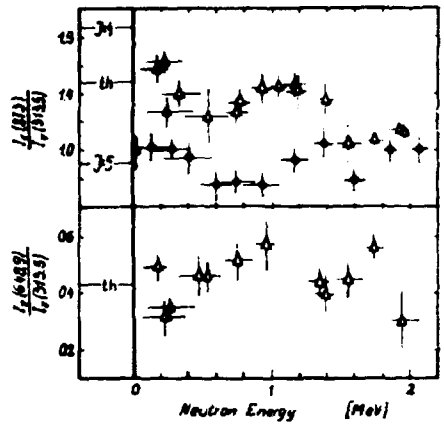

Fig. 5: Ratio of the two strongest γ -transitions between low-energy states. • and Δ measurements for γ -cascades observed at switch off and on regimes, respectively.

taneously the following conditions (see Table I):

i) belong to the group which does not realise spin distribution predicted by the compound nucleus model (i.e. to the group with spins I = 2 or 8, see fig. 4),

ii) have a high value of the spectroscopic factor Sdp,

iii) be directly populated from the compound nucleus decay,

iv) have a population intensity similar to the total (n, γ) cross section or to the b-parameter energy dependence,

v) not be strongly switched off by applying the coincidence technique

Figs. 7-13 present schematically the selected data and the realisation of the mentioned conditions.

As it is seen only the cases shown in figs. 7-10 are interesting. All the presented levels have an important single-particle component $\nu h_{9/2}$ or $\pi g_{9/2}^{-1}$ coupled to the rest of the nucleus. Taking into account that the population of the analysed states results from the high-energy γ -transitions, and the single-particle components are of high l-value type, we can assume that the compound nucleus decay proceeds via exit states [15]. Its decays may be described as single particle transitions in a field of the core, the rest of nucleus in the excited or ground state. Figs. 11-13 show the cases when the states under consideration are not fed in the first step of the γ -cascade.

Cumulating the single particle data (Table II), possible cores and characteristics of investigated levels [16] it is possible to suggest the configurations of compound nucleus responsible for the population of low-energy states.

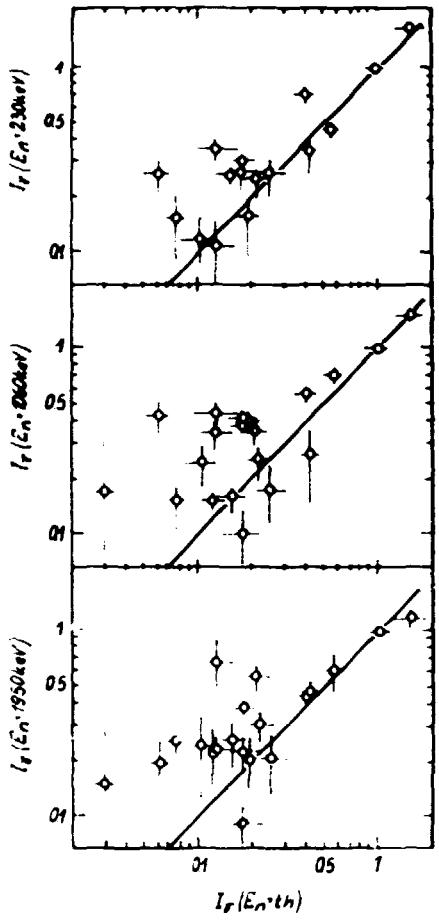

Fig. 6: The observed population intensities measured in the coincidence regime versus the population intensity of the same states for thermal neutrons when coincidences are switched off.

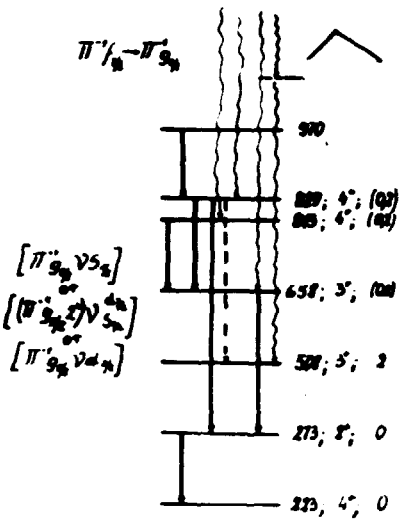

Fig. 7: Interpretation of the results for the case when the 3 i-v conditions are realised.

Figs. 7-13 show our interpretation of the data. We suggest the type of single particle component in the compound nucleus and in the low-energy states which plays a dominating role in the high-energy γ-transitions left-hand part of the diagrams. Since only some of the diagrams have configurations with maximum for E_n = 1 MeV, it is proposed to treat such configurations as the source of the nonstatistical effect and the b-parameter phenomenon. It is impossible to extend our knowledge on the characteristics of the proposed configurations, because the information about the wave function of the low-energy states is limited.

5. Summary

As a result of the discussion of the rich and variegated experimental material the gross structure of the intermediate configurations existing in ^{116}In at excitation energy $E^{*} \cong 7.8$ MeV has been detected and explained. Of course, the suggestion presented in Section 4 should be veryfied on other paths because in fast-neutron reactions many resonances and reaction channels with different spins and parities take part. The poor energy resolution of the neutron beam, because of the intensity problem, allowed to study the substructure with a width

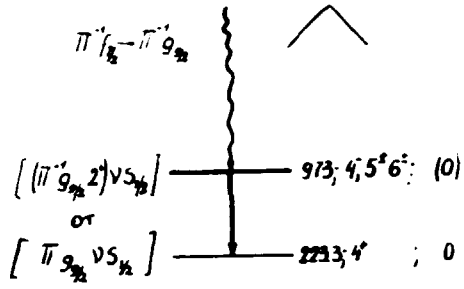

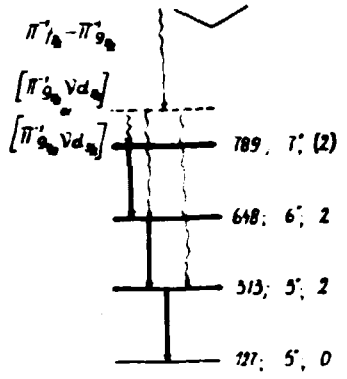

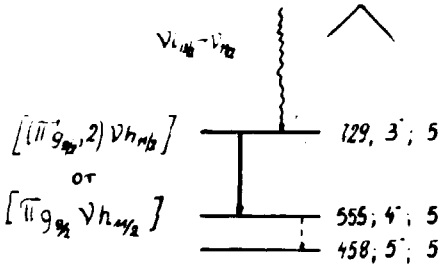

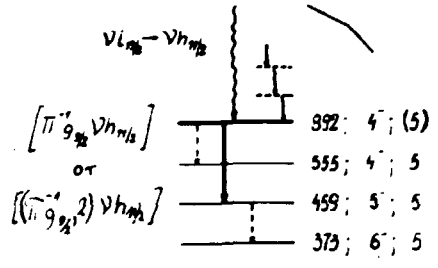

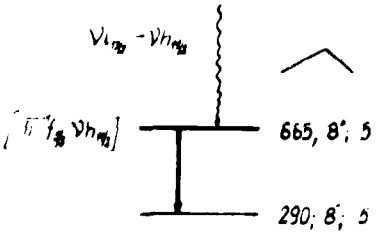

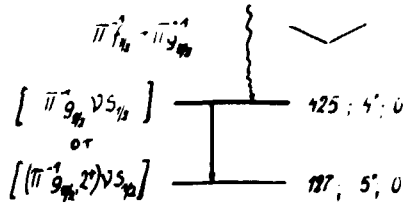

Fig. 8, Fig. 9, Fig. 10, Fig. 11, Fig. 12, Fig. 13 - see caption to Fig. 7

Table 1: Data concerning low-energy states (see Section IV - conditions i-v)

E^{π}	J^{π}	Sdp	S_γ	E_γ	E_n = th			E_n=230±150 keV			E_n=1060±100 keV			E_n=1950±130 keV			
					$\frac{I_\gamma(E_\gamma)}{I_\gamma(186)}$	± Δ [%]	I_γ	$\frac{I_\gamma(E_\gamma)}{I_\gamma(186)}$	± Δ [%]	I_γ	$\frac{I_\gamma(E_\gamma)}{I_\gamma(186)}$	± Δ [%]	I_γ	$\frac{I_\gamma(E_\gamma)}{I_\gamma(186)}$	± Δ [%]	I_γ	
1019	$4^-,5^-$		53.6	126.4	0.18	15	25.2	0.02	90	0.6	0.10	35	2.5	0.08	35	1.4	0.02
973	$4^-,5^-,6^-$		36.0	749.6	0.06	20	8.3	0.27	20	7.9	0.45	20	11.1	0.20	30	3.6	0.95
970.3	$4^\pm,5^\pm,6^+$			141.2	0.11	20	15.2	0.13	15	3.8	0.19	15	4.7	0.21	15	4.9	0.25
892.6	4^-		68.1	384.5	0.11	12	15.5	0.11	9	5.1	0.08	10	2.0	0.09	30	1.6	0.33
				433.7	0.26	20	35.4	0.26	20	7.8	0.18	30	4.5	0.21	35	3.8	0.22
829.1	4^+		11.6	171.1	0.13	18	18	0.11	40	3.3	0.35	20	8.8	0.24	5	4.4	0.18
				556.1	0.07	10	10	0.06	15	1.9	0.19	20	4.9	0.13	22	2.5	0.19
813.3	4^+		11.5	155.3	0.11	22	14.6	0.13	25	3.8	0.24	24	6.1	0.24	40	4.4	0.26
789.3	7^+		9.3	140.5	0.10	20	13.7	0.11	15	3.4	0.17	24	4.3	0.25	15	4.4	0.25
744.8	3^+		7.1	471.8	0.18	15	25.3	0.31	20	8.1	0.42	6	9.3	0.39	12	3.9	0.32
735,7	$4^+,5^+$		7.7	608.3	0.14	30	18.8	0.37	14	11.0	0.44	16	11.1	0.68	30	12.3	0.59
729	3^-	0.81	32.7	173.8	0.18	11	20	0.31	6	9.2	0.42	10	10.4	0.39	6	7.0	0.46
665.6	8^+	0.51		315	0.03	10	4				0.18	70	4.5	0.15	45	2.6	
				375,9	0.13	15	17.6				0.16	5	4.0	0.23	30	4.1	
658.1	3^+		7.7	385.1	0.46	12	14.3	0.29	9	9.2	0.63	10	15.9	0.52	30	9.4	0.64
648.9	6^+	0.66	10.6	335.4	0.43	10	59	0.33	20	10.0	0.26	50	6.6	0.48	8	8.7	0.17
556.8	2^-		70.0	556.8	0.15	10	20	0.19	15	5.5	0.05	20	1.2	0.12	22	2.1	0.27
508.2	3^+	0.81		284.9	0.20	8	27	0.14	30	4.3	0.40	8	10.0	0.20	30	3.7	0.16
425,9	4^+	0.26	6.1	202.6	0.08	6	10.6	0.14	35	4.3	0.14	21	3.5	0.25	5	4.5	0.41
				298.7	0.40	9	55	0.72	5	21.6	0.58	5	14.5	0.45	8	8.1	0.39
313,5	5^+	0.51	12.1	186.2	1.00	12	138	1.00	5	30	1.00	5	25	1.00	5	18.0	0.22
273	2^+		2.4	273	1.48	15	197	1.66	5	49.8	1.49	7	37.3	1.14	5	20.6	0.25

I_γ - relative intensity per capture x 10^3 ; $I_\gamma(186) = I_\gamma(E_\gamma = 186$ keV)

$S_\gamma = I / (D\, E^3_\gamma)$ $[10^{-9}$ MeV $^{-3}]$; $\eta = I_\gamma$ (coinc. on) / I_γ (coinc. off)

of the order of 10^2keV, only. This means that only simple configurations could be observed.

Table 2: Possible single particle transitions for excitation energy of particles clouse to 9 MeV

Single particle transitions	Γ^{γ}_{sp} (eV)
$\nu i_{13/2} \longrightarrow \nu h_{11/2}$	226
$\pi f_{7/2} \longrightarrow \pi d_{5/2}$	162
$\pi f_{7/2} \longrightarrow \pi g_{9/2}$	4
$\pi h_{11/2} \longrightarrow \pi g_{9/2}$	30
$\pi' f_{7/2} \longrightarrow \pi' g_{9/2}$	297

References

[1] Y. Baudinet-Robinet, C. Mahaux, Phys. Rev. C9 (1974) 723;
[2] F. Corvi, M. Stefanon, to be published in Nucl. Phys.;
[3] J.S. Brzosko, M. Herrmann, J. Piotrowski, G. Szeflinska, Z. Szefliński, Proc. Int. Conf. on Nucl. Phys., Munich 1973, Warsaw Univ. Report IFD/10/1973;
[4] J.S. Brzosko, E. Gierlik, A. Soltan, Z. Wilhelmi, Acta Phys. Pol. B2 (1971) 95;
[5] D. Rabenstein, Nucl. Phys. 197A (1972) 129;
[6] J.S. Brzosko, M. Herman, J. Piotrowski, G. Szeflińska, Z. Szefliński, Warsaw Univ. Report IFD/8/1973;
[7] N. Starfelt, Nucl. Phys. 53 (1964) 397;
[8] J.S. Brzosko, E. Gierlik, A. Soltan, Z. Wilhelmi, Can. J. Phys. 47 (1969) 2049;
[9] J.S. Brzosko INR-report 1271/I/PL/1971 - Poland;
[10] A. Gilbert, A.J.W. Cameron, Can. J. Phys. 43 (1965) 1447;
[11] E.M. Auerbach, P.G.J. Percy, ANL-report 745 (1962);
[12] G.A. Bartholomew, F.C. Khanna, Proc. of the Symposium on Neutron Capture γ-ray Spec. 1974, Petten, Holland;
[13] J.S. Brzosko, see lecture "Present Status of the Radiative Capture of Neutrons" on this Symposium;
[14] D.M. Brink, Doctorat Thesis, Oxford Univ., (1955);
[15] J.S. Brzosko, J. Piotrowski, A. Soltan, Z. Szeflinski, Nucl. Phys. A189 (1972)545;
[16] E.M. Baranger, Advances in Nuclear Physics 4 (1971) 261;

FURTHER MEASUREMENTS OF THE PROBABILITY OF α -CLUSTER PREFORMATION BY MEANS OF (p, α) REACTIONS IN HEAVY ELEMENTS

L. Milazzo-Colli, G.M. Braga-Marcazzan, M. Milazzo, R. Bonetti
Instituto di Fisica dell'Università, Milano

1. Introduction

It was shown in previous papers [1, 2, 3] that the dominating reaction mechanism in(p, α)reactions on a number of heavy nuclei at $\sim$ 20 MeV incident proton energy is the pre-compound emissions of the α -particle, which is assumed to be a preformed α -like cluster in the target nucleus. This mechanism is described in detail in the above-mentioned papers on the basis of the "exciton model".

In the formulation of the theory of α -emission by pre-compound mechanism a coefficient ψ is introduced that acts as a normalization coefficient, which can be interpreted as a preformation probability of the α -like-clusters in the target nucleus. The value of this coefficient is extracted by fitting the experimental results.

This paper reports new measurements on (p, α) reactions on the nuclei ^{139}La, ^{140}Ce, ^{150}Sm, ^{156}Gd, ^{171}Yb, ^{203,205}Tl, ^{206,207,208}Pb, ^{209}Bi and ^{232}Th done under experimental conditions similar to those reported in previous papers [1 , 2]. It is also reported the analysis of ^{197}Au(p, α) and ^{181}Ta(p, α) at incident proton energies varying between 20 and 42 MeV obtained in somewhat different experimental conditions by Iori et al. [4]. It is shown below that the precompound emission mechanism as outlined above is the dominant one with the exception of nuclei near the double shell closure Z = 82, N = 126. The α -cluster preformation coefficients are obtained from analysis of these measurements.

2. Experimental apparatus and experimental results

The measurements were taken using the proton beam of the University of Milano's A.V.F. Cyclotron. In our measurements the α -particles were detected at four angles, 30°, 60°, 90° and 120° with an angular aperture of $\sim$ 5°; solid state surface barrier detectors and standard electronics were used; the detector thickness was 400 μ for the measurements taken at incident proton energies of 20 and 22.8 MeV and 700 μ at 25 and 30 MeV.

Actually, the thickness of the detectors limits maximum energy loss to 7.2 MeV for protons and to 9.5 MeV for deuterons in the measurements at 20 MeV. On the otherhand, the positive Q-value of (p, α) reactions on heavy nuclei and the presence of the Coulomb barrier produce high energy α -particle spectra which cannot contain contributions from other reactions.

At forward angles, however, two proton peaks are present in the spectra. They are due to protons elastically scattered from the target in the detector and scattered again by the silicon nuclei of the detector at 90° to the detector axis so that the protons are completely stopped inside the detector layer. The two peaks correspond to the elastic scattering and to the inelastic scattering at the first excited silicon nucleus level. Overall energy resolution was~150keV.

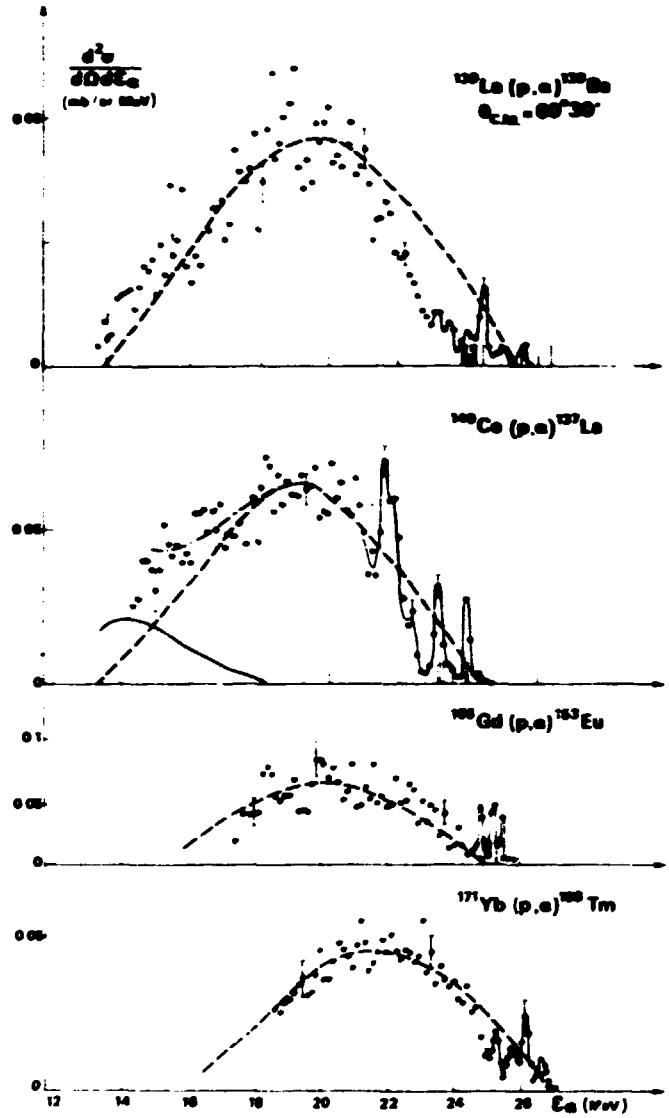

Fig. 1: α-particle spectra from ^{139}La, ^{140}Ce, ^{156}Gd and ^{171}Yb at Ep = 20 MeV, compared with the prediction of α-preformed pre-compound emissione (dashed line) and evaporation (continuous line). Vertical lines indicate the known first excited levels of residual nuclei.

The α-spectra obtained at an angle of 60° are shown in figs. 1, 2, and 3. Figs. 4 and 5 show examples of the spectra at four angles for ^{150}Sm and ^{208}Pb The shape of angular distribution for the other nuclei is very similar.

The energy spectra of emitted α-particles in the nuclei from La to Yb show the shape typical of pre-compound emission (the theoretical shape is also shown in the figure). ^{150}Sm and ^{140}Ce show some low-energy contribution from the evapo-

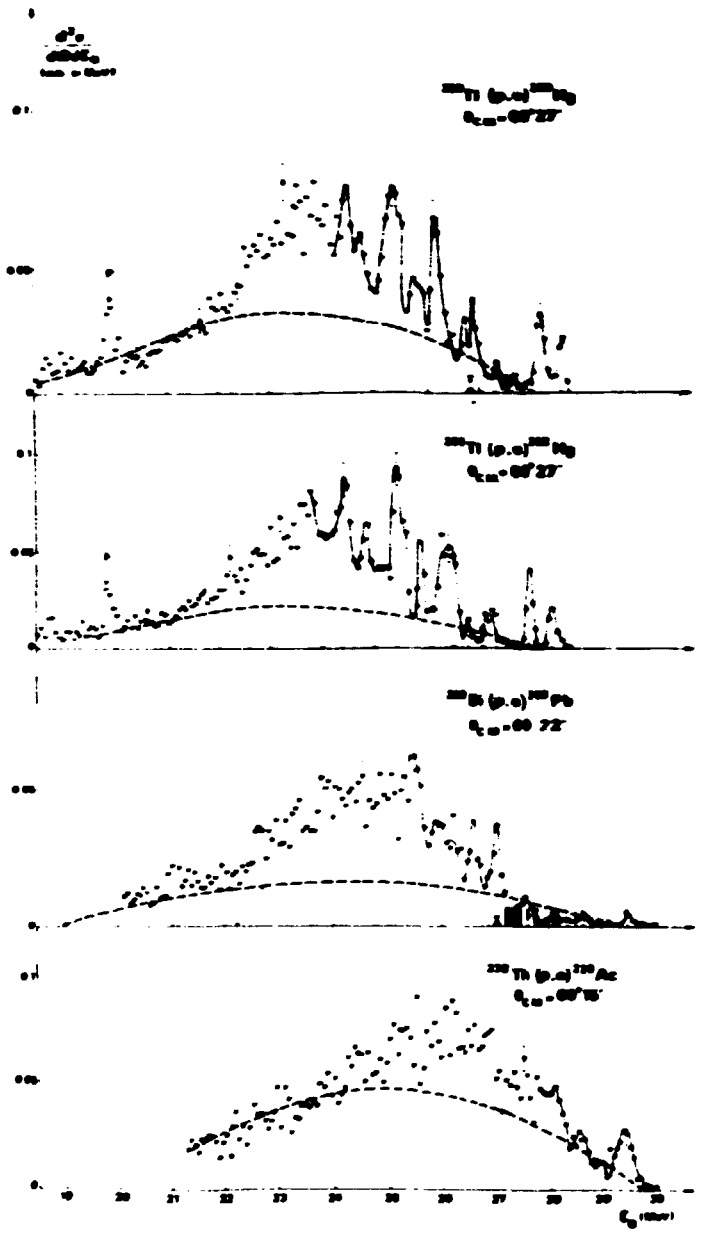

Fig. 2: α-particle spetra from ^{203}Tl, ^{205}Tl, ^{209}Bi and ^{232}Th in the same conditions as fig. 1. In the low part of the spectra peaks due to scattered protons are shown (P).

ration mechanism. At the high-energy end of the spectra a few peaks are often found, which reveal intense transitions to some levels of the final nucleus evidently due to a different effect. In the heavier nuclei (Tl, Pb), the contribution to the spectrum due to precompound emission becomes less and less important, and an α-emission producing a spectrum with higher average energy and well defined structures takes place. This effect, practically the only one present in ^{208}Pb, is similar to what would be expected from "direct interaction". It is

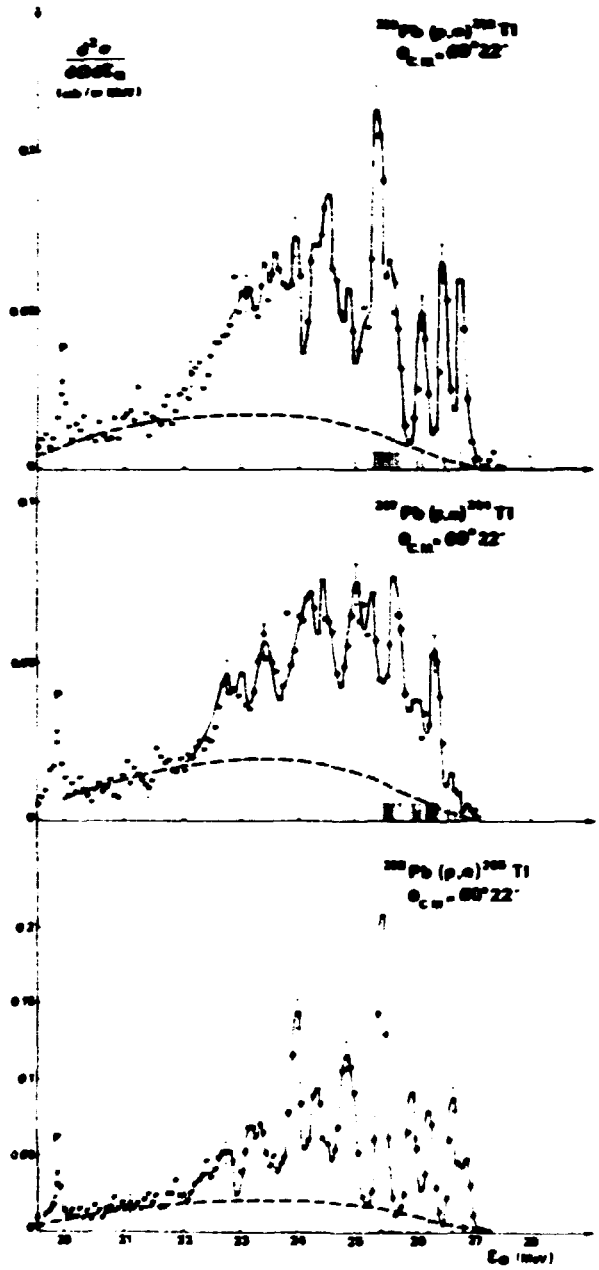

Fig. 3: α-particle spectra from ^{206}Pb, ^{207}Pb and ^{208}Pb in the same conditions as fig. 1.

probably the same as t.e one giving rise to the high energy peaks in Samarium and Cerium, which become the main effect in the lead region. Table 1 shows the integrated cross-section values for both the effects contributing to the (p,α) reactions. Calculation of the direct effect part is only approximate, because the experimental angular distribution is not detailed enough for a strongly angular dependent effect like this one.

Fig. 6 shows the detailed angular distribution of two peaks which has the usual

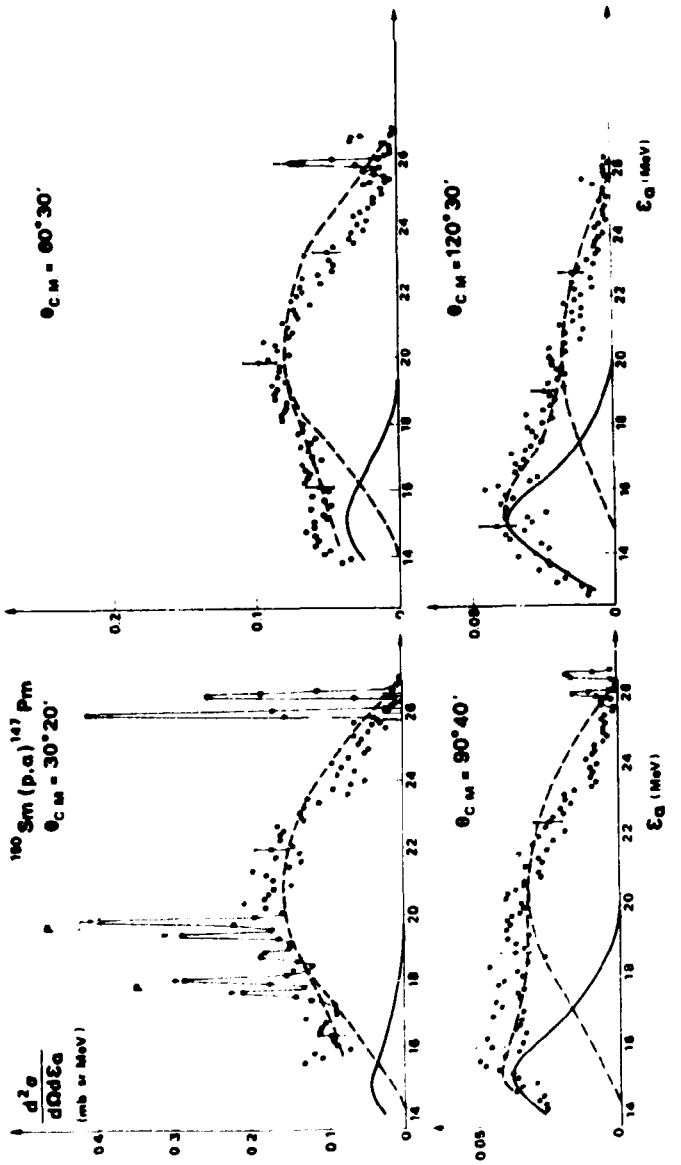

Fig. 4: α-particle spectrum from ^{150}Sm at four angles and Ep = 20 MeV compared with the calculation for evaporation (full line) and α-pre-formed pre-compound emission (dashed line).

direct pattern.

Another interesting fact to be observed in connection with the direct part of the spectrum is that the number of peaks does not increase with proton energy (fig. 7) this shows that only a limited number of low-lying final states contributes to the direct effect. In other words, the end of the direct part at the low energy side is not due to the Coulomb barrier.

Studies of the (p,α) reaction on ^{208}Pb, corresponding to the first excited levels of the residual nucleus ^{205}Tl, have been done by Hopkins et al. [5] at 15 MeV and by C. Glashausser et al. [6] at 35 MeV. The highly selective reac-

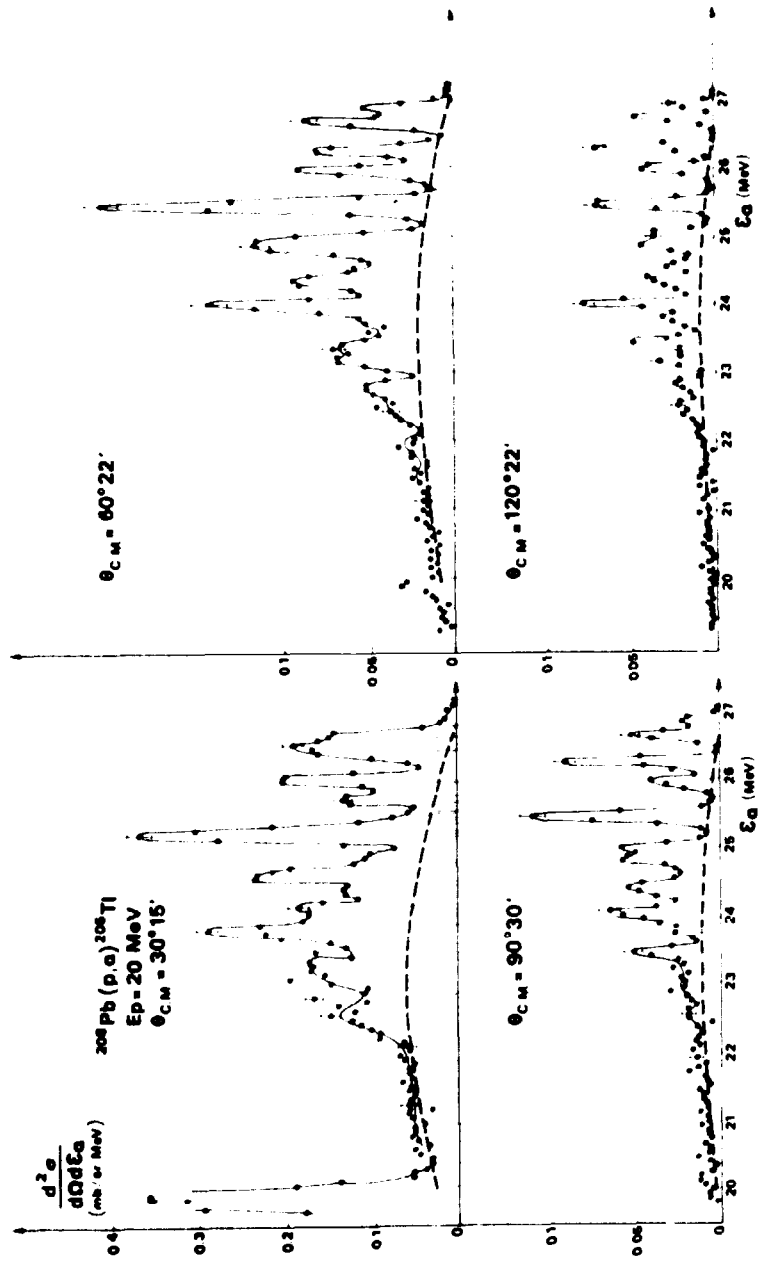

Fig. 5: α-particle spectrum from ^{208}Pb at four angles and Ep = 20 MeV. Dashed line shows the maximum allowed pre-compound emission.

tion mechanism responsible for these transitions was found to be a triton pick-up, dominated by the proton-hole components in the shell-model states of the residual nucleus.

As our measurements show, only a small number of these states contribute to the direct reaction; proton-hole levels with an excitation energy of more than $\sim$ 4 MeV are not involved.

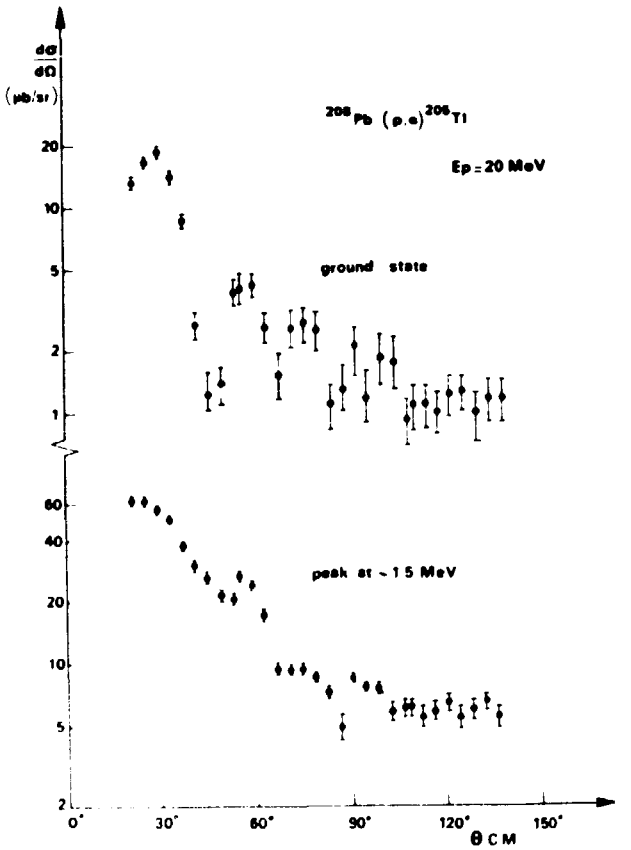

Fig. 6: Angular distributions of the peaks corresponding to transitions to ground state and to unresolved levels at 1.5 MeV excitation energy in ^{205}Tl.

3. Analysis of the results

The precompound mechanism was studied recently by Feshbach, who developed an exact quantum mechanical calculation for this process [7, 8]. The result was a formula for emitted particle energy distribution which is just the same as the one obtained in the perturbation theory [9, 10, 11] which is widely used in the interpretation of experiments.

As already pointed out, an important approximation in the description of precompound emission is the use of the equidistant spacing model in the calculation of level density. It is well known that this model provides a good description of the level density of nuclei with proton and neutron numbers far from magic numbers [12].

The level density parameter "a" in these cases has a well defined meaning and its value, at an excitation energy of $\sim$ 8 MeV, is known with an accuracy of $\pm$ 5 %. Recently, the experimental values of "a" were justified by theoretical calculations done by Huizenga et al. [13] based on the Nilsson model, in which pairing effects were included.

For nuclei near closed shells, matters are complicated by the fact that nuclei level densities cannot be represented by a formula with a constant "a".

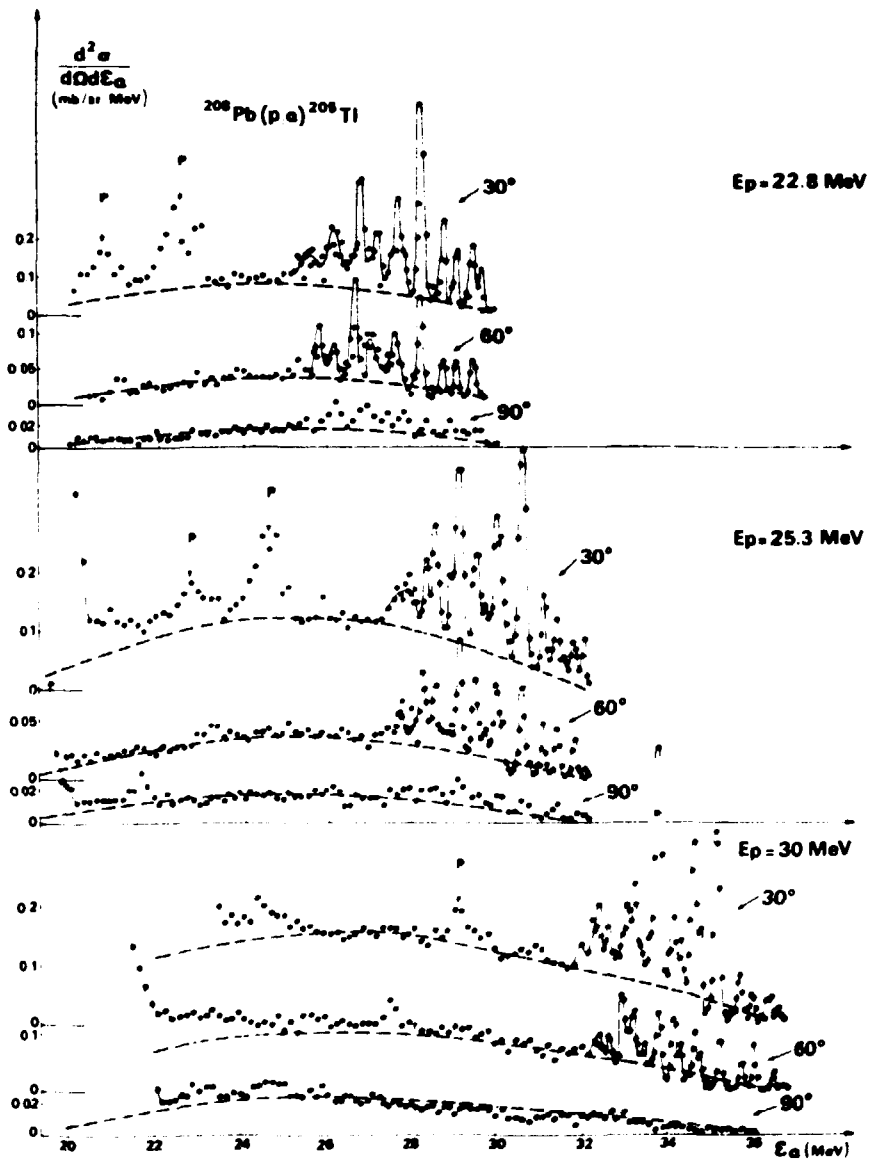

Fig. 7: α-particle spectra from ^{208}Pb at three angles (ϑ = 30°, 60°, 90°) and at different incident proton energies. Dashed lines represent the α-preformed pre-compound emission.

This point was also studied recently by Williams et al. [14]. It was found that the level density, calculated in accordance with the Nilsson model, corresponds to a low value of "a" for the first few MeV of excitation energy and that it gradually increases until it reaches a value such as would be expected without shell effect, after which it remains constant. A similar situation exists for the "few-exciton states" level density.

Albrecht and Blann [15] have in fact made preliminary calculations of the level density function of few-exciton states for a set of nuclei around the closed shells at Z = 50 and Z = 82 on the basis of the Nilsson single-particle levels. Their results seem to show that the average value of the few-exciton density states is fairly well approximated by the equidistant spacing model (Ericson's formula), whereas at the closed shells the level density curve calculated on the Nilsson model may differ a great deal from Ericson's calculation.

The few-exciton level densities are very important in our calculations aimed at determining the theoretical absolute value of the cross-section needed ir order to extract the parameter φ (α-cluster preformation factor). We therefore obtained the few exciton level densities from the analysis of nuclear reactions going through precompound mechanism in the nuclei with nearly closed shells that we had studied. A good measurement of neutron emission under proton bombardment at $\sim$ 18 MeV on ^{208}Pb was done by Verbinsky and Burrus [16] . As they show, the high-energy part of the neutron spectrum can be fitted by a precompound emission spectrum, starting with an n = 3 exciton number. The absolute value fitting of this neutron spectrum can be obtained by the pre-compound theory developed in our previous work [3], where the value of the matrix element representing the two-body interaction was the one determined in the study of (n,p), [17] (n,n') [3] and (p,n) [18] reactions. The level density parameter "a_c" of the composite nucleus-which is formed at 25 MeV excitation energy - was kept as a free parameter. For the "a_r" of the residual nucleus, which is left at rather low energy (less than 10 MeV), we took the value found in slow neutron experiments.

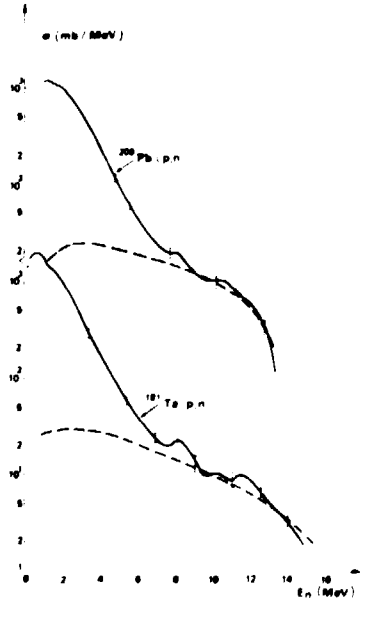

Fig. 8: The neutron spectra from ^{208}Pb(p,n) and Ta(p,n) (taken from reference [23]) at Ep=17,6MeV and Ep=18 MeV respectively, together with the calculated pre-compound emission (dashed-line). The low energy part of the spectrum is due to evaporation.

Fig. 8 shows how the (p,n) reaction on ^{208}Pb is fitted by pre-compound calculations, where the "a_c" value is 12.0MeV^{-1}. This value is about 50 % higher than the "low energy value" which is $\sim$8. A similar variation of the parameter "a" with the excitation energy was obtained by Williams in the above-mentioned paper on ^{208}Pb level density function.

As a test of the validity of our calculations, we applied the same porcedure to the Ta (p,n) reaction studied experimentally by Verbinsky and Burrus. In fig. 8 we show the fitting obtained for the absolute values. In this nucleus, which is far from the closed shell, the level density parameter is constants with the energy. There are therefore no free parameters in the fitting. The result is very good.

From these results, we deduced that the "a_c" value for the closed shell minimum

must be increased slightly to describe level densities at an excitation energy of 20-30 MeV, but the closed shell effect is still far from being cancelled out.

The three-exciton level density corresponding to that "a_c" value was used to calculate the (p,α) cross-section, where the composite nucleus excitation energy ranges from 25 to 35 MeV. For nuclei other than ^{208}Pb near the closed shell we took the "a_c" values from the interpolated curve shown in fig. 9.

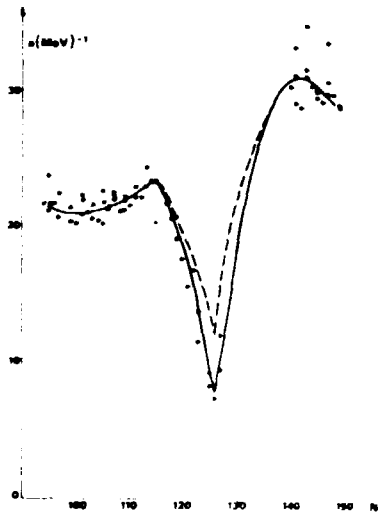

Fig. 9: Behaviour of the parameter "a_c" as a function of the neutron number N. Black points are taken from slow neutron data analysis 15 ; continuous line gives the average trend, the dashed line gives the value used in these calculations for the composite system excited at 25-35 MeV.

Table 1 lists the φ values which were calculated for all the nuclei considered. Values for the quantities of interest to the calculation are also given.

The separation of the direct part from the precompound one is made on the basis of the spectrum shape. The contents of the peaks is attributed to direct mechanism and the continuum part, extrapolated in the peak region attributed to precompound emission.

The separation is thought to be too uncertain in the case of Pb ^{207,208} at 20 and 22.8 MeV and it is not considered. For these nuclei the φ value is deduced from the higher energy measurements, where the precompound contribution is important.

For the other nuclei near doubly closed shell, ($Tl^{203,205}$, Pb^{206} and Bi^{210}) the precompound part calculated in this way has the meaning of maximum allowed quantity.

On order to study more extensively the behaviour of the α-prequilibrium emission with the energy variation of the incident proton, we have analyzed the reaction ^{197}Au (p,α) and ^{181}Ta(p,α) measured at incident proton energy between 20 and 42 MeV for the former case and between 20 and 30 for the latter [4].

These measurements have been taken with an energy resolution such that peaks eventually present and due to direct effect should be smeared out. An example of this can be seen comparing the measurement of Au (p,α) at 18 MeV by Henning [19] and the present one at 20 MeV. The first shows strong peaks and the second shows only a smooth shape. This fact does not allow us to distinguish between contribution to the spectrum due to direct effect in the low energy measurements. But, considering Henning's result we can attribute at least half of the spectrum to direct effect. Increasing the energy, the direct effect contribution remain confined to the highest energy part of the spectrum, as shows clearly in lead, and it is less and less important.

Taking these facts into account Au and Ta α spectra can be fitted very well using a φ -value constant at all the energies, as figure 10 and 11 shows. This

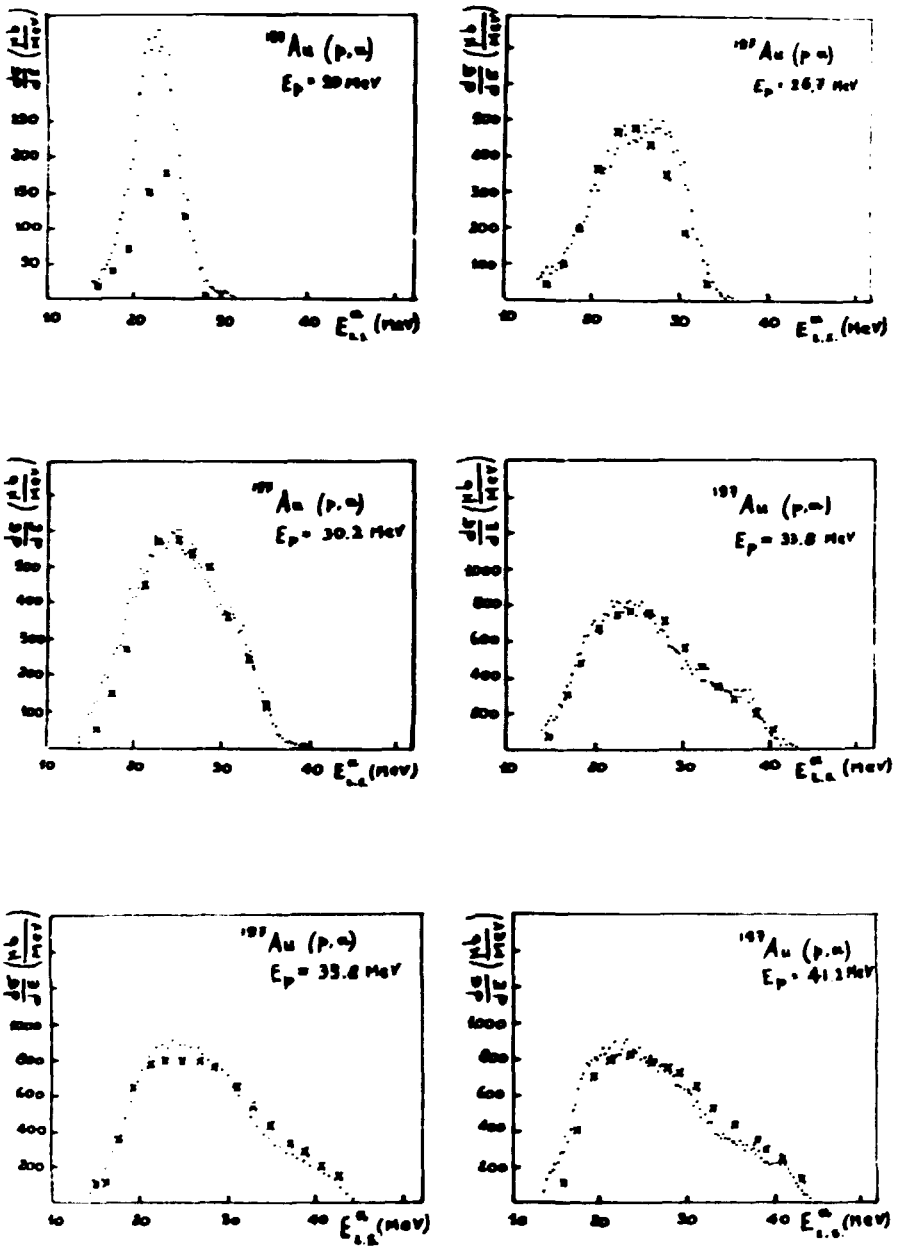

Fig. 17: α-spectra from $^{197}Au(p,\alpha)$ taken at different energies, compared with preequilibrium emission, calculated with $\varphi = 0.09$

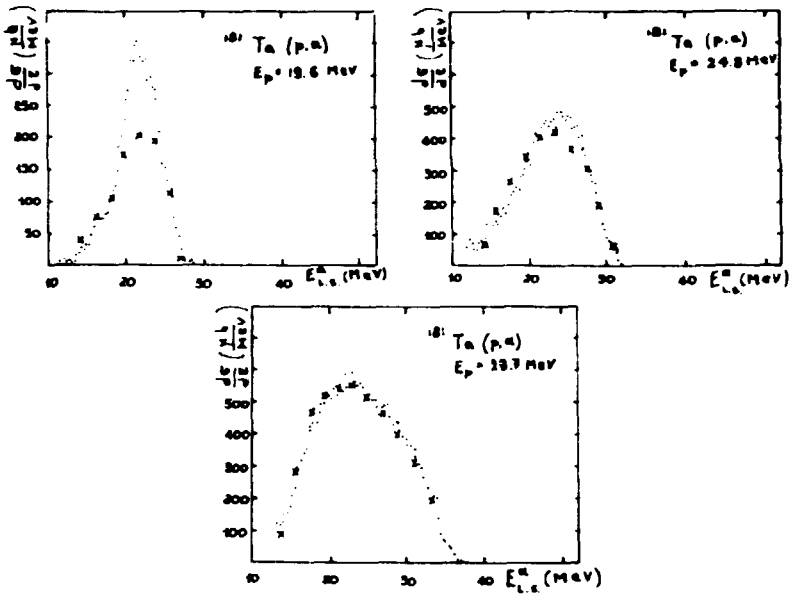

Fig. 11: Same as fig. 10 for ^{181}Ta (p,α), γ = 0.07

result is in agreement with the physical meaning of this quantity, which represents the probability for the incoming proton of exciting and α-cluster in the target nucleus, therefore a quantity related to the internal structure of the target nucleus.

An interesting aspect of this calculation is that the contribution of the terms with $n > n_0$ becomes more and more important as the energy increases, therefore determining the spectrum shape.

References

[1] G.M. Braga-Marcazzan, L. Milazzo-Colli, M. Milazzo, C. Signorini, Nuovo Cimento Lett. 6 (1973) 357;
[2] L. Milazzo-Colli, G.M. Braga-Marcazzan, M. Milazzo, C. Signorini, Nucl. Phys. A218 (1974) 274;
[3] L. Milazzo-Colli, G.M. Braga-Marcazzan, Rivista del Nuovo Dimento 3 (1973) 1535;
[4] I. Iori et al., Report INFN/BE-73/5 (1973);
[5] F.F. Hopkins, W.J. Courtney, W.R. Coker, C.F. Moore and T. Richard, Z. Phys. 243 (1971) 446;
[6] C. Glashausser, D.L. Hendrie and E.A. McClatchie, Nucl.Phys.A222 (1974)65
[7] H. Feshbach, Proc. Int. Conf. on Nucl. Phys. vol. 2, 631 Munich (1973);
[8] H. Feshbach, Rev. Mod. Phys. 46 (1974) 1;
[9] J.J. Griffin, Phys. Rev. Lett. 17 (1966) 478;
[10] F.C. Williams, Phys. Lett. 31B (1970) 184;

[11] M. Blann, Phys. Rev. Lett 21 (1968) 357, 27 (1971) 337, 28 (1972) 757;
[12] U. Paccini, S. Saetta-Menichella, Energia Nucleare 15 (1969) 54;
[13] J.R. Huizenga, A.N. Behkami, J.S. Sventek, R.W. Atcher, LBL-2314 (1974);
[14] F.C. Williams, J.C. Chan and J.R. Huizenga, Nucl. Phys. A187 (1972) 225;
[15] K. Albrecht and M. Blann, Phys. Rev. C8 (1973) 1481;
[16] V.V. Verbinski and W.R. Burrus, Phys. Rev. 177 (1969) 1671;
[17] G.M. Braga-Marcazzan, E. Gadioli-Erba, L. Milazzo-Colli and P.G. Sona, Phys. Rev. C6 (1972) 1398;
[18] C. Birattari, E. Gadioli, E. Gadioli-Erba, A.M. Grassi-Strini, G. Strini and G. Tagliaferri, Nucl. Phys. A201 (1973) 579;
[19] W. Henning et al. Jahresbericht 1972 des Beschleunigerlaboratoriums der Universität und der Technischen Universität München, and private communication.

(p,n) REACTIONS IN MIDDLE HEAVY NUCLEI

P. Eckstein, H. Helfer, D. Kätzmer, J. Kayser, W. Pilz, J. Rumpf, D. Schmidt, D. Seeliger, T. Streil
Technische Universität Dresden, Sektion Physik
DDR 8027 Dresden, Mommsenstraße 13, GDR

Investigations of (p,n) reactions are able to give contributions to information about the reaction mechanism. At the 10 MeV tandem accelerator such experiments using time-of-flight technique are performed.

1. Experimental procedures

The tandem accelerator in the Central Institute for Nuclear Research Rossendorf is capable of a maximum proton energy of 10 MeV. The maximum proton current is about 3 μA. The pulsing system consists of a chopper 1 and buncher acceleration befor and a chopper 2 after acceleration. Under best conditions, the following parameters are achieved (ref.[1]):

pulse width (with spectrometer) $t_{1/2}$ = (2,0 ± 0,5) ns
pulse distance T = 200 ns (or 1000 ns)
energy range E_p = 3.5 ... 10.0 MeV
averaged proton current I = 300 nA.

The detector consists of a 5" ϕ x 1,5" NE-213 scintillator, directly coupled with a photo multiplier TEU-63. The space charge method for neutron gamma discrimination is used, and in this way a lowest neutron threshold of 0,8 MeV is possible. The flight path in connection with the detector shielding can be chosen between 2,5 and 8 meters (ref.[2]).

Targets are in vacuum evaporated thin films - self-supporting or with backing - with thickness of 0,05 to any mg/cm^2, depending on the actual material.
A specific mode of the computer program NADJA III (ref.[3]) calculates from continuous spectra the cross sections $d^2\sigma/d\Omega dE$ with all corrections. If the neu-

tron groups in the spectra are resolved, a computer program (ref.[4]) calculates the partial cross sections, using a Gaussian curve with exponential asymmetry term.

2. Results from $^{55}Mn(p,n)$ and $^{59}Co(p,n)$ reactions

For both the nuclei mentioned above angular distributions at E_p = 4.12 and 5.00 MeV are measured, additional the excitation function in steps of 0.5 MeV from 3.5 up to 8.5 MeV.
$\sigma_{n_i}(\Theta, E_{p_o})$ and $\sigma_{n_i}(E_p, \Theta_o)$ are extracted for the neutron groups n_0 - n_4, respectively.

The excitation functions both of nuclei don't show correlated fluctuations between the neutron groups. The angular distributions are about symmetrical to 90 degrees and in any cases isotropic. Therefore, a comparison with the prediction of the partial statistical theory seems to be possible. The computer program system ELISA (ref.[5]) allows to calculate absolute partial cross sections for particles with spin 0, 1/2 or 1 and under consideration of 40 output channels. It bases on the theory of MOLDAUER (ref.[6]) with width fluctuation correction. In our case, the p, n and α channels are included.

The comparison of the experiment with the results from ELISA gives a quite good agreement for a number of neutron groups (see also fig. 1 and 2). But it exists also any differences in the absolute height, in the order of Legendre polynomials (n_0 group in fig. 1) and in the 90 degrees symmetry, predicted by the

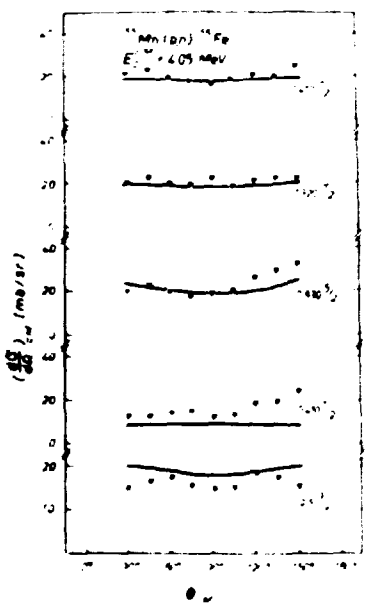

Fig. 1: Angular distributions of the ground state and any excited states of the $^{55}Mn(p,n)$ reaction (points), compared with calculated ones (curves), see also the text

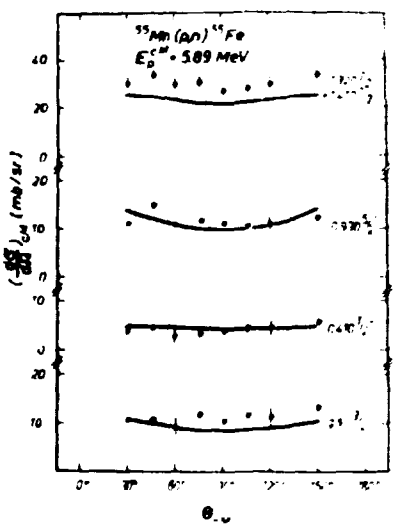

Fig. 2: Similar to fig. 1 at higher bombarding energy

theory (n_1 and n_2 group in fig. 1). But the differences seem to be smaller at the higher energy, than at the lower one. The optical model parameters are taken from (ref.[7]). The present work shows, that the assumption of complete compound mechanism don't seem to be sufficient.
KIM (ref.[8]) found in the ^{55}Mn(p,n) reaction for E_p about 2.3 MeV resonance structure in the excitation function and 90 degrees asymmetry. But in this energy range the influence of analogous states is not negligible. Other results from the ^{59}Co(p,n) reaction (ref.[9, 10.11]) are inconsistent and not directly comparable.

3. The ^{109}Ag(p,n) reaction

In steps of 0.5 MeV, angular distributions and excitation function from 5.0 to 9.0 MeV are measured and the cross sections $d\sigma/dE(E_o,E)$ are extracted. The angular distributions are isotropic. It must be assumed that the reaction mechanism is completely compound one and so a description with the complete statistical theory (see ref.[12]) is possible:

$$\sigma(E) \sim E\,\sigma_{inv}(E)\;\varrho\,(U) \qquad (1)$$

where E is the emission energy of the neutrons, σ_{inv} the inverse cross section and $\varrho(U)$ the level density for the excitation energy U of the residual nucleus. Based on the FERMI gas model, $\varrho(U)$ is given by

$$\varrho(U) \sim U^{-5/4} \exp\sqrt{4aU} \qquad (2)$$

"a" is the level density parameter.
Fig. 3 shows a function derived from (1) and (2) versus $U^{1/2}$, which must give a linear behaviour (it means, the level density parameter "a" is constant). As seen, it is not the case. A more detailed calculation gives the level density parameter value of a = 12 MeV^{-1} for E less about 4 MeV and a = 8 MeV^{-1} from the upper spectrum part. The value a = 16 MeV^{-1} for mass number A = 109 is expected. Therefore pre-equilibrium emission is included (see also ref.[12]) corresponding,

$$\sigma(E) = K_1\sigma_G(E, a) + K_2\sigma_N(E) \qquad (3)$$

where σ_G describes the compound emission according to (1) and σ_N the pre-equilibrium emission (see also ref.[12]).
But in opposite to the procedure of the computer program NONEQUI (ref.[13]) the a-value is set a = 16 MeV^{-1} and the components of equilibrium and pre-equilibrium emission (expressed by K_1 and K_2) are fitted with the experimental spectrum. It seems to correspond more to the physical reality. Any results are shown in fig. 4.

The difference between experiment an theoretical calculation in the high energy part of spectra is not clear up to now. The investigations will be continued.

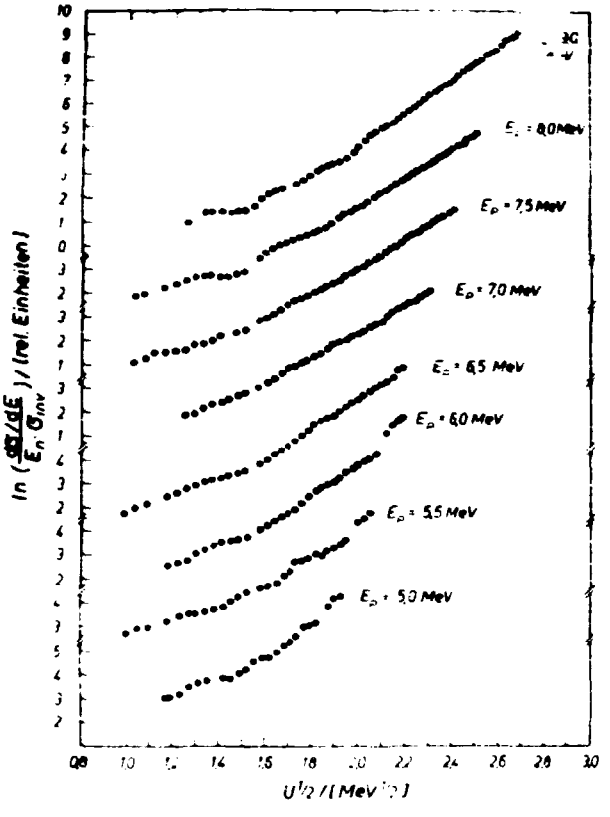

Fig. 3: In the framework of the complete statistical theory, the points should give a linear function, according to formula (2)

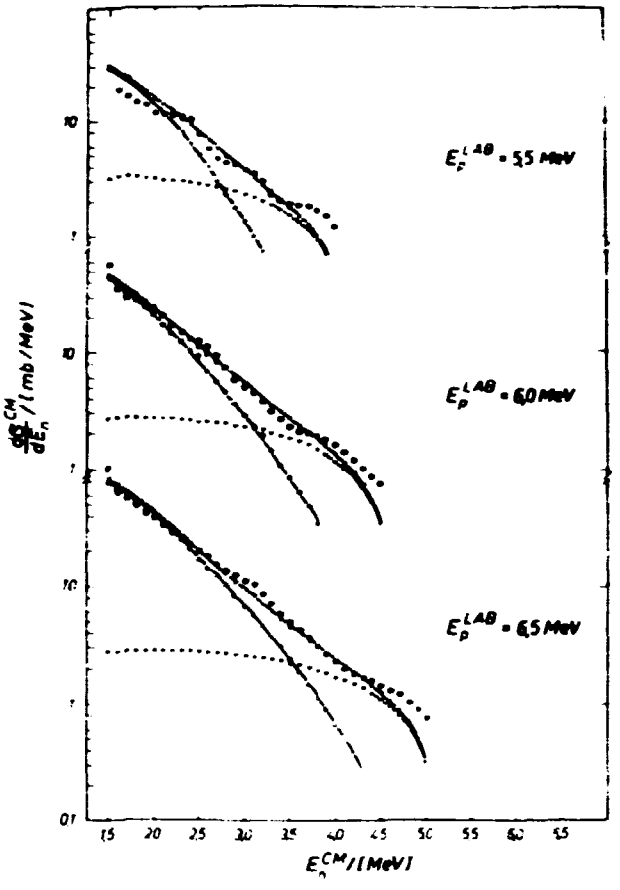

Fig. 4: Experimental points (•) and fitted curve of the total neutron emission (x), consisting of equilibrium (o) and pre-equilibrium (+) contributions

4. References

[1] Eckstein, P. et al., ZfK-295 (1975) 123
[2] Eckstein, P. et al., ZfK-283 (1974) 146
[3] Riera, H.-D. et al., Kernenergie 14 (1971) 115
[4] Rumpf, K., private communication
[5] Kielig, G., thes, Techn. University Dresden 1975
[6] Holdauer, E.A., Phys. Rev. B135 (1969) 642
[7] Beccetti, F.D. and G.W. Greenlees, Phys. Rev. 182 (1969) 1190
[8] Kim, H.-J., Phys. Lett. 5 (1963) 139
[9] Kozkós, M. et al., Tsch. Fiz. Zur. B15 (1965) 151
[10] Dryapachenko, I.P. et al., Yad. Fiz. 5 (1967) 440
[11] Dryapachenko, I.P. et al., Ukr. Fiz. Zur. 16 (1971) 1947
[12] Shahin, F., thesis, Techn. University Dresden 1974
[13] Riera, H.-D. et al., Kernenergie 15 (1972) 384

SESSION III

COMPLEX-PARTICLE FORMATION AND PREEQUILIBRIUM DECAY

E. Betak and P. Oblozinský, Institute of Physics, Slovak Academy of Sciences, 89930 Bratislava, Czechoslovakia

The attempts to describe the process of complex-particle formation and emission are being done within the preequilibrium models of nuclear reactions for several years. Within the exciton model of preequilibrium decay we can record two different approaches [1, 2], from which the second one supposes that a complex particle of any kind is created from excited nucleons only immediately before its emission.

Though the complex-particle formation and its emission should be treated as one process [3], it can be nevertheless presented as a product of corresponding two probabilities. The probability of complex-particle formation γ_β is usually much less than 1, whereas the emission probability itself is comparable with that of nucleons. We know much about α-particle formation in the nuclear ground state because of traditional interest to α-decay [4] and according to many calculations the region of α-formation probability should be rather broad $\approx 10^{-5} - 2 \times 10^{-1}$ (see ref. [5]).

Generally, formation probability can be evaluated on the basis of the overlap integral of wave functions of individual nucleons ψ_i with the cluster wave function Ψ_β. The simplest estimation, originally used for α-particles by Volkoek and Preiswerk [6], can be obtained provided all wave functions are constant in the region in which they should differ appreciably from zero: ψ_i in the nuclear volume V and Ψ_β in the complex-particle volume V_β. It gives

$$\gamma_\beta \equiv \left| \int \psi_1 \cdots \psi_{p_\beta} \; \psi_\beta^* \; d\vec{x}_1 \cdots d\vec{x}_{p_\beta} \right|^2 \approx p_\beta^3 \left(\frac{V_\beta}{V} \right)^{p_\beta - 1} \qquad (1)$$

where p_β is the number of nucleons in the particle β. Assuming radii $\approx r_0 A^{1/3}$ for both composite nucleus and complex particle we find that γ of given kind of the complex particle depends on the mass number A only. There is neither channel energy nor excitation energy dependence. The A-dependence is very sharp mainly for heavier ($p_\beta = 4$) particles, on the contrary to the "experimental" values which show only weak A-trend and indicate channel as well as excitation energy dependence. "Experimental" γ_β (see tab. 1) were obtained from the fit of the high energy parts of the overall complex-particle spectra to the Oak Ridge experimental data from proton-induced reactions on four target nuclei in mass region $51 < A < 209$ with excitation energies up to 71 MeV. Calculations were performed with the code described earlier [7].

Assumption of constant wave functions is rather crude, as obvious corrections lead to the conclusion that eq. (1) gives crude values explaining thus somewhat bad agreement with "experimental" estimations. Firstly, overlap of realistic wave functions, because of their oscillatory character, is less than overlap of constant wave functions. Secondly, only limited portion of nuclear volume V

contains highly excited nucleons with distinctly nonzero wave functions and is available for the formation process.

Knowledge of γ_β enables us to estimate average number of clusters N_β in a nucleus. Following relation has been derived in ref. [8]

$$N_\beta \approx \gamma_\beta \; R_{\beta(p)} \binom{p}{p_\beta} , \qquad (2)$$

where $R_{\beta(p)}$ is simple combinatorial factor (having value of the order of 0.5) and p is the number of excited nucleons. Since to relatively high energy complex-particle spectra contribute essentially only a few low-p states of the composite nucleus, γ_β^{exper} of tab. 1 should be related to those p only. Taking maximum value of γ_β^{exper} and $p = p + 1$ we get (see tab. 1) probably the highest limit of numbers of complex particles with high kinetic energy in the nucleus, a part of which we observe subsequently in the spectra.

Table 1: Formation probabilities and numbers of complex particles

Particle	p_β	γ_β^{exper}	$\gamma_\beta^{theor}{}_{A = 50}$	N_β
deuteron	2	0.024 - 0.12	0.32	0.18
triton	3	0.001 - 0.028	0.097	0.056
helion-3	3	0.002 - 0.020	0.097	0.04
alpha	4	0.0007- 0.094	0.033	0.24

References:

[1] L. Milazzo-Colli and G.M. Braga-Marcazzan, Phys. Lett, B38 (1972) 155
[2] I. Ribanský and P. Oblozinský, Phys. Lett. B45 (1973) 318
[3] H.A. Bethe, Rev. Mod. Phys. 9 (1937) 69
[4] S.G. Kadmenskij, V.I. Furman, Fiz. Elem. Cast. Atom. Yad. 6 (1975) 469
[5] M.K. Basu, Science and Culture 40 (1974) 47
[6] H.A. Tolhoek and P.J. Brussaard, Physica 21 (1955) 449
[7] E. Beták, Comp. Phys. Com. 9 (1975) 92
[8] P. Oblozinský, I. Ribanský, Izv. Ac. Sci.USSR, ser. fiz.39 (1975) No. 9, in press

КАСКАДНО-ЭКСИТОННАЯ МОДЕЛЬ ЯДЕРНЫХ РЕАКЦИЙ

К.К. Гудима, В.Д. Тонеев

Объединённый Институт Ядерных Исследований, ЛТФ, Дубна, (СССР)

Аннотация

Предложена модель, объединяющая черты трех механизмов ядерной реакции - прямого (каскадного), предравновесного и равновесного (компаунд-ядра). На примере двойных дифференциальных распределений частиц, испущенных в протон-ядерных реакциях, обсуждается роль процесса предравновесной эмиссии.

Введение

В последние годы нуклон-ядерные реакции в области промежуточных энергий $T_0 <$ 100 Мэв привлекли широкое внимание тем, что здесь наиболее ярко проявляются эффекты так называемого предравновесного распада ядер. Связанный с этим явлением механизм испускания частиц на стадии установления статистического равновесия в возбужденной ядерной системе занимает некоторое промежуточное положение между прямыми реакциями и распадами через состояния компаунд-ядра и не сводится к какой-то простой их комбинации. Предложенная Гриффином экситонная модель предравновесной эмиссии частиц [1] и её последующее развитие (см. обзоры [2, 3]) позволили понять важность этого механизма, его связь с промежуточной структурой ядер, объяснить ряд интересных физических эффектов.

К сожалению, все модели предравновесного распада, реализующие в той или иной степени идею о релаксации возбужденной ядерной системы за счет столкновений между ее составляющими, не ставят вопроса об угловом распределении продуктов реакции. Наблюдаемая на опыте асимметрия углового распределения вторичных частиц не получила в этом подходе своего объяснения.

В данной работе развита модель, объединяющая характерные черты прямых реакций и предравновесного распада. Обсуждается чувствительность измеряемых величин к этим механизмам.

Описание модели

При обсуждении механизма ядерной реакции мы будем исходить из следующей физической картины. Влетевшая в ядро частица может испытать одно или несколько внутриядерных столкновений, что приводит к образованию возбужденного многоквазичастичного состояния типа "doorway state", которое - в свою очередь - путем испускания частиц может перейти в основное состояние непосредственно или сделать это, пройдя через образование компаунд-ядра. Описанная картина близка к

модели, предложенной Родбергом для объяснения промежуточной структуры ядра [4]. Используя общий формализм теории ядерных реакций, Родберг смог рассмотреть лишь упругое и неупругое рассеяние нуклонов с образованием входного состояния. В нашей работе акцент сделан на реакциях с несколькими частицами в конечном состоянии.

Поведение первичной частицы, а также частиц второго и последующих поколений (если таковые имеются) вплоть до момента поглощения или вылета их из ядра рассматривается в рамках обычной каскадной модели [5, 6]. Подсчет числа захваченных ядром частиц и "дырок", образованных в результате внутриядерного столкновения, определяет входную частично-дырочную конфигурацию оставшегося возбужденного ядра, энергия возбуждения которого находится из баланса энергии. Дальнейшая "судьба" ядра прослеживается на основе модифицированной экситонной модели предравновесного распада, предложенной ранее в Дубне [7]. Следует подчеркнуть, что эта модель построена на решении кинетического уравнения с учетом испускания частиц и трех возможных типов внутриядерных переходов, отвечающих изменению числа частиц-дырок (экситонов) на ± 2 или 0, усредненный матричный элемент оценен из рассмотрения среднего свободного пробега частицы в ядерной материи. Данный вариант экситонной модели учитывает возможность последовательного испускания нескольких частиц и естественно переходит в модель равновесного статистического распада компаунд-ядра для состояний с большим числом квазичастиц [7]. В рамках использованной модели предравновесной эмиссии была успешно объяснена большая совокупность данных по реакции (n, n') при $T_0 \simeq 15$ Мэв [8].

Таким образом, предлагаемая каскадно-экситонная модель рассматривает ядерную реакцию как проходящую в три стадии - каскадную, предравновесную и равновесную (компаунд-ядро) - в отличие от двухэтапного механизма Сербера [9].

Все вычисления выполнены с помощью метода Монте Карло. Для уменьшения дисперсии при расчете энергетических спектров частиц, испущенных под заданным углом, использована модификация метода локального потока, предложенного для расчетов прохождения излучения через вещество [10].

Параметризация модели

Важным моментом в предлагаемой модели является условие перехода от внутриядерного каскада к модели предравновесной эмиссии. В обычной каскадно-испарительной модели быстрые частицы прослеживаются до некоторой минимальной энергии - энергии обрезания $T = T_{обр}$, - составляющей примерно (7 - 10) Мэв. Как показано в [5], вариация в разумных пределах величины $T_{обр}$ не меняет существенно среднего числа частиц в ядерном акте, фактически в этом случае речь идет о том, какие частицы называть каскадными, а какие - испарительными. В качестве нулевого приближения к нашей модели, ниже мы рассмотрим и такой способ "резкого обрезания" для перехода к предравновесному распаду ядра.

В реальном случае следует ожидать некоторого сглаженного - по энергии - обрезания, причем из общих физических соображений ясно, что при переходе к более низким первичным энергиям вклад в поглощение частиц на периферии и во внутренних областях ядра будет меняться, что совершенно не передается приближением резкого

обрезания. Поэтому естественно попытаться связать условие поглощения быстрой (каскадной) частицы со степенью близости мнимой части модельного оптического потенциала к его экспериментальному значению, извлекаемому из анализа опытов по упругому рассеянию частиц на ядрах.

Возникает вопрос: что принять за модельный оптический потенциал? В приближении "слабой связи" мнимую часть оптического потенциала можно выразить через сечение σ рассеяния частицы на ядерных составляющих

$$W_{\text{опт, мод}}(r) = \frac{\hbar}{2}\sigma \cdot \rho(r) \cdot v \,, \qquad (I)$$

где v – скорость налетающей частицы в среде, $\rho(r)$ – плотность ядерной материи, а величина σ должна включать в себя эффект принципа Паули. Учет фермиевского движения предполагает усреднение (I) по соответствующему спектру. Условия применимости этого соотношения выполняются лишь при достаточно высоких энергиях и для центральной области ядра. При этом радиальное поведение плотности $\rho(r)$, как видно из формулы (I), следует за поведением оптического потенциала. В общем случае функция $\rho(r)$ отстает от $W_{\text{опт}}(r)$, что обусловлено конечностью радиуса взаимодействия частиц и эффектом нелинейной связи $W_{\text{опт}}$ и ρ [II]. Поскольку в настоящее время мы не можем последовательно учесть эти факторы, мнимая часть оптического (модельного) потенциала для каскадных частиц оценена в двух следующих вариантах:

А) Оптический потенциал повторяет радиальную зависимость массового распределения, диффузный характер которого учтен в каскадной модели путем разбиения объема ядра на 7 сферических зон с постоянной плотностью равной среднему значению по данной зоне.

Б) Оптический потенциал определяется согласно (I), где в качестве $\rho(r)$ взято распределение Вудса-Саксона, но для значений параметров отвечающих объемной части мнимого оптического потенциала, извлеченного из анализа экспериментальных данных, косвенным образом этот трюк учитывает эффект нелинейной связи $W_{\text{опт}}$ и ρ.

Расчеты, выполненные методом Монте Карло для обоих вариантов, представлены на рис. I, там же нанесены экспериментальные значения мнимой части оптического потенциала $W_{\text{опт, эксп}}(r)$, полученные в двух работах групп авторов [I2, I3]. Интересно отметить, что для $T_0 > 30$ Мэв их результаты заметно отличаются, хотя по величине χ^2 для угловых распределений в упругом рассеянии и даже для поляризационных измерений они практически совпадают. При энергии $T_0 = 60$ Мэв, где различие особенно сильное, значения $W_{\text{опт, мод}}(r)$ находятся между этими данными. Естественно, что при переходе к меньшим значениям T_0 рассчитанная таким образом мнимая часть оптического потенциала не передает максимума поглощения, имеющего место на периферии ядра. К этому следует добавить, что условия справедливости каскадной и оптической моделей не совпадают. В частности, в каскадной модели рассматривается рассеяние на связанных нуклонах, а не на потенциальной яме, как в оптической модели. Таким образом о согласии между $W_{\text{опт, мод}}$ и $W_{\text{опт, эксп}}$ можно говорить лишь с определенной степенью точности, которую мы будем характеризовать параметром близости

$$P = \left| \frac{W_{\text{опт, мод}} - W_{\text{опт, эксп}}}{W_{\text{опт, эксп}}} \right|$$

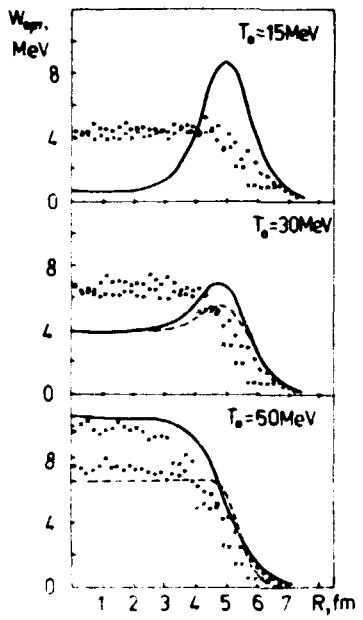

Рис. I Результаты модельного расчета мнимой части оптического потенциала для реакции $p + {}^{56}Fe$ при энергии T_0. (Крестики и кружки - варианты А и Б соответственно, см. текст). Сплошной кривой и пунктиром нанесены экспериментальные значения, полученные в работах [I2, I3].

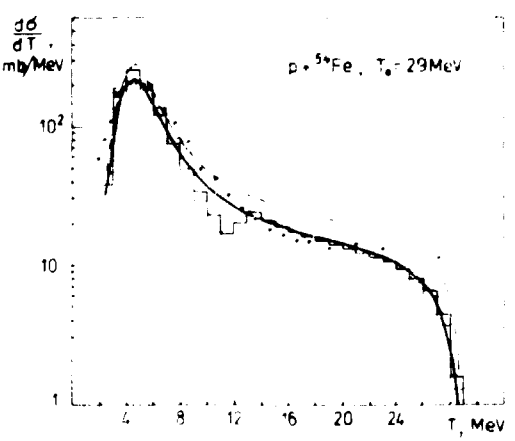

Рис. 2 Расчетный спектр протонов, испущенных ядром при облучении протонами с энергией 29 Мэв.
- - - - каскадно-испарительная модель
——— данная каскадно-экситонная модель, вариант с резким обрезанием,
— — — вариант А,
——— вариант Б,
точки - эксперимент из работ [I4]

Если положить, что 60-мэвный протон удовлетворяет условиям применимости каскадной модели, то - как видно из рис. I - это соответствует значению $P \simeq (0{,}3 - 0{,}5)$. Более точно параметр близости может быть выбран из сравнения с опытом результатов расчета характеристик ядерной реакции.

Все остальные параметры каскадно-экситонной модели фиксированы и взяты теми же самыми, как в моделях внутриядерного каскада [5, 6] и предравновесного распада [7].

Результаты и обсуждения

Рассчитанные в различных предположениях спектры вторичных протонов из реакции $p + {}^{56}Fe \rightarrow p + \ldots$ показаны на рис. 2. Как видно из представленных результатов, использование варианта с резким обрезанием приводит к появлению нефизического провала в спектре частиц вблизи $T_{обр}$. При переходе к большим значениям энергии бомбардирующего протона провал маскируется выбором величины шага в гистограмме, но при $T_0 \simeq$ I5 Мэв его влияние резко искажает общую форму спектра. Подключение механизма предравновесной эмиссии улучшает согласие с опытом, сглаживая теоретическую кривую.

Следует заметить, однако, что проинтегрированный по всем углам энергетический спектр не является очень чувствительной характеристикой реакции, поэтому даже обычная каскадно-испарительная модель дает разумные результаты. Наибольшую чувствительность к

механизму предравновесной эмиссии обнаруживают спектры протонов, испущенных в область задних углов, что демонстрируется на рис. 3. В частности, выход протонов с энергией T >(I5 - 20) Мэв практически целиком обусловлен процессом неравновесного распада ядер. Этот эффект не может быть имитирован никакой вариацией параметров обычной каскадно-испарительной модели.

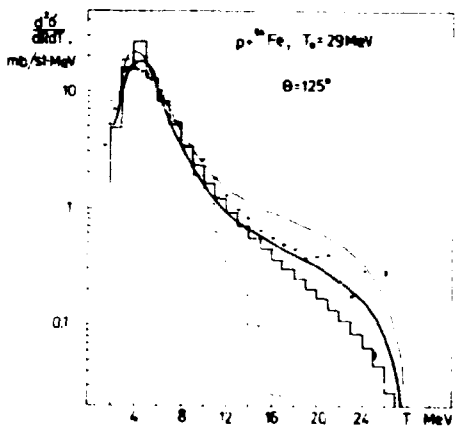

Рис. 3. Спектр протонов, испущенных под углом I25° в реакции $p + {}^{56}Fe \rightarrow p + \ldots$ при T_0 = 29 Мэв. Все обозначения - как на рис 2.

Благодаря высокой чувствительности к предравновесной компоненте согласие с опытом в спектрах испущенных назад протонов явилось основным критерием для выбора величины параметра близости P. Оптимальные значения P оказались равными (0,5 - 0,6) и (0,2 - 0,3) для вариантов А и Б соответственно. Увеличение значения P завышает выход быстрых частиц, что более заметно при небольших энергиях, скажем, $T_0 \simeq$ I5 Мэв. Значения P ниже указанных границ приводят к повышению энергии возбуждения входного канала, что влияет на спектр частиц, испущенных назад, и это проявляется тем раньше, чем выше энергия бомбардирующей частицы.

Необходимо подчеркнуть условность разделения каскадного и предравновесного механизмов в данной модели. Это разделение, а соответственно и выбор основано на предположении об изотропии углового распределения предравновесной компоненты, вся анизотропия приписывается каскадным нуклонам. В действительности возбужденная многоквазичастичная система, образованная в результате прохождения каскада частиц, может сохранить некоторую "память" об инициирующей каскад частице и тем большую, чем меньше число возбужденных частиц-дырок. Последовательно учесть этот эффект сейчас не представляется возможным, однако понятно, что эффективно это отвечало бы выбору более узкого интервала по параметру близости P.

Поскольку варианты А и Б дают близкие результаты, все приведенные ниже данные относятся к варианту Б с P = 0,3, а в качестве $W_{опт, эксп}$ взяты результаты анализа, выполненного Бочетти и Гринлисом [I2]

Результаты вычислений, представленные на рис. 4 - 5, позволяют проследить зависимость формы энергетического распределения протонов от энергии первичного протона и от ядра-мишени, там же указаны вклады от всех трех механизмов испускания. Видно, что предложенная модель хорошо воспроизводит изменение формы спектров при переходе от легких ядер мишеней к более тяжелым, правильно предсказывает абсолютный выход частиц. Проведение абсолютных вычислений оказалось возможным благодаря использованию модели внутриядерного каскада. Относительный вклад каскадных и предравновесных частиц зависит как от T_0, так и от массового и зарядового

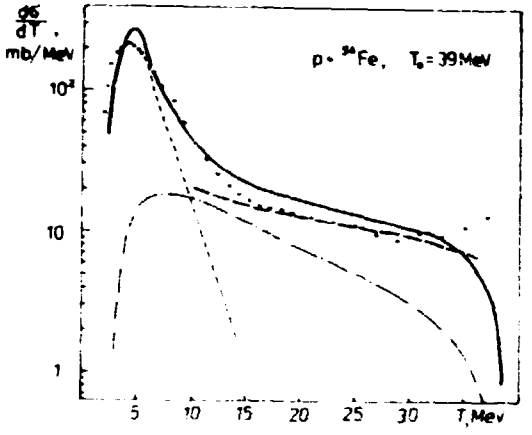

Рис. 4 Проинтегрированный по углам спектр вторичных протонов из реакции $p + {}^{54}Fe \rightarrow p + \ldots$ при T_0 = 39 Мэв.
– – – – – равновесная компонента,
– – – – предравновесная компонента,
———— сумма всех трех компонент,
— — — — результаты расчета Бланна по гибридной модели с учетом геометрии реакции [2]
точки – эксперимент [I4]

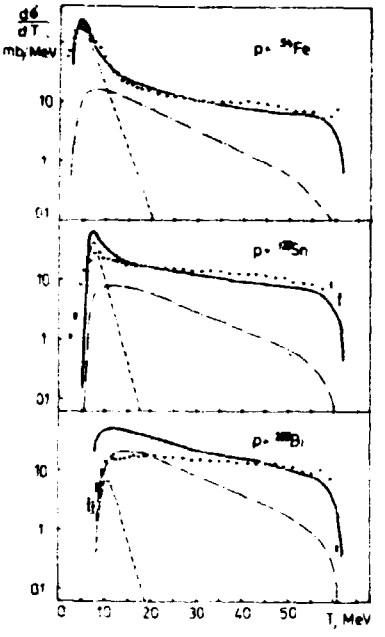

Рис. 5 Спектры протонов, испущенных при облучении ядер железа, олова и висмута протонами с энергией T_0 = 62 Мэв. Все обозначения – как на рис. 4

чисел ядра-мишени, причем если рассматривать лишь проинтегрированные по углам спектры, как это делается в предравновесном подходе, то вклады этих двух механизмов невозможно локализовать какой-то узкой энергетической областью. Соотношение между этими компонентами меняется также и в зависимости от угла вылета вторичных протонов (см. рис. 6).

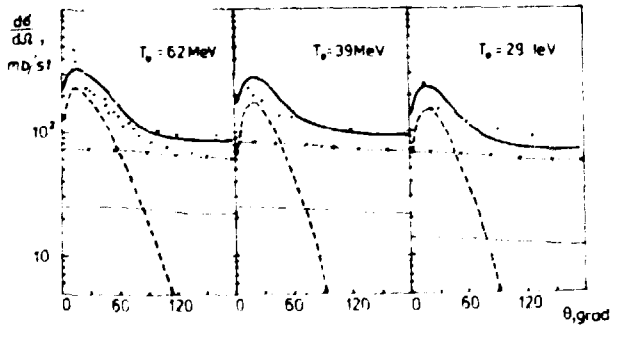

Рис. 6 Угловое распределение протонов из реакции $p + {}^{54}Fe \rightarrow p + \ldots$ при энергии T_0.
—×—×— равновесная компонента,
— — — — предравновесная компонента,
– – – – – каскадная компонента,
———— сумма всех трех
экспериментальные точки взяты из работ [I4].

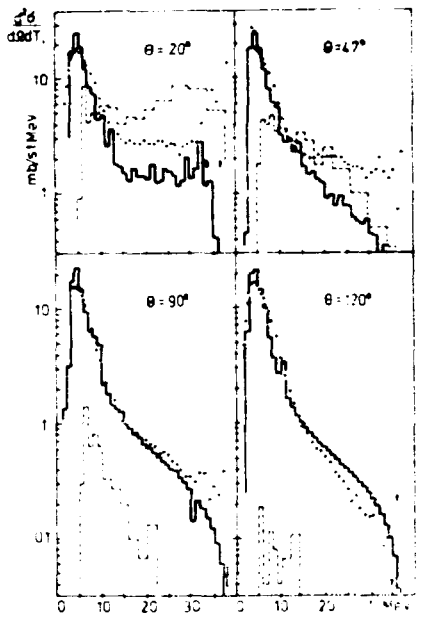

Рис. 7 Спектры вторичных протонов, испущенных в реакции $p + {}^{59}Co \to p + \ldots$ под углом θ при T_0 = 39 Мэв. Сплошная гистограмма - наш расчет, пунктирная - расчет Бертини и др. по каскадно-испарительной модели [15]. Экспериментальные точки взяты из работа [14].

Пример расчета двойных дифференциальных сечений дан на рис. 7. И в этом случае согласие с опытом достаточно хорошее, а в области больших углов - заметно лучше, чем результаты, полученные в рамках каскадно-испарительной модели. Как уже отмечалось, проинтегрированные по углам энергетические спектры являются не очень чувствительной характеристикой, что позволило ряду авторов использовать для них минимально измененную предравновесную модель вплоть до энергии $T_0 \simeq 60$ Мэв (ср. рис. 4).

Заключение

Таким образом, предложенная каскадно-экситонная модель успешно воспроизводит двойные дифференциальные сечения для вторичных нуклонов. Приведенные результаты еще раз подчеркивают важность учета предравновесных процессов, показывают, при каких условиях их вклад может стать превалирующим. В то же время следует помнить, что граница раздела между тремя рассмотренными механизмами ядерной реакции - прямым (каскадным), предравновесным и равновесным (компаунд-ядро) - весьма условна и относительна. Дальнейший прогресс в этом направлении связан как с более детальным и строгим теоретическим рассмотрением проблемы, так и с необходимостью новых прецизионных измерений. В частности, представляет интерес изучение корреляций между испущенными частицами, пример успешного применения такого подхода дают исследования процессов множественного рождения частиц в столкновениях высокоэнергетических адронов.

Литература

[1] J.J. Griffin, Phys. Rev. Lett. 17, 478 (1966)

[2] M. Blann In: Proceedings of the Europhysics Study Conference on Intermediate Processes in Nuclear Reactions
Vlitvice Lakes, Yugoslavia (Aug. 31- Sept. 5 1972)
Ed. by N. Cindro, P. Kulisic, T. Meyer-Kuckuk

[3] К. Зайдель, Д. Зелигер, Р. Райф, В.Д. Тонеев, ЭЧАЯ, 6, № 4, 1975

[4] L.G. Rodberg In: "Intermediate structure in nuclear reactions"
Ed. by H.P. Kennedy and R. Schrils, Univ. of Kentucky Press, Kentucky, 1968, p. 65

[5] В.С. Барашенков, В.Д. Тонеев, Взаимодействие высокоэнергетических частиц и атомных ядер с ядрами, Атомиздат, Москва, 1972

[6] В.С. Барашенков, К.К. Гудима, В.Д. Тонеев, 36 415 (1969).
Препринты ОИЯИ, Р2-4065, Р2-4066, Дубна, 1968
[7] К.К. Гудима, Г.А. Сосков, В.Д. Тонеев, Яд. физ. 21, 260, 1975
[8] Д. Зелигер, К. Зейдель, В.Д. Тонеев, В сб. "Interactions of fast neutrons with nuclei" , ZfK-271, Dresden, 1974, p.65
[9] R.Serber. Phys. Rev. 72, 1114, 1946
[10] В.Г. Золотухин, С.И. Ермаков, В сб. "Вопросы физики защиты реакторов", М., Госатомиздат, 1963, стр. 171
[11] Е.Е. Бальбуцев, И.Н. Михайлов, Препринт ОИЯИ Р4-8474, Дубна, 1974
[12] F.D.Becchetti, Jr., G.W.Greenlees. Phys.Rev. 182 , 1190 (1969)
[13] J.J.H.Menet, E.E.Gross, J.J.Malanify, A.Zucker. Phys.Rev. C4 , 1114 (1971).
[14] F.E.Bertrand, R.W.Peelle. Phys.Rev. C8, 1045 (1973); Reports ORNL-4469 (1970), ORNL-4471 (1970), ORNL-4638 (1971).
[15] H.W.Bertini, M.D.Harp, F.E.Bertrand. Phys.Rev. C10, 2472 (1974).

INVESTIGATION OF THE (n,2n) REACTION BY THE STATISTICAL MODEL

E. Holub, Laboratory for Nuclear Spectroscopy, Institute "Rudjer Bošković", Zagreb, Yugoslavia
and
O. Bersillon, N. Cindro [x] and J. Jary, Service de Physique Nucléaire, CEN Bruyères-le-Châtel, 92120 Montrouge, France

x) Permanent address: Laboratory for Nuclear Spectroscopy, Institute "Rudjer Bošković", Zagreb, Yugoslavia

1. Introduction

A large number of experimental (n,2n) cross sections have been obtained by various techniques during the last 20 years. This has enabled many authors to compare the existing experimental (n,2n) cross sections with theoretical estimates and make a systematics of (n,2n) cross sections.

(n,2n) cross sections have been mostly compared with predictions of the statistical theory and some semiempirical ready-to-use formulas such as the Pearlstein [1] estimates.

The overall conclusion drawn from these systematic studies is that the simple evaporation theory used in Pearlstein semiempirical formulas agrees within 20 % with about two thirds of the measured cross sections [2]. This statement holds for incident neutron energies around 14.7 MeV.

It has been recently pointed out that experimental total (n,2n) cross sections exhibit a systematic trend in the deviation from the Pearlstein estimates [3]. This trend appeared when the comparison was made for constant values of the excess energy $U_R = E_n + Q(n,2n)$ rather than for constant bombarding energies E_n. The necessity of such a comparison appears clearly from the simplest evaporation formulas like the Weisskopf one, where the cross section for the emission of two consecutive neutrons is given in terms of essentially only one parameter, namely U_R:

$$\sigma(n,2n) = \sigma_{ne}\left\{ 1 - \left(1 + \frac{U_R}{\theta}\right) \exp\left(-\frac{U_R}{\theta}\right)\right\}$$

where σ_{ne} is the nonelastic cross section and θ the (residual) nuclear temperature [4].

In an earlier paper Holub and Cindro [3] investigated the comparison of experimental (n,2n) cross sections and the Pearlstein estimates at constant values of U_R. They noticed that most of the data in the region of $U_R = 6 \pm 1$ MeV are systematically overestimated by the Pearlstein estimates. In fact, a χ^2-fit to a straight line in a σ_{exp}/σ Pearlstein ratio as a function of mass number A gave a line

$$\frac{\sigma_{exp}}{\sigma_{Pearlstein}} = -0.00038\ A + 0.95\ ,$$

indicating that for nuclei heavier than A≈100 and for $U_R = 6 \pm 1$ MeV the Pearlstein calculations overestimate the experiment by about 10 % on an average. This difference was conjectured to be due to the effect of preequilibrium processes

in neutron emission.

We should stress, at this point, that the Pearlstein expression is not a purely statistical formula, but rather a statistical model-based semiempirical formula, as it contains σ_{nM}/σ_{ne} as a scaling factor (σ_{nM} is the cross section for all reactions where neutrons are emitted, except elastic scattering). We thought, therefore, that in order to detect systematic departures from the statistical predictions (and to ascribe them to nonstatistical processes) a comparison with a statistical model a priori calculation was necessary. As to the choice of experimental data for this comparison, we used data published from 1970 on whenever possible, i.e., we used activation data obtained by the Ge(Li) detection technique, as well as recent data obtained by the large-scintillator method [5]. Otherwise, earlier data from different authors were averaged and their mean value taken for comparison.

2. An a priori compound nucleus evaporation calculation

In the present work we study in detail the applicability of equilibrium processes to (n,2n) reactions. To this end, we undertook a systematic calculation of (n,2n) cross sections using a statistical model, keeping all the input parameters fixed or smoothly varying with A.

2.1. Ingredients of the calculation. The calculation was based on the 1-independent statistical model; a computer code was used to calculate simultaneously (n,p), (n,α), (n,n'), (n,2n) and (n,3n) cross sections [6].

The input parameters were the total nonelastic cross section σ_{ne}, the inverse cross sections for neutrons, protons and alpha particles (which we denote by $\sigma^{n}_{inv}(\epsilon)$, $\sigma^{p}_{inv}(\epsilon)$ and $\sigma^{a}_{inv}(\epsilon)$, respectively) and the appropriate level density parameters. By including either experimental or calculated (using the Weisskopf single-particle transition rates) values for Γ_γ, it was also possible to calculate the (n,γ) cross section.

(i) The values of nonelastic cross sections $\sigma_{ne}(E_n)$ were taken from the optical model calculations of Mani et al. [7].

(ii) The inverse cross sections for neutrons $\sigma^{n}_{inv}(\epsilon)$ were calculated using the optical model code by Smith [8]. A local equivalent of a nonlocal potential with the Woods-Saxon form for the real and the Woods-Saxon derivative for the imaginary part of the potential was used. The optical model parameters were the following:

V_o = 71 MeV
W_o = (7 + 0.4 E) MeV
$R_{oR} = R_{oI}$ = 1.21 fm β (nonlocality) = 0.85 fm
a_R = 0.65 fm
a_I = 0.47 fm
V_{So} = 7 MeV

The above parameters were chosen in such a way as to obtain maximal agreement between the value of $\sigma^{n}_{inv}(\epsilon)$ calculated by this code and the values obtained by Lagrange and Delaroche [9] from coupled-channel calculations

for the nuclei ^{148}Sm and ^{232}Th, as well as an extended optical model analysis for the nuclei ^{93}Nb and ^{197}Au. We note that $\sigma^{n}_{inv}(\epsilon)$ around 14 MeV was practically equal to the σ_{ne} of ref. [7].

(iii) The values of inverse cross sections for proton emission $\sigma^{p}_{inv}(\epsilon)$ were taken from the optical model calculations of Mani et al. [10] and those for alpha particle emission from the calculations of Huizenga and Igo [11].

(iv) The level density parameter a was systematically taken from Gilbert and Cameron [12]. Following the same reference, the excitation energies of the residual nuclei were split into two regions by an energy E_o. For excitation energies below E_o, the constant temperature density model was applied, and for excitation energies above E_o, the Fermi gas level density model was applied. The value of E_o was calculated using the procedure described in ref.[12]. The values for pairing and shell corrections were also taken from Gilbert and Cameron [12].

(n,2n) cross sections were calculated for about 80 nuclei, for incident energies satisfying the condition that the excess energy was in the region U_R = 5-7 MeV. We made this choice having in mind the following reasons:

(i) For most nuclei, the Q-value for the (n,2n) reaction is about -8 to -9 MeV and most of experimental data for (n,2n) cross sections are for incident energies between 14 and 15 MeV. Thus, the bulk of available data corresponds to the excess energy range U_R = 5-7 MeV.

(ii) In this energy range we are well above the (n,2n) threshold, and still below the (n,3n) threshold; we shall see that this fact has important consequences as to the sensitivity of the calculated cross sections to the variation of input parameters.

(iii) As mentioned in the introduction, a systematic deviation from the statistical predictions was observed in this energy region.

2.2. Sensitivity of the model to the choise of input parameters. We shall now discuss a crucial point in the analysis, that is the sensitivity of the results of the model calculation to the choice of input parameters. Among all the parameters, the level density parameter a and the neutron inverse cross sections $\sigma^{n}_{inv}(\epsilon)$ may considerably influence the calculated cross sections, while leaving at the same time a considerable freedom of choice of values.

It is well known that the average values of the level density parameter a given in ref. [12] may differ from the values deduced from observation [13]. We checked the influence of the two sets of values for the level density parameter a on the calculated (n,2n) total cross sections for the ^{148,150,152} and ^{154}Sm isotopes in the incident energy range from 14 to 16 MeV. The results for the total cross sections obtained using the calculated and observed value for a, respectively, are shown in Table 1. The cross sections obtained for the two sets of a values are quite similar and certainly well within the uncertainties of the method. In addition, we drastically varied the value of a from 16 to 24 MeV^{-1} and calculated the total (n,2n) cross section for ^{152}Sm at an incident neutron energy of 14.5 MeV. The corresponding relative change in the calculated cross sections was found to be only 7 %.

The influence of two different sets of values of neutron inverse cross sections

is shown in Table 2. The (n,2n) cross sections were calculated for ^{148,150,152,154}Sm and ^{197}Au using the optical-model [8] and the coupled-channel [9] values for $\sigma^{n}_{inv}(\epsilon)$, for incident energies in the range between 14 and 15 MeV. In all cases the differences in the cross sections around 14 MeV (corresponding to $U_R = 6 \pm 1$ MeV) were rather small (~5 %).

It is important to note that the effect of the variation of the two crucial parameters a and $\sigma^{n}_{inv}(\epsilon)$ becomes considerable as we move to lower incident energies, approaching the (n,2n) reaction threshold. We stress that this variation had no appreciable influence on the calculated (n,2n) total cross sections only for incident energies corresponding to excess energies in the range U_R = 5-7 MeV. Thus, we felt safe in using the model in this restricted energy range.

3. Results

3.1. Comparison with other systematic calculations. As mentioned before, we calculated the total (n,2n) cross sections for about 90 nuclei in the excess energy range of $U_R = 6 \pm 1$ MeV. There exist at present several semiempirical and empirical formulas for (n,2n) cross sections, for instance those by Pearlstein [1], Adám and Jéki [14] and S. Chatterjee and A. Chatterjee [15]. For 73 nuclei and incident energies corresponding to the above region, we made a comparison between the experimental results of the total (n,2n) cross sections and the results of the calculations from refs. [1, 14, 15] and present work, respectively. Fig. 1 shows the histograms of the relative differences between the experimental values and the different calculations. The semiempirical formulas by S. Chatterjee and A. Chatterjee [15] and Adám and Jéki [14] give rather wide histograms symmetric around 0 % deviation. On the other hand, the results of Pearlstein [1] and the present calculations predominantly overestimate the experimental values up to ~ 20 %. For the Pearlstein [1] semiempirical estimates, the same has already been concluded in Section 1, and it appears that the present calculation gives similar results.

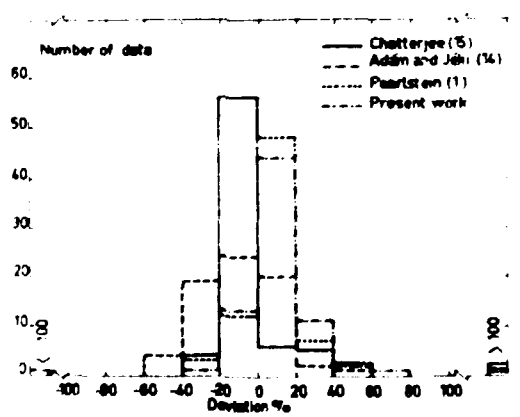

Fig. 1: Distribution of the relative differences between experimental values and calculations of (n,2n) cross sections as given by S. Chatterjee and A. Chatterjee [15], Adám and Jéki [14], Pearlstein [1] and present work, respectively.

3.2. Comparison with experimental data. To study in more detail the comparison of the present calculations with experimental data, we plotted the $\sigma_{exp}/\sigma_{calc}$ ratio as a function of atomic mass number in the chosen excess energy range of 6 ± 1 MeV. Fig. 2 shows the result of this investigation. The least-square fit

to a straight line of the data points in fig. 3 gives

$$\frac{\sigma_{exp}}{\sigma_{calc}} = -0.000061\ A + 0.92\ ;$$

(in this calculation the very low point for A = 58 corresponding to ^{58}Ni has been omitted, as it seems that more accurate experimental data are needed). The least-square line obtained by using the present systematic statistical theory calculation, where no parameters were adjusted, is close to that obtained earlier by Holub and Cindro [3] and discussed in the introduction. The bulk of the calculated values for the total (n,2n) cross sections overestimates the experimental values by about 10 %. A feature observed more clearly in the present results is the peak in the mass region between A = 140 and 180.

4. Discussion

The main point arising from the preceding results is whether the observed systematic discrepancy between the experimental and calculated values for (n,2n) cross sections is significant. In other words, would a suitable change of input parameters bring the calculated values in accordance with the experimental results?

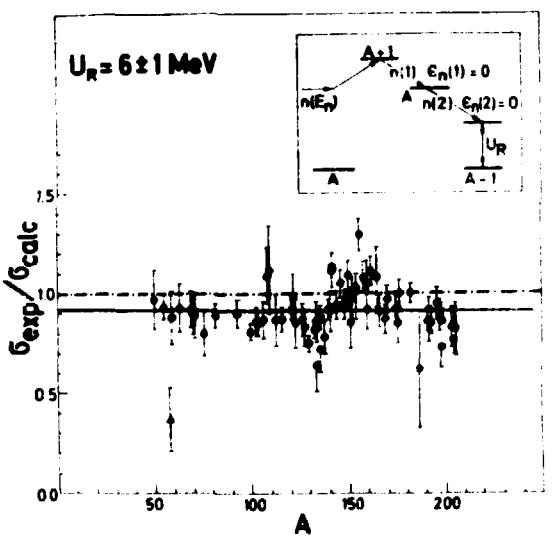

Fig. 2: Ratios of experimental (n,2n) cross sections to the present compound nucleus calculations versus the atomic mass number of the target nuclei for $U_R = 6 \pm 1$ MeV. The full line represents the linear function $y = \frac{\sigma_{exp}}{\sigma_{calc}} = -0.000061 \cdot A + 0.92$, obtained by a leastsquare fit to the data. (The point denoted by Δ is for ^{58}Ni and is not included in the least-square fit).

We have already seen that no systematic variation of the level density parameter a and the neutron inverse cross sections $\sigma^n_{inv}(\epsilon)$, applied within reasonable limits and in a more or less smooth way, could change the calculated values in such a way as to shift the least-square line to unity. On the other hand, the inverse cross sections for protons and alphas and the choise of Γ_γ have no appreciable influence on the value of σ_{calc} for incident neutron energies around 14 MeV.

The only remaining parameter is the nonelastic cross section σ_{ne}. Its values were taken from Mani et al. [7]. Although a systematic uncertainty in the optical model cross sections of ref. [7] is not unconceivable, there is no other independent evidence for the need of, say, a decrease of by 10 %. Besides, this decrease would even worsen the disagreement around A = 150, and, moreover, its effect on the calculated cross sections may be more complex: a consequent decrease of $\sigma_{inv}(n)$ values used at neighbouring energies would soften the primary neutron emission spectrum and thus tend to increase the total (n,2n) cross sections. Thus, explanations calling for an extension of the model appear to be

Table 1: Influence of the level density parameter a on the calculated (n,2n) total cross sections: Comparison of the results obtained using an average value of a (a_{calc}, ref.[12]) and values of a obtained from experiment (a_{obs}, ref.[13]).

	^{148}Sm		^{150}Sm		^{152}Sm		^{154}Sm	
E_n (MeV) \ σ_{calc} (mb)	with a_{calc}	a_{obs}	with a_{calc}	a_{obs}	with a_{calc}	a_{obs}	with a_{calc}	a_{obs}
14.0	1999	1956	2017	1923	2006	1967	2092	2123
14.5	2016	2004	2023	1947	2016	1996	2090	2122
15.0	2026	2015	1954	1905	1938	1966	2014	2077
16.0	1882	1872	1491	1513	1442	1639	1551	1767

Table 2: Influence of the inverse neutron cross sections on the calculated (n,2n) cross sections: Comparison of the calculated (n,2n) cross sections obtained with two different sets of inverse neutron cross sections ($\sigma^{n,OM}_{inv}$, from optical model calculations, ref.[8] and $\sigma^{n,CC}_{inv}$ from coupled-channel calculations, ref. [9]).

	^{148}Sm		^{150}Sm		^{152}Sm		^{154}Sm		^{197}Au	
E_1 (MeV) \ σ_{calc} (mb)	with $\sigma^{n,OM}_{inv}$	$\sigma^{n,CC}_{inv}$	with $\sigma^{n,OM}_{inv}$	$\sigma^{n,CC}_{inv}$	with $\sigma^{n,OM}_{inv}$	$\sigma^{n,CC}_{inv}$	with $\sigma^{n,OM}_{inv}$	$\sigma^{n,CC}_{inv}$	with $\sigma^{n,OM}_{inv}$	$\sigma^{n,CC}_{inv}$
14.0	1999	2005	2017	1986	2006	1910	2092	2027	2374	2276
14.5	2016	2021	2023	1996	2016	1945	2090	2048	2371	2285
15.0	2026	2026	1954	1925	1938	1925	2014	2035	2367	2295
16.0	1882	1850	1491	1524	1442	1626	1551	1814	2344	2269

more likely. A natural way is to include nonequilibrium processes in the neutron emission mechanism. This point is extensively discussed in ref. [16] and other contributions to this Symposium.

The second feature deduced from fig. 2 is the peak in the $\sigma_{exp}/\sigma_{calc}$ ratio for mass numbers between A = 140 and 180. We are not inclined to ascribe it to possible systematic errors in the experimental (n,2n) cross sections in this mass region. Several explanations, for instance in terms of the nuclear Ramsauer effect or in terms of the deformability of the nuclei in this mass region, come to mind, but none appear to coherently explain the observations. Thus, this phenomenom remains an open problem.

We acknowledge the contributions of Mme Z. Cindro and Mr. J.P. Martin in numerical calculations presented in this paper. Two of us (E.H. and N.C.) wish to acknowledge the hospitality of Dr. A. Michaudon and the Service de Physique Nucleaire of the CEN Bruyeres-le-Chatel, where these calculations were performed.

References

[1] S. Pearlstein, Nuclear Data A3 (1967) 327;
[2] Z.T. Bödy and J. Csikai, Atomic Energy Review, Vol. 11, No 1, March 1973
[3] E. Holub and N. Cindro, Phys. Lett. 56B(1975) 143;
[4] J. Blatt and V.F. Weisskopf, Theoretical Nuclear Physics, J. Wiley and Sons, N. York 1967, p. 379;
[5] J. Frehaut and G. Mosinski, Contrib. to this Symposium and refs.therein;
[6] J. Jary, to be published;
[7] G.S. Mani, M.A. Melkanoff and I. Iori, Rep. CEA No. 2380 (1963);
[8] W.R. Smith, Computer Physics Communication 1 (1969) 106;
[9] C. Lagrange, JAERI-M 5984 /INDC (JAP) 25F/, 1975, p. 58; C. Lagrange and J. Delaroche, in Contrib. IAEA Consultant Meeting on the Use of Nucl. Theory in Neutron Nuclear Data Evaluation, Trieste, Dec. 1975, (Review paper 5) and private communication;
[10] G.S. Mani, A.M. Melkanoff and I. Iori, Rep. CEA No 2379 (1963);
[11] J.R. Huizenga and G. Igo, Nucl. Phys. 29 (1962) 462;
[12] A. Gilbert and A.G.W. Cameron, Can. J. Phys. 43 (1965) 1446;
[13] S.F. Mughabghab and D.I. Garber, BNL 325, Neutron Cross Sections, Vol. 1 (1973);
[14] A. Adám and L. Jéki, Acta Phys. Hung. 26 (1969) 335;
[15] S. Chatterjee and A. Chatterjee, Nucl. Phys. A125 (1969) 593;
[16] N. Cindro and J. Frehaut, Contrib. to this Symposium, Section 1.4

PRESENT STATUS OF THE RADIATIVE NEUTRON CAPTURE MECHANISMS - NONSTATISTICAL EFFECTS

J.S. Brzosko, Institute of the Experimental Physics University of Warsaw and the Department of Physics, the Bialystok Division of the Warsaw University

Abstract

This paper is devoted to the description of the present status of our knowledge about neutron radiative capture mechanisms. In the first section there are given a review on mathematical description of the neutron capture cross section and possible sources of correlation effects. The point of lecture is the explanation of connections between the intermediate structures and correlation effects. In one of the sections the explanation of the bump in γ-ray spectra is discussed. The typical experimental results are presented.

1. Introduction

During recent years physicists working in radiative capture of the neutrons have focused investigations on nonstatistical effects. Especially, they paid attention to the correlation between the different radiation channels. As supplementary data, informations concerning the elastic scattering of the neutrons and γ-rays or capture of the neutron in (d,pγ) and (d,p) processes have been presented. The present state of the subject is published in the proceedings from last conferences [1]-[4]. Situation in nuclear reactions was clear during the fifth decade. Two approaches - a statistical model of compound nucleus (CN) [5],[6] and a direct reaction model (DI) [34],[35] were used.

First of all, the reactions induced by neutrons for low and middle energies have been a good example for realisation of statistical conditions. The experimental value of the resonance width revealed the lifetime of the resonances of 10^{-15}s. It is enough for about 10^6 elementary internuclear two-body interactions. After all, the cross-section for low energy capture showed nice resonances that constituted 99 % of the energy-integrated cross-section. This make suggestion to most physicists that decay of the CN can be treated in term of the statistical model. Improved quality of the measurements especially of high-resolution projectiles and outgoing particles have allowed to observe disagreement experimental data and statistical predictions.

It has been observed:

- anomalous amplification in high energy part of the γ-ray spectra [7],[8],
- correlation between intensity population of the same levels in (n,γ) and (d,p) reactions [9],[10],
- gamma and neutron widths correlations [11],
- excitation functions fluctuations [12],[13].

The effects mentioned play an important part in the resonance reaction and have been not treated as direct process fraction. These processes violate statistical picture of the reaction and must be newly interpreted.

2. Compound Nucleus and Intermediate Configurations - Review Based on S-Matrix Theory

In the separate neutron resonances region, the amplitude of the (n,γ) reaction may be written in the form (ignoring a phase - factor $ie^{i\varphi}$):

$$S_{nf} = \sum_{\lambda} \frac{\Gamma_{\lambda n}^{1/2}\,\Gamma_{\lambda f}^{1/2}}{E_\lambda - E - \frac{i}{2}\Gamma_\lambda} - S_0 \tag{1}$$

$\Gamma_{\lambda n}$ and $\Gamma_{\lambda f}$ are the neutron and photon absorption widths, respectively. E is the energy of the compound system: projectile and target, E_λ and Γ_λ are energy and width of the resonance λ, respectively. S_0 is smoothly varying with energy part. It contains potential capture term and part proceed from tails of the distant resonances $|E_{\lambda'} - E| \gg \Gamma_\lambda$.

The (n,γ) cross section is defined as:

$$\sigma_{n\gamma} = 4\pi\,|S_{nf}|^2 \tag{2}$$

Since, the energy resolution in incoming and outgoing channels is limited, experimental data give us the average reaction amplitudes. It is easy to show [14] that after averaging the slow-varying part of the S_{nf}, the amplitude $S_{nf}(s.v)$ has form:

$$S_{nf}(s.v) = Re\,\langle S_{nf}\rangle \tag{3}$$

The fast varying part of the S_{nf} produces fluctuations and adequate cross section can be written as:

$$\sigma_{n\gamma}^{f} = \langle |S_{nf} - \langle S_{nf}\rangle|^2\rangle = \left\langle \frac{\Gamma_{\lambda n}\Gamma_{\lambda f}}{\Gamma_\lambda D}\right\rangle - \left(\pi s_{nf}\right)^2 \tag{4}$$

D is the density of λ resonances per energy unit,

$$s_{nf} = \frac{1}{\pi}\,Im\langle S_{nf}\rangle = \frac{\langle \Gamma_{\lambda n}^{1/2}\Gamma_{\lambda f}^{1/2}\rangle}{D} \tag{5a}$$

$$s_n = \frac{\langle \Gamma_{\lambda n}\rangle}{D}\ ;\ s_f = \frac{\langle \Gamma_{\lambda f}}{D} \tag{5b}$$

The formulas (5) contain definitions of the strength function s.

The existence of the statistical condition in compound system is related to realization the next relations:

$$\sum_{\lambda \in \Delta E} \Gamma_{\lambda n}^{1/2}\,\Gamma_{\lambda f}^{1/2} \cong 0 \tag{6}$$

and

$$\frac{1}{\Delta E}\sum \Gamma_{\lambda n}\ ;\ \frac{1}{\Delta E}\sum \Gamma_{\lambda f} \tag{7}$$

are slowly varying function of the energy, and

$$|S_0| \ll \left|\sum_{\lambda \in \Delta E} \frac{\Gamma_{\lambda n}^{1/2}\,\Gamma_{\lambda f}^{1/2}}{E_\lambda - E - \frac{i}{2}\Gamma_\lambda}\right| \tag{8}$$

The first condition means independent decay of the CN in all channels. It is the result of many component construction of the wave functio~ and randomly distributed phases of the components. This leads to additive sum of the resonance and background cross sections. Additionaly, neighbour resonances can be treated as constructed on similar way basing on the same configurations. The role of the distant resonances and potential term can be neglected (8).

There are many examples of experiments where energy spread of the projectile beam is higher than resonance spacing $\Delta E \gg D_\lambda$ or resonances are strongly overlapped $\Gamma_\lambda \gg D_\lambda$. As the result, many resonances are excited simultaneously. Taking into account conditions (6 ÷ 8) the formula (4) may be written as:

$$\langle \sigma_{nf}^{JL} \rangle \cong \frac{\langle \Gamma_{\lambda n} \rangle}{D} \cdot \frac{\langle \Gamma_{\lambda f} \rangle}{\langle \Gamma_\lambda \rangle} \tag{9}$$

This formula demonstrates independence of the creation and decay of the compound nucleus - the fundamental property of Bohr's theory.

Let us introduce a number definitions iluminating equations discussed above.The amplitudes of the transmission width used in eq. (1) tell us about overlap the resonance wave function and reaction channel or final state f.

$$\Gamma_{\lambda n}^{\eta_L} \propto \langle \lambda | \chi_E \rangle \quad ; \quad \Gamma_{\lambda f}^{\eta_L} \propto \langle \lambda | E1 | \chi_f \rangle \tag{10}$$

where: $|\lambda\rangle$ - is the isolated state of the CN,
$|\chi_E\rangle$ - is the projectile state in the complex potential,
$|\chi_f\rangle$ - is the final state of the system,
$E1$ - is the electric dipole operator. Those transitions are taken into account, only.

One can assume that residual potential is a superposition of two body interactions. Then, the $|\chi_f\rangle$ state can be written in orthonormal set of configuration constructed as:

$$|\chi_f\rangle = \sum_t C_t^f |\Psi_f \Phi_t\rangle \tag{11}$$

In such an explanation the simplest component of the $|\chi_f\rangle$ consists of a target in its ground state and highly excited quasi-particle $|\Psi_{l_0} \Phi_0\rangle$. The next group of the configurations is constructed as quasi-particle in field of the 1p1h type excited core, $|\Psi_{f1} \Phi_{1p_1 n}\rangle$. A further step of complexity will involve $|\Psi_{f2} \Phi_{2p2n}\rangle$ configurations and so on.

The $|\chi_E\rangle$ states can be presented in similar form, there is a natural continuation of the shell model states on positive energy region:

$$|\chi_E\rangle = \sum_t C_t^E |\Psi_E \Phi_t\rangle \tag{12}$$

In eqs. (11) and (12) the antisimmetrization effects are omitted. Detailed discussion on these effects you can find in papers [15], [16] and Feshbach [3].

Let us now turn to experiments with poor energy resolution of projectiles, energy resolution is 10^2 keV in order. As a classical example of this type of data

the averaged excitation function for elastic scattering of the neutrons can be given. The mentioned excitation curve exhibits a broad, so-called giant resonance ($\Gamma_{GR} \cong 4$ MeV) [17]. The existence of the giant resonances can be explained as an interaction of the projectile and the average complex potential of the target. Solution of the problem of the particle moving in complex potential induced existence of the macroscopic amplitude of the reaction. By analogy to the eq. (1) one can obtain:

$$\hat{S}_{nf} = \sum \frac{G_{mn}^{\frac{1}{2}} \; G_{mf}^{\frac{1}{2}}}{E_m - E - \frac{i}{2} G_m - iW} + S_o \tag{13}$$

where G_{mn} and G_{mf} describe the single particle resonance width for absorption of the neutron and photon, respectively. E_m and G_m are the energy and width of a single particle resonance m. W - is the depth of the imaginary part of the optical potential and the width for transition from $|\Psi_m \Phi_o\rangle$ configuration to next complexity. For neutron elastic scattering the eqs. (1) and (13) lead to the relations:

$$S_{nn} = \sum_{\lambda} \frac{\Gamma_{\lambda n}}{E_\lambda - E - i\Gamma_\lambda} + S_c^n \tag{14}$$

$$\hat{S}_{nn} = \sum_{m} \frac{G_{mn}}{E_m - E - \frac{i}{2} G_m - iW} + S_o^n \tag{15}$$

The relations between $\Gamma_{\lambda n}$ and G_{mn} can be obtained from mean value of the difference between the eqs. (14) and (15). The mean value must be equal to zero:

$$\langle \hat{S}_{nn} - S_{nn} \rangle \stackrel{def}{=} 0 \tag{16}$$

In a separate resonance region the eq. (16) leads to dependences:

$$\pi \frac{\langle \Gamma_{\lambda n} \rangle}{D} \cong \frac{G_{mn}\left(W + \frac{1}{2} G_{mn}\right)}{(E_m - E)^2 + \left(W + \frac{1}{2} G_m\right)} \tag{17}$$

and

$$\sum \Gamma_{\lambda n} \cong G_{mn} \tag{18}$$

- the strength of the single particle configurations is distributed among a large number of CN resonances. Its distribution is determined by the Lorentzian form.

Similar information concerning relation between macro and micro-structure gives us the neutron strength function as a mass number function, $\frac{\langle \Gamma_n \rangle}{D}$ ($E \cong 0$). The mass number increasing plays the same role as an increasing in the projectile energy. The single particle levels localised on a top of the potential depth are shifted down as a mass number increase. The giant resonances observed in neutron strength function are shown on fig. 1 [18].

The (n,n') excitation function measured with energy resolution of 0,01 MeV, fig. 2, reveals fine resonance structure built on a giant resonance macrostruc-

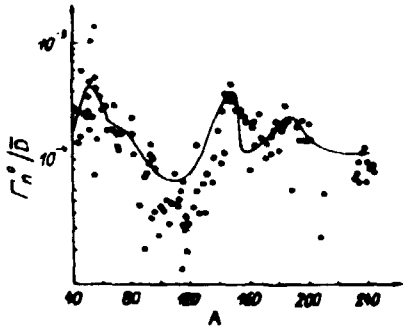

Fig. 1: The neutron strength function: experimental points and theoretical predictions based on optical model [19].

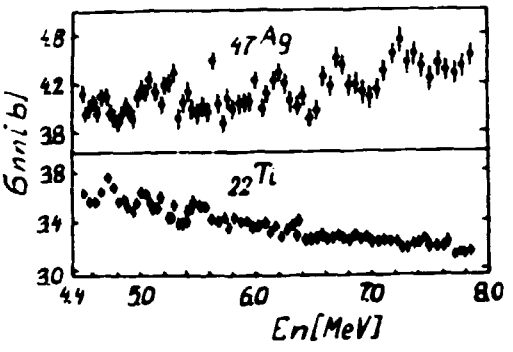

Fig. 2: The (n,n') excitation function measured with energy resolution of 0.01 MeV [1]

ture. This substructure ($\Gamma \sim 0.1 \div 0.2$ MeV) may be understood as neutron scattering on the two quasiparticle excited target, $|\Psi_E \Phi_{1p1h}\rangle$.
An equivalent model quasiparticle - vibration configuration might be assumed. The data mentioned involve a similar relation to eqs. (17) and (18), this means that $|\Psi_E \Phi_{1p1h}\rangle$ configuration is realy observed in the experiment and its strength is distributed among many CN resonances. This reasoning should be repeated for succesively incrasing complexity of the substructures. Generally, increasing step of the configuration complexity involves decreasing of the macroresonances width. Extraction of the defined type of the configuration leads to the conditions:

$$\Gamma_{n+1} \ll I \ll \Gamma_n \quad ; \quad \Gamma_{n+1} \ll \Delta E \ll \Gamma_n \tag{19}$$

where: I - is the energy interval in which experimental data are averaged, ΔE - is the energy resolution of the incoming and outgoing reaction channels.

Normally, it is very difficult to analyse the inter-mediate structure because macroresonances are not equidistant and one can to account of the interference effects. (For identification of the intermediate resonances tests proposed in [19] are useful!).

Up-to-date physicists know a good evidence concerning the role of the scattering states $|\Psi_E \Phi_o\rangle$ type and doorway states one step more complicated i.e. $|\Psi_E \Phi_{1p1h}\rangle$ type. (The doorway state means the intermediate state between incoming or outgoing configuration and more complicated configuration included to a set of CN).

The basic result of this type of investigations is the explanation of the role of averaging the experimental data and using them as a method for the intermediate structure investigations and tests for CN concept.

3. The Correlation Analysis as an Investigati : Method of the Simple Configuration Contri[illegible]ted to the Total Wave Function of the Highly Excited States

In section 2 there were presented troubles in extraction of the intermediate configuration basing on the measured structure of the excitation curves. The correlation coefficient method omits these difficultes.

The correlation $\varrho(a_i; b_i)$ between quantities a_i and b_i is defined as:

$$\varrho(a_i; b_i) = \frac{\sum_i (a_i - a)(b_i - b)}{\left[\sum_i (a_i - a)^2 \cdot \sum_i (b_i - b)^2\right]^{1/2}} \tag{20}$$

where a, b are the mean values.

Using the above definition to the radiation widths amplitude $\Gamma_{\lambda\gamma_i}$ and neutron widths amplitude $\Gamma_{\lambda no}$ or to the spectroscopic factors S_{jk}, one can denote eq. (20) as follows:

$$\varrho\left(\Gamma_{\lambda c}^{1/2}; \Gamma_{\lambda c'}^{1/2}\right) = \frac{\sum_\lambda \Gamma_{\lambda c}^{1/2} \Gamma_{\lambda c'}^{1/2}}{\left[\sum_\lambda \Gamma_{\lambda c} \sum_\lambda \Gamma_{\lambda c'}^{1/2}\right]} = \frac{\langle \Gamma_{\lambda c}^{1/2} \Gamma_{\lambda c'}^{1/2} \rangle}{\left[\langle \Gamma_{\lambda c} \rangle \langle \Gamma_{\lambda c'} \rangle\right]^{1/2}} = \frac{Im\, S_{cc'}}{\left[Im\, S_{cc} \cdot Im\, S_{c'c'}\right]^{1/2}} \tag{21}$$

- where c and c' represent reaction channels.

The relations include the fact that mean value of the width amplitudes are zero and take to account eqs. (3÷ 5).

In experiment one can measure the widths and square of the spectroscopic factors, but for theoretical purposes, it is more convenient to work with the width amplitude correlation i.e. $\varrho(\Gamma_{\lambda c}^{1/2}; \Gamma_{\lambda c'}^{1/2})$. Provided that the correlation arises from a linear relation like $\Gamma_{\lambda c}^{1/2} = \alpha \Gamma_{\lambda c'}^{1/2} + d_\lambda$ [20], [21], where d_λ is random, this is related to the width - correlation thus:

$$\varrho\left(\Gamma_{\lambda c}; \Gamma_{\lambda c'}\right) \cong \left[\varrho\left(\Gamma_{\lambda c}^{1/2}; \Gamma_{\lambda c'}^{1/2}\right)\right]^2 \tag{22}$$

Confirmation that $\varrho(\Gamma_{\lambda c}^{1/2}; \Gamma_{\lambda c'}^{1/2}) \neq 0$ means violation of the statistical conditions eq.(2) and indicates the existence of intermediate structure configurations.

In particular case the radiation width amplitude can be derived in terms of the components coupled to intermediate structure of a different step of complexity. Then, it is assumed that a series of two-body interactions occurs and the following cases are allowed:

$$|\Psi_E\ \Phi_c\rangle \rightleftarrows |\Psi_{E'}\ \Phi_{1p1h}\rangle$$

$$|\Psi_{E'}\ \Phi_{1p1h}\rangle \rightleftarrows |\Psi_{E''}\ \Phi_{1p'1h'}\rangle$$

$$|\Psi_{E'}\ \Phi_{1p1h}\rangle \rightleftarrows |\Psi_{E''}\ \Phi_{2p2h}\rangle$$

The compound system is described as the particle and hole excitations [20], [22], [23], [24]. In equivalent way the phonon excitation makes a good representation. Both models assume that equipartition of energy of the system is realised as

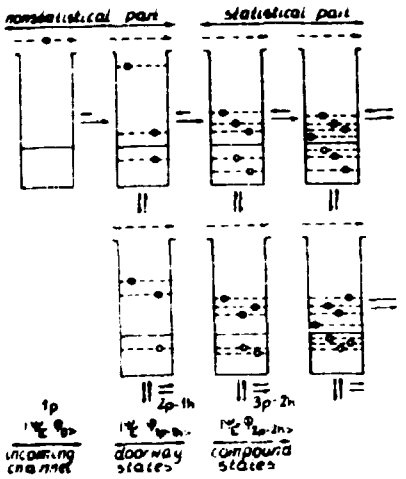

Fig. 3: Diagramic representation of the two body interactions chain. The potential wells represent various nuclear configurations. The horizontal arrow shows a particle scattering mode involve particle-hole creations or recombitations. Its length qualitatively represent transition probability between configurations.

excitation of the succesive step of freedom. Practically, the set of configuration has been devided into two parts. One of them contains a thousands of the complex configurations, condition (19) is not realised and eq. (6) is true. This part may be treated statistically. Another part contains the numerous simple configurations, condition (19) is true and this part involves nonstatistical effects.

Type of the experiment, efficency, energy and angular resolution define the possibility to extract the fine class of configurations, better one of them. A satisfied extraction one can obtain in γ -ray transitions measurement to low - energy states of the final nucleus. There are aproximated by wave function of the simple quasiparticle configurations, first of all 2p1h type.

This fact allows to interpret the emission of high energy γ -rays feeding selectively the low-energy states in accordance with step of overlap of the simple configuration of the C.N. and the exit channel. Hence, one can observed selective feeding of the low-energy states. The role of the exit channels is discussed in numerous papers [L. Papinou -1], [15], [25].

To find an interpretation that would account for all these phenomena is quite challenging. The S-matrix is found to be the sum of three parts, a direct-single particle term, a term which involves doorway state interactions, and a term which proceeds through the C.N. The Beer's results [40] for the resonance region can be summarized by an expression for a partial radiation width amplitude:

$$\Gamma^{J_\lambda}_{\lambda\gamma_i} = \underbrace{A_1 S_{jk} \Gamma^{J_\lambda}_{\lambda n_0}}_{1} + \underbrace{A_2 \Gamma^{J_\lambda}_{\lambda n_0}}_{2} + \underbrace{S_{jk} \Gamma^{J_\lambda}_{\lambda\gamma_{SDk}}}_{3} + \underbrace{\Gamma^{J_\lambda}_{\lambda\gamma_{SDj}}}_{4} + \underbrace{\Gamma^{J_\lambda}_{\lambda\gamma_j}(stat.)}_{5} \qquad (23)$$

Fig. 3 diagrammatically summarizes the connections among the configurations which lead to eq.(23).

The first term of eq.(23) (fig. 4) describes the process in which $|\Psi_E \Phi_0\rangle$ configuration is produced during collision of the incident neutron and nucleus. Another way is due to the nucleus emerging from the C.N. proceeding through the doorway configurations $|\Psi_E \Phi_{1p1h}\rangle$, moving into the exit channel and in the end radiating to a single - particle component of the final state. The transition amplitude is proportional to the resonance neutron width amplitude $\Gamma^{J_\lambda}_{\lambda n_0}$ and to the final state neutron width $\Gamma^{J_\lambda}_{jn_0} \sim S_{jk}$. The γ -ray emission is realised

on two ways. One of them is a transition of a valency nucleon, it is the so called valency model [18], channel capture [26] or radiation on the way out [27]. Second one is realised as anihilation 1p1h system and leads to the same single-particle final configuration. We take into account configurations 2p1h strongly coupled to incoming channel only. In result γ-ray emission and neutron emission may take place at the same doorway, the so called common doorway. The γ-ray radiation can be finished in one step or the system can oscillate between exit channel and C.N. before radiating. The cyclic process allows a "multiplier" effect is represented by a coefficient A_1.

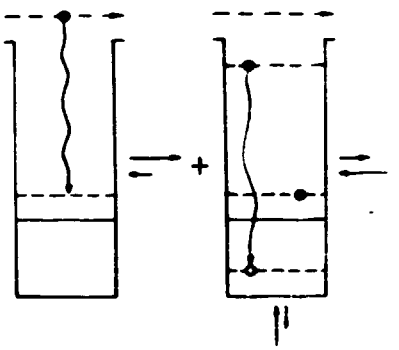

Fig. 4: Diagramoc representations of the processes described by the first term of Eq.(23). Curly vertical arrows show γ-emission.

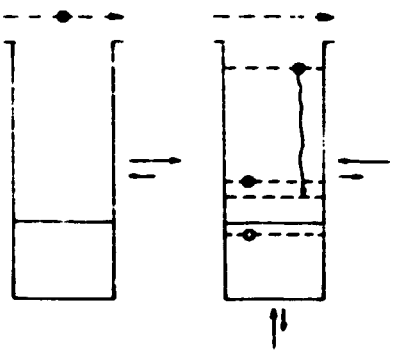

Fig. 5: Representation of the second term of Eq.(23)

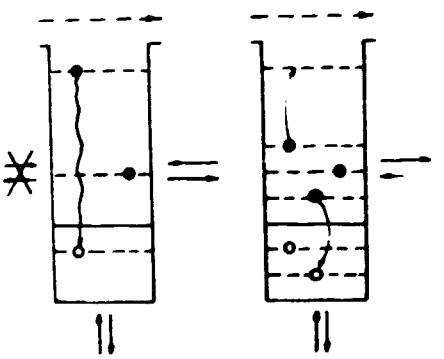

Fig. 6: Representation of the third term of Eq.(23)

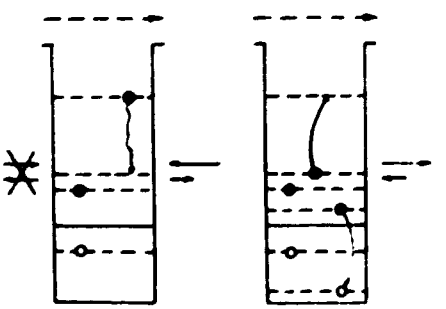

Fig. 7: Representation of the bourth term of Eq.(23)

In the second term the internuclear collisions also proceed to the 2p1h configurations, strongly coupled to incoming channel but in the end, radiates to a particle-hole $|\Psi_{E'}\Phi_{1p1h}\rangle$ portion of the final state (fig. 5). The amplitude is proportional to $\Gamma^{\downarrow}_{\lambda n_0}$ and "multiplier" factor A_2. First two terms are based on an assumption that particle-hole system is decoupled off giant E1 resonance. The processes shown in (fig. 5) and right part of the (fig. 4) have been discussed in doorway state model [28], [29], [30] and common doorway model [21]. The third term (fig. 6) has not connections with incoming channels. The C.N.

evolutes via 3p2h configurations to 2p1h one. At the end an immediate radiation to a single-particle component occurs via annihilation of a particle-hole pair. The amplitude contains a spectroscopic factor proportional to the final state neutron width $\Gamma_{j\alpha}^{n_2} \sim S_{j\alpha}$ and 1p1h annihilation amplitude of the decaying configuration $\delta_{\cdot} \Gamma_{\lambda\gamma\mathcal{D}_k}^{n_2}$.

The fourth term (fig. 7) is the result of γ -transition of one of the 2p1h type configuration to another one. This process proceeds after entering the exit configuration from C.N. in a similar way as in the third term. In this case radiation to the nonsingle-particle final state component involves the retention of the 1p1h pair but the de-excitation of the attached single-particle part, and can be achieved by $\Gamma_{\lambda\gamma\mathcal{D}_j}^{n_2}$. The third and fourth terms are based on 2p1h configurations uncoupled to incoming channels. This case was analysed in papers [31], [32] and in exit state model [33].

The fifth term is the result of γ -radiation from 3p2h, 4p3h and more complicated configurations of the CN and can be treated statistically.

The expressions we have obtained encompass several special cases which we shall now examine:

i) The statistical model is realised and partial radiation width amplitudes are random and normally distributed. One consequence of the model that correlations dissapear:

$$\rho\left(\Gamma_{\lambda n_0}; \Gamma_{\lambda\gamma j}\right) = \rho\left(\Gamma_{\lambda\gamma j}; \Gamma_{\lambda\gamma j'}\right) = \rho\left(\Gamma_{\lambda\gamma j}; S_{jk}^{\lambda}\right) = 0$$

It is important that the resonance averaged partial radiation widths are near-equally for the final state of the same spin and provided they are the same multipolarity [47].

ii) Many 2p1h configurations contribute to γ -transitions but numerous strongly overlap incoming channel-correlations are negligible.

iii) A single-particle transition is important and is reached via randomly related 2p1h configurations from the CN.
A result correlations are large [40]:

$$\rho\left(\Gamma_{\lambda n_0}; \Gamma_{\lambda\gamma j}\right) \cong \frac{\left(A_1 S_{jk} + A_2\right)^2 \langle \Gamma_{\lambda n_0} \rangle_\lambda}{\langle \Gamma_{\lambda\gamma j} \rangle_\lambda} \cong 1,$$

$$\rho\left(\Gamma_{\lambda\gamma j}; \Gamma_{\lambda\gamma j'}\right) \cong \frac{\left(A_1 S_{jk} + A_2\right)\left(A_1 S_{j'k} + A_2\right) \langle \Gamma_{\lambda n_0} \rangle_\lambda}{\left[\langle \Gamma_{\lambda\gamma j} \rangle_\lambda \langle \Gamma_{\lambda\gamma j'} \rangle\right]^{1/2}} \cong 1$$

$$\rho\left(\Gamma_{\lambda\gamma j}; S_{jk}^{\lambda}\right) \cong 1$$

iv) Many randomly related 2p1h configurations are connected to incoming channel and very few of them are involved in γ -ray emission. The correlation is small due to small "multiplier" coefficents, $A_1 = A_2 \cong 0$,
and

$$\rho\left(\Gamma_{\lambda\gamma j}; S_{jk}^{\lambda}\right) \cong \rho\left(\Gamma_{\lambda\gamma j}; \Gamma_{\lambda n_0}\right) \cong 0$$

If the same 2p1h configurations radiate to several final states, then $\rho(\Gamma_{\lambda\gamma j}; \Gamma_{\lambda\gamma j'})$ may be large and described by correlation (term third and

fourth in eq.(23)). It would be taken into account that each excited state has an E1 giant resonance built on it [36]. This fact effects the partial radiation width correlation decreasing it if in γ-transitions take part many different dipole resonances. In this situation:

$0 < \varsigma \leq 1$ - for 2p1h configurations decoupled off the E1 giant resonance,

$0 < \varsigma \leq 1$ and $\Gamma_{\lambda\gamma j} \propto E_\gamma^5$ - for 2p1h configurations coupled to one E1 giant resonance,

$0 \leq \varsigma < 1$ and $\Gamma_{\lambda\gamma j} \propto E_\gamma^3$ - for 2p1h configurations coupled to several E1 giant resonances.

v) A singel isol[illegible] 2p1h configuration plays a dominant role in exit channel and is respons[illegible] for radiation to several final states, then $\varsigma(\Gamma_{\lambda n_0}; \Gamma_{\lambda\gamma j}) = \varsigma(\Gamma_{\lambda\gamma j}; \Gamma_{\lambda\gamma_0 j}) = 1$. The case is similar to iii). Difference is that final states under consideration contain a small S^2_{jk} and correlations is $0 \leq \varsigma(\Gamma_{\lambda\gamma j}; S^2_{jk}) < 1$.

As an additional information one can use parameter $R = \langle \varsigma(\Gamma_{\lambda n_0}; \Gamma_{\lambda\gamma j}) \rangle_j$ defined as the averarge value $\varsigma(\Gamma_{\lambda n_0}; \Gamma_{\lambda\gamma j})$ over many final states j. An equally important correlation parameter is $T = \langle \varsigma(\Gamma_{\lambda\gamma j}; \Gamma_{\lambda\gamma j'}) \rangle_j$. The parameters R and T are near-zero for non-zero correlations, when several 2p1h configurations are involved in the radiation.

4. Experimental Evidence of Intermediate Structures

In this section typical experimental examples of nonstatistical effects have been presented. A main part of data is related to nuclei 3S and 4S or 3P shells. They are localised on the top of the potential well.

1. The resonance-resonance interference effects and direct processes

It is practical, experimentally, to measure in detail the partial cross-section for a given final state. It can be fitted by a formula (1) containing a sum of Breit-Wigner amplitudes and a slowly varying background, representing potential capture and distant resonances portion [Chrien - 4]:

$$\sigma^j_{n\gamma} \cong \left| S^0_j + \sum_\lambda \frac{\Gamma^{1/2}_{\lambda n_0} \Gamma^{1/2}_{\lambda\gamma j}}{E_\lambda - E - \frac{i}{2}\Gamma_\lambda} \right|^2 \qquad (24)$$

If resonances are well separated the attention should be focused on the off-resonance regions and for appreciable correlations, the S^0_j terms may be discernable. By this method the Brookhaven group determines the S^0_j term extract. It is 10^{-2}b in order in the numberous transitions. An example is shown on fig. 8.

2. The average cross sections

The case discussed in sec. 3 i) predicts that cross-section averaged over many resonances [37] should not exhibit correlations. However, for nuclei in 3P giant resonance region i.e. molibdenum isotopes, may be violated statistical distributions of the transition intensity. Riamawi and Chrien [4] are making use of an external 24 keV, Fe - filtered, neutron beam on a FWHM of 2 keV. An example a comparison of a reduced intensity of γ-transitions $I_\gamma E_\gamma^{-n}$, $(1 \leq n \leq 5)$ and spec-

troscopic factors of the final states is shown in fig. 9. It can be stressed that population intensity of the same spin states are different and quantities S^2_{jk} and $\Gamma_{\lambda\gamma_j}$ are strongly correlated. The authors suggest and $|\psi_{p\frac{1}{2}}\ \Phi_c\rangle \rightarrow |\psi_{s\frac{1}{2}}\ \Phi_c\rangle$ valency components as a source of the observed nonstatistical effects.

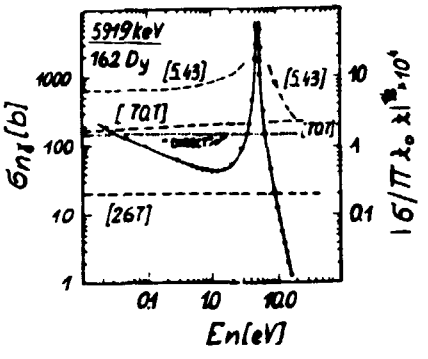

Fig. 8: Excitation function $^{161}Dy(n,\gamma)^{162}Dy$ reaction E =5.961 keV [Chrien - 4]. Dashed and dotted line - predictions based on eq.(24)

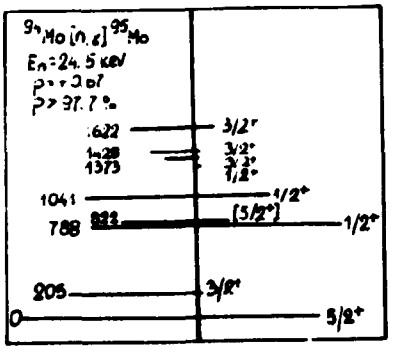

Fig. 9: Comparision of a reduced intensity of γ-transitions and spectroscopic factors of the final states. The (n,γ) experiment [Riamawi - 4] based on 24 keV, Fe filtered neutron beam.

3. The correlation $\Gamma_{\lambda\gamma_j}$ and S^2_{jk}

The radiative capture in the case of the "neutron magic" nuclei can involve either valency transition or potential capture role. In thermal neutron energy region the type of capture mechanism is relatively easy to separate taking into account consideration its different γ-rays energy dependences:

- potential capture [26]:

$$\sigma_{n\gamma} \cong \text{const}\ (Z,A) \cdot E_n^{-1}\ S^2_{jk}\ E_\gamma\ , \tag{25}$$

- capture via distant levels [20]:

$$\sigma_{n\gamma} \cong \varrho(\Gamma_{\lambda n0}\,;\,\Gamma_{\lambda\gamma_j})\,\sigma_n(abs.)\,\underbrace{\frac{\langle\Gamma_{\lambda\gamma_j}\rangle_j}{D}}_{\sim E_\gamma^3} \tag{26}$$

σ_n(abs.) - the neutron absorption cross-section,

- valency capture [25] or channel capture [26]:

$$\sigma_{n\gamma} \cong \text{const}\ (Z,A,J) \cdot E_n^{-1/2}\ S^2_{jk}\ \Gamma_{\lambda n0}\ E^3 \tag{27}$$

- statistical capture treated as simultaneuos excitation of many E1-giant resonances [38] can be written as [18]:

$$\sigma_{n\gamma} \cong \text{const.} \cdot \sigma_n(abs.)\ \underbrace{E_\gamma \sigma_\gamma\ (abs.)}_{\sim E_\gamma^5\ f(E_R,\Gamma_R)} \tag{28}$$

Above approximation is reasonable far from the E1 giant resonance maximum. $f(E_R \Gamma_R)$ - is a function of E1 giant resonance parameters and informs on the wave function of the final state.

From a comparison eqs. (25 ÷ 29) one might hope to obtain the method for the reaction mechanism to define. The potential and valency captures are directly proportional to spectroscopic factor of the final state, and the models differ in γ-rays energy dependence. Using this, the intensity ratios of two strongest γ-rays populating final states with large are considered [Mughabghab - 4]. On fig. 10 the experimental ratio of the intensities is compared with a calculated ratio based on the relation $I_\gamma \propto (2J+1)E_\gamma^n$. The agreement is reasonably good for the majority of cases when a reduction factor n = 1 for A = 24 ÷ 64 and n = 1,6 for A=136÷146 is considered. This cases indicate that capture process can be interpreted in term of hard sphere capture. The similar way for analysing the radiative capture mechanism is to study the variation of the $S(E_\gamma^{-n} \Gamma_{\lambda\gamma i}; S_{jk}^2)$ with the reduction factor n and optimalization of the correlations. The summary of both methods is schematically illustrated on fig. 11 [4]. The capture mechanism suggestion (fig. 11) is consistent with other experimental informations concerning the subject [4].

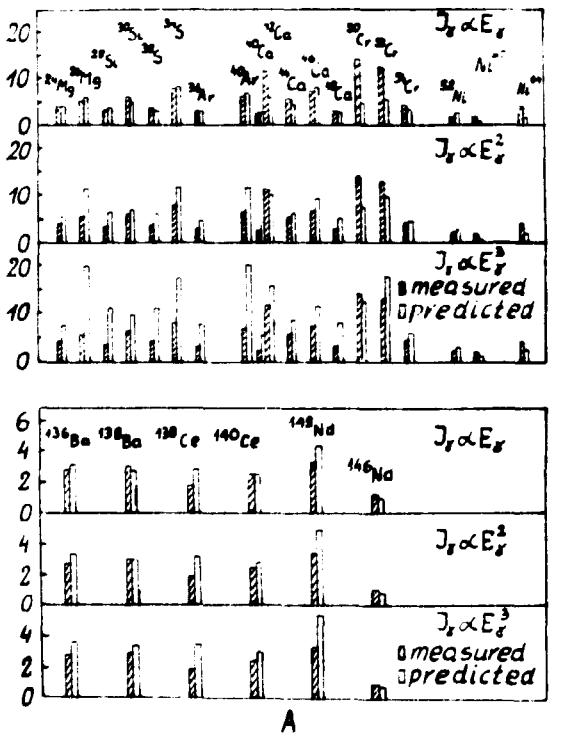

Fig. 10: Comparison of measured and predicted intensity ratios of two strongest γ-rays in two mass regions [Mughabghab-4]

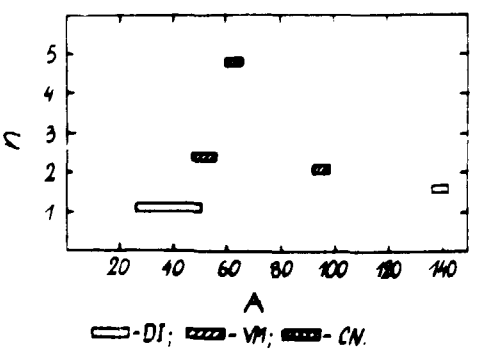

Fig. 11: Diagramic representation of optimal value of the n with atomic mass. The capture mechanism suggesion: DI, valency model VM and CN are consistent with other experimental information

4. Capture mechanism in the resonance neutron region

High energy γ -transitions for resonance capture can not be explained in term of the direct or valency model. The important part of the cross section is coupled to more complex configurations. The analysis of data is based on correlation but conclusions are not so clear as for thermal and off-resonance region. As additional information one can use correlation between (n,γ) and (γ,n) reaction or comparison of measured and predicted absolute values of the partial cross-sections. In sect. 3 it has been shown that simultaneuos correlations $\varsigma(\Gamma_{\lambda n_0}; \Gamma_{\lambda\gamma_j})$ and $\varsigma(\Gamma_{\lambda\gamma_j}; S^2_{jk})$ and $\sigma_{n\gamma} \alpha E_\gamma^3$ dependence do not mean valency process.

Up to date for resonance neutrons, we know numerous examples of different kinds of the process [4]:

- hard sphere capture i.e. ^{138}Ba [Mughabghab - 4]
- distant level capture i.e. ^{162}Dy, ^{164}Dy [Cole, Chrien -4]
- valency capture i.e. ^{24}Mg, ^{98}Mo [39]
- capture via doorway state i.e. ^{28}Si, ^{93}Nb, ^{124}Nd [Mughabghab - 4]
- statistical capture i.e. ^{127}I, ^{197}Au [Jain - 4].

These results are not complete and it is difficult to discuss a general trend.

5. Correlation of the integrated γ - spectra and neutron widths

As it has been mentioned in Sec. 3 iii) for dominance a one single particle configuration in γ-transition, and population it via many 2p1h configurations, one can predict large correlation $\varsigma(\sum_i \Gamma_{\lambda\gamma_j}; \Gamma_{\lambda n_0})$. In the experiment the integrated intensity ratio of the total intensity $E_\gamma > 5$ MeV to that for $E_\gamma < 1,5$ MeV is obtained for each resonance. If one assumes that the low γ-ray energy spectra are constant then this ratio measures $\sum_i \Gamma_{\lambda\gamma_j}$. Significant correlations are reported: $\varsigma = 0.96$ for 1+ resonances in ^{159}Tb [Jain - 4], $\varsigma = 0.40$ for Ti, Cr, Fe, Ni isotopes [41] and $\varsigma = 0$ for ^{59}Co [Spencer - 4].

5. High Energy Average γ-ray Spectra

The anomalous amplification in the γ-ray spectra, so called "bump" measured in the fifth decade was a first information concerning nonstatistical effects in CN decay. Up to date the bump has been observed for nuclei in the range around: A = 60, 110, 140, 200. The experimental material is based on (n,γ) [7], [8], [48], [49], (γ,γ') [R. Lucas - 4], [50] and $(d,p\gamma)$ [51] reactions (fig.12) for wide excitation energy range of the CN different energies of projectile. The γ-rays in bump region are generally of E1 type.

The anomalous amplification of the high energy part of the γ-spectra has been observed for all mass numbers. They take part in 50 % of radiative capture events (fig. 13). They accounted of numberous. A region has a special property- the γ-transitions are concentrated in region - 5,5 MeV and the distribution width is about 0,5 MeV.

The existence of the bump can be explained as a result of the strength func-

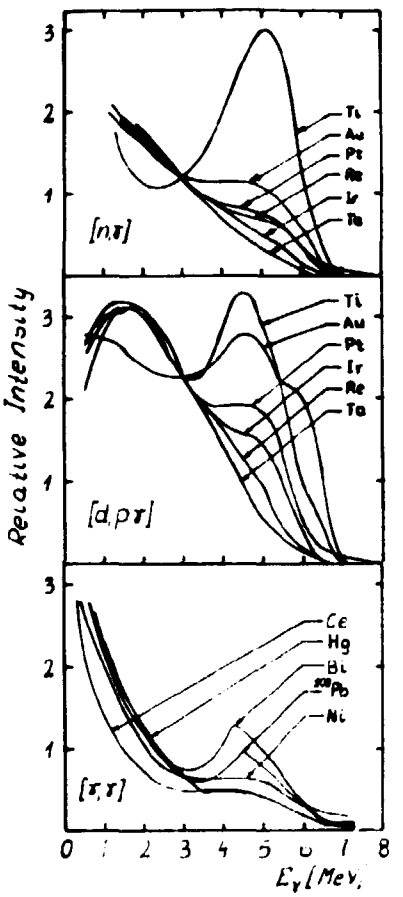

Fig. 12: The experimental data concerning high-energy part of γ-spectra induced in (n,γ), (d,pγ) and (γ,γ) reactions. [49], [51], [Lucas - 4]

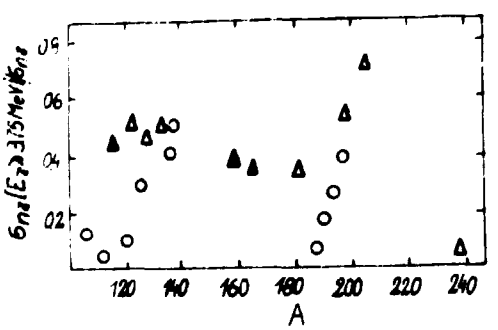

Fig. 13: Relative participation of high-energy part of γ-rays in total (n,γ) cross sections. Δ - E_n=0.4 MeV [50] O - E_n = th [Nucl. Data T].

tion shape around 5.5 MeV γ-ray energy. The anomalous form of the strength function is supported by the excitation curve data. In it a macroresonances were observed near 5.5 MeV γ-ray energy.

Different kind of experimental data strongly suggests that the γ-rays in bump region are coupled to a single particle transition component. For mass number:

A $\cong$ 60 γ-transitions are interpreted in term of valency model,

A $\cong$ 140 and A $\cong$ 200 first of all, high energy γ-rays are single particle transitions in field of the 1p1h or one-phonon excited core. [31], [33], [43], [44].

At present the basic question is the nature of the decoupling of E1 single particle transitions of low l-values from the E1 giant resonance. Generally, all E1 strength of the nuclear states is removed from energy region of the 1p1h states and relocated in giant resonance (Brown-Bolstereli model).

In numerous cases decoupling may be expected:

- The principial quantum number for the particle and hole components are different and 1p1h configuration is decoupled from the giant resonance. Additionally, when only such states are allowed $3p^{-1}2d$ configuration is decoupled [21] i.e. in ^{208}Pb the $3p^{-1}4s$, $2f^{-1}3$ and $3p^{-1}3d$ are decoupled.
- The 1p1h configuration is itself spread in energy by mixing into complicated configurations and only a fraction of configuration is coupled to the giant resonance [45].
- The 1p1h and giant resonance interaction is complex, it creates conditions for weak coupling [52].

Let us assume that in 5.5 MeV region the γ-ray strength function has a structure and it is understood from the point of view of the theory. In this case the bump

is the result of a properity of the strength function and can not be treated as nonstatistical effect. Of course, if correlation is observed, i.e. $\varrho(\Gamma_{\lambda\gamma j}, \Gamma_{\lambda n_0}) \neq 0$ or $\varrho(\Gamma_{\lambda\gamma j}, S^{+}_{j\pi}) \neq 0$ this means an existence of intermediate structure. Such an examples are known.

6. Summary

The status of studies on neutron radiative capture reflects present tendencies in investigations and understanding of nuclear reactions. The material resulting from reactions (n,γ) played an important role in assessing nonstatistical effects and directed it to studying intermediate structures.

Interpretation of statistical theory of C.N. includes a situation where wave function of the high excited state has many components [15], [40], [33], [Soloviev - 4], [Mahaux - 4]. Selection of analysed components depends on the energy resolution of the bemas used for experiment and on the exit channels or the final states of the nucleus type [25], [Papinou - 1].

Statistical approach consists in an account that the components of the wave function of the C.N. are not correlated. The probability of decay of each of them within the intranuclear chain interactions and particle or photon emission is proportional to the decay width in a definite channel. This approach differs from that one applied previously when a statistical description of population of the nuclear levels after reaction was additionally included. Recently, subtle techniques have made possible separation of final states heaving the same configuration in the wave function. Population of such states is governed by another laws than the remained groups and these properties are the key for understanding the composed structures in a C.N.

Such approach enables to understand the correlations for reaction channels (section 3) and makes clear the occurrence of the structure in excitation curves. Mostly generalized approach to the description of radiation width and correlation coefficients has been presented in the Beer's paper [40]. Particular models analysing extreme situations of the Beer's model [26], [20], [33], [15] are known, but are based on various mathematical formalisms.

The variety of this formalism applied leads to an apparent desorientation. However the fact that the results of aclency model have been confirmed with four various approaches speaks for its reliable physical basis (projection operator formalism [27], S matrix formalism [25], [42], quasiparticle-phonon excitation [Soloviev - 4], shell model [Mahaux - 4]).

Present state of our knowledge incude that decomposition of the radiation width amplitude eq. 23 causes that configurations 3p2h and more complex are treated statistically. Improving of the techniques and of studying other types of reactions can reveal the effects of more complex components, for example in reactions of $(n,\gamma\alpha)$ tyne [Popov -2] or in heavy ion reactions [3].

Let us return to the traditional reaction mechanisms. Fig. 3 suggests that the main part of intranuclear collisions is the evolution to more complex configurations, and later the oscillations between simple and complex configurations. Such a way of description of the event seem to confirm long life-times of the neutron resonances, and on the other hand, a fact that majority of the reaction

cross-section shows connections with simple configurations. Explanation of this fact is related to a rather small radiation width of high complexity configurations and in particular, to very small partial widths for transitions to low energy states. In generall, the probability of photons emission to the states described by the simple components i.e. low energy levels plays an important role [Brzosko - 4]. In special cases, as for instance for magic nuclei, one expects [Mahaux - 4] that the probability of transition of valency or doorway configuration to more complex configurations is less than particles or photons emission probability; in this case the cascade of internuclear collisions would stop at the beginning that could correspond to traditional direct or semi-direct reactions.

Both mechanisms are the source of the same type of correlations and fluctuations in the excitation curves if the same configuration is formed in the two mechanisms. The difference is in the quantity of cross-sections predicted in both approaches. It cannot be the criterion of the mechanism at the present step, rather qualitative, of the theory.

It seems that the part of research discussed above has already created a successful tool for investigations of the wave function components of highly excited nuclei.

References

[1] Lecture Notes in Physics 22 (1973), Springer-Verlag Berlin, Heidelberg, New-York. Proceedings of the Europhysics Study Conference on Intermediate Processes in Nuclear Reactions, Plidvice Lakes, 1972;

[2] Proceedings of the Conference on Nuclear Structure Study with Neutrons, Budapest, 1972;

[3] Proceedings of the International Conference on Nuclear Physics, Munich, 1973;

[4] Second Int. Symposium on Neutron Capture Gamma Ray Spect. and Related Topics, Petten, 1974;

[5] N. Bohr, Nature, 137 (1935) 344;

[6] H. Feshbach, Nucl. Spectroscopy Pt. B, ed. F. Ajzenberg- Selove, Academic Press, New York (1960);

[7] B.B. Kinsey "Beta and Gamma-Ray Spectroscopy", North-Holland, Amsterdam, 1955;

[8] L. Groshev, Dohl. Akad. Nauk, USSR, 100 (1955) 651;

[9] B.B. Kinsey, G.A. Bartholomew, Phys. Rev. 93 (1954) 1260;

[10] D.H. Wilkinson, A.M. Lane, Phys. Rev. 97 (1955) 1199;

[11] A.G.W. Cameron, Can. J. Phys., 37 (1959) 322;

[12] K.K. Seth, Phys. Lett. 16 (1965) 157;

[13] A.D. Carlson, H.H. Barshall, Proc. Intern. Conf. Study Nucl. Structure with Neutrons, North-Holland-Antwerpen (1966) 101;

[14] G.E. Brown, Rev. Mod. Phys., 31 (1959) 893;

[15] V.G. Soloviev, Phys. of Elementary Particles and Atomic Nuclei, Vol. 3, Part 4;

[16] A.M. Lane, R.G. Thomas, E.P. Wigner, Phys. Rev. 98 (1955)693;

[17] H.H. Barshall, Phys. Rev. 86 (1952) 431;

N. Narson, S. Darden, Phys. Rev. 94 (1954) 1678;
[18] J.E. Lynn, The Theory of Neutron Resonance Reactions, Clarendon Press, Oxford, 1968, p. 326;
[19] Y. Baudient-Robinet, C. Mahaux, ref. 3, 5.199;
[20] M. Beer, Phys. Rev. 181 (1969) 1422;
[21] A.M. Lane, Ann. Phys. 63 (1971) 171;
[22] M. Blann, 4th Summer School on Nucl. Phys., 1971, Rudziska, Poland, Ed. Warsaw University p.3;
[23] H. Feshbach, Rev. Mod. Phys. 46 (1974) 1;
[24] H.A. Weidenmüller, VI-th Summer School on Nucl. Phys. 1973, Nikolajki, Poland, Nucleonika 19 (1974) 401;
[25] J.S. Brzosko, Report UW-IFD 5/72 presented on Conf. /1/;
[26] A.M. Lane, J.E. Lynn, Nucl. Phys. 17 (1960) 563, 586;
[27] L. Estrada, H. Feshbach, Ann. Phys. 23 (1963) 47;
[28] B. Block, H. Feshbach, Ann. Phys. 23 (1963) 47;
[29] A.P. Jain, Nucl. Phys. 50 (1964) 157;
[30] V.I. Popov, Izv. Akad. Nauk. USSR Ser. fiz. 32 (1968) 2050; Lebedev-Fiz-Tekh-Inst. Report 44 (1969);
[31] E.D. Earle, M.A. Lane, G.A. Bartholomew, Proc. Intern. Conf. on Statistical. Prop. of Nuclei, Albany (1971), Plenum Press, /Ed. K.B. Garg/ N.Y. 1972, 263;
G.A. Barthomew "Proc. of the Int. Symp. on Neutron Capture γ-ray, Spectroscopy, Studsvik, 1969, p. 553 Vienna IAEA, 1969;
[32] K. Rimawi, R.E. Chrien, J.B. Garg, M.R. Bhat, D.T. Garber, D.A. Wasson, Phys. Rev. Lett., 23 (1969) 1041;
[33] J.S. Brzosko, J. Piotrowski, A. Soltan, Z. Szeflinski, Nucl. Phys. 189 (1972) 545;
[34] H. Feshbach, C.E. Porter, V.F. Weisskopf, Phys. Rev. 96 (1954) 448;
[35] G.R. Satchler, Ann. Phys. 3 (1958) 275;
[36] N. Rosenzweig, Nucl. Phys. A118 (1968) 650;
[37] L.M. Bollinger, G.E. Thomas Phys. Rev., 62 (1970) 1951;
[38] D.M. Brink, Nucl. Phys. 4 (1957) 215;
[39] F.S. Mughabghab, Int. Conf. on Photonuclear Reactions 1 (1973) 301, Ed. B.L. Berman;
F.S. Mughabghab, R.E. Chrien, O.A. Wasson, G.W. Cole, M.R. Bhat, Phys. Rev. Lett., 26 (1971) 1118;
[40] M. Beer, Ann. Phys., 65 (1971) 181;
[41] R.G. Stieglitz, R.W. Hockenberry, R.C. Block, Nucl. Phys. A163 (1971)592;
[42] A.M. Lane, S.F. Mughabghab, Phys. Rev. in press
[43] G.A. Bartholomew, E.D. Earle, A.J. Ferguson and I. Bergqvist, Phys. Lett. B24 (1967) 47;
[44] A.M. Lane, Proc. Int. Conf. on Statistical Properties of Nuclei, Albany, 1971, J.B. Garged, Plenum Press N.Y. 1972, p. 271;
[45] B. Gyarmati, A.M. Lane, J. Zimanyi, Phys. Lett 50B (1974) 316;
[46] M. Potokar, Phys. Lett. 46B (1973) 346;
[47] R.E. Chrien, D.I. Garber, O.A. Wasson, M. Beer, Bull. Amer. Phys. Soc. 14 (1969) 105;
[48] I. Bergqvist, N. Starfelt, Nucl. Phys. 39 (1962) 353, 529;

[49] J.S. Brzosko, E. Gierlik, A. Soltan, Z. Szeflinski, Z. Wilhelmi, Acta Phys. Polon B2 (1971) 489;
[50] J.S. Brzosko, Report INR-1271/PL;
[51] G.A. Bartholomew, I. Bergqvist, E.D. Earle, A.J. Ferguson, Can. J. Phys, 48 (1970) 687;
[52] M. Potokar Phys. Lett. 46B (1973) 346;

SESSION IV

DIRECT INELASTIC NUCLEON SCATTERING TO HIGHER EXCITED FINAL STATES

E. Arnst and R. Reif
Technische Universität Dresden, Sektion Physik, DDR 8027 Dresden, Mommsenstraße 13, GDR

Recent experimental investigations of inelastic proton and deuteron scattering with bombarding energies of 17 MeV and 12 MeV demonstrate a strong correlation of the transition strength of both reactions up to excitation energies of the nucleon separation energy [1]. From these results one can conclude, that the final states in both reaction are excited by a similar mechanism simple in nature. One can expect that first order direct processes are not only responsible for the transitions to low-lying collective states but contribute to a large extent also to the smooth back-ground as well as some resonance-like structure (giant resonances [20]) of the continuous spectra for higher inelasticity.

In a previous paper [2] the spectra and angular distributions for different excitation energies in the reaction $^{116}Sn(p,p')$, E_p = 17 MeV have been calculated with statistical assumptions on the phase and energy distribution of the two quasi-particle components of the nuclear wave functions in the mutual interaction. In extending these investigations the inelastic scattering of 14 MeV neutrons from ^{40}Ca and ^{56}Fe was considered and compared with experimental data of Hermsdorf et al. [3]. The microscopic approach to inelastic nucleon scattering has been used mainly with an effective two-body interaction of Gaussian shape and a range of 1.7 fm. Excitations up to about the nucleon binding energy were treated. In order to get absolute differential cross sections the strength of the effective interaction have been chosen to reproduce the collective excitations. The cross section obtained for each final state was transformed to a continuous spectrum according to the resolution of the time-of-flight spectrometer using a Gaussian distribution function. The calculated spectra are also compared with results from the Hybrid model [4] for precompound decay with a transition rate from the optical model.

$^{40}Ca(n,n')$

The inelastic proton scattering experiments performed with high-energy resolution for 25 MeV [5] and 17.1 MeV [6] protons allow to analyse the double differential cross sections of inelastic scattered neutrons. The first broad bump at an excitation energy between 3 MeV and 5 MeV corresponds mainly to the excitation of the 3^- phonon state at 3.73 MeV and a 5^-, 4.49 MeV level, while the 0^+, 3.904 MeV states contributes only with a cross section of 10 % of the collective state. Also the second broad peak is built up from the excitation of negative parity states (3^- (6.285 MeV), 1^- (6.948 MeV), 2^- (6.026 MeV and 6.751 MeV)) and some states of positive parity (2^+ (6.909 MeV) and 4^+ (6.505 MeV)). In the calculations the negative parity states have been taken into account only using the 1p1h wave functions of Gillet and Sanderson [7], which are given in RPA for the 3^- and 5^- levels and in a modified TDA (diagonalization of the symmetric

Table 1: Optical parameters for DWBA calculations (in MeV and fm)

	r_o	a_o	r_D	a_D	V_{ls}	r_{ls}	a_{ls}
$^{40}Ca(n,n')$ ref. [9]	1.25	0.65	1.25	0.7	5.5	1.25	0.65
	$V = 49.3 - 0.33E$, $W_{surf} = 5.75$						
$^{56}Fe(n,n')$ ref. [12]	1.17	0.75	1.26	0.58	6.2	1.01	0.75
	$V = 56.3 - 0.32 - 24\frac{N-Z}{A}$						
	$W_V = 0.22E - 2.7$, $W_D = 11.8 - 0.25E + 12\frac{N-Z}{A}$						

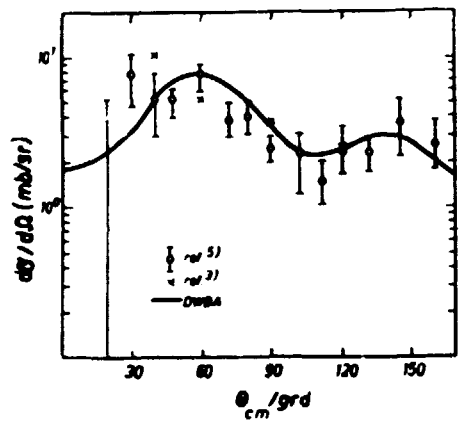

Fig. 1: Differential cross section for the excitation of the 3⁻, 3.73 MeV level in $^{40}Ca(n,n')$, E_n = 14 MeV calculated in DWBA in comparison with experimental data from refs. [7, 19].

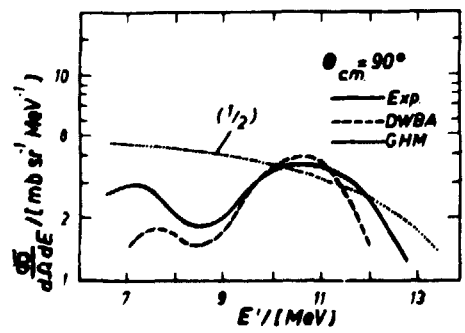

Fig. 2: Spectrum of neutrons inelastically scattered from ^{40}Ca. Solid line: experimental data [7]. Dashed line: DWBA calculation described in the text. Dotted line: angle integrated spectrum calculated from the Hybrid model.

part of the RPA matrix) for the higher excited states. The form factor have been computed with a Woods-Saxon potential (r_o=1.29 fm, a = 0.65 fm, V_{ls} = 6 MeV [8]) taking into account the single particle levels $1d_{5/2}$, $2s_{1/2}$, $1d_{3/2}$, $1f_{5/2}$, $2p_{1/2}$, $2p_{3/2}$, $1f_{7/2}$. The depth of the potential was adjusted seperately to reproduce the neutron single particle energies of ref. [7]. For the non-normal parity states a value of V_1/V_0 = 0.3 for the ratio of Bartlett and Wigner forces have been used. In order to perform the DWBA calculations the optical parameters given by Rosen et al. [9] have been used. The optical parameters for the outgoing channel have been determined from interpolation formula given there.

$^{56}Fe(n,n')$

The level schema of ^{56}Fe is known from inelastic proton scattering experiments at 17.5 MeV [10] and 50 MeV [11] incident energy. In order to compose the neutron spectrum the excitation of 2^+, 4^+ and 3^- levels are taken into account. More than 30 states with these values of spin and parity are known

Table 2: Single neutron (n) and proton (p) transitions in $^{56}Fe(n,n')$. Ground state configuration: $(1f_{7/2})^{-2}(p)$, $(2p_{3/2}, 2p_{1/2}, 1f_{5/2})^2(n)$ L: transfered angular momentum, π : parity

L	initial state	final state
2^+	$1f_{7/2}$ (p)	$2p_{3/2}$, $1f_{5/2}$
	$1f_{7/2}$ (n)	$2p_{3/2}$, $1f_{5/2}$
	$2p_{3/2}$ (n)	$2p_{1/2}$, $1f_{5/2}$
4^+	$1f_{7/2}$ (p)	$2p_{3/2}$, $2p_{1/2}$, $1f_{5/2}$
	$1f_{7/2}$ (n)	$2p_{3/2}$, $2p_{1/2}$, $1f_{5/2}$
3^-	$1f_{7/2}$ (p)	$1g_{9/2}$
	$2p_{3/2}$ (n)	$1g_{9/2}$
	$1f_{5/2}$ (n)	$1g_{9/2}$

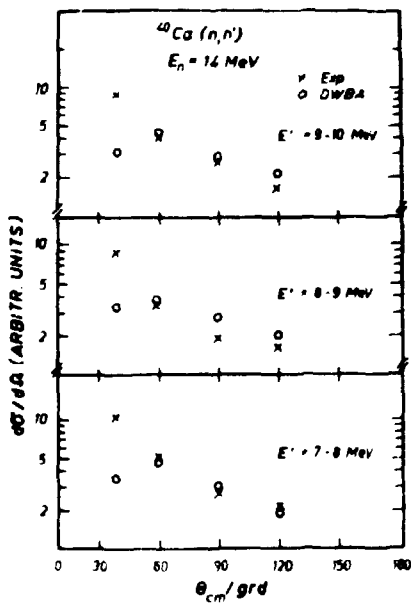

Fig. 3: Calculated and measured angular distribution of inelastically scattered 14 MeV neutrons for different regions of the energy of outgoing neutrons.

up to about 7.5 MeV. Among them are the collective excitations 2^+, 0.849 MeV, 4^+, 3.159 MeV and 3^-, 4.512 MeV, which were calculated with a collective model form factor in complex coupling. The coupling parameters were chosen to reproduce the relative transition strengths observed in the proton scattering. The non-collective states were calculated as an incoherent superposition of the single particle transitions in the neutron and proton configurations shown in table 1, which are possible from the ground state configurations $(1f_{7/2})^{-2}$ for protons and $(2p_{3/2}, 2p_{1/2}, 1f_{5/2})^2$ for neutrons above closed shells. The mean potential of Woods-Saxon shape was adjusted to the experimental single particle energies $\varepsilon_{2p_{3/2}} = 7.65$ MeV and $\varepsilon_{2p_{1/2}} = 6.59$ MeV. The strength of the effective interaction was chosen to reproduce the observed relative transition strength to the collective excitations in the inelastic proton scattering. The optical parameters of Becchetti and Greenless [12] were used in the DWBA calculation with different parameter values for the incoming and outgoing channel.

The distribution of the single particle transitions over the range of excitation corresponds to a Lorentz form with an energy independent spreading width of 7 MeV for all transitions, which is near to the strong coupling limit. Such a value is consistent with other strength function phenomena. From (d,p) stu-

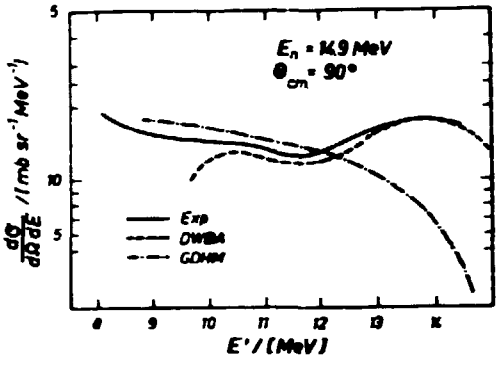

Fig. 4: Same as Fig. 2. ^{56}Fe(n,n').

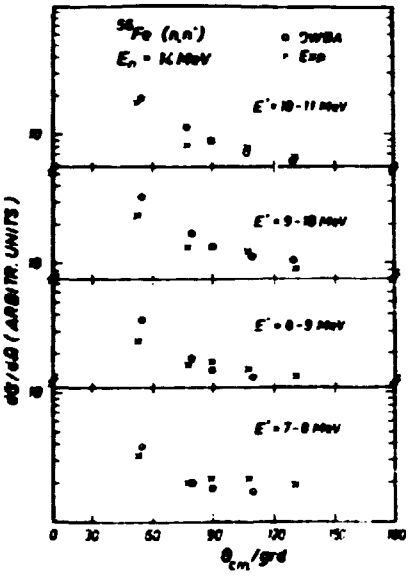

Fig. 5: Same as Fig. 3. ^{56}Fe(n,n').

dies one gets a $2p_{1/2}$ strength function of $\Gamma \approx 2$ MeV in ^{61}Ni [19]. Stripping reactions on deformed rare earth nuclei show also for excitation energies below ≈4 MeV a large spreading width for the single particle states, increasing with excitation energy according to a quadratic law [15]. As mentioned in ref. [14], for the width of the giant dipole resonance at E_x = 13.4 MeV in ^{208}Pb one has measured 4.1 MeV. The width of the giant quadrupole resonances observed at lower energies have a width of about 6 MeV [13].

The results given in fig. 1-5 may be summarized as follows:

1. In ^{40}Ca(n,n') the differential cross section for the first group of inelastically scattered protons (E' = 10-11 MeV) in which the excitation of the 3^- level is dominating is quite well reproduced with a reasonable strength of the effective interaction of V_o = 38 MeV.

2. The gross structure observed in the experiment is indicated and results from the energy distribution of the final states or of the elementary excitations.

3. Normalizing the transition strength to the collective excitations the absolute spectrum of inelastically scattered neutrons is reproduced within a factor of two up to excitation energies of about 7 MeV.
   The shape of the spectrum calculated in DWBA resembles the spectral shape predicted by the Hybrid model.

4. The forward peaked angular distribution in the high-energy precompound region is reproduced.

5. The missing transition strength at higher excitation energies expresses partly the neglect of transitions to positive parity states or of the truncation of the space of single particle states in ^{40}Ca or ^{56}Fe, respectively. But it also indicates the influence of higher-order effects.

Similar results have been obtained within a collective model approach by Lewis [16] and with simplifying assumptions on the form factor and using plane waves instead of distorted waves by Lukjanov et al. [19]. Also Tsai and Bertsch [17] came to such conclusions in the response formalismus for the transition strength.

From these results one can propose an approach to the evaluation of inelastic nucleon scattering data, which should have the advantage (compared with the Exciton or Hybrid model) to reproduce the high-energy tail of the spectra together with the angular distribution. The spectra may be decomposed in (i) an evaporation part giving rise to isotropy or symmetry around 90° in the angular distribution, (ii) a direct part, which may be calculated in collective model coupling distributing the strength of different multipole transitions according to energy weighted sum rules and (iii) a precompound part calculated from a precompound model excluding the $n_o = 3$ term.

References

[1] Cohen, B.L. et al., Phys. Rev. 39 (1974) 1025
[2] Reif, R., acta phys. slovaka 25 (1975) 208
[3] Hermsdorf, D. et al., ZfK-277 (1974)
[4] Blann, M., Nucl. Phys. A213 (1973) 570
[5] Bruhn, C.R. et al., Phys. Rev. 38 (1973) 915
[6] Gray, W.C. et al., Nucl. Phys. 57 (1965) 542
[7] Gillet, V. and E.A. Sanderson, Nucl. Phys. A91 (1967) 292
[8] Shaw, R.R. et al., Proc. Phys. Soc. 86 (1965) 513
[9] Rosen, L. et al., Ann. Phys. (N.Y.) 34 (1965) 96
[10] Peterson, R.J., Ann. Phys. (N.Y.) 53 (1969) 40
[11] Mani, G.S., Nucl. Phys. A165 (1971) 225
[12] Beccetti, F.D. and G.W. Greenless, Phys. Rev. 182 (1969) 1190
[13] Arvieux, J. et al., Nucl. Phys. A247 (1975) 238
[14] Lewis, M.B., Phys. Rev. C11 (1975) 145
[15] Back, B.B. et al., Nucl. Phys. A222 (1974) 377
[16] Lewis, M.B., Phys. Rev. 29 (1974) 1878
[17] Tsai, S.F. and G.F. Bertsch, Phys. Rev. C11 (1975) 1 [illegible]
[18] McDonald, W.J. and J.M. Robson, Nucl. Phys. 59 (1964) 321
[19] Lukjanov, A.A. et al., Jadernaja Fizika, 21 (1975) 67
[20] Satchler, G.R., Nucl. Phys. A195 (1972) 1

DETERMINATION OF THE EFFECTIVE RANGE PARAMETERS OF THE NEUTRON-NEUTRON-INTERACTION

B. Kühn, Zentralinstitut für Kernforschung der AdW der DDR Rossendorf,
DDR 8051 Dresden, Postfach 19

It is well known, that the nucleon-nucleon interaction at small energies is described in good approximation by the effective range theory. It turns out in this theory that the interaction can be characterized by only two parameters, the scattering length a and the effective radius r. A fundamental problem of nuclear forces is the question of charge dependence, that means the question wether the forces between two protons, between neutron and proton and between two neutrons are the same if the electromagnetic forces are switched off. As the scattering length depends very sensitively on the strength of the potential it is the proper parameter for checking this problem.

The proton-proton and the neutron-proton scattering legnths can be measured directly in scattering experiments. Due to the lack of neutron targets a direct observation of the neutron-neutron scattering is not possible. The only possibility up to now to observe the neutron-neutron interaction is the study of nuclear reactions from which simultaneously emerge two neutrons. Such reactions are:

$$\begin{aligned} d + n &= p + n + n \\ d + d &= p + p + n + n \\ t + n &= d + n + n \\ t + d &= {}^3He + n + n \\ t + t &= {}^4He + n + n \\ \pi^- + d &= \gamma + n + n \,. \end{aligned} \qquad (1)$$

The two emerging neutrons interact in the final state and from this effect the effective range parameters can be extracted.

The principle of determining the scattering length from these reactions is based on the principle of detailed equilibrium. According to this principle the cross sections of the reactions depend on the cross section of the neutron-neutron scattering in the final state. In the effective range theory this cross section can be expressed in the following form

$$\sigma_0(k^2) = \frac{4\pi}{k^2 + \left(-\frac{1}{a_{nn}} + \frac{1}{2} r_{nn} k^2\right)^2} \qquad (2)$$

Here k is the wave number of the relative motion of the neutrons. For $k \to 0$, that means relativ energy towards zero, formula (2) reduces to

$$\sigma_0(0) = 4\pi a_{nn}^2 \qquad (3)$$

We see, the scattering length can be determined measuring the cross section at zero energy. But in three particle reactions the cross sections depends not only on that of the neutron-neutron interaction but also on seveveral other factors. Therefore a method based on formula (3) doesn't work. For small k

($\frac{1}{2} r_{nn} k^2 \ll \frac{1}{a_{nn}}$) we can derive from equation (2) the following approximation

$$\sigma_0(k^2) = \frac{4\pi}{k^2 + \frac{1}{a_{nn}^2}} \qquad (4)$$

It represent a peak of the cross section at $k^2 = 0$ which decreases to its half value for $k^2 = 1/a_{nn}^2$.

These very simple considerations show the main conditions for the experiment. We have to observe the reactions (1) in such kinematic conditions in which the relative energy of the neutrons is near zero.

For the extraction of the scattering length from the experimental spectra several theoretical methods were used. The most simple, already expressed in equation (4), is the Migdal-Watson approximation. Further theoretical approaches are the impuls approximation, the Born approximation and the graph summation method. All these approximations consider in more or less detail only the main features of the three particle system and of the wave functions of the initial and final states. They are applicable only in the region of the peak of final state interaction, that means at small relative energies of the neutron pair. This is also *the reason, why up to now no measurements of the effective radius* r_{nn} *were produced*. It follows from equation (2), that r_{nn} has a remarkable influence on the spectra only at higher energies were the spectra are already obsured by effects not included in the approximations. Recently, however, at least for the three nucleon system d + n solutions of the exact three particle theory, the Faddeev equations, could be calculated. By this means the determination of the scattering length is possible with more confidence and it isn't further hopeless to attemot a measurement of the effective radius also. Such an experiment is in preparation in our group at Rossendorf.

Now some words concerning the experimental methods. In all the reactions (1) we have three particles in the final state. To fix a certain kinematic of the final state it is necessary to measure the energy and the direction of two particles. This can be done by means of two detectors, arranged at different angles and working on a coincidence circuit which allows to registrate a two dimensional spectrum in a multichannel analyser. Fig. 1 shows the general arrangment of the experiment. On the axis of the two dimensional plot of the spectrum we have the energies of the two registered particles. Due to the kinematics of the three particle reaction all true events are collected on a certain line in this plane, the kinematik locus (fig. 2). It is easy to choose the angle setting of the detectors in such a way, that on a certain point of the kinematic locus the relativ energy of the neutrons is zero. In the neighbourhood of this place the peak of the final state interaction is to be expected. As one knows the values of the relativ energy along the whole kinematic locus the scattering length can be adjusted by fitting the theoretical spectrum according to equation (2) or (4) to the experimental results.

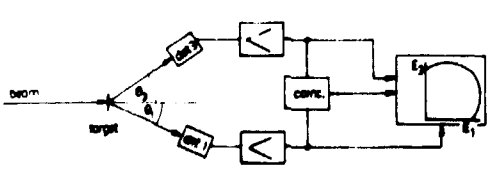

Fig. 1: Scheme of a kinematically complete experiments

This is the most advantageous method,

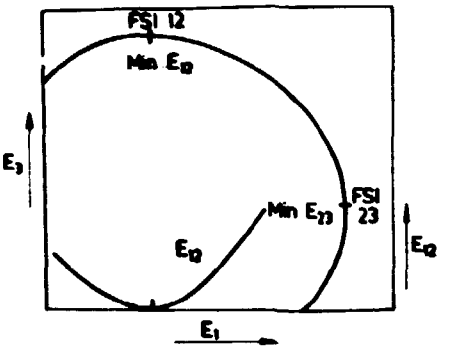

Fig. 2: Kinematic locus of a three particle reaction. On the locus are shown the places of the final state interaction of the particle paire (12) and (23). The curve E_{12} demonstrates the dependence of the relative energy E_{12} of the particle pair (12) on the energy E_1.

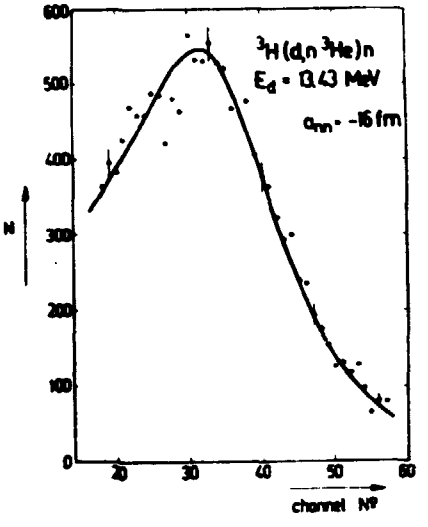

Fig. 3: Two dimensional spectrum of the reaction t(d, ^{3}He n)n projected on the time of flight axis of the registered neutron. From the spectrum a_{nn} = -16.0 fm was derived.

We have produced two experiments in this way. The first was based on the reaction t(d, ^{3}He n)n [1] and the second on the reaction t(t, ^{4}He n) n [2]. Fig. 3 and 4 show the spectra obtained, projected on the time of flight axis of the registered neutron.

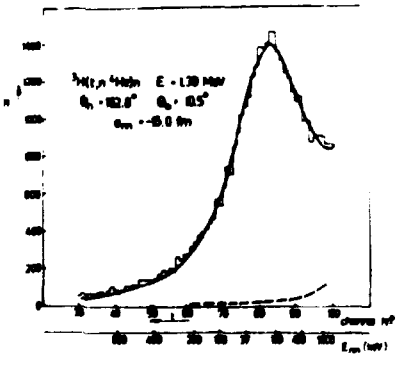

Fig. 4: Two dimensional spectrum of the reaction t(t, ^{4}He n)n projected on the time of flight axis of the registered neutron. From this spectrum a_{nn} = -15.0 fm was derived.

Many measurements were produced by kinematically incomplete experiments, that means, only one of the emerging particles was registered. In this way one integrates over the kinematics of the second particle and a one dimensional continuous spectrum is obtained. If final state interaction is dominent, this spectrum exhibits a peak at the high energy end. The form and the width of the peak can be related to the scattering length. This method is more simple from the experimental point of view but it hardly provides results of the same reliability as the kinematically complete method. Especially it is difficult to take into account the finite experimental resolutions in angle and energy.

Up to now about 40 measurements of a_{nn} were published using all reactions (1), different experimental methods and different theoretical approximations. It isn't possible to discuss all these results in such a short lecture. This was done in detail in a paper published in the Dubna journal "Physics of Elementary Particles and Atomic Nuclei" [3]. It follows from this discussion, that about

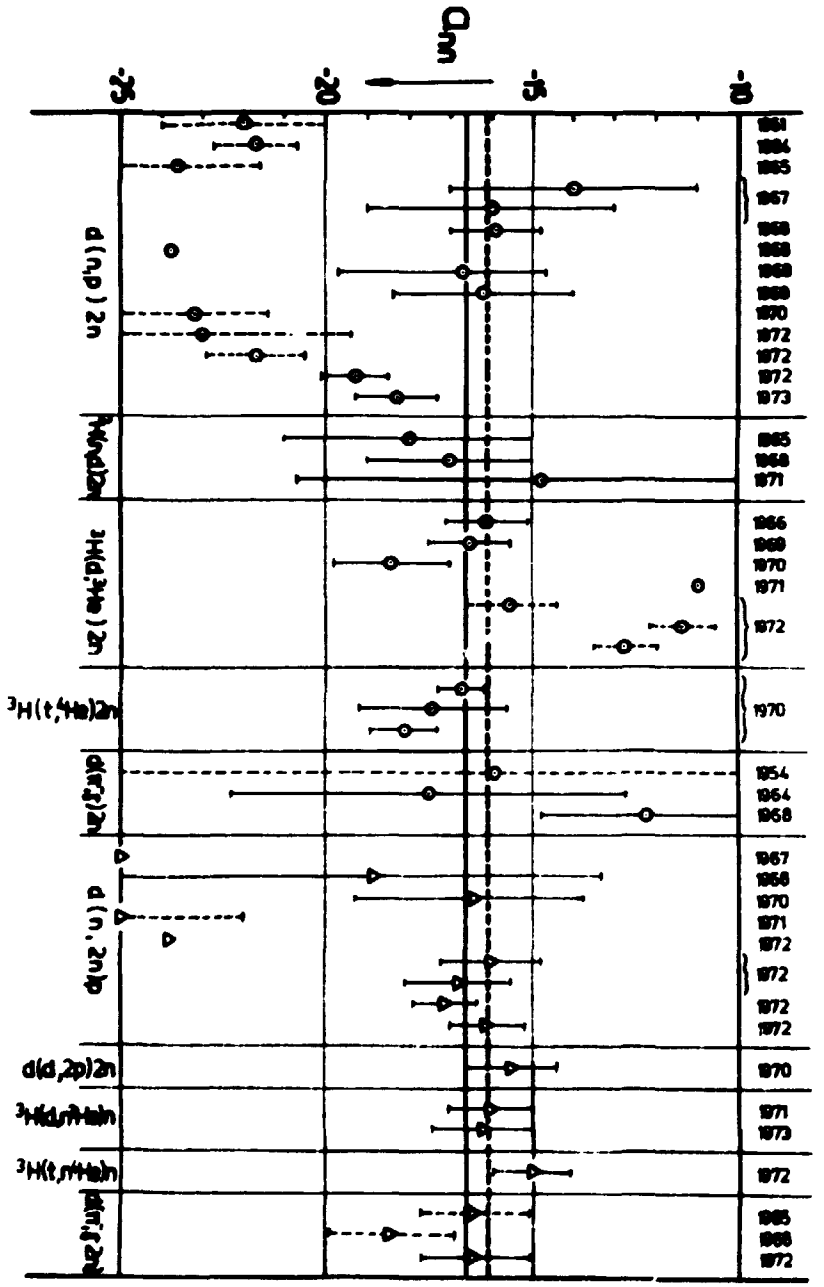

Fig. 5: Graphical compilation of the measured values of a_{nn}. The horizontal full line shows the weighted average value of all accepted values. The broken line the average value of the kinematically complete measurements alone.

10 published values must be excluded from further consideration due to unsufficiencies in the experiments or in the interpretation. This is true especially for these measurements, which resulted in values near - 23 fm.

In fig. 5 all results are compiled. Results with broken error bars were excluded. Kinematically complete measurements are designated by triangles. The about 30 reliable results fullfill the conditions of a standard distribution. This is shown in fig. 6. From this distribution the following weighted average of the scattering length could be obtained:

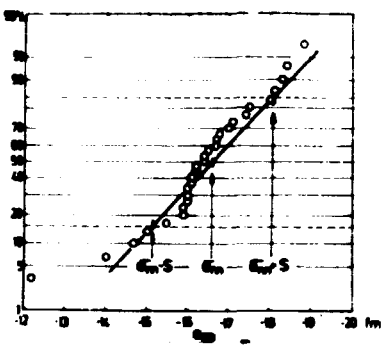

Fig. 6: Standard distribution of the accepted values of a_{nn}.

$$\overline{a_{nn}} = - 16.61 \text{ fm.}$$

In the averaging procedure the results were weighted by the errors given by the authors. The more reliable kinematically complete measurements were taken into account with twofold weight. The standard deviation of the average value is

$$S = \pm 1.45 \text{ fm}$$

and the right value can be found with 95 % confidence in the intervall

$$\overline{a_{nn}} = - 16.61 \pm 0.54 \text{ fm.}$$

This value can be compared with the pp and np scattering lengths. The difference between the np scattering length for the singulett state

$$a^s_{np} = - 23.715 \pm 0.0015 \text{ fm.}$$

and $\overline{a_{nn}}$ is well established. That means, the nucleon-nucleon interaction is charge dependent. This effect can be explained by the mass differences of charged and uncharged pions and ϱ -mesons exchanged in the interaction.

For a comparision of a_{nn} and a_{pp} it is necessary to calculate from the experimental value of a_{pp} a theoretical one for uncharged protons. The result of this calculation depends on the nuclear proton-proton potential. The well known local realistic potentials lead to a value of

$$a_{pptheor} = - 17.2 \text{ fm.}$$

The uncertainty due to different potentials is $\pm$ 0.2 fm i.e. very small. H. Kumpf has shown, that nonlocal contributions in the interaction result in an increasing difference to a_{nn} [4]. Therefore there exists apparently also a slight violation of charge symmetry of nuclear forces. By means of meson theory violation of charge symmetry may be described by meson mixing during the exchange. Henley and Keliher discussed the influence of $\varrho^0 - \omega^0$ and $\eta^0 - \pi^0$ mixing and found an effect of the right order.

We see, that the determination and comparision of the scattering lengths throw light on rather fine details of the nucleon-nucleon interaction.

References:

[1] R. Grötzschel, B. Kühn, K. Möller, J. Mösner, G. Schmidt, Nucl. Phys. A176 (1971) 261;
[2] B. Kühn, H. Kumpf, S. Parzhitsky, S. Tesch, Nucl. Phys. A183 (1972) 640;
[3] B. Kühn EPAN (1975) 347;
[4] H. Kumpf, Jadernaja Fizika 17 (1973) 1156;
[5] E.M. Henley, T.E. Keliher, Nucl. Phys. A189 (1972) 632;

PRE-EQUILIBRIUM MODEL DESCRIPTION OF NUCLEAR DE-EXCITATION FOLLOWING THE ABSORPTION OF π^- AT REST - PART I - MEDIUM HEAVY NUCLEI

E. Gadioli and E. Gadioli-Erba
Instituto di Fisica dell'Università, Milano, Italia

Abstract

The exciton model is used for describing the de-excitation of a medium-heavy nucleus which absorbs a π^- at rest. Particle multiplici ties and spectral distributions and the yield of isotopes produced are calculated and compared with the experimental findings. The comparison shows that the model allows one to describe in a quantitatively correct way the de-excitation process.

1. Introduction

The absorption of π^- at rest in nuclei has been studied in the past by means of nuclear emulsions, neutron dosimetry and activation techniques.
More recently the angular correlation of fast nucleon pairs emitted by excited nuclei and the spectrum of neutrons coming out during the de-excitation process have been measured by means of coincidence and time of flight methods.
The availability of meson factories and the possibility of using π^- beams for biomedical applications renewed the interest in the field [1-3].
The above mentioned measurements aimed to deduce:

a) the average number of neutrons emitted per pion absorbed (neutron multiplicity) and their energy spectrum,
b) in the case of nuclear emulsion experiments, the fraction of pion absorptions without the emission of ionising particles, the prong distribution of α stars, the energy spectrum of charged particles emitted, the ratio between the number of emitted α's and protons,
c) in a few cases the yield of different isotopes produced,
d) the angular correlation of fast n-n and n-p pairs and the ratio of n-n to n-p emissions.

All the experimental results reported up to now concur to strengthen the hypothesis that the pion interacts with a small number of nucleons which have an appreciable probability of escaping befor sharing their energy with other nucleons. The simplest hypothesis consists in assuming that the pion is absorbed by a couple of nucleons, a neutron and a proton or two protons. A model of this

process was developed by Brueckner et al. [4] and thereafter many theoretical refinements have been introduced.

A review of the field which reports a detailed list of references on this subject has been written by Koltun [5].
Coincidence measurements show that the emission from the de-exciting nucleus of two fast neutrons is much more likely than the emission of a neutron-proton pair and, in addition, the two particles are emitted at 180° to each other much more frequently than at a different angle [6, 7]. A great simplification in the calculations to be reported later is achieved by assuming that the total momentum of the absorbing couple of nucleons is zero. This assumption is certainly not accurate [5, 7] but should have a minor influence on most of the results we will obtain and will be retained for simplicity.

The sequence of processes developing in the nucleus after pion absorption can be schematized as follows.

Due to the short range of nuclear forces the pion absorption is assumed to occur in a rather well localized region of the nucleus. The two interacting nucleons that share the rest energy of the pion acquire an energy of approximately 70 MeV and an opposite momentum. By interacting with the surrounding nucleons they start a cascade process which eventually leads to the compound nucleus state. Due to their high energy, the nucleons excited in the first stages of the cascade process have an appreciable probability of being emitted without sharing their energy. As a consequence the average energy of the excited nucleus at the end of the fast stage of the de-excitation process is expected to be considerably lower than the rest mass energy of the absorbed pion ($\sim$ 140 MeV). The nucleus further de-excites by evaporation of low energy particles and γ rays.

On the basis of this mechanism, De Gabbata et al. [3] reported a Monte Carlo calculation which provided a qualitative agreement with nuclear emulsion data concerning pion absorption in Ag and Br. Less satisfactory results have been obtained by Fertini [9]. The above referred mechanism seems to be well suited for a preequilibrium emission model description and detailed calculations that gave results in a reasonable agreement with experimental findings have been undertaken.
This paper reports the results concerning π^- absorption in medium heavy nuclei ($A \geq 80$).

2. Summary of experimental results concerning π^- absorption in medium-heavy nuclei

2,1. Nuclear emulsion data

The results obtained by different authors [3, 10-12] before 1956 have been summarized by Demeur et al. [13]. Further results have been reported by Azimov et al. [14] and Brown and Hughes [15].

The σ stars produced in π^- absorption in an heavy nucleus (Ag, Br) have been discriminated against those produced in a light nucleus (C,N,O) according to different criteria:

a) the total charge of σ stars,
b) the influence of the Coulomb barrier that forbids that charged particles be emitted from an heavy nucleus with energy lower than $\sim$ 3-4 MeV in the case of protons and $\sim$ 6,5 MeV in the case of α particles,
c) the presence of tracks of slow Auger electrons emitted during the mesic stage of the absorption process,
d) the use of emulsions of different compositions.

The distribution of prongs due to ionizing particles, obtained as an average of the data reported by the above quoted authors, is reported in Table 1 and fig.1.

Table 1: Prong distribution of heavy emulsion nucleus σ stars

n	Percentage of stars with n prongs (%)	
	Exp.	Theor.
0	36	41.1
1	40.7	39.2
2	15.8	17.2
3	5.5	2.5
4	1.54	0.10
5	0.57	-

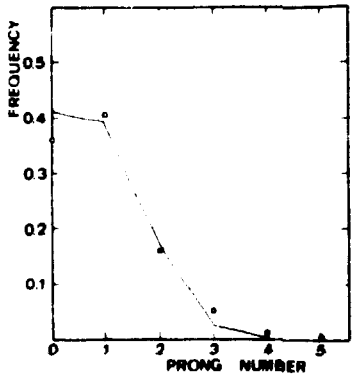

Fig. 1: Prong distribution of heavy emulsion nucleus σ stars. The open points give the experimental percentage of stars with n prongs. The full line curve is the theoretical distribution.

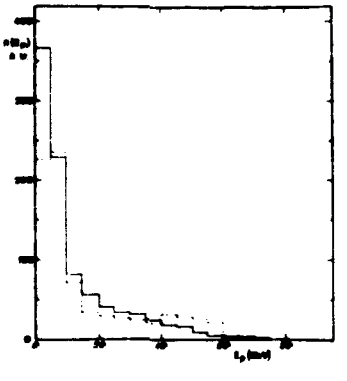

Fig. 2: The full line histogram gives the experimental energy distribution of charged particles emitted by Silver and Bromine nuclei assuming that all the particles are protons. The broken line histogram is the theoretical distribution calculated with the same assumption.

The mean number of charged particles emitted per pion absorbed amounts to 0.93.

The ratio between the number of emitted α's and the number of particles of unit charge has been estimated as 0.3 ± 0.04.

The energy distribution of charged particles emitted has been obtained by Azimov [14] (see. fig. 2) from the range distribution under the assumption that all the particles were protons.

This assumption causes an overestimation of the low energy particle yield but should effect in a minor way the high energy portion of the spectrum.

A considerably lower number of charged particles emitted per pion absorbed has been reported by Fowler and Hayes [16] as a result of an experiment performed usin water-soaked emulsions. Their results are summarized in Table 2.

Table 2:

	Number of particles per π^-		Mean Kinetic Energy (MeV)	
	Exp.	Theor.	Exp.	Theor.
protons	0.52 ± .02	0.62	21.4 ± 1.	19.5
α's	0.08 ± .01	0.192	14. ± .6	12.

2.2. Neutron Multiplicities and Spectral Distribution of Emitted Neutrons

The multiplicity of neutrons emitted by medium heavy nuclei during the fast stage of the de-excitation process (fast neutron multiplicity) has been measured in time of flight experiments [17-19]. The different authors agree in estimating that the mean number of fast neutrons emitted is ~ 2. Anderson et al.[17] measured, in the case of Cd, 1.8 fast neutrons per π^- absorbed, Campos Venuti et al. [18] gave, for Cu and Sn, the value 2.1 ± 0.5, Mattersley et al. [19] report for Cu 2.19 ± 0.30. The slow neutron multiplicity, that is the number of neutrons evaporated from excited nuclei surviving after the fast stage of the de-excitation process, has been measured directly by Tongiorgi and Edwards [20], in the case of elements varying from C to Pb, by comparing the density of neutrons produced in π^- absorption and thermalized in a block of paraffin with that of neutrons emitted by a calibrated Ra α Be source. Their results are reported in fig. 3. Total neutron multiplicities have been estimated by means of time of flight experiments [17-19] and activation measurements [21-23].

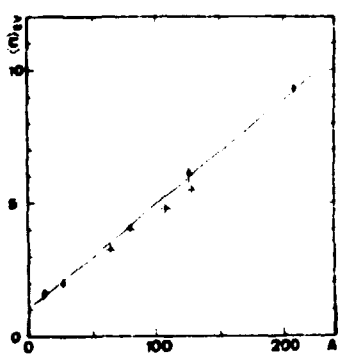

Fig. 3: Slow neutron multiplicities as measured by Tongiorgi and Edwards [20] (open points). The full line drawn through the measured points is as suggested trend. The crosses are the calculated multiplicities.

The different results are compared in fig. 4. The comparison of different results shown that these data are characterized by a considerable uncertainty. The case of lead is striking: two authors agree in measuring a multiplicity ~5 [17,19] and two authors in measuring a multiplicity almost twice (~9.4) [18, 20]. Also the average kinetic energies carried out by slow and fast neutrons are measured with a scanty accuracy. The values reported by different authors greatly differ [17-19]. An indirect estimate of the kinetic energy carried out by fast and slow neutrons can be obtained if one knows the neutrons multiplicities and the energy carried out by charged particles. For instance in the case of Silver Bromide the

average energy decrease due to charged particle emission (kinetic and binding energy) is ~ 24.8 MeV, the total binding energy of emitted neutrons (we assumed a total multiplicity of ~ 5.5 MeV) and the average energy carried away by γ rays amount to ~ 51.3 MeV. As a consequence the total mean kinetic energy carried away by emitted neutrons should amounts to ~ 63.9 MeV.

2.3 Activation Measurements

The yield of radioactive nuclei produced in pion absorption on nuclei ranging from O to Hg has been measured in a series of experiments performed at Chicago University (see ref. [21] and references therein). In some cases also the total percentage yield of the various elements produced can be inferred. In two of the reported cases, namely pion absorption in Br and ^{127}I [21,24] the results allow a detailed comparison with the theoretical predictions. The percentage yield of elements produced in pion absorption in these elements is reported in Tables 3 and 4. In figs. 5 and 6 the isotopic yield of Te and Sb produced in the case of absorption in iodine is reported.

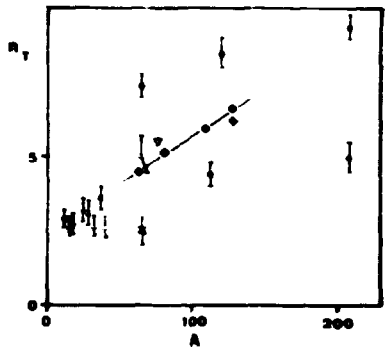

Fig. 4: Total neutron multiplicities. The different data are from Anderson et al. [17] (O), Hattersley et al. [19] (Δ), Turkevich and Fung [22] (x), Campos Venuti et al. [18] (o), Turkevich and Niday [23] (v), Winsberg [21] (+). The calculated multiplicities are also shown (◇). The line drawn through the calculated multiplicities is a suggested trend.

Fig. 6: The same as fig. 5 for Sb isotopes.

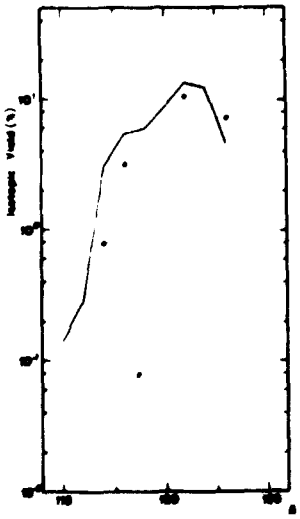

Fig. 5: Percentage yield of Te isotopes produced in π^- absorption in ^{127}I. The open points are the experimental percentages measured by Winsberg [21] The full curve is the predicted yield distribution.

Table 3: Yield of elements produced in π^- absorption in Br. [24]

Element	Percentage Yield (%)	
	Exp.	Theor.
Se	34	37
As	31	33
Ge	21	18
Ga	7	11

Table 4: Yield of elements produced in π^- absorption in ^{127}I [21]

Element	Percentage Yield (%)	
	Exp.	Theor.
Te	58	56
Sb	22	29
Sn	11	14
In	3	1

3. Theory

The exciton model that we intend to apply for describing the deexcitation process outlined in section 1 has been described elsewhere [25-32].

The two nucleons that share the rest energy of the pion are assumed to give rise to two parallel intranuclear cascades each characterized by a I particle-I hole initial configuration.
Coincidence experiments [6,7] which allowed one to mesure the n-n and n-p nucleon pairs arising from π^- capture, indicate that the ratio of the number of n-p to p-p pairs that can absorb the incident pion is approximately 4 [33].
This value has been utilised in present calculations in order to evaluate the probability of starting the de-excitation process with a I_ν, $I\nu^-$ or a $I\pi, I\nu^-$ initial configuration (thereafter the notation π, ν, π^-, ν^-, will be utilised to indicate proton, neutron proton hole, neutron hole states).

The sensitivity of the results obtained to such assumption will be discussed later. The competition between the different decay modes of the intermediate system during the cascade is expressed, as usual, by means of the decay rates for particle emission $W_c^{(n)}(U)$ and exciton exciton interaction $W_{eq}^{(n)}(U)$.

Assuming, in the course of the cascade process, a predominant neutron and proton emission the expression of $W_c^{(n)}(U)$ is given by:

$$W_c^{(n)}(U) = \frac{(2S+1)}{\pi^2 \hbar^3} \frac{m(A-1)}{A} \frac{1}{\omega_{p,h}(U)} \left\{ K_\nu(n) \int_0^{E_{max,\nu}} \sigma_{inv,\nu}(\varepsilon_\nu) \varepsilon_\nu \omega^{(\nu)}_{p-1,h}(U_R^{(\nu)}) \times \right.$$
$$\left. \times \, d\varepsilon_\nu + K_\pi(n) \int_0^{E_{max,\pi}} \sigma_{inv,\pi}(\varepsilon_\pi) \varepsilon_\pi \omega^{(\pi)}_{p-1,h}(U_R^{(\pi)}) \, d\varepsilon_\pi \right\} \qquad (1)$$

where s and m are the spin and the mass of the nucleons, A is the mass of the nucleus which absorpe the pion, n = p+h is the number of particles and holes which characterizes the configuration of the intermediate system considered, $\omega_{p,h}(U)$, $\omega^{(\nu)}_{p-1,h}(U_R^{(\nu)})$ and $\omega_{p-1,h}(U_r^{(\pi)})$ are the state densities of the in-

The decay rates for exciton exciton interactions evaluated according to the semiphenomenologic procedure of refs. [30-32] are reported in fig. 7.

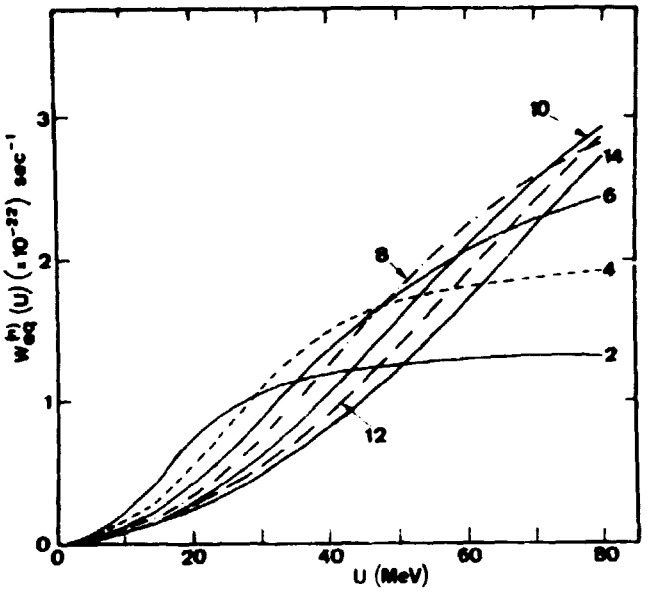

Fig. 7: Decay rates for exciton- exciton interactions as a function of the excitation energy and the exciton number n (n = p+h, p = h).

The calculation of the emission of neutrons, protons during each of the two parallel equibration cascades took into account second and third chance pre-equilibrium emissions (their contribution was small in all the cases considered). At the end of the intranuclear cascade stage of the process a quantity of highly excited nuclei are produced (in the actual case 15) with a percentage yield varying from $\sim$ 0.01, for residual nuclei after the emission of three protons and one neutron, to $\simeq$ 30-35, for residual nuclei after the emission of two neutrons. The mean excitation energies range from $\sim$ 30 to $\sim$ 140 MeV.

All these nuclei further decay by evaporation. The evaluation of the particle emission during this last stage of the process does not introduce any basic difficulty, however, due to the large number of excited nuclei and their great excitation energies, requires a big computing time.

In order to reduce this time, the approximation was been adopted of assuming that the excitation energy of each nucleus, at the end of the fast stage of the de-excitation process, is the calculated mean energy. This assumption has a minor influence on the calculated multiplicities and the spectral shape of emitted particles near the evaporative peak, but is unsatisfactory if one aims to reproduce the isotope yields measured in activation measurements, giving unreasonably small yields for isotopes at the edge of measured distributions. However the following procedure gives reasonably good results: the yield calculated with the above approximation for each isotope is subdivided in three equal portions. The three yields obtained in this way are attributed to the considered isotope and to the ones preceding and following it. The results obtained in this way have been compared with the ones obtained by taking properly into account the calculated energy distributions, at the end of the fast stage, in the case of the production of Te isotopes in π^- capture in ^{127}I. It was found that though the yield of lowest and highest mass isotopes, which contribute with a very small percentage to the total distribution, is again greatly underestimated, the yield of the isotopes in the central region of the distributions is reproduced with a reasonably accuracy ($\simeq$ 10-15 %).

termediate and residual nuclei, $\sigma_{inv,\nu}$ and $\sigma_{inv,\pi}$ are the inverse cross sections that have been calculated according to ref. [34] and $k_\nu(n)$ and $k_\pi(n)$ numerical coefficients which take into account that, depending on the assumed initial configuration and charge conservation, not all the configurations of the composite system and of residual nuclei, corresponding to a given number of particles and holes, are allowed. For the lowest n values the coefficients $k_\nu(n)$ and $k_\pi(n)$ are given in Table 5.

Table 5: Numerical coefficients to be used for evaluating $\nu_c^{(n)}(U)$

Initial configuration: 1ν, $1\nu^-$

k(n) \ n	2	4	6	8
$k_\nu(n)$	2.	1.2	1.0526	1.0145
$k_\pi(n)$	0.	0.8	0.9474	0.9855

Initial configuration: 1π $1\pi^-$

k(n) \ n	2	4	6	8
$k_\nu(n)$	0.	0.8	0.9474	0.9855
$k_\pi(n)$	2.	1.2	1.0526	1.0145

The density of p,h states has been calculated by means of the recursion formulae explicitly reported in ref. [31].

The Fermi energy has been assumed equal to 30 MeV and the density of single nucleon states has been assumed to be constant and equal to $g_o = (3/2)\,A/\varepsilon_f \ MeV^{-1} \approx A/13.3 \ MeV^{-1}$. This calculation allows one to take explicitly into account the finite depth of the potential well to which the single nucleon states are confined that at high energies noticeably reduces the density of hole states. This effect manifests itself as a broad peak in the high energy part of the emitted neutron spectrum due to the fact that, at the beginning of the cascade process, when particle emission is more likely, no residual nucleus states with energy in excess of the depth of the potential well can be excited.

The effect in proton spectrum is greatly reduced due to the small number of 1π, $1\pi^-$ initial configurations. The peak, such as it appears in the calculated spectra, is too sharp due to the simplifying assumption of zero total momentum of the absorbing pair. While the real peak should be broader than the calculated one, the average kinetic energy of the neutrons should be estimated with a reasonable accuracy. The approximation of equidistant spacings of the single nucleon states is partially counterbalanced by the assumption $\varepsilon_p = 30$ MeV, and the average excitation energy of one hole states, most important in the calculation, should be reasonably estimated. In fact a more realistic potential well is expected to be deeper than the one here considered but, on the other hand, the hole states should rarefy near the bottom of the potential well.

All the approximations, introduced in order to simplify the calculations, have a noticeable influence only on the calculated spectral shape of high energy neutrons and protons, but have a negligible influence on most of the quantities we aim to estimate. The effort of eliminating these peculiar approximations does not appear, at present, fully justified since the high energy portions of experimental neutron and proton spectra are measured with a scanty accuracy.

The total element yield are, for each element, reproduced within a few percent. This accuracy is considered sufficient for present work, however a more detailed calculation, in the case for instance of the elements of greater biological interest, should be based on the more accurate procedure.
The evaporative decay of excited nuclei was calculated with a Monte Carlo program like the one developed by Dostrovski et al.[35]. These authors, in order to deduce analytical expressions for the ratios $\frac{\Gamma_n}{\Gamma_f}$ and $\frac{\Gamma_p}{\Gamma_n}$ used simplified expressions for the level density of excited nuclei ($\varrho(U) \propto \exp(2\sqrt{aU})$) and the inverse cross sections for charged particles ($\sigma(E) = \pi R^2(1-V_c/E)$), suggesting the values to be used for R and V_c. However, in order to obtain more accurate results, values for R and V_c different by the ones suggested by these authors have been used. These values are the ones that allow one to reproduce with the analytical expressions of Dostrovski et al. the ratios $\frac{\Gamma_n}{\Gamma_f}$ and $\frac{\Gamma_p}{\Gamma_n}$ and the mean energies of the evaporated particles evaluated with a standard computer code which utilises Fermi Gas Model level density expressions and Optical Model inverse cross sections. In each of the considered cases the procedure above outlined allowed one to obtain, for all the nuclei involved in a given evaporative cascade, values of R and V_c which show a simple dependence on, respectively, A and Z.
In the calculations of pre-equilibrium emissions, pairing energy corrections were not taken into account, the binding energies were taken from Wapstra and Gove [36]. In the calculation of the evaporation stage, the pairing energies were taken from Nemirovski and Adamchuck [37] and the binding energies (most of them are not experimentally known) have been calculated by using the Myers and Swiatecki mass formula [38].

4. Comparison with the Experimental Data

The calculations have been carried on for π^- absorption in Cu, Br, Ag and ^{127}I. Some of the results obtained are summarized in fig. 9 where predicted neutron, proton and α particle multiplicities are reported. The mass dependence of the ratio α/p, the fraction of π^- absorptions without the emission of charged particles (NCP yield) and the average excitation energy $\langle E_{exc} \rangle$ of the compound nuclei after the pre-equilibrium emissions are also shown. One should, however, keep in mind that the model outlined in previous section predicts a very broad distribution for the excitation energy of residual nuclei at the end of the equilibration cascade and the average excitation energy alone cannot characterize this distribution.
Our estimated values for $\langle E_{exc} \rangle$, that agree with the estimate of De Sabbata et al. [9] are considerably lower than the ones reported in refs.[9-11, 19].
The lines drawn through the calculated points are suggested trends and could be used for interpolation. In Addition to the above shown results, the calculation predicts that during the fast stage of the de-excitation process the average total kinetic energy carried away by the protons and the neutrons amounts respectively to ~ 10 and ~ 50 MeV.

4.1 Nuclear Emulsion Data

The calculated distribution of prong of σ stars, for absorptions in Silver Bro-

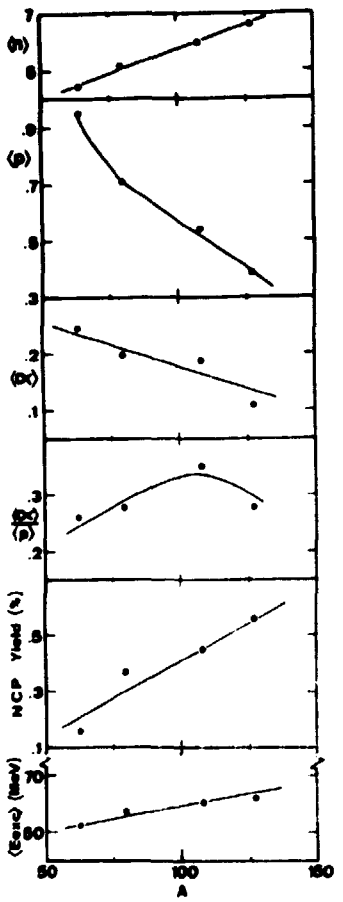

Fig. 8: Some of the predictions of the theory: <n>, <p>, <α>, neutron, proton, α-particle multiplicities. NCP is the percentage yield of absorptions without charged particle emissions, <Ecxc> is the average excitation energy of residual nuclei at the end of the fast stage of the de-excitation process.

mine is compared with the experimental one of section 2.1 in fig. 1 and Table 1. The mean number of charged particles emitted per π^- absorbed is estimated from previous distributions to be respectively 0.98 (experimental value) and 0.81 (theoretical value).

The value we calculated for the ratio between the number of emitted α's and particles of unit charge is 0.31 in good agreement with the estimate of Perkins and Menon et al. [10,11] (=0.30 ± 0.04). As previously reported, Fowler and Hayes gave for the multiplicity of charged particles a value considerably lower than the previous one [16]. These authors, in addition, estimated the mean kinetic energy carried out by charged particles. Our theoretical predictions are compared with their findings in Table 2.

The most relevant discrepancy between the calculated values and the results of Fowler and Hayes concerns the α-particle multiplicity.

The ratio α/p depend's sensitively on the heights of the Coulomb barriers for α's and protons. The mean kinetic energy of α's as deduced by Flower and Hayes is ~ 1.5 MeV higher than the one predicted by our calculations that reproduce reasonably well the ratio α/p as given by the other authors. This fact show that the α barrier height as deduced by Flower and Hayes is higher than the one suggested by previous experiments and seems to indicate that the origin of the discrepancy is the estimate of the yield of α's of lowest energy.

The energy distribution of charged particles predicted by the model is compared with the experimental one of Azimov et al. [14] in fig.2. Since these authors made the assumption that all the particles were protons we also assumed that the α's were counted as protons of about one quarter of their energy. The two distributions show a substantial agreement. The discrepancy on the high energy side is largely due to the assumption of zero total momentum for the absorbing pair. A more realistic consideration of the momentum distribution of the absorbing pair would remove the discrepancy. The discrepancy at the lowest energies, at least in part, could be due to the fact that a percentage of all the stars attributed by Azimov et al. [14] to heavy nuclei pertains to light nuclei. This suggestion is justified by the consideration that a) the prong distribution as given by these authors predicts a larger mean prong number than the ones reported by the other authors and b) the selection criterion adopted by these authors (they separate heavy nucleus from

The comparison between the calculated yield of isotopes of Te and Sb and the measured ones in shown in fig. 5 and fig. 6.

The agreement between the calculated and measured yields is surprisingly good if one takes into account that also at the maximum of the distributions the yield of different isotopes as a small percentage of the yield of all the different nuclides produced.

5. Conclusions

The comparison between the predictions of the model and the experimental results seems to indicate that the exciton model allows one to describe in a quantitatively correct way the de-excitation of a medium heavy nucleus which absorbs a π^- at rest.

This result confirms that this model constitutes a powerful tool for describing the sequence of processes which occur during the equilibration of a nucleus whose excitation energy is initially shared by a small number of particles and holes.

We assumed a value equal to 4 for the ratio of n-p to p-p pairs that can absorb the pion. Some authors suggest that this ratio should be equal to 3. This choice should not alter most of our conclusions but should reduce the number of fast neutrons and should increase the number of fast protons and the ratio of the yields of fast and slow charged particles worsening the agreement between the theoretical predictions and the experimental results.

The authors wish to thank prof. P. G. Sona for useful suggestions and enlightening discussions and prof. G. Tagliaferri for his continuous interest and encouragement.

References

[1] P.H. Fowler, Proc. Phys. Soc. 85 (1965) 1051
[2] M.P. Guthrie, R.G. Alsmiller jr. and H. W. Bertini, Nucl. Instr. Methods 66 (1968) 29
[3] T.R. Raju, Europ. J. Cancer, 10 (1974) 211
[4] K.A. Brueckner, R. Serber and K.M. Watson, Phys. Rev. 84 (1951) 258
[5] D.S. Koltun, Advances in Nuclear Physics, M. Baranger and E. Vogt Edts., Plenum Press, New York - London 1969
[6] S. Ozaki, R. Weinstein, G. Glass, E. Loh, L. Neimala and A. Wattenberg, Phys. Rev. Lett. 4 (1960) 533
[7] M.E. Nordberg jr, K.F. Kinsey and R.L. Burman, Phys. Rev. 165 (1968)1096
[8] V. De Sabbata, T. Manaresi and G. Puppi, Nuovo Cim. 3 (1956) 726; 10 (1953) 1704
[9] H.W. Bertini, Phys. Rev. 31 (1970) 483
[10] D.H. Perkins, Phil.Mag. 40 (1949) 601
[11] M.G.K. Menon, F. Muirhead and O. Rochat, Phil. Mag. 41 (1950) 583
[12] S. Enomoto, Y. Fujimoto, S. Horie and Y. Tsuzuki, Progr. Theor. Phys. 7 (1952) 353
[13] M. Demeur, A. Huleux and G. Vanderhaeghe, Nuovo Cim. 4 (1956) 509

[14] S.A.Azimov, U.G. Gulamov, R.A. Zamchalova, M. Nizametdinova, N.I. Podgoretskii and A. Iuldashev, Soviet Phys. JETP 4 (1957) 632
[15] G. Brown and I.S. Hughes, Phil. Mag. 2 (1957) 777
[16] P.H. Fowler and V.M. Hayes, Proc. Phys. Soc. 92 (1967) 377
[17] H.L. Andersen, E.P. Hincks, C.S. Johnson, C. Rey and A.M. Segar, Phys. Rev. 133B (1964) 392
[18] G. Campos Venuti, G. Prontorotta and G. Matthiae, Phys. Lett. 9 (1964) 45; Nuovo Cim. 34 (1964) 1446
[19] P.M. Hattersley, H. Muirhead and J.N. Woulds, Nucl. Phys. 67 (1965) 309
[20] V. Cocconi Tongiorgi and D.A. Edwards, Phys. Rev. 88 (1952) 145
[21] L. Winsberg, Phys. Rev. 95 (1954) 198
[22] A. Turkevich and S. Fung, Phys. Rev. 92 (1953) 521
[23] A. Turkevich and J.B. Niday, Phys. Rev. 90 (1953) 342
[24] T.T. Sugihara and W.F. Libby, Phys. Rev. 88 (1952) 587
[25] J.J. Griffin, Phys. Rev. Lett. 17 (1966) 478
[26] M. Blann, Phys. Rev. Lett. 21 (1968) 1357
[27] C.K. Cline and M. Blann, Nucl. Phys. A172 (1969) 225
[28] E. Gadioli, Nuovo Cim. Lett. 3 (1972) 515
[29] M.G. Braga Marcazzan, E. Gadioli Erba, L. Milazzo Colli and P.G. Sona, Phys. Rev. C6 (1972) 1398
[30] C. Birattari, E. Gadioli, E. Gadioli Erba, A.M. Grassi Strini, G. Strini and G. Tagliaferri, Nucl. Phys. A201 (1973) 579
[31] E. Gadioli, E. Gadioli Erba and P.G. Sona, Nucl. Phys. A217 (1973) 589
[32] E. Gadioli, E. Gadioli Erba, L. Sajo Bohus and G. Tagliaferri, Rivista Nuovo Cim., to be published
[33] V.I. Fedotov, Soviet J. Nucl. Phys. 2 (1966) 335
[34] E. Gadioli, E. Gadioli Erba and P.G. Sona, Nuovo Cim. Lett. 10 (1974)373
[35] I. Dostrovski, Z. Fraenkel and G. Friedlander, Phys. Rev. 116 (1959)683
[36] A.H.Wapstra and N.B. Gove, Nucl. Data Tables 9, nos 4 and 5 (1971)
[37] F.E. Demirovski and Yu. V. Adamchuck, Nucl. Phys. 39 (1962) 551
[38] J.D. Myers and W.J. Swiatecki, Nucl. Phys. 81 (1966) 1; Ark. Fys. 36 (1969) 343

THE INFLUENCE OF THE CONTINUUM ON THE WIDTHS AND POSITIONS OF RESONANCE LEVELS

I. Rotter, H.H. Marx
Zentralinstitut für Kernforschung Rossendorf, GDR

J. Höhn
Technische Universität Dresden, Sektion Physik, GDR

1. Introduction

The question how strong the continuum changes the resonance parameters calculated in a bound state model has been discussed frequently during the last time (e.g. 1,2). First, there may be threshold effects which can lead to an additional change of the reaction cross section in the neighbourhood of particles decay thresholds because of the enlarged extension of the system. Secondly, the mixing of the resonance levels via the continuum may change the positions as well as the widths of the resonance levels calculated in a bound state model. The changes may be of such a type that they can not be compensated by using effective parameters.

It is the aim of this paper to investigate the influence of the continuum on widths and positions of resonance levels in a case in which the resonance levels have a complicated shell model structure. The calculations are done in the continuum shell model (CSM) for the reaction ^{15}N+n. The $d_{3/2}$ single particle resonance is treated like a bound state up to a cut-off radius in order to define the space of bound states in analogy to the configuration space of the usual shell model (SM). The details of the calculations are given in sect. 2 of this paper while the effects investigated and the results obtained are described in the sects. 3, 4 and 5. Some conclusions are drawn in the last section.

2. The Calculations

The basic equations of the model are given in refs. [3, 4]. The whole wave function of the model is given by

$$\Psi = \zeta + \sum_{RR'} (W_R - \Phi_R) < \Phi_R \left| \frac{1}{H_{QQ}^{eff} - E} \right| \Phi_{R'} > < \Phi_{R'} \left| H_{QP} \right| \zeta > \qquad (1)$$

Here, H_{QP} stands for QHP etc., the operator Q projects onto the space of discrete resonance states and the operator P onto the continuum (P + Q = 1), while H is the Hamilton operator. The functions ζ and W_R are solutions of the equations

$$(H_{PP} - E)\,\zeta = 0 \qquad (2)$$

$$(H_{PP} - E)\,W_R = H_{PQ}\,\Phi_R \,. \qquad (3)$$

The wave functions Φ_R are eigenfunctions of the operator H_{QQ}. The operator

$$H_{QQ}^{eff} = H_{QQ} - H_{QP}\,\frac{1}{H_{PP} - E}\,H_{PQ} \qquad (4)$$

is effective in the Q space.

The method of numerical calculations consists in solving the usual SM problem

$$(H_{QQ} - E_{sh}^{(R)})\ \phi_R = 0 \qquad (5)$$

which gives the eigenvalues $E_{sh}^{(R)}$ and eigenfunctions ϕ_R of the operator H_{QQ}. Using these eigenfunctions, the equations (2) and (3) are solved with the coupled channel method [3, 4].

The diagonal matrix elements

$$\langle \phi_R \mid H_{QQ}^{eff} \mid \phi_R \rangle = U_R - \tfrac{i}{2}\ V_R \qquad (6)$$

contain the energies U_R and the widths V_R of the resonance levels described by the SM wave function ϕ_R. Here, the configuration mixing of the discrete resonance states is taken into account like in a usual SM calculation. The channel coupling, i.e. the interaction of the resonance levels via the continuum, is considered in the eigenvalues $E_R - \frac{i}{2}\ \Gamma_R$ and eigenfunctions $\tilde{\phi}_R$,

$$\langle \tilde{\phi}_R^* \mid H_{QQ}^{eff} \mid \tilde{\phi}_R \rangle = E_R - \tfrac{i}{2}\ \Gamma_R , \qquad (7)$$

which follow from the diagonalization of H_{QQ}^{eff} .

The numerical calculations reported here are performed for the ^{15}N +n reaction. The SM strucutre of the intermediate nucleus ^{16}N and the target nucleus ^{15}N is obtained in the 1p - 1h and 2p - 2h configuration spaces, and the 1 h and 1p-2h configuration spaces, respectively, using a δ -force for the nucleon-nucleon interaction,

$$V(\vec{r}_1 - \vec{r}_2) = V_0\ (a + b\ P_{12}^{\sigma})\ \delta(\vec{r}_1 - \vec{r}_2) . \qquad (8)$$

The parameters are $V_0 = 500$ MeV $\cdot$ fm^3, $a = 1.0$, $b = 0.05$. The parameters of the Woods-Saxon potential are the same as in ref. [3]. Together with the bound states the $d_{3/2}$ single particle resonance is included in the Q-space up to the cut-off radius 7.5 fm, while the $d_{3/2}$ continuum part and the single particle scattering states of the other angular momenta l_j define the P-space. The continuum is restricted to $l \leq 6$ in the coupled channels calculations. The calculations are performed by taking into account four channels corresponding to the two hole states $1/2^-$ (0 MeV) and $3/2^-$ (6.3 MeV) of ^{15}N and to the two states $5/2^+$ and $1/2^+$ at 5.3 MeV of ^{15}N with 1p - 2h strucutre.

3. The Mixing of Resonances via the Continuum

In order to investigate the mixing of the resonances via the continuum in more details, six 0^+ resonance states of ^{16}N are investigated. The energies $E_{sh}^{(R)}$ of these states are chosen different from the eigenvalues of H_{QQ} in such a manner that the distances between the resonances are constant (200 keV). The wave functions ϕ_R are taken from the SM-caloulation without any change.

In fig. 1, the widths V(E) and Γ (E) defined in eqs. (6) and (7) are shown for one of the considered 0^+ levels. The energies $E_{sh}^{(i)}$ of the other levels are chosen in such a manner that $E_{sh}^{(1)} > E_{sh}^{(i)}$ (full line), $E_{sh}^{(1)} < E_{sh}^{(i)}$ (dashed line), and $E_{sh}^{(i)} < E_{sh}^{(1)} < E_{sh}^{(j)}$ (dotted and dash-dotted lines), respectively. The ener-

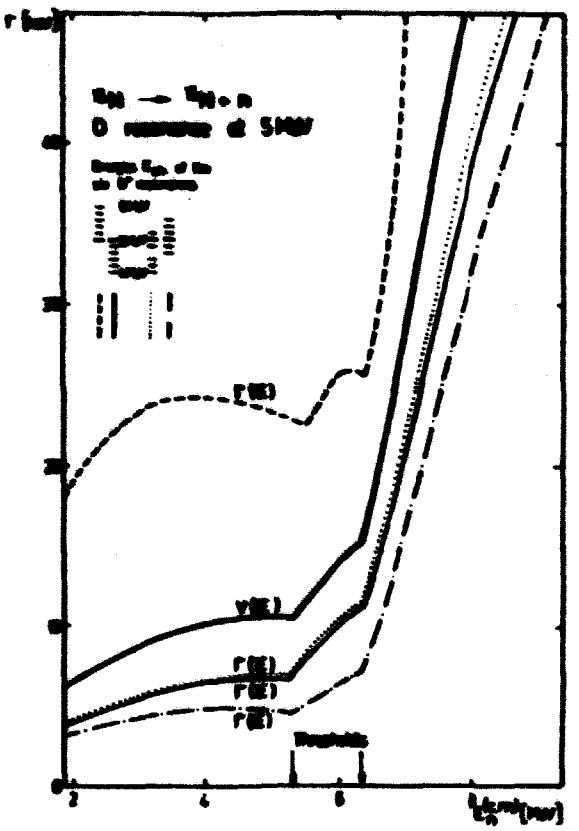

Fig. 1: The energy dependence of the widths V and Γ of the 0^+ resonance state No. 1. The widths Γ_j (E) are given for four different positions of the five surrounding 0^+ resonances. Sequence of the resonances: 1 2 3 4 5 6 (dashed, 2 3 4 5 6 1 (full), 2 3 4 6 1 5 (dotted), 3 2 1 4 5 6 (dash-dotted), see the upper part of the figure. In the case of 5 MeV $\leq E_{sh}^{(R)} \leq$ 6 MeV, the energies E_R(c.m.) and widths Γ_R of all the resonances are: 4,97 MeV - 23 keV, 5,03 MeV - 27 keV, 5,30 MeV - 88 keV, 5,53 MeV - 5 keV, 5,72 MeV - 4 keV, 5,99 MeV - 0,5 keV.

gy dependence of Γ and V is similar in all cases, but $\Gamma(E_R)$ and $V(U_R)$ differ from each other by a factor up to three. In all cases, the width of the resonance lying at the lowest energy is enlarged at the cost of the resonances lying at higher energies. This effect seems to be similar to the effect well known in structure calculations by which the lowest level is most collective. The only difference is that the energy E_R of the lowest resonance is almost not changed compared with U_R in the case considered in fig. 1.

The mixing of the resonances via the continuum would be very different from that shown in fig.1 if the main part of the $d_{3/2}$ single particle resonance inside the nucleus would not be included in the Q space of discrete states. Thus, a mixing of the resonances via the continuum exists though almost all components of the wave functions which have large amplitudes inside the nucleus are taken into account already in diagonalising H_{QQ}.

4. The Influence of the Level Overlapping on the Resonance Parameters

The mixing of the resonances via the continuum is expected to depend on their mutual overlapping. Therefore, it seems to be reasonable to vary the energy distances between the resonances in order to investigate the mixing of the resonances via the continuum.

The calculation are done for five 0^+ resonances of the ^{16}N nucleus. In the first

case, the distance between the positions $E_{sh}^{(R)}$ of the resonance levels are 200 keV, in the second case 100 keV and in the third case 50 keV. The wave functions ϕ_R used in the calculations are not changed.
In the case of small level overlapping the functions ϕ_R are almost pure in the wave functions ϕ_R (nearly 95 % at 200 keV distance and no less than 75 % at 100 keV distance), whereas they are strongly mixed in the ϕ_R if the overlapping is stronger (at 50 keV distance between the $E_{sh}^{(R)}$. In fig. 2, the energies U_R and E_R and the widths V_R and Γ_R of all five resonances are shown which are obtained by changing the distances between the resonances. The shifts $U_R - E_{sh}^{(R)}$ and the widths V_R are not depending on the level distances. The changes in the sequence $U_R^{(i)}$ of the resonances compared with the sequence $E_{sh}^{(i)}$ is connected with the fact that $U_R - E_{sh}^{(R)}$ is different for the different resonance states and sometimes larger than the distances between the resonances. The energies E_R and widths Γ_R containing the coupling of the resonances via the continuum show some regularities in depence on the level overlaping: The width of the lowest resonance level is enlarged at the cost of the widths of the higher lying levels. Moreover, the lowest level is shifted additionally to lower energy and the highest level to higher energy so that the distance Δ between them becomes larger than in the case without channel coupling. The observed effects become larger if the resonance levels are more overlapping. For the lowest and the highest resonance levels the shifts and widths are given in table 1 in the case of 50 keV distance between the energies $E_{sh}^{(R)}$.

Fig. 2: The energies and widths of five 0^+ resonances in ^{16}O before the diagonalization (U_R, V_R) and after the diagonalization (E_R, Γ_R) of the operator H_{eff}. The distances between the SM energies $E_{sh}^{(R)}$ are changed from 50 keV to 100 keV and 200 keV. The obtained distance Δ between the lowest and highest lying resonances is given in the figure.

The effects shown in fig. 2 and in table 1 are of the same type as the effects which are well known from nuclear structure calculations. Like in structure calculations, the lowest level is more collective than the higher lying levels. It should be remarked here that the energy dependence of Γ is smooth for overlapping resonances like for isolated resonances though the absolute value Γ_R strongly depends on the mixing of the resonance level via the continuum.

Table 1: The shifts $E_R - E_{sh}^{(R)}$, $E_R - E_{sh}^{(R)}$ and the widths Γ_R, Γ_R of the lowest and highest lying 0^+ resonance level of ^{16}N. The calculations are performed with five 0^+ resonance levels the positions $E_{sh}^{(R)}$ of which are equally spaced by 50 keV.

Resonance	$E_R - E_{sh}^{(R)}$/keV	$E_R - E_{sh}^{(R)}$/keV	Γ_R / keV	Γ_R / keV
lowest	- 120	- 180	152	237
highest	- 50	0	31	9

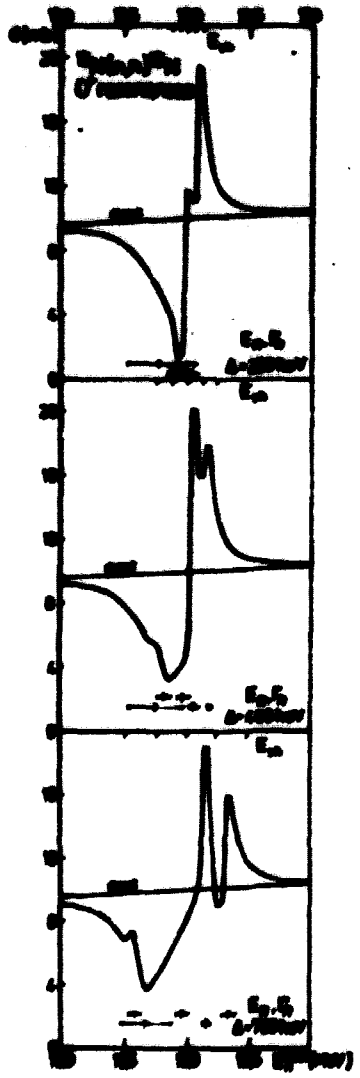

Fig.3: The cross section of the elastic $^{15}N+n$ scattering with five 0^+ resonance states. The distances between the energies $E_{sh}^{(R)}$ are varied from 50 keV to 100 keV and 200 keV. The energies E_R and widths Γ_R of the resonances are shown below the cross section. For Δ see fig. 2

5. The Influence of the Level Overlapping on the Cross Section

For the cases shown in fig. 2 the cross section of the elastic neutron scattering on ^{15}N is calculated (fig.)). Whereas the different resonances can be identified in the case with small level overlapping (200 keV distance between the energies $E_{sh}^{(R)}$), this cannot be done in the case of stronger level overlapping (50 keV distance between the energies $E_{sh}^{(R)}$). In the last case, the peaks in the cross section are connected with interference effects. In all cases, the cross section has an intermediate-like structure the width of which is determined by the distance Δ between the lowest and highest resonances.

In fig. 4, the cross sections of the inelastic channels are shown in the case of 50 keV distance between the energies $E_{sh}^{(R)}$. The intermediate-like structure of the cross section is obtained also in these channels. The position of the centre of gravity depends, however, a little on the values of the partial widths.

The elastic cross section of the $^{15}N+n$ reaction in dependence of the number of resonances is shown in fig. 5. In the first case, the cross section is determined by only one 0^+ resonance (dashed curve). If other 0^+ resonances are added, then the shape of the cross section is changed, but an intermediate-like structure remains which is determined by the value of the interval Δ in which the resonances are lying.

The figs. 3,4 and 5 show that it is difficult to identify different resonances even in the case $\Gamma \approx D$. Also in the case in which the resonance parameters are changed only a little by the

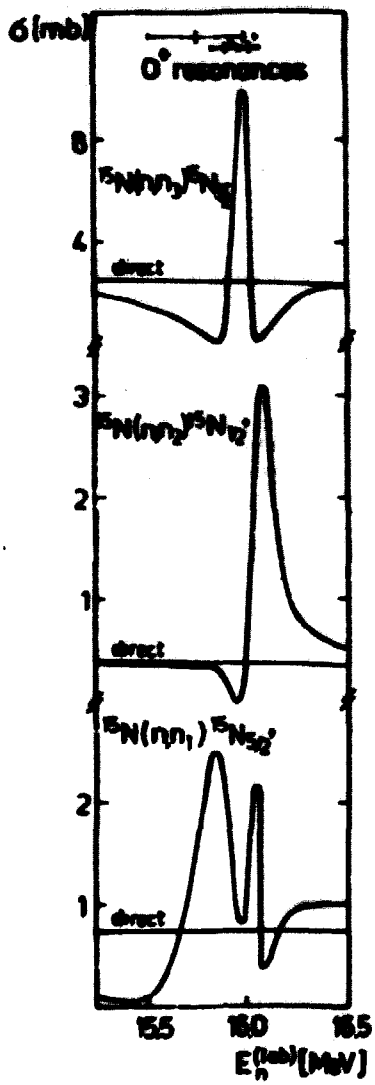

Fig. 4: The cross section of the inelastic $^{15}N+n$ scattering with five 0^+ resonances at 50 keV distance between the energies $E_{sh}^{(R)}$. The energies E_R and widths Γ_R of the resonances are shown in the upper part of the figure.

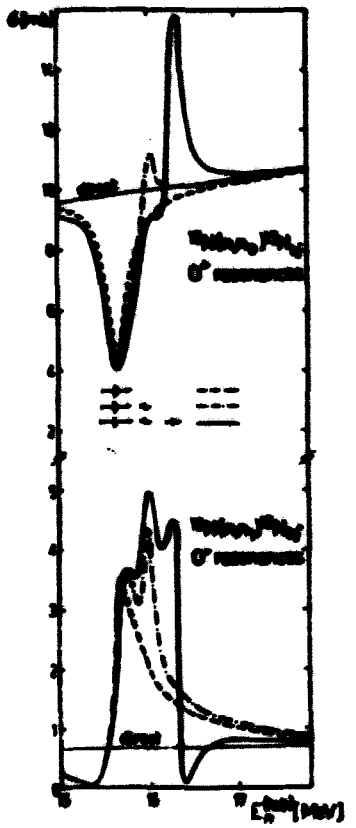

Fig. 5: The cross section of the elastic and inelastic $^{15}N+n$ scattering for a different number of 0^+ resonances. The number, the positions E_R and the widths Γ_R of the resonances are shown in the middle of the figure.

mixing via the continuum, the cross section would have an intermediate-like structure depending on the level density.

5. Conclusions

In this paper the mixing of the resonance states via the continuum is shown to exist even in those cases in which the contribution of the single-particle resonances inside the nucleus is excluded from the continuous spectrum. Effects in the mixing via the continuum are observed which are analogous to effects well known in the mixing of discrete states. The width of the lowest level is found to enlarge at the cost of the widths of the higher lying levels. Furthermore, the interval Δ between the resonances enlarges like in structure calculations.

The cross section shows an intermediate-like structure also in the case with small level overlapping. The distance Δ between the lowest level and the highest level which is characteristic for the energy dependence of the cross section depends on the degree of the level mixing. Therefore, also the shape of the cross section depends on the mixing of the resonances via the continuum.

At higher excitation energies, fluctuations in the level density are of some importance. Therefore, intermediate structures in the cross section may appear at these energies which are connected with level density fluctuations. The "width" of such an intermediate structure which is determined by Δ is larger as it would be expected from the energies $E_{sh}^{(R)}$ obtained in a usual SM calculations. Moreover, two resonance levels mixed strongly via the continuum do not come so close to each other as the CSM calculations without channel coupling predict.

References

[1] C. Mahaux, H.A. Weidenmüller, Shell-Model Approach to Nuclear Reactions, Amsterdam, North-Holland, 1969

[2] C.Mahaux, A.M. Saruis, Nucl. Phys. A177 (1971) 103

[3] H.W. Barz, I. Rotter, J. Höhn, Phys. Letters 37B (1971) 4

[4] I. Rotter, H.W. Barz, R. Wünsch, J. Höhn, Particles and Nucleus (USSR) 6 (1975) 435

УГЛОВЫЕ РАСПРЕДЕЛЕНИЯ ОСКОЛКОВ ПРИ ДЕЛЕНИИ ^{235}U НЕЙТРОНАМИ С ЭНЕРГИЕЙ 24 КЭВ

Е. Дермендиева, Н. Калинкова, Н. Минтов, Н. Чиков

Институт ядерных исследований и ядерной энергетики Болгарской АН, Болгария

Аннотация

Измерено угловое распределение осколков при делении ^{235}U нейтронами с энергией 24 кэв. Экспериментальное распределение аппроксимировано функцией $W(\theta)=1+A\cos^2\theta$ с $A = -(1{,}8 \pm 1{,}6)\cdot 10^{-2}$. Показано, что отрицательный знак анизотропии обусловлен делением через каналы с $J^\pi = 2^+$ и $4^+(K = 2)$.

В работах [1, 2] было обнаружено, что при энергии бомбардирующих нейтронов $E_n \leq 0{,}1$ Мэв угловая анизотропия осколков деления ^{235}U отрицательна. Более поздние исследования [3] подтвердили наличие небольшой отрицательной анизотропии $A < 0$, где

$$A = \frac{W(0^\circ)}{W(90^\circ)} - 1 \qquad (1)$$

По данным работ [2, 3] $|A| \leq 0{,}1$ при 50 кэв $< E_n <$ 150 кэв. Особый интерес, по нашему мнению, представляют попытки авторов работ [2 - 4] объяснить этот эффект. Действительно, следуя работе [2] и предполагая, согласно [5], статистическое распределение K - проекции спина J на ось симметрии делящегося ядра, - в виде

$$F(K) \sim \exp[-K^2/2K_0^2] \qquad (2)$$

с $K_0 \sim 1{,}5 - 2{,}5$, качественно удается объяснить ход угловой анизотропии осколков в зависимости от E_n и спина ядра-мишени I. Однако является удивительным, что при энергии возбуждения делящегося ядра E^*, превышающей высоту наиболее низкого барьера деления $E_f^{3/2,K^\pi}$ на ~ 1 Мэв, остается справедливым статистическое распределение K и ф-ла (2). Количественное описание угловой анизотропии осколков деления неориентированных ядер ^{235}U нейтронами с 50 кэв $< E_n <$ 150 кэв, предпринятое авторами работ [3, 4] на базе концепции двугорбого барьера деления [6] показало, что расчетные значения $|A|$ всегда меньше экспериментальных. Для устранения этого различия авторы вынуждены были предположить во-первых, что при E_n = 100 кэв все акты деления ядер ^{235}U вызваны p-нейтронами и, во-вторых, - высокую степень вероятности деления через канал с $J^\pi = 4^+$, который определяет отрицательный знак анизотропии.

Поскольку данные по анизотропии осколков, полученные в работах [1 - 4] относятся к E_n 50 кэв, было бы интересно исследовать область $E_n <$ 50 кэв, при которой вклад нейтронов с орбитальным моментом $\ell > 1$ становится несущественным.

Для этой цели на одном из горизонтальных каналов реактора ИРТ-2000 был установлен фильтр из Fe, Al и S, выделяющий нейтроны с $E_n \sim 24$ кэв. Устройство фильтра схематически показано на рис. 1, а конструкция фильтра, параметры нейтронного пучка и фоновые условия более подробно описаны в работе [7]. Камера с двумя мишенями из ^{235}U толщиной ~ 1 мг/см^2 устанавливалась в пучке фильтрованных нейтронов с диаметром пучка β = 1 см и максимальной угловой расходимостью $\sim 2^0$ и защищалась кадмием.

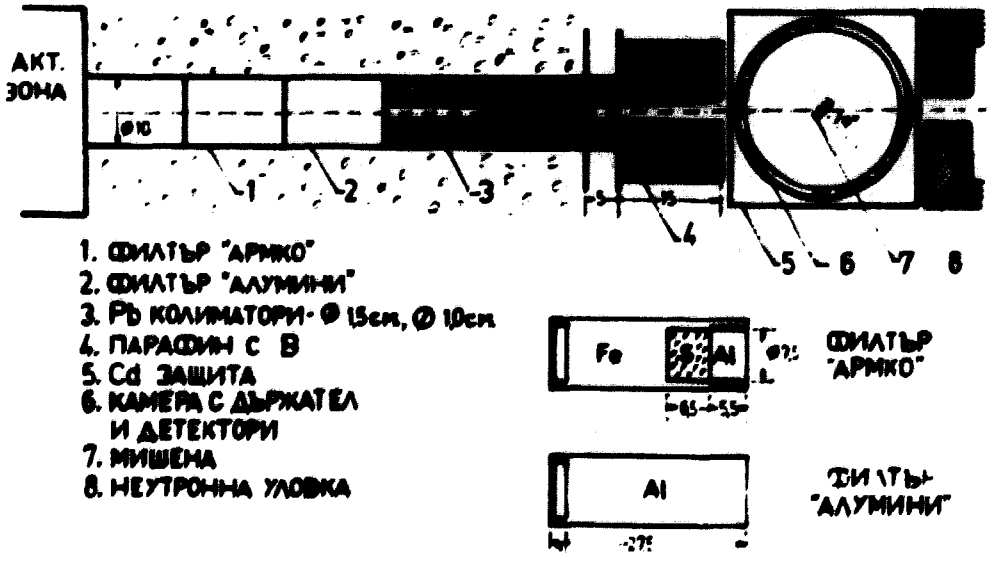

Взаимное расположение мишеней и стекол для регистрации осколков деления ^{235}U показано на рис. I. Для учета влияния толщины урановых мишеней и поправок на геометрию опыта нами было проделано контрольное облучение мишеней тепловыми нейтронами. Метод введения поправок аналогичен описанному в работе [8] . Время облучения мишеней нейтронами с $E_n \sim 24$ кэв $T = 119$ час. Число осколков, зарегистрированных на симметричных относительно плоскости мишеней стеклах суммировалось. Для определения фона, т.е. числа фотоделений ядер ^{235}U гамма-лучами высоких энергий (линия Al с $E_\gamma = 7{,}72$ Мэв, линия Fe с $E_\gamma = 7{,}63$ Мэв) возникающими за счет (n,γ)-реакции на конструкционных материалах активной зоны реактора, было проделано отдельное "фоновое" облучение камеры. При этом пучок нейтронов на выходе фильтра перекрывался пробкой из смеси парафина с бором. Было обнаружено, что угловое распределение осколков фотоделения ^{235}U хорошо описывается функцией

$$f(\theta) = 1 + A' \sin^2\theta, \qquad (3)$$

причем значение анизотропии $A' \sim 0{,}3$. Эта величина близка к полученному в работе [9] значению $A' \sim 0{,}25$ для ^{238}U при $E_\gamma = 7{,}72$ Мэв. Таким образом было установлено, что в условиях нашего эксперимента число фоновых делений не превышало I5 % от полного числа делений при открытом пучке фильтрованных нейтронов.

Угловое распределение осколков деления ^{235}U с вычтенным фоном и введенными поправками представлено на рис. 2. Оно аппроксимировалось функцией вида

$$W(\theta) = 1 + A\cos^2\theta \qquad (4)$$

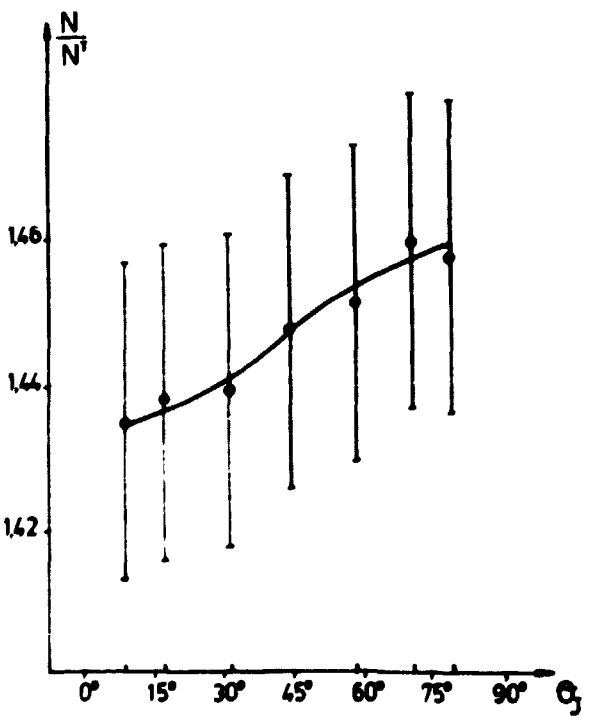

Методом наименьших квадратов было вычислено значение коэффициента A. Оказалось, что $A = -(1{,}8 \pm 1{,}6)\ 10^{-2}$ при уровне значимости $q = 0{,}05$.

Величина A, полученная нами при $E_n = 24$ кэв меньше экспериментальных значений угловой анизотропии при $E_n \sim 50 - 150$ кэв [2, 3]. Качественно этот факт согласуется с уменьшением вклада -волны при меньших значениях E_n. Для выяснения влияния различных факторов на знак и величину угловой анизотропии, мы пытались рассчитать угловые распределения осколков деления, которые в наиболее общем виде описываются выражением

$$W(\theta) = \sum_J (2J+1) T_J \sum_\pi \sum_K (2\delta_{K0}) \cdot T^{J\pi K} \cdot \sum_M \langle l 0 S M | J M \rangle^2 \cdot [d^J_{MK}(\theta)]^2 \qquad (4)$$

Коэффициенты T_ℓ вычислялись по оптической модели. Значения делимостей $f^{J,\pi,K}$ расчитывались в приближении двугорбого барьера деления. Выражение (4) содержит коэффициенты Клебша-Гордана и функции Вигнера, зависящие от J, K, M. При E_n = 24 кэв в соответствии с оптической моделью вклад p-нейтронов составлял ~ 8 % от общего числа делений. При расчетах делимости ядер ^{235}U через каналы с различными значениями J^π, K использовался набор параметров, характеризующих двугорбый барьер деления, который был предложен авторами работ [3, 4]. Были рассмотрены различные варианты, в которых полоса положительной четности с K = 2 лежит на 0,5 Мэв, 0,7 Мэв и 0,9 Мэв выше полосы с K = 0. Оказалось, что отрицательный знак анизотропии обусловлен каналами деления с $J^\pi = 2^+$, $4^+(K = 2)$ и $J^\pi = 4^+(K = 0)$, хотя расчетные значения A были меньше экспериментальных.

Выше отмечалось, что для согласования величин A, полученных расчетным путем и из эксперимента авторы работ [3, 4] считали, что при $E_n \lesssim 100$ кэв все деления вызваны p-нейтронами. По всей видимости, с точки зрения оптической модели это предположение не совсем корректно. Анализ наших результатов показывает, что более правдоподобным кажется предположение об усилении вероятности деления составного ядра ^{236}U через каналы с $J^\pi = 2^+$ и $4^+(K = 2)$ и $J^\pi = 4^+(K = 0)$.

Литература

[1] Нестеров В.Г., Смиренкин Г.Н., Шпак Д.Я., ЯФ, 4 (1966) 993
[2] Смиренкин Г.Н., Шпак Д.Я., Остапенко Ю.Б., Фурсов Б.И. Письма в ЖЭТФ, 11 (1970) 489
[3] Гонин Н.Н., Горюнов В.К., Козловский Л.К., Работнов Н.С., Стависский Ю.Я., Тамбовцев Д.И. Письма в ЖЭТФ, 20 (1974) 507, Прогр. III. Всесоюзной конф. по нейтронной физике, Киев, 9 - 13 июня 1975 г. стр. 42
[4] Козловский Л.К. Автореферат диссертации, Дубна, 1975
[5] Струтинский В.М. Атомная энергия 2 (1957) 508
[6] Strutinsky V.M. Nucl. Phys. A95 (1967) 420
[7] Дерменджиев Е., Илчев Г., Калинкова Н., Митов И., Чиков Н. Доклад на 7. Национальной конф. по физике, Видин, 1976
[8] Бочарова И.Е. и др. ЖЭТФ 49 (1965) 476
[9] Manfredini A. et al Nucl. Phys. A123 (1969) 664

ПРИМЕНЕНИЕ НЕРАВНОВЕСНОГО СТАТИСТИЧЕСКОГО ОПЕРАТОРА Д.Н. ЗУБАРЕВА НА ОПИСАНИЕ ПРЕДРАВНОВЕСНЫХ ПРОЦЕССОВ В ЯДЕРНЫХ РЕАКЦИЯХ

П. Мадлер, Р. Райф, Г. Рэрке

Технический Университет Дрезден, (ГДР)

Исходя из неравновесной статистики открытых квантомеханических систем ставится цель, найти описание и статистических и динамических аспектов временной зависимости ядерных релаксационных процессов.

В работах Д.Н. Зубарева (см. например [1]) описан метод конструкции матрицы плотности в любой момент времени включая сильно неравновесные стадии, который может быть использован при описании предравновесных процессов в ядерных реакциях [2]. Метод довольно общий и сводится к следующему:

Выбирая набор динамических переменных $\{P_m\}$, которые следует учесть в данной физической задаче, можно написать статистический оператор в любой момент времени как

$$\varrho(t) = \frac{1}{Q} \exp(A + B) \qquad Q = \mathrm{Tr}(\exp [A + B])$$

$$A = -\sum_m F_m(t)\, P_m$$

$$B = \int_{-\infty}^{0} dt' e^{\varepsilon t'} \sum_m [F_m(t+t')\, \dot{P}_m(t') + \frac{d}{dt} F_m(t+t')\, P_m(t')]$$

При этом параметры $F_m(t)$ приобретают смысль термодинамический сопряженных параметров, определяющие средние значения P_m, если требовать

$$\mathrm{Tr}(\varrho P_m) = \mathrm{Tr}(\varrho_q P_m)$$

$$\varrho_q = \frac{1}{Q_q} \exp A \qquad Q_q = \mathrm{Tr}(\exp A)$$

Предельный переход $\varepsilon \to +0$ следует выполнить в конце выкладок. В этом пределе $\varrho(t)$ удовлетворяет уравнению Лиувилля.

Для первого применения на релаксационные процессы в ядре мы используем модель ферми-газа и пренебрегаем "охлаждением" ядра.

После небольного числа столкновений налетающей частицы в ядре образуется (сильно неравновесная) система, которую будем подразделять на различные подсистемы состоящие из частиц с энергиями в определенных интервалах.

Переход к равновесию описывается как процесс релаксации между этими подсистемами, которые предполагаются находиться в неком квазиравновесии, которое характеризуется ферми-распределением с параметрами зависящими от времени. Такое рассмотрение возможно, если времена релаксации внутри подсистем меньше времени релаксации между подсистемами [3].

Для простоты сначала рассмотрим лишь две подсистемы: "горячая" ($\varepsilon > \varepsilon_F$) и "холодная" ($\varepsilon \leq \varepsilon_F$) подсистемы. Они связаны взаимодействием V. Полный Гамильтониан системы имеем тогда как

$$H = H_0 + H_0' + H_{int}$$

$$H_0 = \sum_i \varepsilon_i a_i^+ a_i \quad , \ \varepsilon_i \leq \varepsilon_F \quad ; \quad H_0' = \sum_{i'} \varepsilon_{i'} a_{i'}^+ a_{i'} \quad , \quad \varepsilon_{i'} > \varepsilon_F$$

$$H_{int} = \sum_{i,k,e,m} < me|V|ik > a_m^+ a_e^+ a_k a_i \quad ,$$

где индекс i обозначает набор квантовых чисел (в простейшем случае - без учета спина - i есть только импульс $\vec{k}$ частицы). Заштрихованные величины соответствуют "горячей" и не заштрихованные "холодной" системам.

Хотя для релаксационного процесса в ядре трудно ярко выделить различные стадии (кинетическая, гидродинамическая), поскольку длина свободного пробега по порядку сравнима с радиусом ядра мы ограничиваемся гидродинамической стадией, т.е. будем характеризовать релаксационный процесс средними величинами потоков $\langle \dot{P}_m \rangle$. Если не учесть спин частиц, то набор динамических переменных в случае двух подсистем выбирается как

$$\{P_m\} = \{H, H', \vec{P}, \vec{P}', N, N'\} = \{P_1, P_1', P_2, P_2', P_3, P_3'\}$$

- полная энергия H, полный импульс $\vec{P}$ и число частиц N каждой подсистемы.

$$\vec{P} = \sum_{\vec{k}} \hbar \vec{k} a_{\vec{k}}^+ a_{\vec{k}} \quad , \quad N = \sum_{\vec{k}} a_{\vec{k}}^+ a_{\vec{k}}$$

соответствующие термодинамический сопряжённые параметры F_m есть тогда:

$$\{F_m\} = \left\{\beta, \beta', -\beta\vec{v}, -\beta'\vec{v}', -\beta(m - \tfrac{m}{2}V^2), -\beta'(m' - \tfrac{m}{2}V'^2)\right\}$$

$$= \{\beta_1, \beta_1', \beta_2, \beta_2', \beta_3, \beta_3'\}$$

где β - обратная температура

$\vec{v}$ - средняя скорость частиц

m - химический потенциал.

С помощью статистического оператора $\varrho(t)$, который составляется для данного набора P_m и F_m можно считать средние значения потоков

$$\dot{P}_m = \frac{1}{i\hbar}[P_m, H] = -\dot{P}_{m'}$$

которые описывают транспорт энергии, импульса и числа частиц между подсистемами, обусловленный остаточным взаимодействием V.

Разлагая $\varrho(t)$ по интегральному члену B и учитывая только линейный член разложения (слабое остаточное взаимодействие), получается

$$\langle \dot{P}_m \rangle = \sum_i (\beta_i - \beta_{i'}) \int_0^\infty dt e^{\varepsilon t} \langle \dot{P}_m, \dot{P}_i \rangle \qquad i, m = 1, 2, 3$$

где вводились корреляционные функции

$$\langle \dot{P}_m, \dot{P}_i \rangle = \int_0^1 d\tau \, Tr\left\{\dot{P}_m e^{-\tau A} P_i e^{\tau A} e^{-A}\right\} / Tr\, e^{-A} - \langle \dot{P}_m \rangle \langle \dot{P}_i \rangle$$

$$A = -\sum_i (\beta_i P_i + \beta_{i'} P_{i'})$$

Кинетические коэффициенты

$$\langle \dot{P}_{m_i} \dot{P}_i \rangle = \int_{-\infty}^{0} dt\, e^{\varepsilon t} \langle \dot{P}_m , \dot{P}_i \rangle$$

можно, используя теорему Вика, явно представить как функции числа заполнения и квадрата матричного элемента остаточного взаимодействия V включая закон сохранения энергии.

Связав потоки $\langle \dot{P}_m \rangle$ с временными производными $\dot{\beta}_i$

$$\langle \dot{P}_m \rangle = \sum_i \langle P_m, P_i \rangle \dot{\beta}_i$$

получим систему связанных нелинейных дифференциальных уравнений первого порядка для термодинамических параметров:

$$\sum_i (\beta_i - \beta_{i-1}) \langle \dot{P}_m ; \dot{P}_i \rangle = \sum_i \langle P_m, P_i \rangle \dot{\beta}_i \qquad i,m = 1,2,3$$

Если рассмотреть только диагональные члены матриц $\langle \dot{P}_m ; \dot{P}_i \rangle$ и $\langle P_m, P_i \rangle$ и кроме того как простейшее приближение рассчитать их с помощью равновесных значений параметров $\beta_m = \beta_m^0$, то мы получаем простую систему уравнений

$$\langle P_m, P_m \rangle^0 \dot{\beta}_m = (\beta_m - \beta_m') \langle \dot{P}_m ; \dot{P}_m \rangle^0$$

Эти уравнения дают временную зависимость термодинамических параметров β_m, β_m' и тем самым дают распределение частиц по импульсам в любой момент времени

$$n(\vec{p},t) = \left[1 + \exp\left\{\beta'(t)\left(\varepsilon - m'(t) + \frac{m}{2} V'(t)^2 - \vec{V}'(t)\vec{p}\right)\right\}\right]^{-1}$$

(аналогичное выражение для другой подсистемы) если известны их начальные значения в момент времени $t = t_0$. Зная распределение для "горячей" системы в зависимости от времени легко считать спектр испущенных нуклонов, их угловое распределение и т.д. Начальное распределение следует получить из следующих соображений: Каким-либо способом считается распределение после несколько столкновений (в простейшем случае после первого). Оно отнюдь не будет фермиевским распределением. С помощью этого распределения считаются моменты для каждой из подсистем (т.е. энергия, импульс и число частиц). Начальное (фермиевское) распределение, наконец, находится из требования равенства его моментов соответствующим моментам "истинного" распределения. Ясно, что такой способ тем точнее, чем больше число подсистем в которое мы подразделяем всю систему.

Первые расчеты, в которых переходная вероятность $\frac{2\pi}{\hbar}|\langle me|V|\,k\rangle|^2$ заменялась усредненным по конечным состояниям e, m выражением

$$\frac{\sigma(\varepsilon_i + \varepsilon_k)\sqrt{\varepsilon(\varepsilon_i + \varepsilon_k)}}{\Omega \sum_{e,m} \delta(\varepsilon_i + \varepsilon_k - \varepsilon_e - \varepsilon_m)}$$

где $\sigma(\varepsilon)$ - сечение свободного нуклон - нуклонного рассеяния по [4], Ω - объем ядра, дают в случае двух подсистем релаксационные времена около $5 \cdot 10^{-20}$ сек, причем между релаксационными временами энергии, импульса и числа частиц выходит соотношение

$$\tau^\varepsilon < \tau^p < \tau^N$$

Это обстоятельство объясняется тем, что не все процессы связанные с потоком энергии дают и поток импульса или числа частиц между подсистемами.

Данный формализм позволяет дальнейшее улучшение. Чтобы учесть и кинетическую стадию в $\varphi(t)$ следует представить операторы числа частиц в качестве динамических переменных. Легко проделать и обобщение на учет "охлаждения" ядра добавлением дополнительной подсистемы - континуум вне области ядра. Данный метод способен и описать процессы взаимодействия между тяжелыми ионами. Тут основная проблема сводится к удачному выбору динамических переменных.

Литература

[1] Д.Н. Зубарев, Неравновесная статистическая термодинамика, Москва 1971
[2] P. Mädler, R. Reif, G. Röpke and H.-E. Zschau, TU-Preprint 05-30-75
[3] N.N. Bogoljubov, Probleme der dynamischen Theorie in der statistischen Physik, Moskau 1946
[4] N. Metropolis et al., Phys. Rev. 110 (1955) 185

SESSION V

COEXISTENCE OF DIFFERENT NUCLEAR SHAPES IN THE ISOTOPES OF THE LEAD-REGION

S. Prauendorf [x], Zentralinstitut für Kernforschung Rossendorf

x) The lecture is based an common work with V.V. Pashkevich and P.R. May JINR Dubna [1-3].

In order to investigate the coexistence of different nuclear shapes one must have at ones disposal a method to calculate the deformation energy. We shall use the shell-correction-method [4]. According to this approach the deformation energy has the form

$$E(\beta) = E_{LDM}(\beta) + \delta E(\beta) \qquad (1)$$

where β denotes a set of parametere fixing the nuclear shape. The liquid drop part $E_{LDM}(\beta)$ has a smooth behaviour leading to only one minimum of the deformation energy. Therefore a coexistence of nuclear shapes must be caused by the shell-correction $\delta E(\beta)$. This quantity has an oscillating behaviour as a function of the elongation parameter ε. The period is about 0.4. As δE is the sum of a proton and a neutron part one can distinguish two cases:

1. The neutron and proton contributions are oscillating in phase.
2. The two contributions are out of phase.

Let me start with the discussion of case 1. It corresponds to a ground state minimum and a second minimum with a mutual distance of $\Delta\varepsilon = 0.4$. The neutron and proton shell-corrections are in phase if both the number of neutrons and protons corresponds to the same relative filling of shells. This condition is satisfied for the β-stable nuclei from the rare-earth till the actinide region. For the actinides there is a deformed ground state minimum at $\varepsilon = 0.2 - 0.3$ and the famous second minimum at $\varepsilon = 0.6 - 0.7$, which appears as an isomer in the fission process. With decreasing mass number both minima move to smaller deformation. In the Pb-isotopes the first minimum corresponds to the spherical ground state and the second minimum lies at $\varepsilon = 0.4$. For still lighter nuclei the first minimum moves to negative deformations and the deformation of second minimum further decreases. After the Os-Pt-nuclei, where both minima have approximately the same energy, the second minimum becomes the deformed ground state of the rare-earth region. A second minimum analoge to the fission isomeric state is again expected for the rare-earth nuclei. However, because of the very steep barrier of E_{LDM} the corresponding minimum of δE is flattened out.

As the second minimum in the actinids has been discussed in detail elsewhere, let me consider the nuclei around ^{208}Pb. On fig. 1 the deformation energy of the Pb-isotopes is shown. In double magic ^{208}Pb there are very pronounced first and second minima. The energy difference between the two minima amounts to 15 MeV. With decreasing neutron number the pronounced structure gets more flat and the second minimum gradually disappears. This reflects the fact that with decreasing neutron number the neutron and proton shell-corrections are getting out of phase. Going along the line of β-stability both parts remain in phase. As the liquid drop barrier is lower for larger mass number the energy difference between

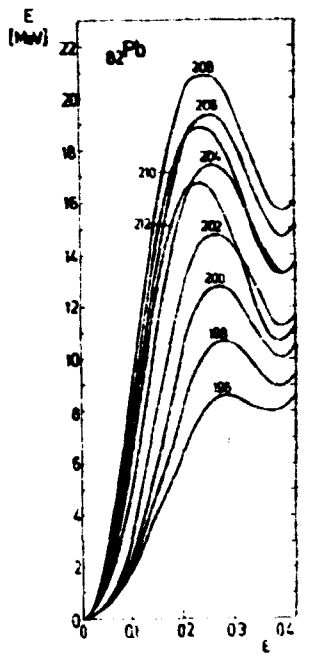

Fig. 1: The deformation energy of the Pb-isotopes 2 . The single particle schema is the same as in ref. [1]. The strength of pairing is given by $\bar{\Delta} = 12\ \mathrm{MeV}/A^{1/2}$ (for definition see ref. [4])

the two minima decreases with increasing proton number.

In our calculations only axial-symmetric shapes are considered. Thus we cannot exclude that the second minimum becomes a saddle point if three-axial shapes are taken into consideration. Calculations for the Pt-nuclei 5 and the actinide region 6 show that the barrier between the minima persists when γ-deformation is allowed. The level structure near the fermi-surface, which is reponsible for the shell effects, does not very strongly change when going from Pt to Th (for $\varepsilon = 0.4$). This is revealed by the fact that the second minimum for axial deformations has a rather constant shape for all nuclei in the considered region. Thus, it is very likely that in the whole Pt-region the second minimum seen for axial shapes remains a minimum if three-axial shapes are taken into account.

Let me now discuss the population of the second minimum. We assume that a compound nucleus is formed by means of some nuclear reaction.

The compound nucleus deexcites by evaporating neutrons. When the excitation energy gets lower than the barrier between the minima the nucleus can stay within the second minimum because in this case the transition rate between the minima is limited by the rapidly decreasing penetration factor of the barrier. Therefore as a rough estimate the ratio of population is given by the ratio of the level-densities in the two minima taken at the energy where the transition rate T_b through the barrier equals the transition rate of γ-decay T_γ. The most rapid decay mode is E1 with a single particle estimate of $T_{E1} = 10^{15} s^{-1}$.

In order to estimate the transition rate from the second to the first minimum the barrier is approximated by a parabola. If, furthermore, a constant mass parameter B is assumed for the deformation mode T_b reads

$$T_b = 2\pi\omega \exp\left(-\frac{\pi}{\hbar\omega}\sqrt{B(E_b - E)}\,\Delta\varepsilon\right) . \qquad (2)$$

where E_b is the energy of the top of the barr ... $\Delta\varepsilon$ is its width at the energy E. Taking for B the semiempirical value of ref. [7] at $\varepsilon = 0.3$ and A=210 and for $\hbar\omega = 10^{20} s^{-1}$, which corresponds to $\hbar\omega = 0.5$ MeV (see e.g. ref. [4]), one obtains

$$\log (T_b) = 3.05\sqrt{(E_b - E)}\,\Delta\varepsilon , \qquad (3)$$

where T_b is measured in s^{-1} and E in MeV. From (3) it is found that $T_{E1} > T_b$ for $E < E_b - 1$ MeV. Hence, the ratio n_1/n_2 of population of the first and second minima is given by

$$\frac{n_1}{n_2} = \exp\left(2\sqrt{a_2\,(E_b - E_2 - 1\ \mathrm{MeV})} - 2\sqrt{a_1(E_b - 1\ \mathrm{MeV})}\right), \qquad (4)$$

where a_1 and a_2 are the parameters of the single-particle level-densities in the two minima. E_2 denotes the energy of the second minimum measured from the first one. If the nucleus is non-suprafluid in the first minimum one should still add to E_2 the pair-correlation energy. Assuming for a_1 and a_2 the values of the fermigas plus a shell correction (taken from ref. [4]) one obtains for ^{210}Po $n_1/n_2 = 10^{-5}$. In heavier nuclei the ratio increases because E_2 decreases. In the case of ^{216}Rn n_1/n_2 amounts to 10^{-4}.

Considering the dependence of n_1/n_2 on the angular momentum it is neccessary to count the thermal energy from the minima of deformation energy for a given value of angular momentum (up to now we have referred to angular momentum equal to zero). The rotational energy in the second minimum is given by that of an axial rotator. The moment of inertia obtained from the cranking model (see e.g. ref. [8]) has approximately a constant value of 50 MeV^{-1} in the whole lead-region. As for the first minimum it is not possible to calculate the rotational energy in the same way, because the nuclei considered are nearly spherical. However, one can refer to the experimental yrast-levels. For example, one obtains for ^{208}Pb that n_1/n_2 increases by a factor of 15 if the angular momentum equals to $6\hbar$.

As shown by the calculations of ref. [9] (for ^{208}Po) the energy of the yrast-levels increases more slowly at higher angular momentum approximately corresponding to the rigid body value of the moment of inertia. Therefore, for angular momentum of the order $10\text{-}20\hbar$ the ratio of population should again decrease, because the moment of inertia in the second minimum is still reduced by the pairing (compare ref. [8]). Only for angular momentum larger than about $30\hbar$ the energies of the two minima may become comparable. However, at those large values of angular momentum one expects appreciable changes of the shell structure [10] which may completely change the shape of the function $E(\vartheta)$ we are referring to.

When the system is caught in the second minimum it decays to the ground state. This is expected from the calculated decay-rates for tunneling into the first minimum, which are given in table 1. The transition rates for collective E2-transition are greater than $T_{E2}(2^+ \rightarrow 0^+) = 10^9 s^{-1}$. Therefore, in most cases the barrier is high enough that the system may reach the ground state of the second minimum by emitting E1- and E2-radiation. The ground state of the second minimum decays by emission of γ -radiation or by emission of neutrons if the second minimum lies above the neutron binding energy. As both processes are fast in comparison with tunneling through the barrier the decay-time of the ground state of the second minimum is determined only by T_b. If the energy of the second minimum lies above the threshold of neutron emission (see table 1) this decay mode should prevail.

Let me now turn to case 2, when the oscillations of δE_p and δE_n are out of phase: In this case the first minima of δE_p and δE_n correspond to different deformations. This may lead to two minima of the deformation energy at relatively small deformation. One is caused by the protons the other by the neutrons. The minima are less pronounced because δE_p and δE_n partly cancel each other.

Table 1:

Nuclid	lg (T_b [s^{-1}])	E_2 [MeV]	Nuclid	lg (T_b [s^{-1}])	E_2 [MeV]
$_{82}Pb^{198}$	16	9	$_{84}Po^{208}$	6	12
$_{82}Pb^{200}$	13	10	$_{84}Po^{210}$	4	13
$_{82}Pb^{202}$	11	11	$_{84}Po^{212}$	4	12
$_{82}Pb^{204}$	9	13	$_{84}Po^{214}$	2	8
$_{82}Pb^{206}$	6	15	$_{86}Rn^{202}$	14	4
$_{82}Pb^{208}$	4	15	$_{86}Rn^{204}$	11	5
$_{82}Pb^{210}$	3	13	$_{86}Rn^{206}$	9	7
$_{82}Pb^{212}$	4	10	$_{86}Rn^{208}$	8	9
$_{84}Po^{200}$	14	6	$_{86}Rn^{210}$	6	10
$_{84}Po^{202}$	10	8	$_{86}Rn^{212}$	4	12
$_{84}Po^{204}$	7	9	$_{86}Rn^{214}$	3	9
$_{84}Po^{206}$	8	10			

A situation like that is expected if the number of one kind of particles is near the closure of a spherical shell while the number of the other kind of particles lies near the closure of a deformed shell x).

As an example I shall discuss the very neutron deficit isotopes of mercury [1]. The proton number of 80 is only two units away from the closure of the spherical shell. Going away from the line of β-stability the neutron number approaches the closure of the deformed shell 102 corresponding to the stable deformed rare-earth nuclei. Therefore, one expects the coexistence of an almost spherical shape and a deformed shape with $\varepsilon = 0,2 - 0,3$. On fig. 2 the deformation energy of ^{184}Hg is shown. In the ground state the nucleus is slightly oblate with $\varepsilon = -0,12$. However, at the very low energy of 0,29 MeV there is a prolate minimum with $\varepsilon = 0,23$.

In order to calculate the deformation energy of the higher levels of the yrast-line we have added to expression (1) the rotational energy of an axial rotator, i.e., a term $I(I+1)/2\Theta$, where $J(\beta)$ is the moment of inertia of the cranking model (for details see refs. [1,8]). The moment of inertia is smaller in the oblate than in the prolate minimum. Therefore, the rotational levels are more closely spaced in the prolate minimum than in the prolate one leading to a preferrance of the prolate shape with increasing angular momentum. In the 2^+-state the two minima are almost degenerated, however, the 4^+-state is already prolate.

x) Shells for arbitrary shapes can be defined by the minima of the level density (see ref. [4]).

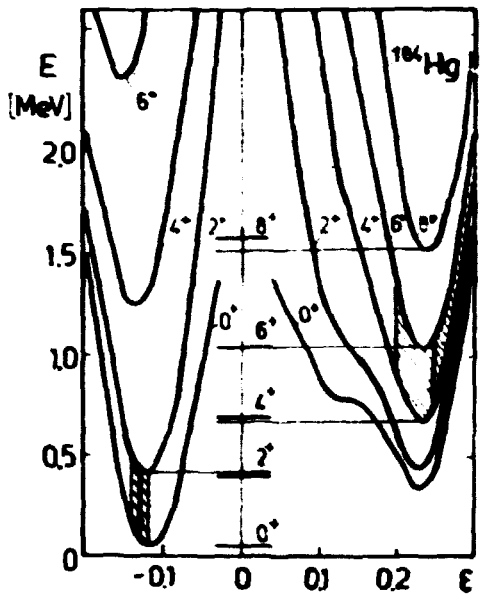

Fig. 2: Deformation energy of the rotational states in ^{184}Hg (taken from ref.[1]). The heavy bars indicate the experimental yrast-levels. The arrows indicate the deformation calculated from the BE2-value of the corresponding transition. The shadowed area is the experimental error.

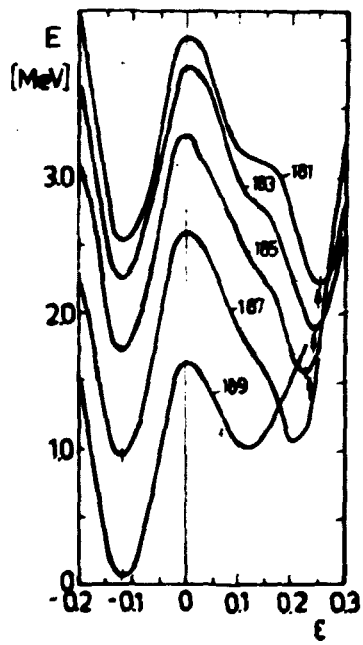

Fig. 3: The deformation energy of the odd-mass Hg isotopes (taken from ref.[1]). The arrows indicate the experimental values of deformation (see text).

As can be seen in fig. 2 this transition from the oblate to the prolate shape provides a rather peculiar spacing of the yrast-levels, which is experimentally observed. The large energy of the $2^+ \longrightarrow 0^+$ transition corresponds to the small oblate deformation. Above the 4^+ - level the rotational band corresponding to the large prolate deformation is seen. In addition it is also possible to reproduce the experimental E2-lifetimes, which are a direct measure of the quadrupole-moment. The deformation calculated by means of the rotor model from the experimental BE2-values of the $6^+ \longrightarrow 4^+$ and $2^+ \longrightarrow 0^+$ transitions are indicated by the arrows in fig. 2.

The experimental results for ^{186}Hg are similar to the discussed ones and are also reproduced with good accuracy. In accordance with the experimental findings the oblate-prolate-transition occurs in ^{188}Hg between the 4^+- and the 6^+-state. This shift is due to the gradually increasing difference between the energies of the two minima. The same lifting up of the prolate minimum appears in the odd-mass isotopes. It can be seen that the isotopes $^{181-185}Hg$ have a large prolate ground state deformation, whereas the heavier isotopes are oblate in the ground state. This jump in the ground state deformation permits a natural explanation of the sudden decrease of the mean-square radius between ^{185}Hg and ^{187}Hg, which has been measured in optical pumping experiments. From the experimental value of $\Delta r^2 = \langle r^2 \rangle - \langle r^2 \rangle_{oblate}$, where $\langle r^2 \rangle_{oblate}$ is obtained by linear extrapolation of the experimental values for the isotopes heavier than ^{185}Hg, and the theoretical de-

formation of the oblate minimum one obtains a (semi) experimental value of the prolate deformation. In fig. 3 it is shown that the experimental and the theoretical equilibrium values of deformation coincide with an excellent accuracy. Even the slight increase of deformation between ^{185}Hg and ^{181}Hg is reproduced. Our calculations indicate that all even mass isotopes heavier than ^{180}Hg are oblate in the ground state. The different shapes of adjacent even- and odd-mass isotopes can be traced back to a different loss of pair-correlation energy when a level in the oblate or in the prolate minimum is blocked by the odd neutron.

A still open question is the γ-dependence of the deformation energy. Calculations [11] for ^{182}Hg show a very flat barrier of 0.2 MeV between the minima. This seems to be in accordance with the experimental BE2-value of the $4^+ \rightarrow 2^+$ transition in ^{184,186}Hg which does not indicate any noticable hindrance for the prolate-oblate transition. However, in the experimental study of ref. [12] it is claimed that the 2^+- and 0^+-levels in the prolate minimum are seen. This would indicate a noticable barrier between the two minima.

Let me finish with a discussion of the overall trends in the Pt, Hg, Pb region as predicted from calculations of the deformation energy [1, 2, 3]. In the Pt-isotopes because of the smaller proton number the oblate minimum lies higher and at a larger deformation than in the adjacent Hg-isotopes. Therefore, the very neutron deficite isotopes $^{184-188}$Pt are already prolate in the ground state. With increasing neutron number the prolate minimum is lifted up. In ^{190,192}Pt both minima are degenerated. The heavier isotopes are oblate in the ground state. In ^{196}Pt the second minimum at $\varepsilon \approx 0.4$ appears which, as already discussed, is typical for all β-stable nuclei in the lead-region. The experimental spectra of the Pt-isotopes do not indicate any barrier between the minima. This is in accordance with the calculations of ref. [13] where a smooth γ-dependence or a flat minimum at $\gamma \neq 0$ is predicted. As already mentioned the prolate and oblate minima are degenerated in ^{180}Hg. Thus, all heavier Hg-isotopes are oblate in the ground state. The low lying prolate minimum in $^{184-188}$Hg leads to the interesting phenomena discussed above. All Pb-isotopes heavier than ^{184}Pb are spherical in the ground state. This corresponds to the proton number 82. For the lightest isotopes the low-lying prolate minimum again appears. It disappears for the isotopes heavier ^{190}Pb. As shown in fig. 4 the coexistence of the spherical and deformed shape in ^{186}Pb should lead to a very

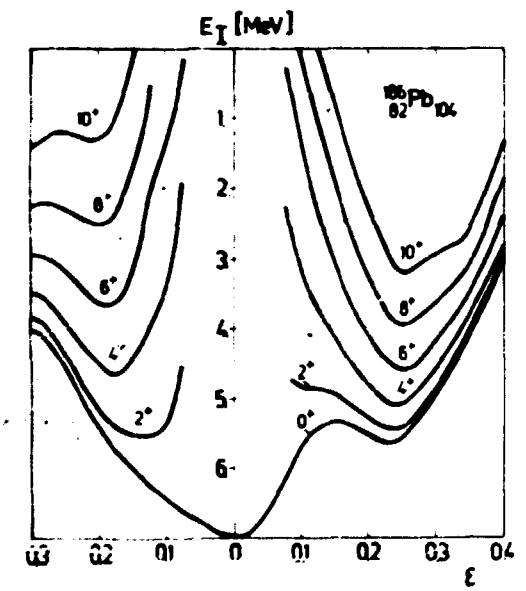

Fig. 4: The deformation energy of ^{186}Pb [2]. The single particle schema is the same as in ref. [1]. The pairing is treated as in ref. [8].

interesting spectrum: One expects a phonon triplet of 0^+, 2^+, 4^+ and a rotational band with a large moment of inertia and a band-head at about 0.5 MeV.

References

[1] S. Prauendorf, V.V. Pashkevich, Phys. Lett. 55B (1975), 365
[2] S. Prauendorf, V.V. Pashkevich, to be published
[3] S. Prauendorf, F.R. May, V.V. Pashkevich, to be published
[4] M. Brack etal., Rev. Mod. Phys. 44 (1973) 320
[5] U. Götz et al., Nucl. Phys. A192 (1972) 1
[6] V.V. Pashkevich, Nucl. Phys. A133 (1969) 400
[7] I. Randrup et al., Nucl. Phys. A217 (1973) 221
[8] S. Prauendorf, Preprint JINR-E4-9101 (1975) and Nucl. Phys. to be puslished
[9] I.R. Grover, Phys. Rev. 157 (1967) 832
[10] K. Neergard, V.V. Pashkevich, Preprint JINR-P4-8947
[11] A. Peassler et al., Phys. Lett. 39B (1972) 579
[12] J.H. Hamilton et al., Phys. Rev. Lett. 35 (1975) 562
[13] I. Ragnarsson et al., Nucl. Phys. A233 (1974) 329

SEARCH FOR γ -DECAY OF THE SHAPE ISOMER IN MUONIC ^{238}U

R. Arlt, G. Musiol, H.-G. Ortlepp, TU Dresden, Sektion Physik, WB Kernphysik
8027 Dresden, Mommsenstraße 13
W.-P. Fromm, Zentralinstitut für Kernforschung Rossendorf
Dz. Gansiorig, S.M. Polikanov, U. Schmidt, G.N. Sorin
Vereinigtes Institut für Kernforschung Dubna, UdSSR

1. Introduction

The phenomenon of the spontaneously fissioning isomers [1] can be interpreted as fission from a shape isomeric state e.g. a state characterized by a much larger nuclear deformation than the ground state. Theoretical calculations [2] on the base of the liquid drop model with shell and pairing corrections included are able to describe the shape isomerism qualitativly. In the framework of this model isomeric fission occurres from a state at the second minimum of the potential energy curve at large quadrupole deformation.

A systematical study of all hitherto known fission isomers [7] shows that their formation cross sections are decreasing in going from Z = 94 to lower Z-values and for Z< 92 no isomers are known at all. Calculations of the double-humped fission barrier [8] predict a higher outer than inner barrier for Z< 94, which was experimentally supported [9]. Whereas for shape isomers with Z ≥ 94 fission in the dominating deexcitation channel for nuclei with Z< 94 and lowered inner barrier γ -decay into the first minimum should compete with fission. A strong γ -branch would allow to regularize the observed formation cross sections and to establish precise excitation energies for the shape isomeric state. Search experiments for the observation of the shapeisomeric γ -decay have been performed by various groups employing the reactions ^{235}U (d,p) ^{236m}U [10], ^{238}U(p,n)

^{238m}Np [10] and ^{238}U (d,pn)^{238m}U [11]. Only the authors of [11] succeded to observe γ-transitions from the shape isomeric decay and precised the excitation energy of this state to 2.559 MeV. One possibility to get physical information about the existence of large deformations is the observation of rotational states in the second minimum through which the shape isomeric state is populated. In [3] the conversion electrons from such highly converted γ-transitions precurring the isomeric fission of ^{240}Pu were observed. From the energy spacings of this states a moment of inertia as high as twice that of the ground state band was determined, which strongly supports the conception of shape-isomeric states with large deformations.

Another independent method would be the use of the sensitiveness of the muon to the nuclear charge distribution as was proposed in [4]. According to calculations from [5, 6] the high quadrupole moment of the shape-isomeric state should lower the muonic binding energy for the 1s state by several hundred keV. Correspondingly the barrier heights would be changed, allowing the isomeric state more easily to backtunnel and depressing the fission channel. The observation of an energetically shifted shape-isomeric state in the presence of the muon would give another hint for the validity of the double-humped barrier description. Furthermore the lifetime of the shape-isomeric state in the muonic atom would be changed, because one has to take into account the capture of the muon on the 1S state by the nucleus. A presumption for a successful search of the γ-branch in muonic atoms is a sufficiently stron excitation of the shape-isomeric state by the muonic cascade. From the different lifetimes observed for delayed fission [13, 14] and electronic decay of the muon [15] in muonic ^{238}U a strong population of the shape isomer was postulated [12].

The aim of the present work is to search for delayed γ-radiation after formation of muonic atoms of ^{238}U.

2. Experimental Arrangement

The measurements were performed at the separated μ^--beam of the Dubna synchrocyclotron. A special extension of the muon channel into the heavy shielded, so called low background laboratory, was used. At this site the effect to background ratio was much improved compared with an earlier run [22] with the experimental arrangement in the main experimental hall and in comparision to the experiment [23].

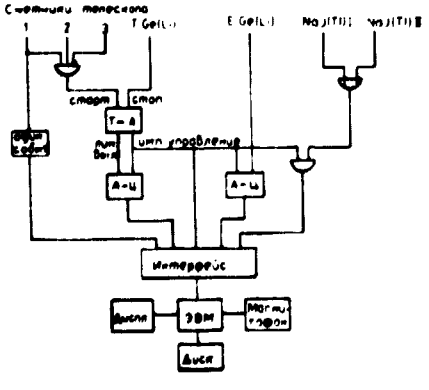

Fig. 1: Blockdiagramm of the electronic device withaut amplifiers, delayblocks and -lines and stabilisation

A simplified block diagram of the electronic apperatus is given in fig. 1. The μ-stop signal was registered by means of a scintillation counter telescope fulfilling the coincidence relation 123. With an typical intensity of the μ^--beam of $10^4 s^{-1}$ the number of μ-stops in the 115 g uranium target amounts to 650 s^{-1} The γ-radiation was recordet by means of a 60 cm^3 Ge(Li) diode (2.8 keV FWHM at 1 MeV) and two NaJ(Tl) crystals (8 cm diameter by 8 cm length). The timing system [24] provides us with an integral time resolution of 7 ns FWHM for the energy range from E = .1...4.7 MeV in the Ge(Li)-branch.
The experiment was operated on-line with the HP 2116 computer [25]. The following informations were combined and transferred to the computer:

1. the energy of the γ-quantum registered by the Ge(Li)-detector (up to 4.7 MeV in 8192 channels)
2. the time between the μ-stop event and the Ge(Li)-signal (2.5 μs range in 4096 channels)
3. the signal from the inspection circuit, if 3 μs before and after the μ-stop-moment no other muon passes through the first counter (threshold 100 keV)
4. the signal of the NaJ(Tl)-detectors, if at least one of them had registered a hard γ-ray in the time interval from 20 to 120 ns after the Ge(Li)-signal.

The data were stored in the event-by-event mode on magnetic tape. Integral energy and time spectra were sampled and displayed simultaneously. After the 45 hour data-taking run the events were sorted into 4 ground of 8 spectra each.The groups were determined by the presence of the signals indicating single muon and/or delayed NaJ-coincidence events. The spectra were derived according to eight time intervals producing one prompt, six successive delayed and one calibration spectra. The internal calibration lines were provided by radioactive sources of ^{56}Co and ^{152}Eu registered as chance coincidence in the course of the experiment. The time scale was calibrated with a 10 MHz frequency generator.

In the delayed spectra from muonic atoms the main part of the background activity is formed by γ-radiation following the nuclear muon capture. As far as we are mainly interested in the detection of weak delayed lines as they were expected from the decay of the shape isomeric state in muonic ^{238}U, the delayed background should be suppressed as much as possible. Except of measurements with good spectroscopic resolution a delayed coincidence between the Ge(Li)- and the NaJ(Tl)-detectors was introduced. The coincidence condition is fulfilled only in that case where a γ-ray registered by the Ge(Li)-detector was followed by other γ-rays in a time interval typical for nuclear muon capture. Therefore all events from μ-capture without precurring γ-activity could be removed from the delayed spectra. The efficieny of the delayed coincidence circuit was measured to be about 10 % from the intensity ratio of prompt muonic X-rays with and without the coincidence signal. The registration of very short halflifes cannot be improved by this additional coincidence condition.
With the spectrometer described a lower intensity detection limit for delayed γ-rays of about 0,3 % per one stopped muon was reached.

3. Results and Discussion

The prompt peak has for the γ-rays recordet from the ^{238}U target a FWHM of 7ns.

The decay time of the delayed γ-rays was determined by the least squares method for two exponential decays, the longer one should account for the muon capture in constructional materials of small Z and was found to be (760 ± 120) ns. The lifetime of the component belonging to the μ^--capture in ^{238}U τ = (78,5±1,5)ns remains unchanged within error limits if the second decay is emitted. In table 1 the lifetimes for μ-capture in ^{238}U measured via fission, γ-rays and electronic decay are compared. For the assumption of a strong population of the shape isomeric state by the muon a shortened lifetime for fission as well as for the γ-decay channel with respect to the free decay of the muon is essential [12].

Table 1: Intensity of the delayed γ-transitions with $T_{1/2}$ = 9 ns per μ-stop in the muonic atome ^{239}U

E_γ (keV)	708 ± 1	817 ± 1	834 ± 1	962 ± 1	1015 ± 1	2215 ± 1,5	3131±2
I_μ (%)	0,6±0,2	0,4±0,2	0,5±0,3	0,4±0,2	0,65±0,25	0,5±0,2	0,5±0,2

The prompt spectrum exhibits all features of the complex interaction of the muon and the heavy deformed nucleus. Results of the investigation of the dynamic quadrupole hyperfine splitting of muonic X-rays are given in a forthcoming paper [16]. The calibrational spectrum developed from γ-events separated by more than 200 ns from the μ-stop moment shows in addition to the γ-transitions from the decay of ^{57}Co and ^{152}Eu γ-rays known from the radioactive decay of ^{238}U. The main interest in this investigation was devoted to delayed γ-ray activities which can be produced in different ways. Except of the γ-ray decay of shape isomeric states excited by radiationless transitions in the muonic cascade which was searched for, delayed γ-lines are emitted in the nuclear μ-capture process, by the capture of neutrons emitted in connection with μ-capture and by inelastic scattering of neutrons, by de-excitation of spin isomers excited in fission fragments as well as in the target nucleus.

A careful search for delayed activities revealed two groups of γ-rays distinguished by their halflives. The first group of transitions has a lifetime of about 75 ns, which is typical for the μ-capture process in uranium nuclei. The energies and intensities of these lines are in good agreement with the transitions observed in the $^{238}U(n,\gamma)$-reaction [17,18]. That means, that the neutrons emitted from the nucleus after μ-capture, where an energy of about 95 MeV is released, produce secondary reactions in the thick uranium target. Transitions from the $^{238}U(n,n')$-reaction however have not been found. Also transitions from the excited residual nuclei after the $^{238}U(\mu,xn)^{238-x}Pa$ reaction could not be identified.

Nuclear muon capture can be accompanied by fission too, for ^{238}U the delayed fission branch has a partition of 3 % per captured muon [14]. The complex γ-ray spectrum produced by the deexcitation of isomeric states in the variety of fission fragments was studied in very detail using the spontaneous fissioning ^{252}Cf [19]. Every isomeric transition from a fission fragment produced by muon capture induced fission is fed by a delayed process with respect to the μ-stop moment. Lines from fission fragments should therefore appear in our spectra with

enlarged lifetime. Caused by the small probability of the fission process and the wide spread-out of its intensity by the statistical nature of this phenomenon, no γ -transitions from fission fragment isomers could be detected with an intensity exceeding 0,3 % per stopped muon.

The second group comprehenses delayed γ -transitions with a shorter mean lifetime of about 13 ns. In general the existence of a γ -line was admitted if in a series of successive spectra the counting rate of neighbored channels was higher than the background. Unfortunately for this short lifetime region the additional delayed coincidence with the NaJ(Tl)-counters was not applicable. A total of seven transitions were found in different time windovs. The decay of their intensities is presented in fig. 2 together with a least squares fit of the corresponding lifetimes. The intensities of the transitions are summarized in table 2. The normalization of the delayed intensities to the number of μ-stops was performed with the intensity of the muonic 4f-3d transition in the prompt spectrum and the percentage of this transition determined by a cascade calculation [26] starting with statistical distribution at n = 20. The reduction of the intensity of the detected main components of the muonic 4f-3d transition group due to dynamic quadrupole interaction [27] was taken into account using the charge distribution parameters of [28] in the calculation for ^{238}U.

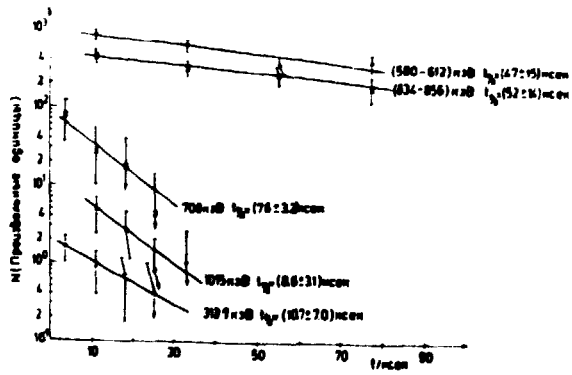

Fig. 2: Halfe-lifes ($T_{1/2}$) of the muonic ^{238}U γ -lines

Table 2: Intensity of the delayed γ -lines ($t_{1/2}$ = 9 ns) per μ-stop in $^{238}(U+\mu)$

E_γ (keV)	708±1	817±1	834±1	962±1	1015±1	2215±1,5	3131±2
I/μ-stop (%)	0,6±0,2	0,4±0,2	0,5±0,3	0,4±0,2	0,65±0,25	0,5±0,2	0,5±0,2

Because of the short lifetime of the γ -transitions under consideration any explanation of their existence with processes connected with the capture of the muon from the 1s-state is not concessive. In principle, prompt fission after radiationless excitation of the nucleus by the muon could excite isomers in the fission products which then would be recorded with their natural lifetimes. Prompt fission, however, occurres only in 0,2 % of the μ-stops in the ^{238}U target [14]. Therefore, even in the case where all fission events would produce two definite fragments with full excitation of a short-lived isomeric state, this intensity would be lower than the detection limit of this experiment.

Further one has to investigate, whether or not the short-lived transitions observed could be explained by an isomeric state in ^{238}U. The level structure of ^{238}U has been studied from the decay of ^{238}Pa [29], by means of coulomb excitation [30] and by (n,n',γ)-reactions [20]. The ground state band was followed up to the 14 member at about 1,5 MeV. No short-lived isomeric transitions were reported so far. Also in the accurate investigation of the ^{238}U (d,pn) reaction by Russo [11] no isomeric states were found. The existence of such isomers, however, cannot be excluded in this mass region. For example, the study of the ^{236}U(d,pn) reaction [10] dedicated the detection of the γ-branch from the shape-isomeric state yielded in a new isomer in the first minimum with $K,I^{\pi} = 4,4^-$ at 1.052 MeV excitation energy in ^{236}U second isomer with $K,I^{\pi} = 2,2^-$ at 0.687 MeV and a halflife of 4,4 ns is also known in ^{236}U. Because of the high excitation energy of the state observed in this experiment ($\approx$ 2 MeV) and the limited possibilities of the excitation of states with significant spin difference to the ground state by the muon, the identification of the observed delayed γ -rays with the de-excitation of a yet unknown spin- or K-isomeric state is very improbable.

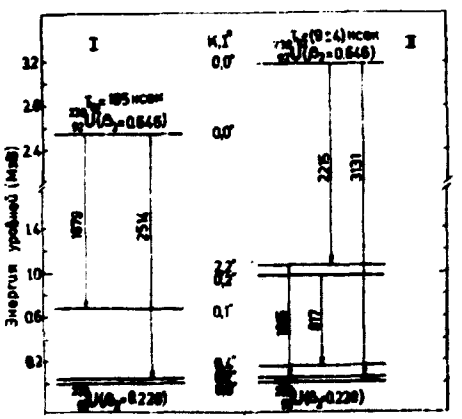

Fig. 3: Decay schema of the proposed ^{238}U shape isomere
I: from the (d,pn)-reaction [11]
II: with the muon on the 1s-orbit

Two of the seven transitions from table 2 fit into the level scheme of ^{238}U (fig. 3). The 1015 keV transition represents the deexcitation of the lowest member of the γ-vibrational band (K=2) to the 2^+ state of the ground state band, the 818 keV transition de-excites the 2^+ member of the second rotational band to the 4 state of the groundstate band. It should be mentioned that the $4^+ \rightarrow 2^+$ (E_γ = 103 keV) and $2^+ \rightarrow 0^+$ (E_γ = 45 keV) transitions in the experimental arrangement could not be recorded due to their low energy and high conversion. Furthermore, all lines with intensities lower than 0,3 % are undetectable, thus, in the case of branching at one level the de-excitation path may be lost. In addition all transitions recorded in the presence of the muon on the 1s-state are splitted and shifted due to the influence of the interaction of nucleus and muon. The magnitude of the magnetic hyperfine splitting of nuclear levels is of the order of 1 keV, and in most cases larger than the isomeric shift. The intensities of the delayed transitions and the therefore limited energy accuracy are not sufficient to extract this peculiarities from the data. Therefore in fig. 3 all levels are shown like unsplitted ones. The isomeric shift has a minor influence on the level energies, if the nuclear charge distribution (or deformation) for the levels under consideration are neuvely equal. For large differences in the shape of the nuclear charge distribution the isomeric shift becomes the dominating part of the muonic-nuclear interaction. Hence a large shift of the shape isomeric levels relative to states from the first

minimum has to be expected.

In ruling out other possibilities for short-lived high-energy transitions the two transitions with E_γ = 2215 keV and E_γ = 3131 keV can be ascribed as the decay of the shape isomeric state in muonic ^{238}U to the 2^+ levels of ground-state and γ -vibrational band. The level schemes for the γ -ray decay of the shape isomer in ^{238}U [11] and muonic ^{238}U are shown together in fig. 4. Three of the obeerved delayed transitions could not be placed in the decay scheme. It is possible, that intermediate states with low spin at energies higher than the γ -vibrational band are connected by this transitions with the shapeisomeric decay. There is no experimental information of states with low spin in the excitation band brom 1.2 to 2.5 MeV in ^{238}U available at present. The most striking features comparing the two level schemes presented in fig. 3 are the large isomer shift for the shape isomeric state in the presence of the muon of ΔE = 617 keV and its shortened lifetime. In the early work of Zaretzki [5] an estimation of ΔE = 500 keV for the isomer shift in muonic actinide nuclei was given. To account for the change in the barrierheight one can use the change in the binding energy of the muon in the 1s-state. The binding energy of the muon was calculated by solving the Dirac equation for a deformed Fermi type charge distribution.

$$\rho(r) = \rho_0 \left[1 + \exp\left(4 \ln 3 \; \frac{r - c\,(1 + \beta_2 Y_{20} + \beta_4 Y_{40})}{t}\right)\right]^{-1}$$

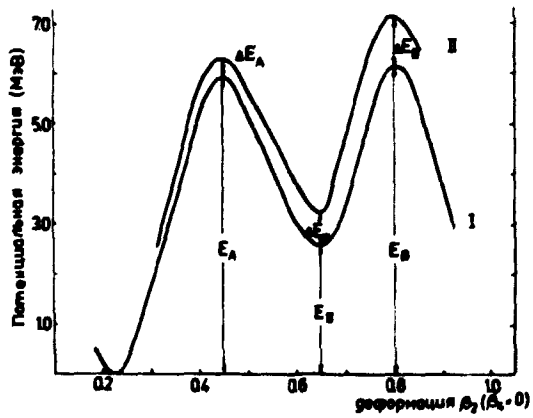

Fig. 4: Potential barriere of ^{238}U without (I) and with (II) muon on the 1s-orbit. Parameters from references: E_A = (5,90±0,20) MeV [9], E_B = (6,12±0,20) MeV [11], E_{II} = 2,559 MeV [11], $\hbar\omega_A$ = 1,00±0,10 [9], $\hbar\omega_B$ = 0,62±0,10 [9]. Parameters from solving the Dirac-equation with $\rho(\beta) = [r - c\,(1+\beta Y_{20}]\,/t$, c = 7,10 f, t = 1,80 f): ΔE_A = 320 keV, ΔE_B = 990 keV, ΔE_{II} = 640 keV. Experimental result of the isomeric shift is ΔE_{II} (exp.) = 617 keV.

For the parameter β_4 values determined as giving minimal potential energy for every β_2 value calculations of Pashkevich [31] where used. In fig. 4 the potential energy curve for ^{238}U and muonic ^{238}U are shown together. The value of the isomer shift of states in the second minimum ΔE_{II} = 620 keV is in good agreement with the experimental value. The results of a recent paper of Leander and Möller [6], where the nonrelativistic Schrödinger equation for a charged particle in the Coulomb potential of a deformed charge distribution was solved, are in good agreement with the values given for the charge in the muonic binding energy

of fig. 4. The experimental lifetime t_{exp} = 13 ns of the delayed γ-rays observed comprehenses the lifetime t_{iso} of the shape isomeric state in the presence of the muon and the lifetime $t_{/u}$ of the muonic atom itself:

$$\frac{1}{t_{iso}} = \frac{1}{t_{exp}} - \frac{1}{t_{/u}}$$

The value for t_{iso} can be compared with the lifetime of the shape isomer estimated on the base of parabolic fission barriers. In this framework the barrier penetrability is given as

$$P_{A,B} = \exp\left(-2\pi \frac{E_{A,B} - E_{II}}{\hbar\omega_{A,B}}\right)$$

with E_{II} as excitation energy of the shape isomeric state and the curvature parameters $\hbar\omega_{A,B}$ for the inner barrier A and the outer barrier B respectively. For equal penetrabilities fission will dominate over γ-decay by a factor of about $10^{6.5}$ [8]. Using for the partial lifetime of fission decay of the isomer the expression

$$t_{iso,f} = \frac{1}{n \cdot P_B} = \frac{6 \cdot 10^{-21}}{P_B}$$

where n is the number of barrier assaults per second fo. the vibrational frequency in the second minimum of $\hbar\omega$ = 1 MeV, the partial lifetime for γ-decay of the isomer becomes

$$t_{iso,\gamma} = \frac{6 \cdot 10^{-15}}{P_A}$$

Table 3: Parameters of fission barrier of $^{238}_{92}U$

	$\hbar\omega_A$(MeV)	$\hbar\omega_B$(MeV)	$\hbar\omega_{II}$(MeV)	E_A(MeV)	E_B(MeV)	E_{II}(MeV)	$t_{i\gamma}$ (ns)	
$^{238}_{92}U$	1.00	0.62	0.9	5.90	6.10	2.60		a)
	1.18	0.63	1.0	5.90	6.12	2.559	200	b)
$^{238}_{92}$(U+/u1/2s)	1.18	0.63	0.9	6.22	7.10	3.176	11	

a) ref. [7]
b) ref. [9]

In table 3 the estimated partial lifetimes for ^{238}U and muonic ^{238}U are compared. The barrier parameters where taken from ref.[9]. The augmentation of the fission barrier was calculated as described above. The shortening of the isomeric decay with the muon in the nuclear system is reproduced. However, there are ways left open to enhance the agreement between the experimental and the theoretical values. For example the curvature parameters of the fission barrier were taken not modified by the barrier height changes by the muon. Furthermore damping of nuclear states according to the theory of Lynn [21] was not included

since it was felt that the scarce experimental material did not permit to give such refinements physical significance. The most astonishing fact is the large population probability of the second minimum by the muonic cascade. Radiationless transitions which are responsible for the excitation of the isomeric state establish about 15 to 20 % of the muonic cascade. The total intensity of the γ-rays deexciting the shape isomeric state was found to be 1.6 % in this experiment. Therefore the feeding probability for the shape isomeric state by radiationless transitions is of the order of 10^{-1}, which is surprisingly high compared with the corresponding values for neutron induced excitation or charged particle reactions of 10^{-3} and 10^{-4} respectively. The physical reason for this phenomenon could be resonance excitation of states in the second minimum via vibrational states in the first well. Such resonances were observed in neutron subthreshold excitation work [32], but at present more experimental material should be accumulated to yield in a better understanding of the excitation process governing the discussed effect.

References

[1] Polikanov, S.M., Zh. Eksp. Theor. Fiz. 42 (1962) 1464
[2] Strutinsky, V.M., Nucl. Phys. A95 (1967) 420
[3] Specht, H.J. et al., Phys. Lett. 41B (1972) 42
[4] Polikanov, S.M., Preprint VIK Dubna, 1971
[5] Zaretsky, D.F. et al., Nucl. Phys. 28 (1961) 177
[6] Leander, G., et al., Phys. Lett 57B (1975) 245 (3)
[7] Britt, H.C., Atomic Data and Nucl. Data Tabl. 12 (5) (1973) 407
[8] Nilson, S.G. et al., Nucl. Phys. A140 (1970) 275
[9] Back, B.B. et al., Phys. Rev. C9 (1974) 1924
[10] Borggreen, J. et al., Nucl. Phys. A218 (1974) 621
Brinckmann, H.F. et al., Phys. Lett. 43B (5) (1973) 386
[11] Russo, P.L. et al., Nucl. Phys. A240 (1975) 13
[12] Bloom, S.D., Phys. Lett. 48B (5) (1974) 420
[13] Sens, J.C., Phys. Rev. 113 (1959) 679
Diaz, J.A. et al., Nucl. Phys. 40 (1963) 54
Budick, B. et al., Phys. Rev. Lett. 24 (1970) 604
[14] Chultem, D. et al., Nucl. Phys. A247 (1975) 452
[15] Hashimoto, O. et al., Preprint LBL 3850
[16] Fromm, W.D. et al., to be published
[17] Souverly, M.G. et al., Ann. Nucl. Scc. Engeng 1 (718) (1974) 409
[18] Groshev, L.V. et al., Nucl. Data Tables 5 (3-4) (1969) 416
[19] John, W. et al., Phys. Rev. C2 (1970) 1451
[20] McMurray, W.R. et al., Zeitschrift für Physik 253 (4) (1972) 289
[21] Lynn, J.E., AERE M 2505 (1971)
[22] Arlt, R.-D. et al., ZFK Gemeinsamer Jahresbericht 1975, ZfK-295
[23] Kaplan, S.N. et al., 6. Int. Conf. on High Energy Phys. and Nucl. Struct. Santa Fe 1975
[24] Akimov, Yu.K. et al., Nucl. Instr. Meth. 104 (1972) 581
[25] Andert, K. et al., JINR P6-856 4 (1975)

[26] Hüfner, J. cascade calculation after Eisenberg Y. et al., Il Nuov. Cim XIX (1961) 1195
[27] Acker, H.L., Nucl. Phys. 87 (1966) 153
[28] De Wit, S.A. et al., Nucl. Phys. 87 (1967) 657
[29] Trautmann, N. et al., Z. f. Naturforschung 23a (12) (1968) 2127
[30] Gross, E. et al., Phys. Rev. Lett 35 (1975) 565
[31] Pashkewich, V.V., private communication
[32] Specht, H.J., Int. Conf. on Nucl. Physics vol 2, Munich 1973

ПОИСК ИЗОМЕРИИ ФОРМЫ В ИЗОТОПАХ ПОЛОНИЯ

Р. Арльт, М. Ёнь, Г. Музиоль, Г. Хайзер+, Г. Хоффманн

Технический Университет Дрезден, (ГДР),
+ЦЯИ Россендорф, (ГДР)

I. Введение

В теоретических работах ряда авторов [I] было предсказано существование второго минимума потенциальной энергии ядер в районе свинца как функция от параметра деформации. Авторы работы [2] рассматривают причина этого эффекта и его зависимость от числа нейтронов и протонов. Кроме того они дают численные результаты свойств второго минимума в ряде ядер около $^{208}_{82}Pb$, полученные на основе собственных вычислений. Второй минимум согласно этим расчетом характеризуется следующими свойствами:

I) второй минимум расположен около $\varepsilon \sim 0,4$, глубина его достигает несколько Мэв (см. рис. I, работы [2]),

2) энергия основного состояния второго минимума в ряде случаев расположена выше энергии связи нейтрона (таблица I, работа [2]),

3) экстраполируя свойства ядер от Pt до Th можно ожидать сохранение второго минимума даже в случае, когда допускается γ-деформация,

4) второй минимум должен быть особенно выражен в ядрах около полосы β-стабильности, то есть в ядрах, которые легко можно исследовать в реакциях с легкими заряженными частицами или нейтронами.

Факт существования второго минимума установлен экспериментально в области актинидов. Целью настоящей работы является поиск таких свойств у ядер около $^{208}_{82}Pb$, которые позволили бы проверить экспериментально результаты работ [I, 2] и начинать соответствующие эксперименты.

2. Распад состояний второго минимума

Когда второй минимум потенциальной энергии существует над уровней, превышающем энергию связи нейтрона, тогда в нём при достаточной его глубине в следствии ядерных реакций могут возбуждаться квазисвязанные состояния. Разрядка этих состояний может идти разным путем. Проникновение внешнего барьера (рис. I, канал I) ведёт к спонтанному делению. Так как этот барьер достаточно широк в ядрах около свинца, этот вид распада мало вероятен. В работе [3] было например показано, что сечение этого канала должно быть меньше 0,I мкбарн. Вторым каналом распада состояний во второй яме является проникновение внутреннего барьера (рис. I, канал II). Время жизни для разрядки уровней этим процессом оценивалось в работе [2]. Оно составляет от 10^{-15} до 10^{-3} сек в различных ядрах

данной области. При этом ядро может испускать заряженные частицы, нейтроны или γ-кванты. Из за кулоновского барьера испускание заряженных частиц сильно подавляется, так что в основном остается испускание нейтронов и γ-квантов.

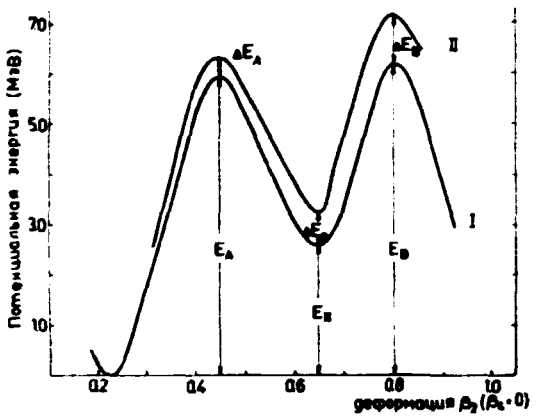

Рис. I Схематическое изображение распада ядер около ^{208}Pb из основного состояния второго минимума

Вероятность эмиссии нейтронов должно расти с увеличением энергии основного состояния во втором минимуме, а также в том случае, когда дочернее ядро ^{A-1}Z обладает малоэнергетическим состояния с низким значением спина. В другом случае, когда энергия второго минимума близко или ниже энергии связи нейтрона, или когда дочернее ядро отличается большим значением спина предимущественным каналом распада будет испускание каскад γ-квантов. Как известно, процессы эмиссии нейтронов и γ-квантов происходят за очень короткое время по сравнению с временем, необходимым для прозачивания барьера, в этом случае внутреннего. Таким образом существование второго минимума может привести к появлению изомерии формы.

3. Проводимые нами эксперименты и полученные результаты

3.I Возбуждение состояний во втором минимуме в реакции $(\alpha, n\gamma)$

При облучении свинцовой мишени с 27 Мэв-ными α-частицами на ядрах $^{207}_{82}Pb$ происходит реакция $(\alpha, 2n)$. Энергия возбуждение компаундядра $^{211}_{84}Po$ достаточно для испарения двух нейтронов. После испускания первого возможны две пути дальнейшей разрядки. Либо остаточная энергия возбуждения снимается испусканием еще одного нейтрона и γ-квантов $(\alpha, 2n, \gamma)$ либо она освобождается только испусканием γ-квантов, хотя энергия возбуждения после эмиссии первого нейтрона больше энергии связи нейтрона $(\alpha, n\gamma)$. Последний процесс может вести к заселению состояний во второй яме ядра $^{210}_{84}Po$. В работе [2] вероятность такого процесса оценивается как 10^{-3} - 10^{-5} по сравнению с переходом ядра в первый минимум.

3.2 Поиск задержанных γ-квантов

Облучалась мишень из естественной смеси изотопов свинца 27 Мэв-ными α-частицами на циклотроне Ц-120 ЦИЯИ в Россендорфе. Регистрировались спектры мгновенных и задержанных γ-квантов. В качестве сигнала стоп были использован синхроимпульсы циклотрона. Методика обще известная гамма спектроскопия с $Ge(Li)$-детекторами. Поиск задержанных γ-квантов проводимая на хорошо излученных низко-энергетических переходах изотопов Po, учитывая что распад высоко возбужденных состояний с большой вероятностью идет через этие уровни. В эксперименте мы искали слабые

задержанные компоненты этих переходов. В изотопах Po известно много состояний с временами жизни в наносекундной области. Поэтому мы искали только в милли- и микросекундной областях.

В мгновенном спектре были идентифицированы переходы между низколежащими уровнями изотопов Po от A = 206 до A = 211. В исследованной области времени не были найдены задержанные компоненты изотопов Po. Задержанные γ-лучи также не были найдены. Экспериментальный результат позволяет таким образом оценить лишь верхний предел сечения распада изомерного состояния Po по каналу испускания γ-квантов. Он составляет около I мбарн.

3.3 Поиск задержанных нейтронов

Выведенный пучок 27 Мэв-ных α-частиц циклотрона Ц-120 был тщательно сфокусирован, чтобы предотвратить попадение отдельных частиц на стены коно провода или на диафрагму. Все α-частицы были заторможены в толстой мишени. Эти меры были необходимы для того, чтобы вне мишени не образовались нейтрона. В качестве нейтронных детекторов использовались однослойные ионизационные камеры деления с изотопами ^{238}U и ^{232}Th и сцинтилляционный спектрометр с кристаллом из стильбена и схемой для (n,γ)-дискриминации. Фактор поддавления γ-квантов составлял 10^{-4} при энергии нейтронов выше I Мэв и скорости счета $\approx 10^3$/сек.

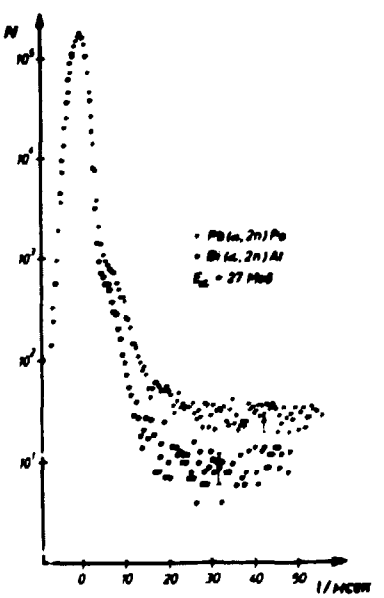

Рис. 2 Спектра задержанных нейтронов, снятые при помощи сцинтилляционного детектора с кристаллом стилбен при установлении порога n,γ-дискриминации на энергию нейтронов равную I Мэв.

Первые измерения были проведены в наносекундной области. В качестве мишени были использованы свинец и висмут в естественном составе изотопов. В обоих случаях во временном спектре (рис. 2) наблюдался короткий экспоненциальный участок с периодом полураспада 2,5 нсек. Этот эффект также имеет место при облучении алюминия. Причиной его может быть разброс α-частиц по времени. В этом диапазоне времени других задержанных эффектов не удалось наблюдать. Соответствующая оценка верхнего предела сечения распада возможных изомеров по нейтронному каналу составляет приблизительно 100 мкбари с периодом полураспада от 20 нсек до 100 нсек.

Однако, как видно из рис. 2 фон задержанных нейтронов в случае свинца приблизительно в три раза больше нежели в случае висмута. При этом нормировка проводилось по мгновенному пику. Возможна следующие варианты объяснения:

I) Может быть, что мгновенный энергетический спектр в двух рассматриваемых случаях мишени сильно отличается, так что проведенная нормировка недопустима.

2) Если спектры мгновенных нейтронов в достаточной мере отличаются друг от друга, тогда спектры рассеивания, регистрируемые в детекторе после отражения на спектрах помещения могут отличаться еще более сильно.

3) В четно-четных изотопах Po могут возбуждаться сравнительно много спиновых изомеров, которые разряжаются через γ-каскады. Если они частично не были охвачены (n,γ)-дискриминацией, тогда это приведет к повышенному фону в экспериментах со свинцовой мишенью.

4) Возможно существование долгоживущего состояния в одном из изотопов Po, которое излучает задержанные нейтрона. Для проверки этого предположения в ближайшее время проводится эксперимент во микросекундном диапазоне времени.

Авторы работы считают своим приятным долгом поблагодарить С.М. Поликанову за стимулирующие дискуссии, групп циклотрона ПИЯИ в Россендорфе за предоставление пучка, Х. Функе за поддержку, а В. Вагнер за помощь при проведении экспериментальных работ.

Литература

[I] В.В. Паникевич, ОИЯИ Р4 - 4383, Дубна 1969
C.F. Tsang et al., Nucl. Phys. A140 (1970) 275
M. Mosel et al., Phys. Rev. Lett. 25 (1970) 678
M. Mosel et al., Phys. Rev. C4 (1971) 2185
[2] S. Frauendorf, S.R. May, V.V. Paschkewitsch (siehe diese Veröffentlichung)
[3] S. Björnholm et al. Nucl. Phys. A156 (1970) 561

О ПОСТАНОВКЕ НОВЫХ ЭКСПЕРИМЕНТОВ ПО ИССЛЕДОВАНИЮ СВОЙСТВ СПОНТАННО ДЕЛЯЩЕГОСЯ ИЗОМЕРА ^{242}Am НА ИМПУЛЬСНЫХ РЕАКТОРАХ ИБР-30 И ИБР-2 ЛНФ ОИЯИ

Е. Дермендиев

Институт ядерных исследований и ядерной энергетики Болгарской АН,
София (Болгария)

Аннотация

Показано, что нейтронные спектрометры по времени пролета на базе импульсных реакторов ИБР-30 и ИБР-2 ЛНФ ОИЯИ могут быть использованы для постановки новых экспериментов:

а) по измерению среднего числа нейтронов на акт изомерного деления $\overline{\nu}_{if}$ ядра ^{242}Am,

б) по исследованию корреляции между вероятностями изомерного деления и делительными ширинами нейтронных резонансов ^{241}Am.

Введение

Открытие изомерного деления ядер ^{242}Am [1] с точки зрения представлений о процессе деления, основанных на модели жидкой капли казалось явлением необычным и трудно объяснимым. Однако открытие большого числа спонтанно делящихся изомеров дает основание предполагать, что такой "способ" деления тяжелых возбужденных ядер не является чем-то исключительным. Скорее наоборот - большинство изотопов тяжелых ядер при определенных условиях испытывают изомерное деление. В настоящее время на базе концепции двугорбого барьера деления [2] можно довольно правдоподобно объяснить ряд свойств спонтанно делящихся изомеров [3, 4].

Изучение подбарьерного деления ядер ^{237}Np [5], ^{240}Pu [6], ^{234}U [7] привело к открытию явления "группирования" нейтронных резонансов и "модуляции" их силы. Пока эти факты можно понять только используя представление о барьере деления с двумя минимумами и двумя взаимодействующими через промежуточный барьер системами уровней составного делящегося ядра в минимумах [8].

Среди многих интересных проблем, связанных с изомерно делящимися ядрами можно выделить и такие, которые являясь важными для понимания процесса изомерного деления и получения новой информации о нем, в то же время могут быть решены методами нейтронной спектроскопии ядер и, в частности, с использованием импульсных реакторов ИБР-30 и ИБР-2 ЛНФ ОИЯИ.

Ниже будут рассмотрены возможности постановки экспериментов по исследованию характеристик деления спонтанно делящегося изомера ^{242}Am на реакторах ИБР-30 и ИБР-2.

I. Измерение среднего числа нейтронов $\bar{\nu}_{if}$ на акт изомерного деления ^{242}Am

I. В 1971 г. по предложению С.М. Поликанова нами была рассмотрена возможность постановки эксперимента по измерению среднего числа нейтронов $\bar{\nu}_{if}$ на акт изомерного деления ^{242}Am. Суть опыта состоит в сравнении величины $\bar{\nu}_{if}$ для составного ядра ^{242}Am, образованного при облучении ^{241}Am тепловыми нейтронами со средним числом нейтронов $\bar{\nu}_{th}$ при делении ^{241}Am тепловыми нейтронами.

В принципе, измерение величины $\bar{\nu}_{if}$, которая сама по себе представляет несомненный интерес, является важным еще и по следующей причине. В настоящее время обычно предполагают, что изомерное деление - это спонтанное деление ядра из основного состояния во II-ой яме (см. рис. I).

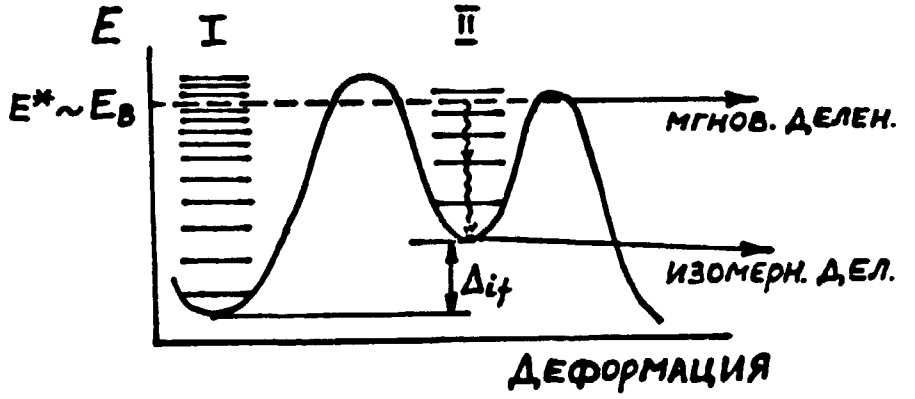

Поскольку энергия основного состояния во II-ой яме Δ_{if} меньше энергии возбуждения E^* составного ядра на величину разности $E^* - \Delta_{if}$ то можно предположить, что значение $\bar{\nu}_{if}$ будет отличаться от $\bar{\nu}_{th}$ и, что $\bar{\nu}_{if} < \nu_{th}$ Количественная оценка этого эффекта весьма затруднительна, однако можно надеяться, что известная формула [9]

(I) $$d\bar{\nu}/dE^* \sim 0{,}101$$

окажется справедливой и при значениях $E^* < E_B$, где E_B - энергия связи нейтрона в составном ядре.

Выбор ядра-мишени ^{241}Am обусловлен следующими соображениями:

а) К настоящему времени достоверно известно лишь одно спонтанно делящееся изомерное ядро, - ядро ^{242}Am, которое образуется в реакции с тепловыми нейтронами [10]. Ядро-мишень ^{241}Am имеет относительно большое сечение деления на тепловых нейтронах - $\sigma_f^{th} = 3{,}13$ барн /11/, кроме того для ядра ^{242}Am определена величина $\sigma_{if}/\sigma_f^{th} \sim 10^{-4}$ [10].

б) Период полураспада по отношению к изомерному делению $T_{1/2}^{if}$ для ^{242}Am 14 мсек. Ядро ^{242}Am обладает наибольшим среди изученных делящихся изомеров значением $T_{1/2}^{if}$, и поэтому является наиболее благоприятным объектом для исследований на импульсных реакторах ИБР-30 и ИБР-2. Ниже этот вопрос обсуждается более подробно.

Используя формулу (I) и следующие значения: $E^* \sim 5{,}5$ Мэв, $\Delta_{if} \sim 3$ Мэв, $\overline{\nu}_{th} = 3{,}12$ [I2] можно получить оценку для ожидаемого изменения $\overline{\nu}_{if}$ по сравнению с $\overline{\nu}_{th}$:

(2) $$\Delta\overline{\nu} \cong 0{,}10I,\ E^* \cong 0{,}10I.(5{,}5-3) = 0{,}253$$

Относительное изменение

(3) $$\Delta\overline{\nu}/\overline{\nu}_{th} \approx 8\ \%$$

Таким образом оценка по максимуму дает для ожидаемого эффекта величину ~8 %.

2. Постановка опыта по измерению $\overline{\nu}_{if}$

Для определения $\overline{\nu}_{if}$ предлагается следующая схема опыта (см. рис. 2).

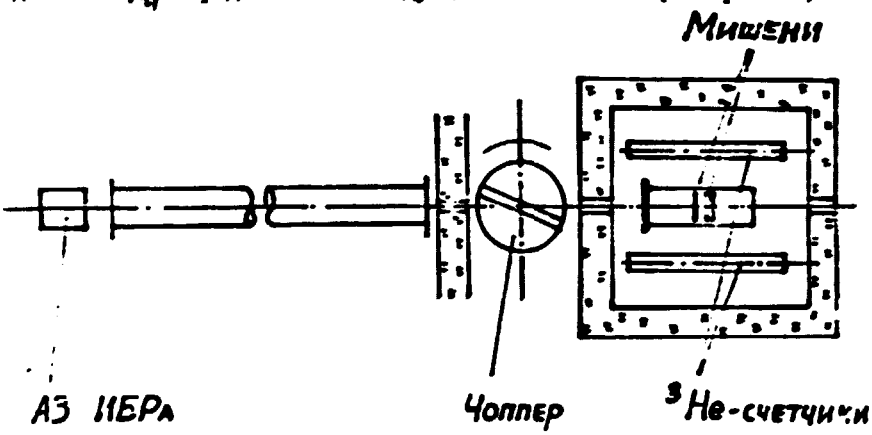

Используются две мишени из ^{241}Am с одинаковой площадью S (принимаем $S = 20$ см^2):
а) тонкая мишень с толщиной слоя $\varsigma_1 \sim 2$ мг/см^2,
б) толстая мишень с толщиной слоя $\varsigma_2 \sim 25$ мг/см^2.

Общее количество ^{241}Am не превышает ~ I г. Тонкая мишень ставится в детектор осколков (искровая камера, газовый сцинтилляционный счетчик) и служит для счета осколков деления N_{f1}^{th} и N_{f1}^{if} при тепловом и изомерном делении ядер америция. Толстая мишень устанавливается вблизи тонкой мишени так, чтобы обе мишени пронизывались одним и тем-же потоком нейтронов. Рядом, вне пучка, устанавливается детектор нейтронов, который регистрирует число нейтронов N_n^{th} и N_n^{if} при тепловом и изомерном делении соответственно. Прерыватель нейтронного пучка, синхронизированный с импульсами ИБРа, пропускает на мишени только тепловые нейтроны. Во время облучения мишеней нейтронами соответствующая электронная аппаратура регистрирует осколки $/N_{f1}^{th}/$ и мгновенные нейтроны деления $/N_n^{th}/$. В интервалах времени, когда нейтронный пучок перекрыт, регистрируются величины N_{f1}^{if} и N_n^{if} .

Число тепловых делений N_{f1}^{th} регистрируемых детектором осколков:

(4) $$N_{f1}^{th} = N_{f0}^{th}\ \varepsilon_f$$

где N_{f0}^{th} - полное число делений в тонком слое,
ε_f - эффективность детектора осколков.

Число мгновенных нейтронов деления, регистрируемых детекторами нейтронов:

$$(5) \qquad N_n^{th} = \left(\frac{N_{f1}^{th}}{\varepsilon_f} + N_{f=2}^{th} \right) \cdot \bar{\nu}_{th} \cdot \omega \cdot \varepsilon_n$$

Здесь $N_{f=2}^{th}$ - полное число делений в толстом слое,
ω - телесный угол регистрации нейтронов,
ε_n - эффективность регистрации нейтронов теплового деления.

Предполагается, что в ф-ях (4) и (5) и далее фон учтен. Аналогичные формулы можно написать и для изомерного деления:

$$(6) \qquad N_{f1}^{if} = N_{f=1}^{if} \cdot \varepsilon_f$$

$$(7) \qquad N_n^{if} = \left(\frac{N_{f1}^{if}}{\varepsilon_f} + N_{f=2}^{if} \right) \bar{\nu}_{if} \, \omega \, \varepsilon_n$$

После несложных преобразований получим:

$$(8) \qquad \bar{\nu}_{if} = \bar{\nu}_{th} \cdot \frac{N_n^{if}}{N_n^{th}} \cdot \frac{N_{f1}^{th}}{N_{f1}^{if}}$$

Таким образом, зная величину $\bar{\nu}_{th}$ и измеряя остальные величины, из формулы (8) можно определить $\bar{\nu}_{if}$.

3. Численные оценки

На основании результатов работы [13] для реактора ИБР-30 принимаем средний поток тепловых нейтронов $\bar{\varphi}_{th} = 10^{13}$ н/сек 4π. Детекторная аппаратура устанавливается на расстоянии $L = 10$ м от активной зоны ИБР-30 (выбор величины L рассматривается ниже). Приближенно величина N_{f1}^{th} определяется по формуле

$$(9) \qquad N_{f1}^{th} \sim \bar{\varphi}_{th} \cdot \frac{S}{4\pi L^2} \cdot \sigma_f^{th} \cdot n_1 \cdot \varepsilon_f$$

Принимая $\bar{\varphi}_{th} = 10^{13}$ н/сек 4π, $S = 20$ см^2, $L = 10$ м, $\sigma_f^{th} = 3{,}13$ барн, $n_1 = 5 \cdot 10^{18}$ яд/см^2 $\varepsilon_f = 0{,}4$,
получаем $N_{f1}^{th} = 100$ дел/сек.

За 250 час: $N_{f1}^{th}(250) = 10^8$ дел/250 ч.

Число изомерных делений за 250 час:

$$N_{f1}^{if}(250) = N_{f1}^{th}(250) \cdot \frac{\sigma_{if}}{\sigma_f^{th}}$$

Поскольку для ядра ^{242}Am $\sigma_{if}/\sigma_f^{th} \sim 10^{-4}$, то

$$N_f^{if}(250) = 10^4 \text{ дел/250 час.}$$

Регистрацию мгновенных нейтронов можно осуществить при помощи:

а) ^3He - счетчиков,

б) сцинтилляционного счетчика с разделением импульсов от "n" и "γ" по форме импульса.

При наличии достаточного количества ^{3}He - счетчиков, этот метод имеет ряд преимуществ. Поэтому здесь обсуждается эффективность детектора нейтронов на базе ^{3}He - счетчиков. Предполагается, что диаметр $\varnothing$ = 3,5 см, давление ^{3}He p = 10 ати эффективность регистрации быстрых нейтронов (E_n = 1 Мэв) $\varepsilon_{n1} \sim 5 \cdot 10^{-3}$ и эффективность регистрации тепловых нейтронов $\varepsilon_{n2} \sim 1$.

Возможны два варианта использования ^{3}He - счетчиков:

а) с замедлителем нейтронов,
б) без замедлителя нейтронов.

Какой из них более выгоден - в смысле максимального отношения эффект/фон, оптимального времени для проведения эксперимента и т.д. - покажет опыт.

Ниже рассматриваются оба варианта.

Полное число тепловых делений в обеих мишенях:

$$N_{f_0}^{th} \sim \overline{\varphi}_{th} \cdot \frac{S}{4\pi L^2} \cdot \sigma_f^{th} \cdot (n_1 + n_2) \qquad (10)$$

при $n_1 = 5 \cdot 10^{18}$ яд/см^2 и $n_2 = 6{,}25\ 10^{19}$ яд/см^2

$$N_{f_0}^{th} \cong 3{,}4 \cdot 10^3 \text{ дел/сек},$$
$$N_{f_0}^{th}(250) \cong 3{,}10^9 \text{ дел/250 час}.$$

Полное число изомерных делений

$$N_{f_0}^{if}(250) = 3 \cdot 10^5 \text{ дел/250 час}.$$

Число нейтронов деления, которые регистрируются детектором нейтронов без замедлителя:

$$N_n^{th}(250) \approx N_{f_0}^{th}(250) \cdot \omega_n \cdot \varepsilon_{n1} \cdot \overline{\nu}_{th} \qquad (11)$$

При $\omega_n \sim 0{,}5$, $\varepsilon_{n1} \sim 5 \cdot 10^{-3}$ и $\overline{\nu}_{th} = 3{,}12$

$$N_n^{th}(250) = 2{,}3 \cdot 10^7 \text{ н/250 час}$$
$$N_n^{if}(250) = 2{,}3 \cdot 10^3 \text{ н/250 час}$$

При использовании замедлителя нейтронов вокруг ^{3}He-счетчиков

$$N_n^{th}(250) \cong 5 \cdot 10^9 \text{ н/250 час}$$
$$N_n^{if}(250) = 5 \cdot 10^5 \text{ н/250 час}$$

Таким образом, оценки показывают, что такой эксперимент на ИБР-30 является невозможным.

4. Требования к чистоте мишеней из ^{241}Am

Примеси спонтанно делящихся ядер создают нежелательный фон. В зависимости от требуемого соотношения между уровнем фона спонтанного деления и "эффектом" в таблице I приводятся допустимые количества для некоторых спонтанно делящихся изотопов.

5. Выбор базы, прерыватель пучка, электроника

При измерениях $\bar{\nu}_{if}$ для ^{242}Am на ИБР-30 (частота импульсов f = 5 сек$^{-1}$) наиболее подходящим является пролетное расстояние с L ~8 - I5 м. В таблице II приводится время пролета для нейтронов разных энергий $E_н$ при L = I0 м.

Таблица II

$E_н$ эв	I0	5	2	I	0,5	0,2	0,I	0,0I	0,005	
T мксек	224	326	5I0	723	I020	I620	2240	7230	I0200	
	пучок перекрыт					облучение				перекр.

Облучение мишеней нейтронами проводится в следующей последовательности. В течении I,5 - I,8 мсек после вспышки ИБРа пучок перекрыт, затем в интервале времени I,5 мсек - I0 мсек после момента вспышки мишени облучаются, после чего вплоть до следующей вспышки реактора пучок снова перекрывается. Такому режима облучения мишеней удовлетворяет прерыватель (чоппер) со скоростью ~ I50 об/мин. Возможны разные варианты конструкции чоппера, однако каждая из них должна максимально ослаблять пучок в момент перекрытия. Требования к синхронизации вращения чоппера с импульсами ИБРа повидимому не являются слишком жесткими. Из таблица II видно, что смещение во времени момента открывания пучка может достигать величины δ~(0,5 мсек/200 мсек) I00 % = 0,25 % без существенного изменения его интенсивности.

Заключение

Выше было показано, что при измерении величины $\bar{\nu}_{if}$ за не слишком большое время измерения (~ 250 час) число зарегистрированных актов изомерного деления ^{242}Am может быть доведено до ~ $I0^4$, а число зарегистрированных мгновенных нейтронов изомерного деления ~ $I0^5$ (^{3}He - счетчики с замедлителем). В тоже время при требуемой чистоте ^{241}Am (см. табл. I) фон от спонтанного деления примесей может быть сделан достаточно малым. Спонтанное деление ^{241}Am создает заметный фон, однако он может быть учтен с необходимой для опыта точностью.

Таблица I[А]

Максимально допустимое содержание спонтанно делящихся изотопов в америциевой мишени

Изотоп	$T_{1/2}^{sf}$ (год)	$T_{1/2}^{\alpha}$ (год)	N^{sf} $(г \cdot час)^{-1}$	Содержание изотопа * (г/г)
^{236}Pu	$3{,}5 \cdot 10^{9}$	2,7	$5{,}8 \cdot 10^{7}$	10^{-5}
^{238}Pu	$4{,}9 \cdot 10^{10}$	90	$4 \cdot 10^{6}$	10^{-4}
^{240}Pu	$1{,}2 \cdot 10^{11}$	$2{,}4\ 10^{3}$	$1{,}6 \cdot 10^{6}$	$3\ 10^{4}$
^{242}Pu	$6{,}7 \cdot 10^{10}$	$6{,}6\ 10^{3}$	$2{,}9 \cdot 10^{6}$	$1{,}7\ 10^{-4}$
^{241}Am	$2{,}3 \cdot 10^{14}$	$4{,}7\ 10^{2}$	10^{2}	-
^{244}Cm	$1{,}4 \cdot 10^{7}$	18,4	$1{,}4 \cdot 10^{10}$	$3{,}5 \cdot 10^{-8}$
^{246}Cm	$3 \cdot 10^{7}$	$4\ 10^{3}$	$6{,}4 \cdot 10^{9}$	$8 \cdot 10^{-8}$
^{249}Cf	$1{,}5 \cdot 10^{9}$	470	$1{,}3 \cdot 10^{7}$	$4 \cdot 10^{-5}$
^{250}Cf	$1{,}4 \cdot 10^{4}$	10	$1{,}3 \cdot 10^{12}$	$4 \cdot 10^{-10}$
^{252}Cf	66	2,2	$2{,}9 \cdot 10^{15}$	$2 \cdot 10^{-13}$

* - предполагалось, что фон от спонтанного деления для данного изотопа должен быть в 50 раз меньше числа изомерных делений ^{242}Am

Таблица I[Б]

Максимально допустимое содержание изотопов с большим значением σ_f^{th} в америциевой мишени

Изотоп	σ_f^{th} (барн)	Содержание изотопа * (г/г)
^{235}U	580	10^{-4}
^{239}Pu	754	10^{-4}
^{241}Pu	1060	$5 \cdot 10^{-5}$
^{242}Am	6000	10^{-5}
^{244}Am	2300	$2{,}5 \cdot 10^{-5}$

* - предполагалось, что фон от деления ядер данного изотопа тепловыми нейтронами должен быть в 50 раз меньше числа изомерных делений ^{242}Am

Наиболее неопределенным является вопрос о "собственном" фоне искровой камеры и ^{3}He - счетчиков. Источниками этого фона являются рассеянные нейтроны, космическое излучение и др., а также аппаратурные эффекты (наводки, разряды и др.). Если исходить из требования, чтобы "собственный" фон камеры и ^{3}He - счетчиков был в 10 раз меньше полезного эффекта, то тогда фон искровой камеры не должен превышать 1 имп. за 15 мин. а фон гелиевых счетчиков - 1 имп./мин.

Таким образом, при подходящих условиях измерения величины $\overline{\nu}_{if}$ можно надеяться на точность в определении $\overline{\nu}_{if}$ ~2 - 3 %.

Выше было отмечено, что измерение величины $\overline{\nu}_{if}$ для спонтанного делящегося изомера ^{242}Am представляет несомненный интерес для физики деления. Действительно, если окажется, что $\overline{\nu}_{if} < \overline{\nu}_{th}$, то этот факт будет рассматривать как важный аргумент в пользу гипотезы двугорбого барьера.

Важность такого эксперимента по нашему мнению очевидна. Что касается численных оценок, то они тоже свидетельствуют о возможности постановки такого эксперимента уже на реакторе ИБР-30.

С целью повышения точности измерений, этот эксперимент в будущем может быть продолжен на реакторе ИБР-2. С другой стороны, многократное возрастание интенсивности нейтронного пучка открывает новые методические возможности (использование совпадений "осколок - нейтрон" и др.) для более точного определения $\overline{\nu}_{if}$

II. Измерение отношения вероятностей изомерного и мгновенного делений σ_{if}/σ_f в нейтронных резонансах ^{241}Am

Анализ величины σ_{if} и σ_f для изомерного и мгновенного делений в тепловой области для ^{242}Am [10] и при делении быстрыми нейтронами для ^{242}Am и ^{244}Am [14] показывает, что имеется "очень сильная корреляция между двумя процессами - мгновенным делением и образованием делящихся изомеров... Существование указанной корреляции позволяет заключить, что образованию делящихся изомеров предшествует возникновение колебаний, соответствующих делительным степеням свободы" [3].

Выше было отмечено, что ядро ^{242}Am, образующееся при бомбардировке ^{241}Am нейтронами, обладает наибольшим значением $T_{\frac{1}{2}}^{if}$ = 14 мсек и благодаря этому оно является подходящим объектом для исследования процесса изомерного деления методами нейтронной спектроскопии. С другой стороны в интервале $E_н \leq$ 10 эв значения делительных ширин Γ_f в нейтронных резонансах ^{241}Am отличаются в несколько раз. Например $\Gamma_f/\Gamma(E_н$ = 0,575 эв) = 0,34 ± 0,05, $\Gamma_f/\Gamma(E_н$ = 10,05 эв) = 3,2 ± 0,6 [15]. Полагая Г = 50 Мэв [15], получаем Γ_f ~0,17 Мэв и ~1,6 Мэв соответственно. Исходя из отмеченной выше корреляции между вероятностями мгновенного и изомерного делений и наличия довольно сильной флюктуации величин Γ_f было бы интересно измерить отношения σ_{if}/σ_f в первых низколежащих резонансах ^{241}Am.

Нейтронный спектрометр по времени пролета на базе импульсного реактора ИБР-2 будет иметь рекордную интенсивность резонансных нейтронов и, что особенно важно для исследования изомерного деления, сможет работать с малой частотой повторения нейтронного импульса ($f \sim 5 - 50$ сек$^{-1}$). Таким образом ИБР-2 является наиболее подходящей для предлагаемой работы установкой.

Схема опыта. Измерения будут вестись на короткой базе /$L = 15 - 30$ м/. Как и в предыдущем эксперименте перед мишенью (или мишенями) из ^{241}Am ставится прерыватель нейтронного пучка, вращение которого происходит синхронно с импульсами ИБРа. Прерыватель настраивается на данный резонанс и в момент облучения мишени регистрируются мгновенные деления. При перекрытом пучке регистрируются изомерные деления.

Следует отметить, что конструкция прерывателя нейтронного пучка для данного эксперимента должна удовлетворять ряду довольно жестких требований:
а) Большая светлосила при достаточно низком фоне.
б) Высокая степень синхронизации оборотов прерывателя с импульсами ИБРа.
в) Возможность настройки на данный временной интервал, который соответствует данному нейтронному резонансу в широком диапазоне $E_н \sim 10^{-2} - 10$ эв.

Так например, для резонанса при $E_н = 0{,}575$ эв интервал в 0,1 эв (0,575 $\pm$ 0,05эв) соответствует времени облучения $\Delta T \sim 140\mu$ сек, а для резонанса при $E_н = 5{,}48$ эв интервал $E_н = 0{,}5$ эв соответствует $\Delta T = 40\mu$ сек. Здесь мы не будем касаться технических проблем, связанных с реализацией такого прерывателя нейтронного пучка, поскольку этот вопрос само по себе является достаточно сложным. Ограничимся лишь обсуждением вопросов физического характера.

Численные оценки. Для расчетов использовались данные по Γ_f/Γ для резонансов ^{241}Am из работы [15], причем для определения значений в резонансах полагали, что $\Gamma = 50$ Мэв.

Для средней мощности реактора ИБР-2 принималось значение $P = 3000$ квт. Значения нейтронных потоков в резонансах определялись из графика рис. 5 в работе [13] для $P = 3000$ квт. База $L = 17$ м.

Для регистрации осколков деления используется многослойный детектор осколков (многослойная искровая камера). Число мишеней - 10, толщина каждого слоя $\varsigma \sim 2$ мг/см^2, площадь $S = 10$ см^2. Общее количество $^{241}Am \sim 0{,}2$ г.

Сумма счетов делений в резонансе определяется по известной формуле

$$(12) \qquad \sum N_f = \Pi \cdot \varepsilon_f \cdot \frac{\Gamma_f}{\Gamma} \cdot A ,$$

где Π - поток нейтронов (сек. см^2 эв)$^{-1}$,
ε_f - эффективность детектора осколков,
A - вавовская площадь резонанса.

Таблица III

E_0 эв	$\frac{\Gamma_f}{\Gamma} \cdot 10^{-2}$	Γ_f Мэв	$\sigma_0 \Gamma_f$ барн эв	Π для P=3000 квт =17 м $(см^2 сек\ eV\ PL)^{-1}$	$\sum N_{f_0}$ мгнов дел/сек	$\sum N_{f_0}(24)$ мгнов дел/24час	$\sum N_{f_0}^{if}(24)$ изомерн дел/24час
0,306	0,76±0,12	0,38	$12,5 \cdot 10^{-3}$	10^8	300	$2,5 \cdot 10^7$	$2,5 \cdot 10^3$
0,575	0,34±0,05	0,17	$1,5 \cdot 10^{-3}$	$4,5 \cdot 10^7$	16	$1,6 \cdot 10^6$	160
1,27	0,74±0,07	0,37	$11 \cdot 10^{-3}$	$2,5 \cdot 10^7$	65	$5,5 \cdot 10^6$	550
5,06	0,55±0,25	0,20	$0,8 \cdot 10^{-3}$	$6,5 \cdot 10^6$	1,3	$1,1 \cdot 10^5$	11
5,48	1,01±0,10	0,50	$6,2 \cdot 10^{-3}$	$6 \cdot 10^6$	9	$7,5 \cdot 10^5$	75
10,05	3,2±0,6	1,6	$7,2 \cdot 10^{-3}$	$3,5 \cdot 10^6$	6	$5 \cdot 10^5$	50

Для тонкой мишени:

(I3) $$A = \frac{I \cdot n}{2} \cdot \sigma_0 \Gamma ,$$

где n – число ядер мишени на $см^2$,
σ_0 – значение полного сечения в максимуме резонанса,
Γ – полная ширина резонанса.

Суммарный счет делений в сек со всей площади мишени и всех мишеней

(I4) $$\sum N_{f_0} = \sum N_f \cdot 10S.$$

Окончательно ($S = 10$ $см^2$, $n = 5 \cdot 10^{18}$ $см^{-2}$, $\varepsilon_f = 0{,}3$)

(I5) $$\sum N_{f_0} = 2{,}36 \cdot 10^{20} \cdot \Pi \cdot \sigma_0 \Gamma_f$$

Число изомерных делений в резонансах можно оценить, полагая что

(I6) $$\sum N_{f_0}^{if} \sim 10^{-4} \cdot \sum f_0$$

Все исходные данные вместе с результатами расчетов приводятся в табл. III.

При оценке допустимого содержания спонтанно делящихся примесей в мишенях из ^{241}Am исходили из требования, чтобы число фоновых отсчетов в резонансе при $E_n = 5{,}48$ эв было в 2 раза меньше величины $\sum N_{f_0}^{if}$ (5,48) ~ 75. При этом концентрацию изотопов из табл. II следует уменьшить еще в 3 раза, а собственный фон детектора осколков должен быть меньше I имп./час.

Заключение. Наблюдение изомерного деления составного ядра ^{242}Am в нейтронных резонансах ^{241}Am, может, в какой то мере, пролить свет на возможную корреляцию между вероятностями мгновенного деления и образования спонтанно делящегося изомера ^{242}Am. С этой точки зрения предлагаемый эксперимент представляет определенный интерес.

Заслуживает внимания и то обстоятельство, что параметры импульсного реактора ИБР-2 наилучшим образом удовлетворяют требованиям данного эксперимента.

В заключение автор выражает благодарность С.М. Поликанову за ценные обсуждения.

Литература

[1] С.М. Поликанов и др. ЖЭТФ, 42 (1962) 1964
[2] V.M. Strutinsky, Nucl. Phys. A95 (1967) 420
[3] С.М. Поликанов, УФН, 107 (1972) 685
[4] Ю.П. Гангрский, Препринт ОИЯИ Р6 - 4307 (1969)
[5] D. Paya et al., Int. Symp. Nucl. Str. /IAEA, Vienna, 1968, p.483
[6] E. Migneco, J. Theobald, Nucl. Phys. A112 (1968) 603
[7] G.D. James, E.R. Rae, Nucl. Phys. A118 (1968) 313

[8] E. Zynn "Physics and Chemistry of Fission" (IAEA) 1969 p. 449
[9] F. Manero, V.A. Conshin, Atomic En. Review 10 (1972) 637
[10] Ф.П. Гангрский и др. ЯФ, 10 (1969) 65
[11] E.K. Hullett et al., Phys. Rev. 102 (1956) 1621
[12] A.H. Jaffey, J.L. Lerner, Nucl. Phys. A145 (1970) 1
[13] В.В. Голиков и др. Сообщения ОИЯИ, 3 - 5736 (1971)
[14] Т. Надь и др. Препринт ОИЯИ, Р7 - 5162 (1970)
[15] Ю.Ф. Герасимов, "Nuclear Data for Reactors" IAEA, 1966, CN-23/112

КИНЕТИЧЕСКИЕ ЭНЕРГИИ ОСКОЛКОВ И ДИНАМИЧЕСКИЕ ЭФФЕКТЫ ПРИ ДЕЛЕНИИ ^{239}Pu РЕЗОНАНСНЫМИ НЕЙТРОНАМИ

Е. Дерменджиев

Институт ядерных исследований и ядерной энергетики Болгарской АН,
София (Болгария)

Аннотация

Обсуждается возможность наблюдения динамических эффектов, связанных с относительным движением осколков в момент деления составного ядра ^{240}Pu

В каналовой теории деления [1] предполагается, что деление тяжелых ядер S-нейтронами реализуется через малое число каналов деления с определенными значениями спина и четности J^π составного ядра и проекции K спина на ось симметрии ядра. Четные значения J^π и, в частности, $J^\pi = 0^+$ для составного ядра ^{240}Pu связаны с повышенным выходом симметричного деления, по сравнению с делением через канал с $J^\pi = 1^+$ для того же ядра [2]. Предполагалось, что такие характеристики деления, как средняя кинетическая энергия осколков E_K и среднее число нейтронов на акт деления $\bar{\nu}$, которые определяются массовыми распределениями осколков [3,4], также должны зависеть от выхода симметричных способов деления и, следовательно, от величины J [5,7], хотя последние работы [8,9] свидетельствуют об отсутствии заметной зависимости между $\bar{\nu}$ и спином J.

Ожидаемое при делении ^{239}Pu s-нейтронами уменьшение $\bar{E}_K$ за счет более высокого выхода симметричного деления в резонансах с $J^\pi = 0^+$ по сравнению с резонансами, для которых $J^\pi = 1^+$ наблюдалось в работе [10]. Найдено, что значение $\bar{E}_K$ в резонансе при $E_K = 0{,}29$ эв ($J^\pi = 1^+$) превышает на $0{,}75 \pm 0{,}05$ Мэв значение $\bar{E}_K$ в области крыла "отрицательного" резонанса, для которого предполагается $J^\pi = 0^+$.

С другой стороны Андреевым [II], Блинкиной и др. [I2] было предположено, что если энергия возбуждения E^* делящегося ядра больше высоты барьера деления $B^{J^\pi,K}$, то за счет динамических эффектов (ДЭ), связанных с относительным движением еще не разделившихся осколков значение E_K может возрасти на величину $\Delta E = E^* - B^{J^\pi,K}$. В случае деления ^{239}Pu S-нейтронами, такая точка зрения дает основание ожидать для E_K изменения противоположного знака по сравнению с экспериментально наблюдаемым в работе [I0] эффектом.

Действительно, поскольку принятая в настоящее время структура каналов деления составного ядра ^{240}Pu в седловой точке такова, что канал с $J^\pi = 0^+$ лежит ниже канала с $J^\pi = I^+$ примерно на I Мэв [I3], то следует ожидать, что $\Delta E(0^+) > \Delta E(I^+)$. Кроме того, учитывая, что средняя делительная ширина $\overline{\Gamma_f}(0^+)$ превышает $\overline{\Gamma_f}(I^+)$ более чем в 50 раз [I4] и предполагая в резонансах с $J^\pi = 0^+$ большую скорость относительного движения еще не разделившихся осколков [I2] можно ожидать, что $\overline{E_K}(0^+) > \overline{E_K}(I^+)$.

Наблюдение каждого из обсуждаемых выше эффектов изменения $\overline{E_K}$, которые в случае деления ^{239}Pu S-нейтронами имеют противоположные знаки, представляет несомненный интерес. Для наблюдения изменения $\overline{E_K}$, обусловленного ДЭ, предлагается сравнение значений E_K для наиболее вероятных осколков деления.

Известно, что каждому осколку с массой M соответствует распределение кинетических энергий $N(E_K)_M$ с дисперсией $\sigma \sim$ IO - I5 Мэв [4]:

$$N(E_K)_M \sim C \exp\left[-(\tilde{E}_K - E_K)^2/2\sigma\right]$$

Здесь $\tilde{E}_K$ - наиболее вероятное значение E_K для осколка с массой M, C - константа, учитывающая относительный выход осколка данной массы. Вследствие малого выхода осколков симметричного деления ($\sim$ I/600 для ^{235}U и $\sim$ I/I00 для ^{239}Pu) влияние "крыла" $N(E_K)$ для симметричного деления на величину кинетической энергии $\langle E_K \rangle$, которая усредняется по узкому интервалу около значения кинетической энергии для наиболее вероятного способа деления оказывается достаточно малым. Кроме того, в соответствии с законом сохранения импульса изменение E_K для легкого осколка окажется больше, чем для тяжелого осколка. Поэтому сравнивая значения $\langle E_K^L \rangle$ для наиболее вероятного легкого осколка в резонансах с разными спинами, в принципе можно обнаружить обсуждаемые выше ДЭ.

Интересно отметить, что ожидаемые в резонансах составного ядра ^{236}U изменения $\overline{E_K}$, которые обусловлены ДЭ, будут того-же знака, что и изменения $\overline{E_K}$ за счет различных выходов симметричного деления в резонансах с $J^\pi = 3^-$ и 4^-. С другой стороны, значения $\overline{\Gamma_f}(3^-)$ и $\overline{\Gamma_f}(4^-)$ (79 [illegible] и 25 Мэв соответственно [I5]) отличаются не столь сильно, как в случае ^{240}Pu, энергетический интервал между каналами с $J^\pi = 3^-(K = 0)$ и $J^\pi = 4^-(K = I)$ оценивается примерно в 0,5 Мэв или меньше [I3]. Вследствие этого, ожидаемое при делении ^{235}U S-нейтронами изменение $\overline{E_K}$, которое обусловлено ДЭ, может оказаться существено меньше, чем изменение $\overline{E_K}$ при делении ^{239}Pu.

Литература

[I] Bohr, A., Proc. Int. Conf. Peaceful Uses of Atomic Energy, Geneva, 2 (1956) 151
[2] Уиллер Дж., Сб. "Успехи физики деления" Атомиздат, 1963
[3] Апалин В.Ф., Добрынин Ю.П., Захарова В.П., Кутиков И.Е., Михайлов Л.А., Атомная энергия, 8 (1960) 15
[4] Milton, J.C.D. and Fraser J.S., Can. J. Phys. 40 (1962) 1626
[5] Melkonian, E. and Mehta G.K., Physics and Chemistry of Fission (IAEA, Vienna, 1965), v. II, p. 355
[6] Бочваров С., Дерменджиев Е., Кацукеев Н., Physics and Chemistry of Fission (IAEA, Vienna, 1969), p. 593
[7] Weinstein, S. and Block, R.C., Physics and Chemistry of Fission (IAEA, Vienna, 1969), p. 447
[8] Weston, L. and Todd, J., Conf. Neutron Cross Sections and Technology, University of Tennessee, 2 (1971) 861
[9] Shackleton, D. et al., Phys. Letters, 42B (1972) 344
[10] Toreskar, J. and Melkonian, E., Phys. Rev. 4C (1971) 267
[11] Андреев В.Н., "Тезисы совещания по делению ядер", Ленинград, 1961, Изд. АН СССР
[12] Blyumkina, J.A. et al., Nucl. Phys. 52 (1964) 648
[13] Griffin, J.J., Physics and Chemistry of Fission (IAEA, Vienna, 1965) p.23 v.I,
[14] Derrien, H. et al., Nucl. Data for Reactors (IAEA Vienna, 1967) p.195
[15] Ван ин-дя, Ван Ин-чан, Е. Дерменджиев, Ю.В. Рябов, Physics and Chemistry of Fission (IAEA, Vienna, 1965, v.I. p. 287)

КИНЕТИЧЕСКИЕ ЭНЕРГИИ ОСКОЛКОВ ДЕЛЕНИЯ ^{235}U В РЕЗОНАНСЕ 8,8 ЭВ

Г. Илчев, Е. Дерменджиев, Н. Калинкова, Н. Чиков

Институт ядерных исследований и ядерной энергетики Болгарской АН, София (Болгария)

Аннотация

На нейтронном спектрометре по времени пролета на базе импульсного реактора ИБР-30 ОИЯИ в Дубне измерены средние кинетические энергии $\bar{E}_K$ осколков деления ^{235}U в резонансе 8,8 эв и в тепловой точке. Найдено, что $\bar{E}_K(8,8) > \bar{E}_K(th)$ на (1,3 ± 1,5) Мэв.

Измерения средних кинетических энергий осколков $\bar{E}_K$ в S-нейтронных резонансах ^{235}U и ^{239}Pu, для которых значения спинов J известны, могут оказаться полезными для понимания процесса диссипации энергии возбуждения E^* делящегося ядра при разных деформациях ядра в седловой точке [1]. В случае деления ^{239}Pu установлено, что $\bar{E}_K(I^+) > \bar{E}_K(0^+)$ на $\sim 0{,}7$ Мэв [2]. При исследовании вариации $\bar{E}_K$ в резонансах ^{235}U по выходам наиболее высокоэнергетических осколков [3,4] установлено наличие двух групп резонансов с отличающимися на величину $\sim 0{,}65$ Мэв значениями $\bar{E}_K$ [4,5]. Прямые измерения $\bar{E}_K$ для ^{235}U в резонансах при $E_n = 0{,}3$ эв и $E_n \lesssim 0{,}005$ эв (крыло "отрицательного" резонанса), спины которых различны [6], показывают, что $\bar{E}_K(0{,}005\ эв) > \bar{E}_K(0{,}3\ эв)$ [7].

Нами было предпринято измерение E_K в наиболее сильном низкоэнергетическом резонансе ^{235}U при $E_n = 8{,}8$ эв, которая сравнивалась со значением $\bar{E}_K^{th}$ в тепловой точке. Измерения проводились на нейтронном спектрометре по времени пролета на базе импульсного реактора ИБР-30 ОИЯИ в Дубне. Реактор работал в бустерном режиме со средней мощностью 4 - 6 квт, полушириной импульсов ~ 4 мксек и частотой повторения 100 $сек^{-1}$. Камера с урановой мишенью, толщиной ~ 20 мкг/$см^2$ и полупроводниковым детектором с площадью ~ 3 $см^2$ устанавливалась на расстоянии 15 м от активной зоны реактора. Усилительный тракт состоял из высокостабильных предусилителя *NE* 5287 и усилителя *NE* 5259. Регистрация импульсов осуществлялось при помощи двухмерного анализатора с временными "окнами" для амплитудного анализа осколочных импульсов. Ширина "окна" при $E_n = 8{,}8$ эв была равна 64 мксек. Время измерения в резонансе 8,8 эв ~ 65 час. Время измерения в тепловой точке - 11 час. В резонансе при $E_n = 8{,}8$ эв зарегистрировано $\sim 10^4$ осколков, а в тепловой точке $\sim 10^5$ осколков. Обработка данных на ЭВМ показала, что $\bar{E}_K(8{,}8\ эв)$ больше $\bar{E}_K^{th}$ на величину $(1{,}3 \pm 1{,}5)$ Мэв. Хотя по знаку эффекта наши предварительные результаты согласуются с результатами работ [3,4] и могут служить аргументом в пользу того, что спин резонанса 8,8 эв имеет значение $J^\pi = 3^-$ [2,3], однако значительная статистическая погрешность измерений затрудняет интерпретацию найденного эффекта.

Следует отметить, что измерение $\bar{E}_K$ осколков деления ^{235}U в резонансе 8,8 эв, выполненное в настоящей работе, является первым прямым измерением $\bar{E}_K$ в нейтронных резонансах ^{235}U. В то же время оно свидетельствует о том, что несмотря на большие технические трудности, повышение точности в определении $\bar{E}_K$ и увеличение число исследованных резонансов ^{235}U является реальной задачей.

В заключение авторы выражают благодарность Л.Б. Пикельнеру за ценные обсуждения, Ц. Пантелееву, З. Длоухи и В. Назарову за содействие при измерениях.

Литература

[1] S.Bjornholm, Phys. Reports 4 (1972) 325
[2] J. Toraskar, E.Melkonian, Phys. Rev. C4 (1971) 267
[3] L.G.Miller, M.S.Moore, Phys. Rev. 157 (1967) 1055
[4] С. Бочваров, Е. Дермендинев, Н. Кацукеев, "Physics and Chemistry of Fission" (IAEA, Vienna, 1969) 465

[5] В. Дерменджиев, Ц. Пантелеев, Препринт ОИЯИ Р3 - 5081 (1970)
[6] R.Shermer et.al., Phys. Rev. 167 (1968) 1121
[7] Е. Дерменджиев, Г. Ичев, Н. Калинкова, Н. Чиков, Сб. трудов III. Всесоюзной конф. по нейтронной физике, Киев, 1975 (в печати).

ПОЛНЫЕ СЕЧЕНИЯ ВЗАИМОДЕЙСТВИЯ БЫСТРЫХ НЕЙТРОНОВ С КОНСТРУКЦИОННЫМИ ЭЛЕМЕНТАМИ

А.И. Тутубалин, В.П. Божко, В.Ф. Поздний, В.Г. Болдалин

Харьковский Физико-технический институт АН УССР (СССР)

Аннотация

Методом пропускания измерены полные сечения взаимодействия нейтронов с ядрами конструкционных элементов *Al*, *Fe*, *Zr*, *Nb*, *Ta* и *Pb* при энергии нейтронов 14,7 Мэв. В измеренные сечения введены поправки на рассеяние в детектор. Получены следующие значения полных сечений в барнах: 1,76 ± 0,01 (*Al*), 2,58 ± 0,04 (*Fe*), 3,93 ± 0,03 (*Zr*), 4,03 ± 0,03 (*Nb*), 5,59 ± 0,04 (*Ta*), 5,47 ± 0,04 (*Pb*). Проведено сравнение с данными других авторов. Отмечено хорошее согласие измеренных полных сечений с усредненными в интервале 13 - 15 Мэв значениями для всех элементов, за исключением тантала. Для тантала измеренное сечение превышает на 7 % усредненное значение.

1. Введение

Полные сечения взаимодействия нейтронов с атомными ядрами являются важными ядерной-физическими константами, потребность в которых возникает при решении многих практических задач. При проектировании ядерных и термоядерных реакторов знание констант необходимо для выбора конструкционных материалов, расчета отдельных конструкций, защит и т.д. Чтобы обеспечить требуемую точность расчетов, погрешности в исходных константах не должны превышать допустимые пределы. Так, например, для расчетов защиты реакторов величины полных сечений в области энергий нейтронов от 0,1 до 15 Мэв должны быть заданы с точностью 1 - 3 % [1]. В других случаях требования к точности еще более жестки (1 - 2 %).

Для ядер большинство конструкционных элементов данные о полных сечениях получены несколькими исследователями, особенно при энергии нейтронов вблизи 14 Мэв. Приводимые экспериментальные погрешности, как правило, удовлетворяют указанным выше требованиям. Однако, сравнение результатов разных работ показывает, что различия в абсолютных значениях полных сечений в некоторых случаях значительно больше, чем можно ожидать из приведенных авторами погрешностей отдальных измерений (см. рис. 1 - 6).

Большие различия в измеренных полных сечениях обусловлены, по-видимому, неучтенными систематическими ошибками эксперимента, однако, объективная оценка результатов разных работ и исключение систематических ошибок представляют собой довольно сложную задачу. Сказанное хорошо иллюстрируется рис. 2 и 6, на которых представлены данные нескольких авторов [2 - I2] по полным нейтронным сечениям для железа и свинца в диапазоне энергий I3,6 - I5,6 Мэв. Из рис. 2 видно, что результаты работы [3] для железа систематически занижены по сравнению с результатами других работ [2 - 9]. Однако, нахождение источника систематической ошибки затрудняется тем, что результаты этой же работы для свинца (рис. 6) достаточно хорошо согласуются с данными других авторов [2 - 4, I0 - I2]. Отсюда ясно, что для получения более достоверных данных, рекомендуемых в качестве констант для прикладных целей, необходимы повторные измерения, желательно разными методами или в разных экспериментальных условиях.

В настоящей работе изложены результаты измерения полных сечений взаимодействия нейтронов с конструкционными элементами Al, Fe, Zr, Nb, Ta и Pb при энергии нейтронов I4,7 Мэв.

2. Методика эксперимента

Измерения полных сечений взаимодействия выполнены методом пропускания.

Источником нейтронов служила реакция $T(d,n)\alpha$, протекающая при бомбардировке титан-тритиевой мишени дейтронами, ускоренными до энергии ~ 200 кэв.

Образцы исследуемых элементов естественного изотопного состава имели цилиндрическую форму с диаметром 3,3 см и толщиной t от 2,38 до 2,84 см для разных элементов. Образцы располагались на расстоянии L_1 = 30 см от источника нейтронов, расстояние от образца до детектора нейтронов L_2 = I90 см.

В качестве детектора нейтронов использовался сцинтилляционный счетчик, состоящий из пластического сцинтиллятора диаметром D = 7 см и высотой H = 9 см, соединенного коническим световодом с ФЭУ-36.

Для уменьшения фона, обусловленного регистрацией рассеянных в помещении нейтронов, была произведена коллимация узкого пучка эффективных нейтронов путем отбора быстрых совпадений нейтронов с сопутствующими α-частицами, регистрируемыми в в малом телесном угле детектором, установленным под углом I45^0 к направлению пучка падающих дейтронов.

Детектор сопутствующих α-частиц состоял из ФЭУ-36 и тонкой сцинтиллирующей органической пленки, нанесенной на торец цилиндрического световода. Перед сцинтиллирующей пленкой устанавливался танталовый коллиматор, закрытый алюминиевой фольгой для предохранения детектора от засветки рассеянными дейтронами и мягким β-излучением из тритиевой мишени.

Дискриминация γ-излучения из образцов производилась методом времени пролета. Разрешающее время спектрометра по времени пролета составляло около 2 нсек.

3. Результаты измерений и ошибки

Полные сечения определялись из измеренных величин пропускания $T = J/J_0$, где J - поток нейтронов на детектор с установленным образцом и J_0 - поток в отсутствие образца. Определяемое в эксперименте значение полного сечения

$$(I) \qquad \sigma_t' = \frac{1}{n_0 t} \ln \frac{1}{T}$$

где n_0 - число ядер в I см^3 образца.

Измерения потоков J и J_0 производились попеременно через достаточно короткие интервалы времени, чтобы исключить влияние нестабильностей аппаратуры. Для учета влияния медленных дрейфов аппаратуры проводилось несколько серий таких измерений с большим интервалом времени между сериями. Набираемое во всех сериях число отсчетов обеспечивало статистическую точность не хуже 0,3 %. Для нахождения полной ошибки в каждой серии измерений определялось среднее значение пропускания и среднеквадратичная ошибка, а затем по результатам всех серий находилось средневзвешенное значение пропускания и его среднеквадратичная ошибка.

В определенные по формуле (I) полные сечения σ_t' вводилась поправка на рассеяние в детектор [20], величина которой зависит от геометрии эксперимента и массового числа A изучаемого элемента. Истинное значение полного сечения σ находилось из выражения

$$(2) \qquad \sigma_t = \frac{\sigma_t'}{1 - \frac{\Delta\sigma_t}{\sigma_t}} ,$$

где:
$$\frac{\Delta\sigma_t}{\sigma_t} = \frac{\pi}{4} \left(\frac{DL}{L_1 L_2}\right)^2 \frac{\sigma_n(0^\circ)}{\sigma_t} ,$$

$$L = L_1 + L_2 ,$$

$$\frac{\sigma_n(0^\circ)}{\sigma_t} = \frac{(KR+1)^2}{8\pi} ,$$

$K = \frac{1}{\lambda}$ - волновое число нейтрона,

$R = r_0 \cdot A^{1/3} \cdot 10^{-13}$ см.

При введении поправки в полные сечения может вноситься дополнительная систематическая ошибка за счет неопределенности величины r_0. Обычно r_0 выбирается в пределах $(1{,}3 - 1{,}4)\ 10^{-13}$ см, и вносимая погрешность не превышает 10 % от величины самой поправки. В использованной нами геометрии эксперимента величина поправки составляла от I до 3 % величины полного сечения, а вносимая вместе с поправкой возможная систематическая погрешность - соответственно от 0,I до 0,3 %.

Результаты измерений представлены в таблице I. Приведенные ошибки являются полными и для изученных в настоящей работе элементов находятся в пределах от 0,7 до I,5 %. В таблицу включены также результаты проведенных нами ранее [9] измерений полных сечений для разделенных изотопов Fe^{54} и Fe^{56} и предварительные результаты для никеля, измеренные с недостаточно высокой точностью (~2 %).

4. Сравнение с имеющимися данными

Полученные нами при E_n = I4,7 Мэв значения полных сечений представлены для наглядности на рис. I - 6 вместе с некоторыми данными других авторов [2 - I9] в диапазоне энергий примерно от I3,5 до I5,7 Мэв. Из рисунков видно, что для всех элементов, за исключением тантала, имеется достаточно хорошее общее согласие наших результатов с большинством приведенных данных, хотя в отдельных случаях наблюдаются значительные расхождения, превышающие пределы оценочных ошибок.

Для количественной оценки степени согласуемости наших результатов с данными других авторов во второй колонке таблицы I приведены средние значения $(\sigma_t)_{средн.}$, взятые из работы [II]. Эти значения были получены путем усреднения результатов многих работ в интервале энергий от I3 до I5 Мэв. Процедура усреднения [2I] позволяла при некоторых допущениях учесть как статистические, так и систематические ошибки. Из сравнения видно, что для Al, Fe, Ni, Nb и Pb значения σ_t и $(\sigma_t)_{средн.}$ совпадают с точностью I %, т.е. различия лежат в пределах ошибок. Расхождение в случае Zr можно объяснить тем, что для него $(\sigma_t)_{средн.}$ определено с большой (~ 5 %) погрешностью. Усредненные в более узком интервале энергий результаты работ [2, 4, I4] приводят к величине $(\sigma_t)_{средн.}$ = (3,93 ± 0,05) барн, что совпадает с полученным нами значением σ_t = (3,93 ± 0,03) барн (см. также рис. 3). Наибольшее расхождение наблюдается в случае тантала (рис. 5), для которого измеренное нами значение превышает почти на 7 % усредненное значение. Поскольку хорошее согласие для остальных исследованных нами ядер свидетельствует об отсутствии неучтенных систематических ошибок эксперимента, то для выяснения причин расхождения в случае тантала необходимы дополнительные экспериментальные данные в интервале энергий от I4,5 до I5 Мэв.

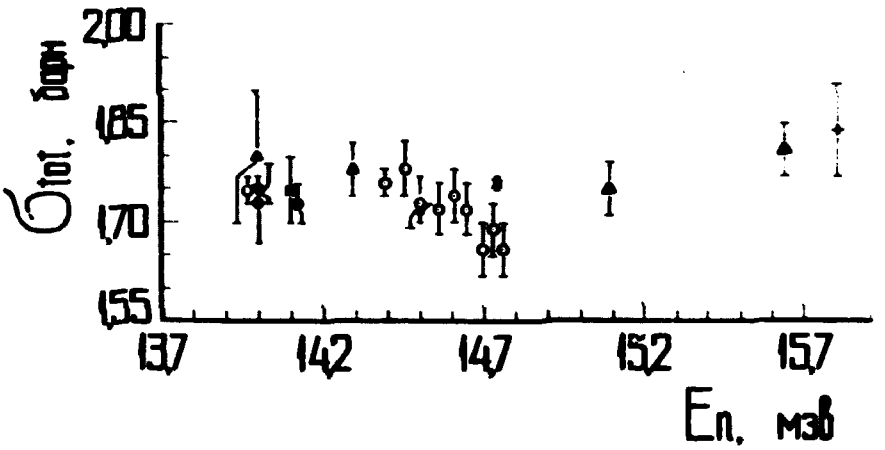

Рис. I Полные сечения взаимодействия нейтронов с Al
Обозначения: ● - [2], ⊙ - [3], ● - [4],
● - [5], ● - [6], ▽ - [13],
▲ - [14], □ - [15], ◆ - [16],
+ - [17], x - наши данные

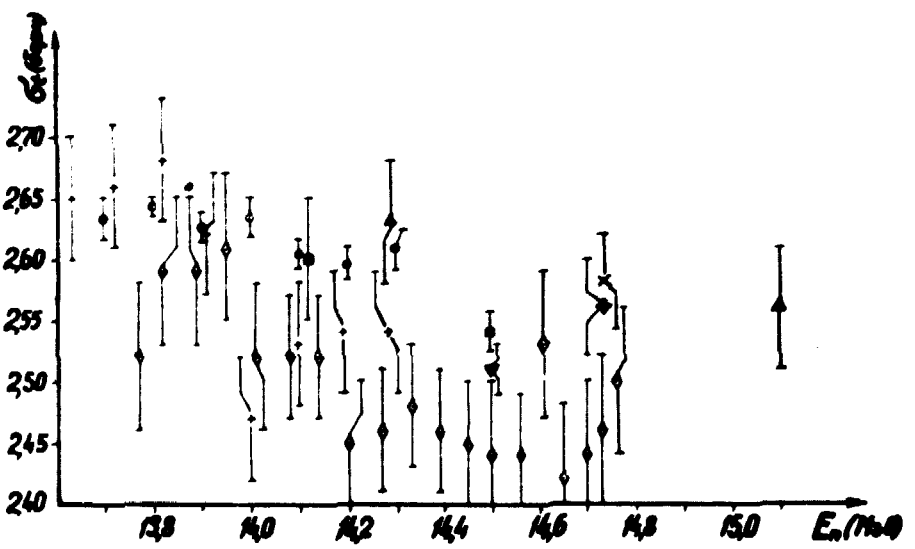

Рис. 2 Полные сечения взаимодействия нейтронов с Fe
Обозначения: ■ - [2], ◇ - [3], ⊡ - [4],
△ - [5], ▽ - [6], + - [7],
⊙ - [8], ◆ - [9], x - наши данные

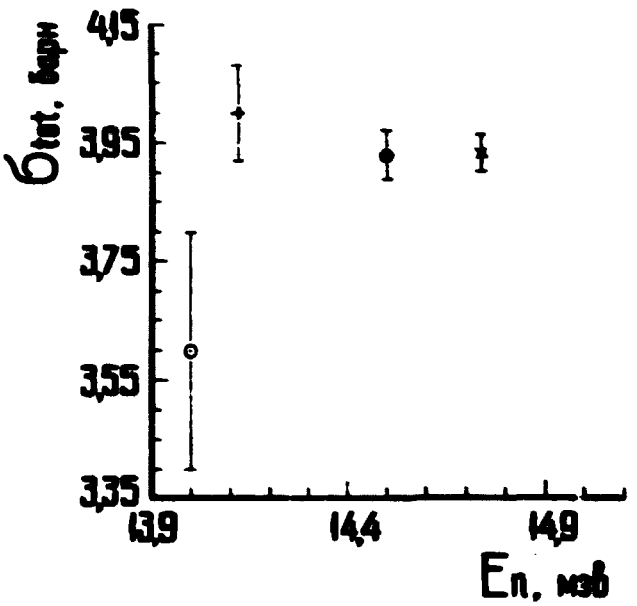

Рис. 3 Полные сечения взаимодействия нейтронов с Zr
Обозначения: + - [2] ● - [4] ⊙ - [14]
x - наши данные

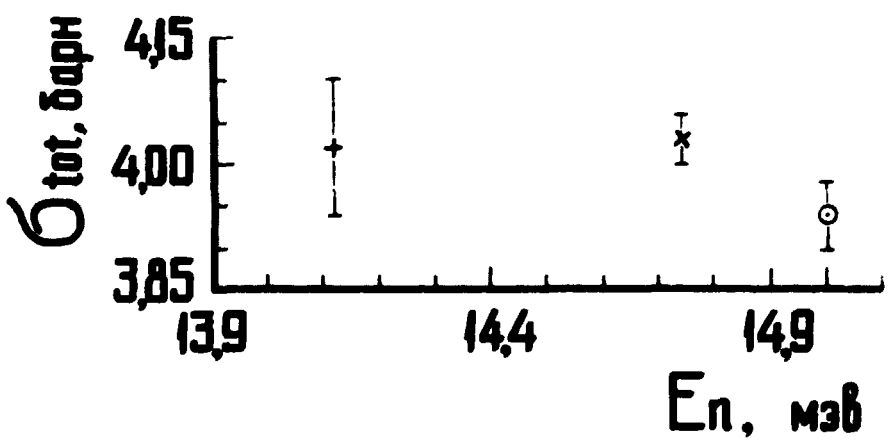

Рис. 4 Полные сечения взаимодействия нейтронов с Nb
Обозначения: + - [2] ⊙ - [18]
x - наши данные

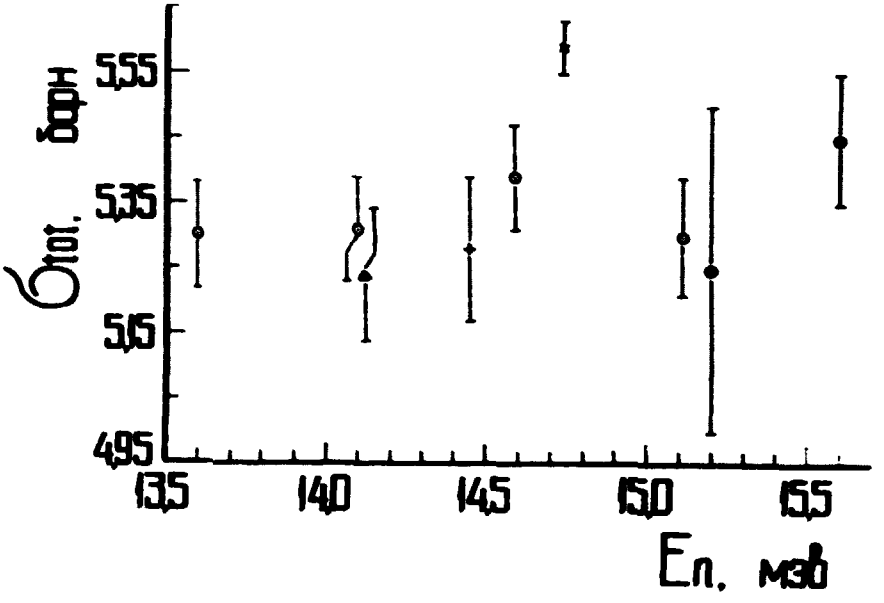

Рис. 5 Полные сечения взаимодействия нейтронов с Ta
Обозначения: △ - [2] + - [3] ⊙ - [10]
● - [19] x - наши данные

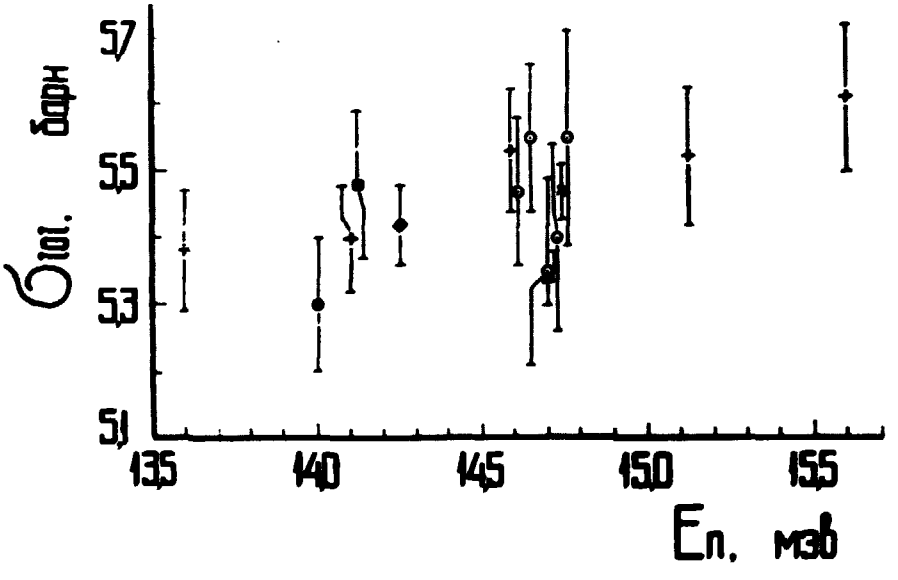

Рис. 6 Полные сечения взаимодействия нейтронов с Pb
Обозначения ⊡ - [2] ⊙ - [3] ◆ - [4]
+ - [10] ▲ - [11] ● - [12]
x - наши данные

Таблица I

Полные сечения взаимодействия нейтронов при энергии I4,7 Мэв в интервале (I3 - I5) Мэв

Ядро	σ_t, барн	$(\sigma_t)_{средн.}$, барн
Al	I,76 ± 0,0I	I,74I2 ± 0,0I27
^{54}Fe	2,55 ± 0,02	-
^{56}Fe	2,56 ± 0,04	-
Fe	2,58 ± 0,04	2,5754 ± 0,0I79
Ni	2,67 ± 0,05	2,68I5 ± 0,0209
Zr	3,93 ± 0,03	3,744I ± 0,2007
Nb	4,03 ± 0,03	4,0033 ± 0,0444
Ta	5,59 ± 0,04	5,2357 ± 0,0473
Pb	5,47 ± 0,04	5,4006 ± 0,0305

Литература

[I] А.А. Абагян, А.А. Дубинин, А.П. Суворов, Нейтронная физика, ч. I, IC, Киев, I972

[2] J.H. Coon, E.R. Graves and H.H. Barschall, Phys. Rev., 98, 562, 1952

[3] J.P. Vervier et A. Martegani, Nucl. Phys., 6, 260, 1958

[4] A. Bratenahl, I.M. Peterson and J.P. Stoering, Phys. Rev., 110, 927, 1958

[5] G.J. McCallum, G.S. Mani and T.G. Ferguson, Nucl. Phys. 16, 313, 1960

[6] I. Angeli, J. Csikai and I. Hunyadi, Acta Phys. Acad. Sci. Hung., 28, 97, 1970

[7] F. Manero, B.H. Armitage, J.M. Freeman, J.H. Montague, Nucl. Phys. 59, 583, 1964

[8] I.C. Albergotti and I.M. Ferguson, Nucl. Phys. 82, 652, 1966

[9] А.И. Тутубалин, А.П. Ключарев, В.П. Божко и др., ядерные константы, вып. II, I7, Атомиздат, I973.

[I0] Jerry P. Conner, Phys. Rev. 109, 1268, 1958

[II] I. Angeli, J. Csikai, I.L. Nagi et al., Acta Phys. Acad. Sci. Hung., 30, 115, 1971

[I2] BNL-325, Second Edition

[I3] J.P. Davidson, Rev. Mod. Phys. 37, 105, 1965

[I4] Leonard S. Goodman, Phys. Rev. 88, 686, 1952

[I5] C.F. Cook and T. W. Bonner, Phys. Rev. 94, 651, 1954

[I6] Claud St. Pierre, M.K. Machwe and P. Lorrian, Phys. Rev. 115, 999, 1959

[17] P.H. Bowen, J.P. Scanlon, G.H. Stafford et al., Nucl. Phys. 22, 640, 1961
[18] APWL-TR 65216 , 1966
[19] R.L. Cassola and R.D. Koshel, Nuovo Cim., 53, 2B, 363, 1968
[20] Дж. Марион и Дж. Фаулер, Физика быстрых нейтронов, т. 2, стр. 5, Атомиздат, 1966.
[21] Z.T. Bödy and K.M. Dode, Acta Phys. Acad. Sci. Hung., 28, 155, 1970

ПРЯМЫЕ ИЗМЕРЕНИЯ ЗАДЕРЖАННЫХ НЕЙТРОНОВ СПОНТАННОГО ДЕЛЕНИЯ ^{252}Cf

В.И. Нефедов, А.Ф. Семенов, Б.И. Старостов

НИИАР Димитровград, (СССР)

Аннотация

С помощью методики, обеспечивающей исключение систематических ошибок, связанных с регистрацией рассеянных нейтронов, подтверждено существование нейтронов деления, излучаемых после момента деления, с временем испускания в наносекундной области.

В ряде работ [I - 6] описаны эксперименты, результаты которых объясняются существованием задержанных нейтронов, испускаемых за 10^{-7} - 10^{-9} сек после момента деления ядра. Испусканием задержанных нейтронов можно объяснить тонкую структуру спектров нейтронов деления [I, 2] и наблюдаемое экспериментально [7] превышение спектра нейтронов спонтанного деления ^{252}Cf над теоретическим в области энергий нейтронов менее 0,7 - I Мэв. Однако имеющиеся данные по задержанным нейтронам имеют недостаточную точность из-за систематических ошибок, возникающих при учете фона рассеянных в окружающих предметах нейтронов и запаздывающих γ-квантов деления [6, 7].

Надежные измерения эффектов от задержанных нейтронов спонтанного деления ^{252}Cf были выполнены с помощью методики, исключающей эти систематические ошибки. На рис. I приведена схема экспериментальной установки, использованной в работе. С помощью этой установки снимались кривые запаздывающих совпадений между моментами регистрации осколков деления ^{252}Cf в вакуумной камере делений и моментами регистрации нейтронов деления кристаллом $^6LiJ(Eu)$. Измерения проводились время-амплитудным преобразователем для двух положений камеры делений. В первом положении камера устанавливалась так, что слой $ZnS(Ag)$, регистрирующий осколки

деления ^{252}Cf, подводился вплотную к кристаллу $^{6}Li](Eu)$. При этом значительно увеличивалась эффективность регистрации задержанных нейтронов, испускаемых осколками деления, попавшими в слой $ZnS(Ag)$. Во втором положении камера поворачивалась на 180^{0} вокруг вертикальной оси. В этом случае эффективность регистрации задержанных нейтронов становится минимальной. Эффективность же регистрации мгновенных нейтронов и фона от рассеянных нейтронов остается неизменной, что обеспечивает надежное выделение эффекта задержанных нейтронов.

Вакуумная камера делений, служащая для регистрации осколков деления ^{252}Cf, представляет собой цилиндр диаметром 210 мм и высотой 150 мм нержавеющей стали толщиной 1,5 мм. В центре камеры перпендикулярно ко дну установлена односторонняя мишень из калифорния диаметром 20 мм. Калифорний нанесен на алюминиевую подложку толщиной 0,2 мм и для предотвращения распыления закрыт золотой фольгой толщиной 100 мкг/см^{2}. Осколки деления регистрировались слоем $ZnS(Ag)$ диаметром 40 мм, нанесенным на боковую поверхность камеры. Вспышки света, возникающие в слое $ZnS(Hg)$ под воздействием осколков деления, регистрировались через кварцевое окно фотоумножителем ФЭУ-97. Интенсивность счета осколков деления была равна 200 дел/сек и не менялась при повороте камеры. Эффективность регистрации осколков деления достигала 90 - 95 %.

Для регистрации нейтронов в работе использовался кристалл $^{6}Li](Eu)$ с фотоумножителем ФЭУ-36. Использование кристалла $^{6}Li](Eu)$ позволяет избавиться от фона запаздывающих γ-квантов деления [4, 8] благодаря высокому уровню дискриминации, соответствующему γ-лучам с энергией 2,2 Мэв, устанавливаемому в регистрирующей аппаратуре для обеспечения полной эффективности регистрации тепловых нейтронов.

В результате измерений были получены временные распределения совпадений для двух положений вакуумной камеры делений. На рис. 2 приведены полученные после вычитания фона случайных совпадений и приведения к одинаковой площади временные распределения совпадений, а также временное распределение совпадений, подтверждающее отсутствие запаздывающих совпадений от γ-лучей деления. Это распределение измерялось с камерой делений, установленной в первом положении для γ-квантов с энергией $E = 2 \pm 0,1$ Мэв, вырезаемых одноканальным дифференциальным дискриминатором.

Из рис. 2 видно, что в области времени задержки, больших 40 - 50 нсек, наблюдается значительное превышение временного распределения, полученного в первом положении камеры делений, над распределением с камерой делений, установленной во втором положении. Наблюдаемое превышение может быть интерпретировано только существованием задержанных нейтронов, испускаемых в наносекундном диапазоне времен задержек после момента деления ядра.

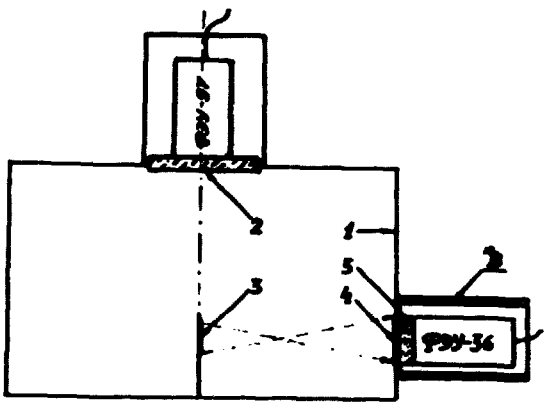

Рис. I Схема эксперимента: I - вакуумная камера делений, 2 - кварцевое окно, 3 - слой калифорния, 4 - слой $ZnS(Ag)$, 5 - кристалл $^6Li\,J(Eu)$, ⌀ 30 x I0 мм

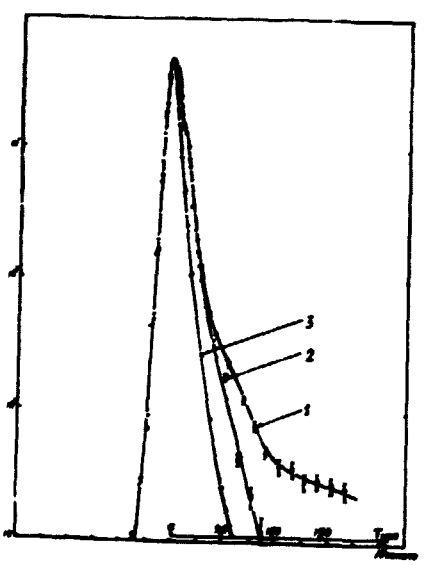

Рис. 2 Временные распределения совпадений: I - распределение для первого положения камеры делений, 2 - распределение для второго положения камеры делений, 3 - распределение совпадений для γ-лучей с энергией 2 ± 0,I Мэв

Литература

[1] Нефедов В.Н., Тонкая структура мгновенных нейтронов деления, Препринт НИИАР, П-52, 1969

[2] Nefedov, V.N., Melnikov, A.K., Starostov, B.I., Delayed neutrons from spontaneous fission of ^{252}Cf. Fission Neutron Spectra IAEA, Vienna, 1972, p. 89

[3] Нефедов В.Н., Мельников А.К., Старостов Б.И., Задержанные нейтроны спонтанного деления ^{252}Cf, Нейтронная физика, ч. 2, с. 19, Киев, 1972, (Материалы I. Всесоюзной конференции по нейтронной физике, Киев, 1971)

[4] Нефедов В.Н., Старостов Б.И., Потаманов В.Н., Периоды испускания и энергетические спектры задержанных нейтронов спонтанного деления ^{252}Cf, Нейтронная физика, ч. 4, с. 155, Обнинск, 1974, (Материалы II. Всесоюзной конференции по нейтронной физике, Киев, 1973)

[5] Нефедов В.Н., Старостов Б.И., Природа превышения спектра нейтронов деления ^{252}Cf над максвелловским распределением в области энергий нейтронов меньше 0,5 Мэв, Нейтронная физика, ч. 4, с. 163, Обнинск, 1974, (Материалы II. Всесоюзной конференции по нейтронной физике, Киев, 1973)

[6] Нефедов В.Н., Старостов Б.И., Семенов А.Ф., Изучение влияния запаздывающих γ -квантов деления при измерении спектров нейтронов деления методом времени пролета, Доклад на III. Всесоюзной конференции по нейтронной физике, Киев, 1975

[7] Meadows, J.W. Phys. Rev. 1957, p. 157, 1076

[8] John, W., Guy F.W., Weselovski T.T. Phys. Rev. C-2, 1970, p. 1451

О КОНКУРЕНЦИИ ЭМИССИИ НЕЙТРОНОВ И ГАММА-КВАНТОВ ПРИ СПОНТАННОМ ДЕЛЕНИИ ТЯЖЕЛЫХ ЯДЕР

О.И. Батенков, И.В. Блинов, В.А. Витенко

Радиевый институт им. В.Г. Хлопина, Ленинград (СССР)

Аннотация

Приведена экспериментальная оценка вероятности испускания нейтронов спонтанного деления Cf^{252} после эмиссии гамма-квантов.

Осколки спонтанного деления тяжелых ядер имеют в среднем угловой момент около $8\hbar$. Хотя это значение не является большим, влияние такого момента должно сказываться на характере процесса снятия энергии возбуждения. В теоретических работах Гровера [1] рассмотрены вопросы конкуренции эмиссии нейтронов и гамма-квантов, испускаемых возбужденными ядрами, обладающими угловыми моментами. Если результаты расчетов Гровера применить к девозбуждению осколков спонтанного деления тяжелых ядер, то можно оценить, что верхний предел вероятности эмиссии гамма-квантов до эмиссии нейтронов может достигать величины 10^{-1} по отношению к общей вероятности. Однако, вероятность такого процесса может быть и значительно меньше, так как точность оценки невелика из-за отсутствия достаточной информации, например, о распределениях угловых моментов и энергии возбуждения осколков деления. Если вероятность более 10^{-2}, то можно попытаться ее определить путем измерения времени эмиссии нейтронов, которое определяется в рассматриваемом случае временем испускания гамма-квантов. В данной работе это время оценивалось путем прецизионного сравнения спектров нейтронов деления при движении эмитирующих осколков в вакууме и в плотной среде. Осколки начинают заметно замедляться в среде через время $\sim 10^{-14}$ сек, а полное время торможения $\sim 10^{-12}$ сек. Если гамма-кванты и соответственно нейтроны испускаются за время большее, чем 10^{-14} сек относительно акта деления, то это может быть замечено по разнице в спектрах нейтронов.

На рис. показаны наши расчетные данные по изменению отношения таких спектров для случаев, когда осколки перед эмиссией нейтронов уже потеряли часть своей скорости в среде (потеря 4 %, 10 % и 20 % скорости соответствует временам замедления $2 \cdot 10^{-14}$ сек, $6 \cdot 10^{-14}$ сек и $1{,}5 \cdot 10^{-13}$ сек [2]. В качестве спектров нейтронов в системе осколка использовались данные из работы [3]. Из рис. видно, что чувствительность метода сильно повышается при регистрации нейтронов низких и, особенно, высоких энергий. Использование не данных по всему спектру в целом, как это было сделано в работе [4], существенно снижает точность эксперимента. Измерения спектров нейтронов деления производились с помощью источника калифорния-252, в котором происходило $10^5 \frac{\text{дел}}{\text{сек}}$. Слой калифорния был нанесен на ни-

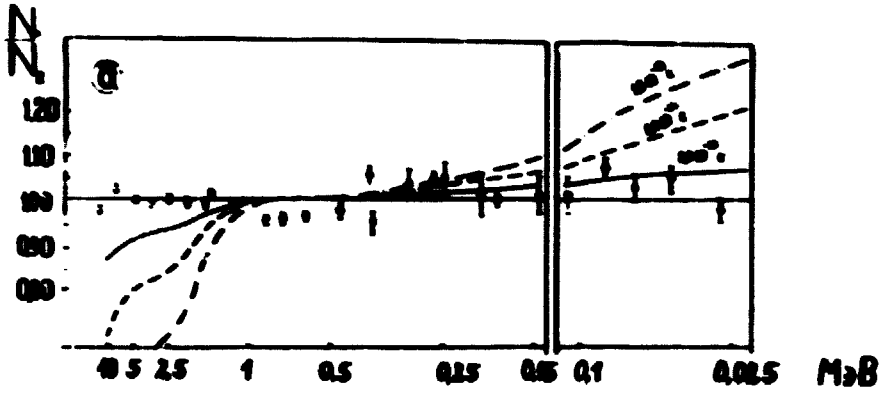

А) Отношение числа нейтронов деления Cf^{252} ($\frac{N_{\theta}}{N_{\theta}}$), вылетевших против направления движения регистрируемых осколков $N_{\theta}(\theta = 180^{\circ})$ и по направлению $N_{\theta}(\theta = 0^{\circ})$ в зависимости от энергии нейтронов.
Точки – экспериментальные данные, полученные с пластмассовым сцинтиллятором (○) и с кристаллом $^{6}Li\,I\,(Eu)$ (●).
Кривые – расчетные данные для разных времен эмиссии нейтронов.

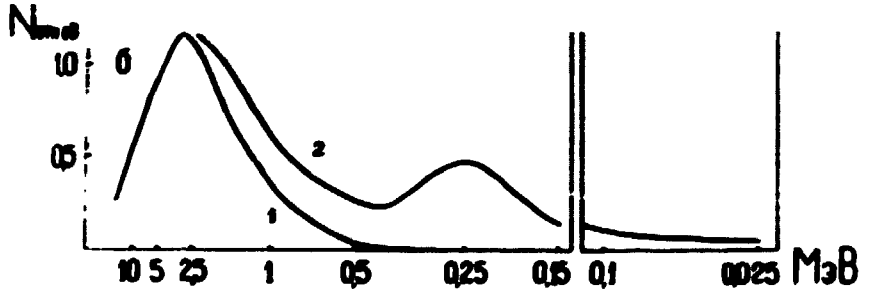

Б) Аппаратурные распределения нейтронов по времени пролета (1 – пластмассовый сцинтиллятор, 2 – кристалл $^{6}Li\,I\,(Eu)$.
В первой части рисунка для удобства изображения области низких энергий масштаб по энергетической шкале изменен.

келевую фольгу толщиной 0,2 мм. Для регистрации осколков применялся кремниевый поверхностно-барьерный счетчик площадью I $см^2$, расположенный на расстоянии I,5 см от слоя Cf^{252}. Для регистрации нейтронов использовались пластмассовый сцинтиллятор в интервале энергий 0,5 - I0 Мэв и кристалл $^6Li\,J(Eu)$ в интервале 0,0- - 2,0 Мэв. Нейтронный счетчик устанавливался под углами 0^0 и $I80^0$ к направлению регистрируемых осколков. Измерения энергии нейтронов производились по методу времени пролета. Временное разрешение установки было около I,5 нсек для обоих типов нейтронных детекторов. Краткое описание использованной аппаратуры дано в работе [5]. Измерения производились на пролетных расстояниях I2,5см, 25 см и 50 см. Было зарегистрировано более $I0^5$ нейтронов под каждым углом.

Результаты измерений (см. рис.) показывают, что несмотря на небольшие отклонения в области средних энергий, спектры не отличаются в пределах экспериментальных ошибок. Путем сравнения экспериментальных данных и расчетных можно оценить, что среднее время эмиссии нейтронов деления Cf^{252} менее I $I0^{-I4}$ сек, а доля нейтронов в временами эмиссии более $I0^{-I3}$ сек не превышает 2 - 3 %.

Авторы выражают признательность И.А. Баку за обсуждение результатов работы и А. С. Вещикову за помощь при измерениях.

Литература

[I] J.R. Grover, Phys. Rev. 157, 4, 802, 814, 1967
J.R. Grover, J. Gilat, Phys. Rev. 157, 4, 872, 1967
[2] Ф. Насыров, Атомная энергия I6, № 5, 449, I964
S. Kahn, V. Forque, Phys. Rev. 163, 290, 1967
[3] H. Bowman, S. Thomson, J. Milton, W. Swiatecki, Phys. Rev. 126, 2120, 1962
[4] J.S. Fraser, Phys. Rev. 88, 536, 1952
[5] И.В. Блинов, В.А. Витенко, И.Т. Крисюк, Препринт РИ № 30, I974

SESSION VI

NUCLEAR DATA EVALUATION AT THE TU DRESDEN - REVIEW AND RESULTS

D. Hermsdorf, G. Kiessig, D. Seeliger
Technical University Dresden, Section of Physics, GDR

Abstract:

This contribution aims at a brief survey on neutron data evaluation activities at the Technical University of Dresden. The mainly used methods, techniques and models will be discussed here by some representative results obtained in cross section evaluation of the system ^{93}Nb+n finished now at the TU.

1. History and present status

Nowadays compilation and evaluation of neutron nuclear data represent a task of world-wide interest, which has been mainly initiated by reactor physics. All efforts concerning measurements and compilations of nuclear data are co-ordinated by the 4-data-centre-system under the guidance of the NDS of the IAEA Vienna organizing the international exchange of data and informations also.

To the contrary, data evaluation is done essentially for use in national libraries. Such evaluated-data-libraries like ENDF/B, KEDAK, UKNDL, LLL NDF as well as SOKRATOR exist or are builded up in various countries. An international exchange is strongly hindered by aspects of the economic and strategic importance of such data as well as by the quite different structure (formats) of these libraries.

To overcome these difficulties, the USSR-evaluated-data-file is planned for free exchange and for use in all socialistic people's republics. In this sense the activities in nuclear data evaluation, which are reported upon here, represent a contribution for completing the SOKRATOR file and making it available as soon as possible.

At the TU nuclear data evaluation has begun in 1972. In agreement with the Centr po Yadernim Dannim (CJD) at Obninsk /USSR we start to evaluate the cross sections for the system ^{93}Nb+n. First preliminary results have been published in the same place in 1973 [1].

In the meantime various methods in mathematics, statistics, and theoretical nuclear physics as well as computer codes have been investigated and elaborated for use in data evaluation. These tools will be described in paragraph 3 of this paper.

2. Aims of data evaluation

Our device is: an evaluator should not be a "book-keeper" but more a physicist having founded experiences in experimental and theoretical nuclear physics and knowledge about the practical demands and the use of his results.
Therefore we restrict ourselves on evaluation of cross sections for the inter-

action of fast neutrons (i.e. neutron incidence energies from roughly 100 keV up to 20 MeV) with, in the next future only non-fissile nuclei. This limitation is not striotly decisive because this energy range in the medium weight mass-region is assumed to be of further increasing interest for the development of fast breeders and thermo-nuclear arrangements especially [2].
The most important fact is, that at the TU this energy and mass range has been investigated quite well concerning measuring techniques and usually applied nuclear reaction models. So, evaluations can be done founding on an estimate of the validity of different experimental results and calculations in the frame of independent reaction mechanisms. This should result in arguments and decisions for data recommendation basing on nuclear physics knowledge as well as experiences in applying theoretical models and informations about their accuracy, limitations and further developments and improvements.

3. Methods used for data evaluation

Fig. 1 shows in form of a block-diagram the main steps and features for obtaining recommended data, on the following context these steps have to be explained taking into consultation illustrative results of the ^{93}Nb-evaluation.

Nuclear data evaluation deals with two problems mainly:
- the handling of a large amount of informations and
- their interpretation, concentration and representation in a way convenient for practical requirements.

To attack such tasks, a large scale computer is needed. At the TU the soviet

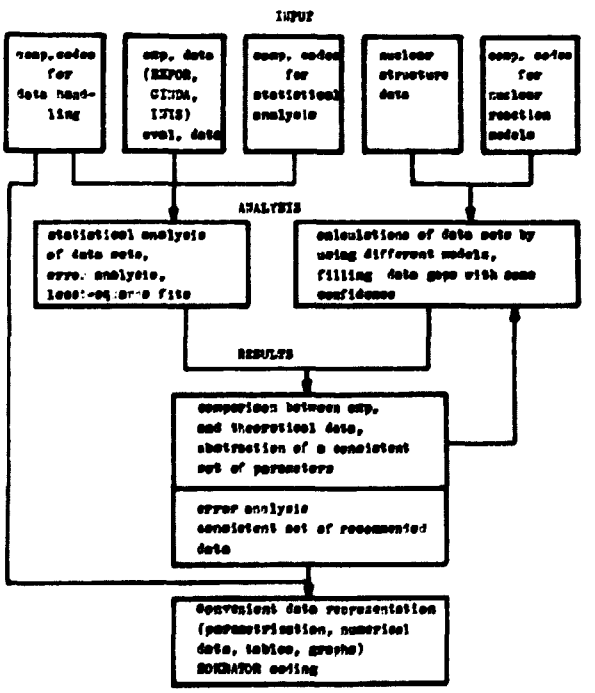

Fig. 1: Block-diagram sketching the main features and steps for obtaining evaluated and recommended data

computer type BESM-6 can be employed for this work. Operational speed, fast memory capacity and the periphery-equipment enable this machine for treating such problems.

3.1. Data handling and managing

Besides several computer codes for the numerical solution of special problems in statistical mathematics and nuclear theory, a comprehensive packet of codes has been prepared for data managing and handling. For instance special codes for magnetic tape transfer and transmission guarantee the compatibility of our internal machine system (1' tapes,11 tracks, Iso-code representation) with other data centres like NDS Vienna and CID Obninsk (1/2' tapes, 7 tracks, BCD-representation). An other code enables us to handle EXFOR-data-tapes by use of selection criteria defined in the EXFOR-dictionary as well as to connect these tapes with data processing programs directly.

3.2. Data processing and analysis in terms of statistical mathematics

If there are a large amount of independent experimental data for a given cross section typ, a statistical analysis is indicated. An example is demonstrated in fig. 2. In such cases, like the total cross sections in ^{93}Nb+n, evaluated data were obtained by fitting experimental results in different manner from simple averaging procedures up to least-squares-fits with weighting functions

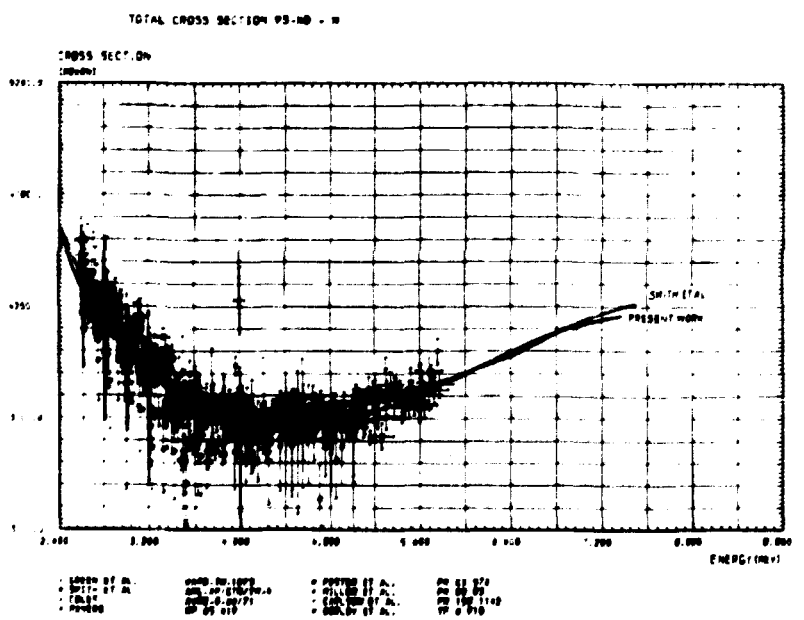

Fig. 2: The ^{93}Nb+n total cross section in the neutron incidence energy range from 2,6 to 5,8 MeV. Present results are compared with data recommended by Smith et al. in ANL-AD/CTR/TM-4

according to experimental errors, estimated validity of experimental techniques and normalization errors by use of standard cross sections. Fitted data can be represented in polynomial expansions (series in energy powers, Legendre or Tschebyshev-polynomials).

In this category a code for automatic drawing of data should be mentioned as an important tool for an effective optical comparison and publication of results.

3.3. Data analysis in terms of nuclear theory

In energy regions or reaction channels where experimental data are scarce, spreading in wider limits than the given errors by different authors or are absent totally, recommended data have to be obtained by use of calculated values. The application of nuclear reaction models yield (in dependence on the rehability of these models) selection criteria for supporting or exclusion of any experimental results as well as the only possibility to define cross section data. Varying from nucleus to nucleus and depending on the investigated energy range, existing theoretical models have to be choosen carefully in order to work with the most successful and powerful tools [3].
We prefer the use of reaction models which enable us to calculate different reaction channels simultaneously and in a consistant manner by use of an unique set of parameters like nuclear structure informations and optical potentials.

Meeting these conditions the following models have been proved successfully in the ^{93}Nb evaluation:

- the optical model [4, 5]
- the Hauser-Feshbach-formalism [4] and
- other statistical models including equilibrium and pre-equilibrium particle emission [6, 7, 8, 9].

Here only the main features can be discussed, whereas they have been published in more detail elsewhere [10, 11, 12].

The use of the optical model (OM)

As known, the OM is very well suited for discription of total and elastic scattering cross sections. In the case of ^{93}Nb+n a systematic examination of several potential parameter sets was carried out in order to verify the partially unknown elastic scattering cross section above 5 MeV neutron incidence energy using the quite exakt knowledge of the energy dependence of the total cross section and some informations about the angular distribution of elastically scattered fast neutrons (see fig. 3).
As an important result this procedure yields a set of transmission coefficients (for inverse cross sections for instance) and the nonelastic cross section, which were used for calculations in the frame of other statistical models.

The use of the Hauser-Feshbach-formalism (HF)

At lower neutron incidence energies up to about 5 MeV compound processes have to be taken into account necessarily for a correct estimation of elastic scattering

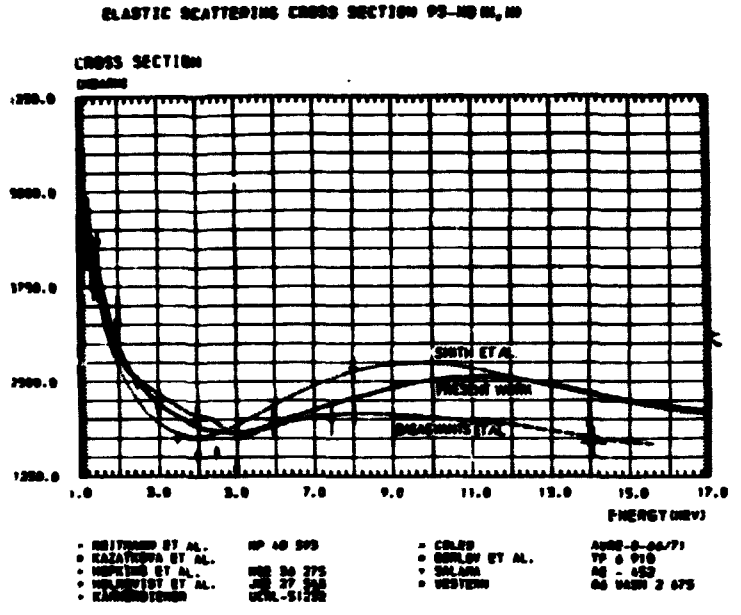

Fig. 3: The ^{93}Nb+n total elastic scattering cross section. Present results are compared with evaluations carried out by Smith et al. and Basasyants et al. in Yad. Konst. 8 (1972) 61

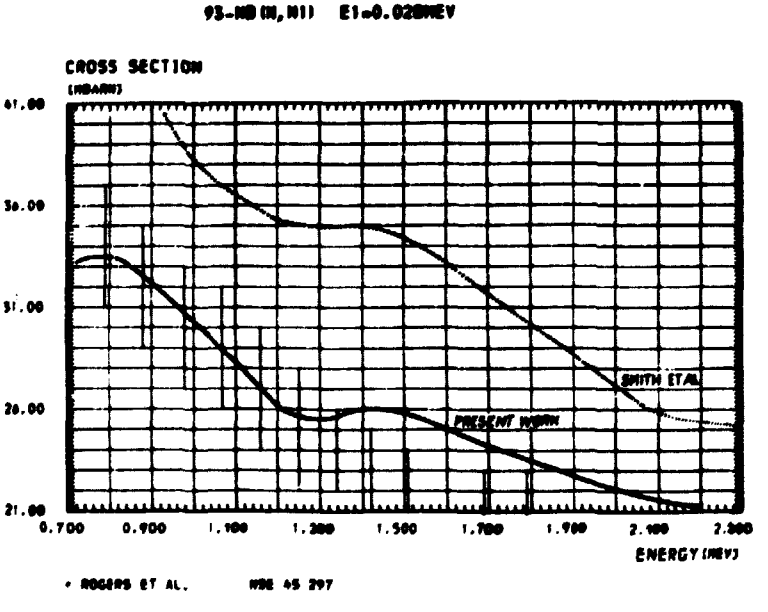

Fig. 4: Excitation function for inelastic neutron scattering to the first excited level of ^{93}Nb as resulting from calculations in the frame of H-F-formalism

cross sections. This were done in the frame of the H-F-model also for calculation of reaction cross sections for the excitation of low-lying isolated levels including all reaction channels like (n,n), (n,p), (n,α) and (n,γ). Taking the whole known spectroscopic informations about the level structure of the different residual nuclei the excitation functions for (n,n_i) processes were treated exactly up to a neutron incidence energy of 1.5 MeV (see fig. 4). Above this energy the continuum region of nuclear levels was considered by use of nuclear level densities with a-parameters.

The use of equilibrium and pre-equilibrium models

As now well established, pre-equilibrium processes play a very important role above some 10 MeV particle incidence energy. To test the applicability of some pre-equilibrium emission models in a more moderate energy range (between 5 to 20 MeV) we used two computer codes basing on the Hybrid-model [8, 9]. They proved very succesful for consistent calculations of the excitation functions for some reaction channels like (n,n'), (n,p), (n,2n), (n,3n), (n,np) and (n,pn) as well as for neutron and proton emission spectra (see figs. 5,6). By pre-equilibrium emission the particle spectra are changed in the high energy part resulting in harder spectra. In order to get an adequate representation of such emission spectra this contribution has to be taken into account necessarily.
This formalism employed for the above mentioned channels has been extended also for the description of reactions with complex particles in the input and or exit channels successfully (see fig. 7).
These models are estimated as very valuable tools for data evaluation [12].

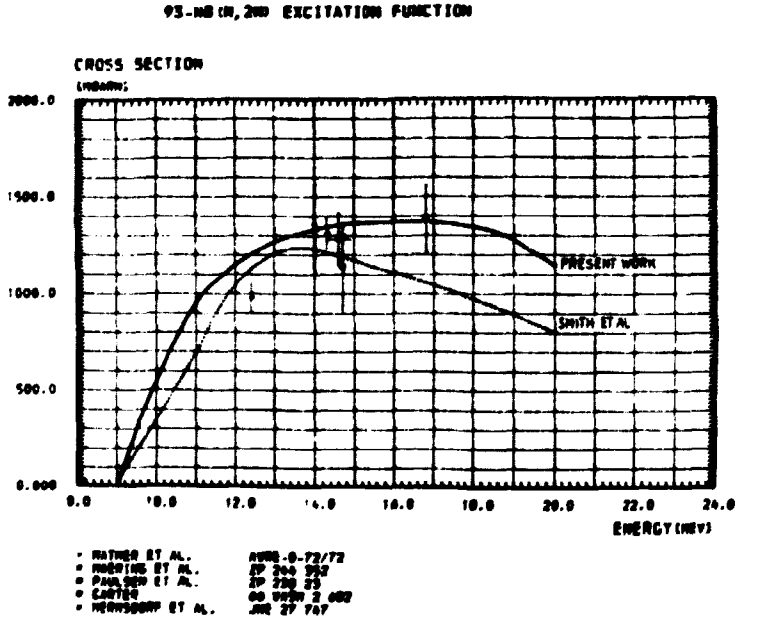

Fig. 5: The $^{93}Nb(n,2n)^{92}Nb^{GS}$ excitation function as result of including pre-equilibrium neutron emission

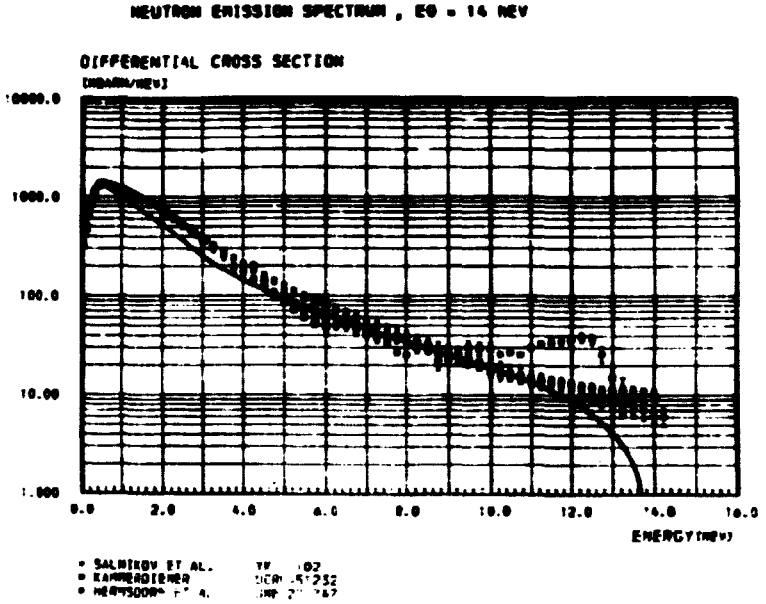

Fig. 6: The spectrum of emitted neutrons after the bombardment of ^{93}Nb with neutrons of 14 MeV incidence energy. The influence of pre-equilibrium neutron emission is evident at high emission energies

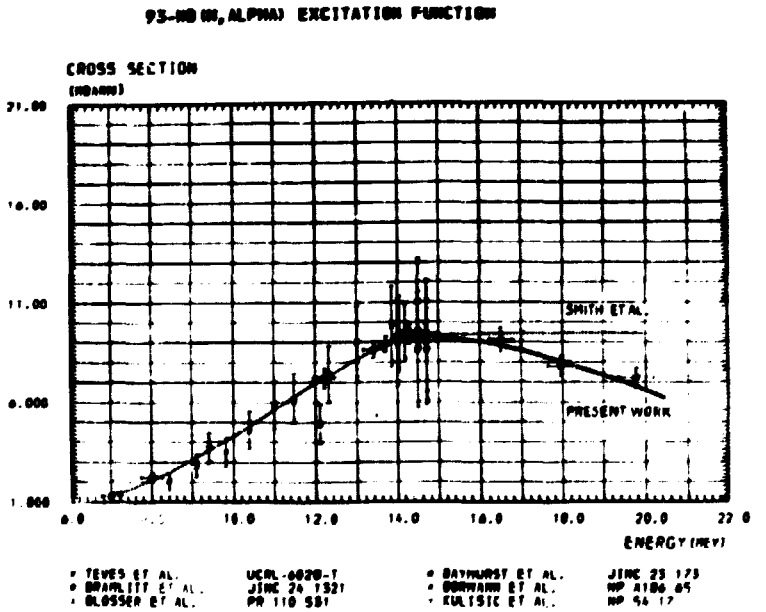

Fig. 7: The ^{93}Nb(n,α) excitation function. Present work includes pre-equilibrium emission of α-particles also

The use of other formulations of the statistical model for equilibrium emission of particles

Basing on the complete statistical model (Weisskopf-Ewing-formalism) there are some known computer codes for data evaluation purposes and a variety of different empirical formulas. We used some of them for comparison. Especially Pearlstein's code [7] has been tested extensively to find a basis for the adjustment of calculated cross sections for some exotic reactions like (n,t), (n,^{3}He), (n,nt+tn), (n,nα+αn) and other, which play a minor role for a consistent evaluated data file.

3.4. Remarks on theoretical methods being in discussion or preparation

To sketch the situation in data evaluation some open problems many not be omited. So, no attention was given to a theoretical description of gamma-ray production cross sections and gamma-ray spectra as well as the angular distributions of inelastic neutron scattering.
Nowa days the growing demands of such data for practical purposes (shielding problems [2]) and for nuclear theory (test of models) cannot be ful filled because of a decisive lack of experimental data.
Some trials were undertaken to calculat excitation functions for γ-ray emission of certain isolated γ-ray energies using the H-P-formalism (see fig. 8) and experimental in formations about branching ratios and γ-ray-multiplicities. Stronger difficulties arise from the treatment of the continuum of γ-rays emitted after neutron capture and reactions like (n,n') and (n,2n). In order to overcome this problems more sophisticated models have to be tested.

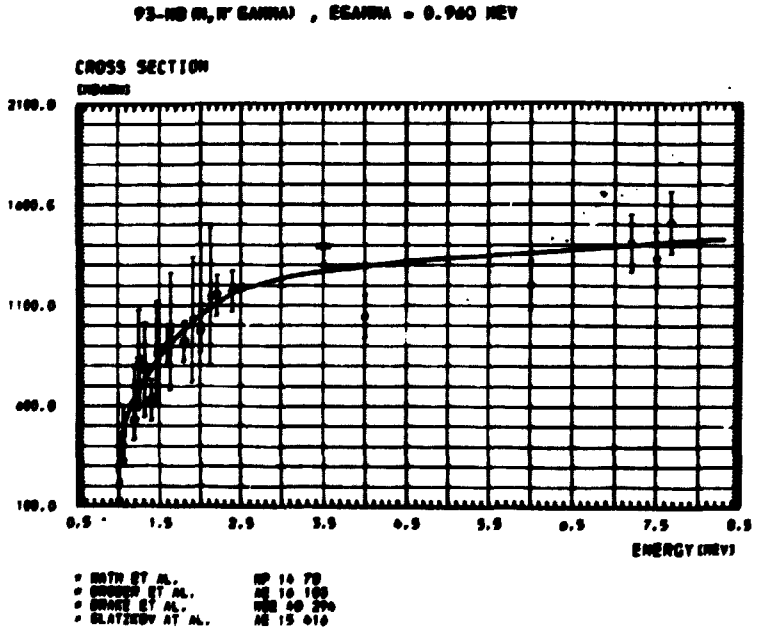

Fig. 8: The production cross section for γ-ray of about 0,96 MeV energy. Full line represents the result of application of the H-P-formalism including γ-ray branching ratios

Analogous conditions exist from the point of a theoretical founded interpretation of angular distributions of inelastically scattered neutrons. Apart from inelastic scattering to resolved levels, which can be described in terms of the H-F-formalism and/or direct reaction models (DWBA) in common, some methods were elabroated for an understanding of the angular dependence of the inelastic scattering of neutrons to contineously distributed levels in nuclei. Results which have been obtained using these models were offered or summarized in some other contributions to this seminary [13, 14, 15].

4. Abstraction of recommended data

Recommended data have been abstracted in two independend ways, i.e. the evaluation of integral cross sections like σ_{nT}, σ_{nX} and $\sigma_{n,n}$ and separatly all partial cross sections, which have to fulfill several conditions (sum rules) for consistency with integral data. This is the only possibility to meet the need for avoiding arbitrary correlations between uncertainties in some cross sections.

An essential problems in this process results from the determination of the reliability of evaluated data, which can be estimated from statistical distribution functions (standard deviations) on the one hand or comparisons between calculated and measured data on the other side.

Now final works are in progress for the representation of all numerical results corresponding to the format and the included laws of the USSR evaluated data library SOKRATOR [16].

References

[1] D. Hermsdorf, G. Kießig, K. Paßkönig, D. Seeliger and R. Storch,. Proc. 3rd Int. Sem. on Nuclear Structure Study iwth Neutrons, Gaussig 1973 ZfK-271, 1974

[2] anon., WRENDA 75, INDC (SEC)-46/U+R+P+S, 1975

[3] P. Guenther, P. Moldauer, A. Smith, EANDC Topical meeting, Tokyo, 1974

[4] G. Kiessig, thesis, TU Dresden, 1975

[5] S. Igarasi, JAERI-1224, 1972

[6] V. Benzi, G.C. Panini, G. Reffo, RT/PI (69) 44

[7] S. Pearlstein, J. Nucl. Energy 27 (1973) 81

[8] D. Herrmann, D. Seeliger, K. Seidel, ZfK-271, p. 80, 1974

[9] K.K. Gudima, G.A. Ososkov, V.D. Toneev, Preprint P4-7821, Dubna, 1974

[10] D. Hermsdorf, G. Kiessig, D. Seeliger, Proc. 3rd Neutronenphysics Conf. Kiev, in press

[11] D. Hermsdorf, G. Kiessig, D. Seeliger, Yadernije Konstante, to be publ.

[12] D. Hermsdorf, G. Kiessig, D. Seeliger, Contr. to the IAEA Consult. meeting, Trieste, 1975, in press

[13] R. Reif et al., Contr. to this seminary

[14] P. Mädler et al., Contr. to this seminary

[15] N. Cindro, Inv. paper to this seminary

[16] V.E. Kolesov, M.N. Nikolaev, INDC (CCP)-13/L, 1970

FAST REACTOR NEUTRON EXPERIMENTS ON CRITICAL ASSEMBLIES

D. Albert, Central Institute of Nuclear Research, Rossendorf near Dresden, GDR

A survey report was given about fast reactor physics investigation at Rossendorf.

The difference between nuclear neutron physics and reactor neutron physics has been pointed out. After having given the explanation what is meant by "critical assembly" and how the Rossendorf assembly SEG is constructed, the task of fast reactor physics experiments is described as a checking of calculational methods and group constants, especially data adjustment.

Then the experimental methods have been characterised which we have concentrated our forces on at Rossendorf:

1. Reactor oscillator (K. Fährmann, G. Hüttel). Application at SEG and at KOBRA (FEI Obninsk). Accuracy of reactivity measurements 10^{-8}. Measurements of central probe reactivities and adjoint flux spectrum by means of different neutron sources.

2. Proton recoil counter spectrometer (D. Albert, W. Hansen). Application at SEG and at BFS-I (FEI Obninsk). Measurement of flux spectrum in the range 2 ... 1200 keV, accuracy $\approx$ 5 % and resolution $\simeq$ 10 % if E $\geq$ 20 keV.

3. Transmission measurements (B. Böhmer, K. Dietze) at neutron beam of IBR-30 (Dubna), total and partial (in inverse shere geometry) as well. Evaluation to resonance parameters in unresolved region and to doppler effect and group constants.

   Such experiments have to be continued up to 1985 in order to get a complete physical understanding of large and diluted fast breeder cores of commercial scale ($\approx$ 1500 MWe).

THE TREATMENT OF RESONANCE CROSS SECTIONS IN REACTOR CALCULATIONS

E. Seifert, Central Institute of Nuclear Research Rossendorf near Dresden, GDR

Reactor physics is a field quite different from nuclear physics. Both fields are coupled by the neutron cross sections. In reactor physics the cross sections are considered as given quantities. In the energy region of interest (below 10 MeV) the cross sections of many materials in a reactor show a typical resonance structure whose correct consideration is of great importance. The Doppler effect as a pure resonance effect is an example for the influence of the resonances on reactor parameters. The Doppler effect plays an important role for the security of fast reactors.

The fundamental quantity in reactor physics is the neutron flux Φ because all the parameters describing a reactor can be calculated with the help of this function. The flux depends on the position vector x, the unit vector of flight direction $\vec{\omega}$ and the energy E (the time t is omitted here). It has to be determined as a solution of an equation of the Boltzmann type [1]:

$$\left[\vec{\omega}\frac{\partial}{\partial \vec{x}} + \Sigma_t(\vec{x},E)\right]\Phi(\vec{x},\vec{\omega},E) = \Psi(\vec{x},\vec{\omega},E) \quad \Big| \text{ + boundary conditions} \qquad (1)$$

with

$$\Psi(\vec{x},\vec{\omega},E) = \sum_{\alpha}\int d\vec{\omega}'dE'\Phi(\vec{x},\vec{\omega}',E')C_{\alpha}\Sigma_{\alpha}(\vec{x},E')f_{\alpha}(\vec{x};E',\vec{\omega}'\to E,\vec{\omega}) + Q(\vec{x},\vec{\omega},E)$$

where

Σ_{α} = macroscopic cross section for the reaction of the type α (elastic, inelastic scattering, fission, n2n-reaction)

C_{α} = mean number of secondary neutrons as a result of the reaction α

f_{α} = transfer function for reaction α

Q = external neutron source (may be zero)

This is a linear equation because we can neglect the interaction between the neutrons themselves as a result of the low density compared with the density of the nuclei. Furthermore the neutrons can be treated as classical particles outside the nuclei.

Disregarding few simple special cases (1) has to be solved numerically. Therefore we need a discrete representation of all variables. But by reason of computation time we cannot choose such a great number or energy points necessary for the resolution of the complicated resonance structure of the cross sections. Therefore the energy group model is usually applied. The energy region of interest is divided into some intervals each of them containing many resonances. (1) is integrated over each interval and the result is the coupled system of "group equations":

$$\left[\vec{\omega}\frac{\partial}{\partial \vec{x}} + \Sigma_{t,n}(\vec{x},\vec{\omega})\right]\Phi_n(\vec{x},\vec{\omega}) = \Psi_n(\vec{x},\vec{\omega}) \qquad (n = 1,2,\ldots,N) \qquad (2)$$

where

$$\Sigma_{\alpha,n}(\vec{x},\vec{\omega}) = \frac{\int_n dE\,\Phi(\vec{x},\vec{\omega},E)\Sigma_{\alpha}(\vec{x},E)}{\int_n dE\,\Phi(\vec{x},\vec{\omega},E)} \qquad (3)$$

are the "effective cross sections" and $\Phi_n = \int dE\, \Phi(\vec{x},\vec{\omega},E)$ are the "group fluxes". The basic question is now whether we can derive good approximations for Φ in order to calculate the effective cross sections (3) or not. If yes then the problem is separated into two independent problems: The calculation of the effective cross sections and the solution of the coupled system of group equations. Obviously an exact separation is impossible.

1. Infinite medium with a homogeneous material composition

All the quantities are independent on $\vec{x}$ and $\vec{\omega}$ and (3) is simplified to

$$\Sigma_{\alpha,n} = \frac{\int_n dE\, \Phi(E)\Sigma_\alpha(E)}{\int_n dE\, \Phi(E)} \tag{4}$$

According to (1), $\Phi(E)$ satisfies the equation

$$\Sigma_t(E)\,\Phi(E) = \sum_\alpha \int dE'\, \Phi(E')\, C_\alpha \Sigma_\alpha(E') f_\alpha(E' \to E) + Q(E) \tag{5}$$

whose solution is no serious problem. With some assumptions for the resonances, simple approximations for Φ can be derived from (5). For example, a widely used approximation is $\Phi(E) \sim 1/\Sigma_t(E)$, valid under the assumption of sufficiently narrow resonances [2]. Some difficulties arise in the case of the broad resonances of the isotopes with medium atomic weight. In order to taken into account these resonances correctly it is sufficient to use some hundreds of energy groups. Then the broad resonances can be resolved, and the narrow resonances which cannot be resolved are considered by the use of effective cross sections shielded by a spectrum like $\Phi(E) \sim 1/\Sigma_t(E)$. Then (5) can be solved numerically in this fine group mesh, e.g. with the very effective "continuous slowing-down method" (CSD). With the solution, effective cross sections can be computed in a more coarse group mesh according to (4).

2. Non-homogeneous material composition, large zones

In large material zones (large compared with the mean free path of the neutrons) we can neglect boundary effects. Far from boundaries we have a spectrum similar to that in an infinite medium. Therefore we can apply the method mentioned above. A computation of such a system consists of the following steps:

a) For each of the different material zones, determine a spectrum $\Phi(E)$ and effective cross sections according to (4).

b) Solve the system of group equations. Usually some further approximations of (2) are necessary. Some of the methods are the following (see e.g. [1],[3]):
   - starting from the differential form of the Boltzmann equation:
     diffusion method
     P_N-method
     S_N-method
   - starting from the integral form:
     collision probability method (CP)
     discrete integral method (DIT)
     Monte Carlo method

   The permitted number of energy groups depends on the geometric complexity of the system. As an example, in an one-dimensional problem we can use some

100 groups, in a two-dimensional one not essentually more than 10 groups and in a three-dimensional one not essentually more than 2 or 3 groups. An exception is the Monte Carlo method (see later).

3. Boundary effects

In the vicinity of boundaries between two zones with a different material composition the flux is a complicated non-separable function of $\vec{x}, \vec{\omega}$ and E. Therefore the effective cross sections are also complicated functions of $\vec{x}$ and $\vec{\omega}$ in the vicinity of such boundaries. The replacement by the cross sections of the infinitely extended medium which are independent on $\vec{x}$ and $\vec{\omega}$ is not justified. But the deviations are of importance only when the diameters of the zones are comparable with the mean free paths of the neutrons. In large zones we can neglect the complicated behaviour of the effective cross sections near the boundaries.

The use of effective cross sections is not very advantageous in order to take into account these boundary effects. There are some alternative methods.

a) emission_density_method

The emission density $\Psi(\vec{x},\vec{\omega},E)$ is defined by the right hand side of (1). It has the meaning of the density of those neutrons which after suffering a collision at $\vec{x}$ will travel in direction $\vec{\omega}$ with energy E. Under the assumption of sufficiently narrow resonances, the emission density is a smooth function of the energy. This result can be obtained by an investigation of the defining expression in (1). As a good approximation, we can assume $\Psi(\vec{x},\vec{\omega},E) \approx \Psi(\vec{x},\vec{\omega})$ [5], within an energy group. Therefore we can proceed as follows.

There is an unique relation between flux and emission density. Therefore we can use the emission density as a basic quantity instead of the flux. Firstly we have to derive the equation for the emission density. Secondly we have to convert this equation into the corresponding system of group equations. As a result, the interaction between neutrons and matter is now described by transmission functions:

$$F_{\alpha,n}(\vec{x}' \to \vec{x}) = \frac{\int_n dE \Psi(\vec{x},\vec{\omega},E) \Sigma_\alpha(\vec{x},E) e^{-\tau(\vec{x}' \to \vec{x},E)}}{\int_n dE \Psi(\vec{x},\vec{\omega},E)} \qquad (6)$$

where τ is the optical distance between $\vec{x}'$ and $\vec{x}$ at E. With the above approximation, (6) can be simplified to

$$F_{\alpha,n}(\vec{x}' \to \vec{x}) \approx \frac{1}{\Delta E_n} \int_n dE \Sigma_\alpha(\vec{x},E) e^{-\tau(\vec{x}' \to x,E)} \qquad (7)$$

The transmission functions are the counterpart of the effective cross sections in the flux equation. As an advantageous property, (7) is independent on the solution function. In the special case of an infinite medium we have $\Psi(E) = \Sigma_t(E)\Phi(E)$. The assumption $\Psi(E) \approx$ const within a group corresponds to the assumption $\Phi(E) \approx 1/\Sigma_t(E)$. But in a finite medium, emission density and collision density $\Sigma_t \Phi$ are different quantities. Nevertheless the method is based on the assumption of sufficiently narrow resonances (NR-approximation [2]).

b) Monte Carlo method

A very important property of this method [4] is the independence of the computation time on the number of energy groups or points chosen for the representation of the cross section functions. The computation time depends on the number of collisions per neutron between start and absorption or leakage. Obviously this number is independent on the way of subdivision of the energy axis into several intervals. Therefore we have the possibility to increase the number of energy groups or even to use a continuous energy variable. In this way all the difficulties can be avoided in a very natural manner. In non-Monte Carlo methods the number of energy groups is strongly limited because their computation time is about proportional to that number.
By the Monte Carlo method we are able to solve the basic equation (1) without any approximations. This concerns also such points as the scattering mechanism, a complicated three-dimensional geometric arrangement etc. At Rossendorf we have some experience in the application of the Monte Carlo method [6]. According to this experience this method works very well at selected problems. The decision between different solution methods must be based on a comparison of the computation times. Such a comparison leads to the general rule: The more complicated the system, the more advantageous the Monte-Carlo-method. With the Monte Carlo method we have the possibility to avoid approximations. The question is whether it is really necessary to avoid that or another approximation. If not (e.g. in the infinite medium) then other and more simple methods give the results with the same accuracy in much shorter times. Therefore the first step in any reactor calculation has to find an answer on the question: What is important to take into account and what can be neglected?

References

[1] Davison, Neutron Transport Theory, Oxford 1958
[2] Williams, The slowing Down and Thermalization of Neutrons, Amsterdam 1966
[3] Weinberg, Wigner, The Physical Theory of Neutron Chain Reactors, Chicago 1958
[4] Spanier, Gelbard, Monte Carlo Principles and Neutron Transport Problems, Reading, Massachusetts 1969
[5] Wintzer, Heterogeneity Calculations Including Space Dependent Resonance Self Shielding, KFK-633, 1967
[6] Barz, Noack, Seifert, Wand, Anwendung der Monte Carlo Methode bei Reaktorberechnungen, Kernenergie 16 (1973) 274

SESSION VII

STOCHASTIC FILTERS FOR NUCLEAR MEASUREMENTS

E. Hentschel, Zentralinstitut für Kernforschung Rossendorf, Bereich 2

The talk is concerned with data processing methods, which are used in space research. Everybody who has seen pictures from other planets like Mars of Venus is impressed by their quality. This high quality, however, is the result of a lot of computations [1]. It is encouraging to use these restauration methods also for nuclear measurements.

Nuclear physicists mainly use fut procedures for data processing. The main features of such procedures are the following ones:

fit procedures: Comparison of the detected signal with an input model

applications:
- many different kind of research, e.g.
- energy spectra (nuclear, X-ray, optical,...)
- comparison between experiment and theory,...

advantages:
- good accuracy
- it is easy to include previous knowledge about the signal
- a well established theory of error

drawbacks:
- The result in some cases is strongly dependent on the start situation
- there is no explicit inclusion of the noise in the theory; the χ^2-criterion is a mathematical one, and it is difficult to define a physical meaningful criterion of fidelity.
- Difficulties arise in cases with large noise.

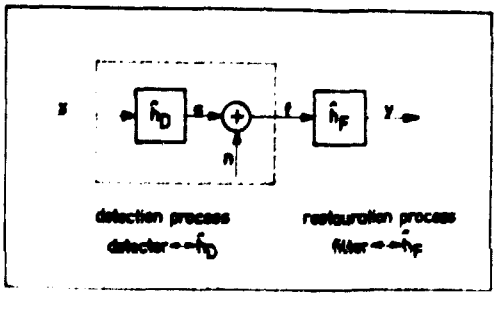

Fig. 1: Model of the measuring process. The ^ denotes an operator acting on the signals which are elements of a Hilfert-space.

Stochastic filters are very useful to overcome the drawbacks of fit procedures. The combination of these methods nowadays seems to be the typical way of modern data processing [1]. What is a stochastic filter?

Let us look to the following model of a measuring process, which is shown in fig. 1. A measurement consists in modern language of two parts: the detection of the signal and the restauration process, which is performed by means of a filter. Because the noise n appearing in the detection process is a stochastic variable, the filter is called a

stochastic filter. It is optimal in the sense of Wiener and Kolmogoroff, if the condition

$$\epsilon^2 = \| x-y \|^2 \qquad \text{Minimum!} \tag{1}$$

is hold. Of course, there existalso other definitions of the optimum and other filter constructions [2], and the scheme given in fig. 1 is the most simple one. However, the Wiener-Kolmogoroff-filter defined by the optimum condition (1) is very useful to learn the handling of the statistical noise, which occurs in nuclear measurements.
With the notations given in fig. 1 we get

$$\epsilon^2 = \| (1-\hat{h}_F \hat{h}_D) x \|^2 + \| \hat{h}_F n \|^2 + 2 \langle (1-\hat{h}_F \hat{h}_D) x \mid h_F n \rangle$$

A widely used assumption is that the noise n and the signal x are uncorrelated. Then one obtaines by taking into account the zero mean value of n

$$\epsilon^2 \approx \| (1-\hat{h}_F \hat{h}_D) x \|^2 + \| h_F n \|^2 \tag{2}$$

By a Fourier-transformation of this equation (this is a unitary transformation and, therefore ϵ^2 is invariant) one obtaines

$$\epsilon^2 = \frac{1}{2\pi} \int_{-\infty}^{\infty} d\omega \left(|1 - H_D(\omega) H_F(\omega)|^2 \cdot S_x(\omega) + |H_F(\omega)|^2 \cdot S_n(\omega) \right) \tag{3}$$

In this equation $H_D(\omega)$ and $H_F(\omega)$ are the transfer functions of the detector and the filter respectively. The functions $S_x(\omega)$ and $S_n(\omega)$ are the spectral power densities of the signal x and the noise n respectively. This are non-negative functions and, therefore, one obtaines the minimum condition for every frequency point and the following expression for the transfer function of the Wiener-Kolmogoroff-filter:

$$H_F(\omega) = \frac{H_D^*(\omega)}{|H_D(\omega)|^2 + (S_n(\omega)/S_x(\omega))^{-1}} \tag{4}$$

It is important to note, that $H_F(\ )$ depends only on $H_D(\ )$ and the so called signal to noise-ratio

$$r^2 = S_x(\omega)/S_n(\omega) \tag{5}$$

which is related to measured things. The square is only a matter of definition, which is convenient for detailed calculations. From the physical meaning of the spectral power density one can find by simple and rough models for the behaviour of nuclear spectra like that given in fig. 2.

$$r^2(\omega) \approx \frac{AG}{1+5B/A} = const \tag{6}$$

The important points is the following one:
From the explicit inclusion of the noise one obtaines a quantitative criterion how to handle the statistics. The choice of r has drastic consequences for the real meaning of the filtering. Let us discuss limiting situations: The case n=o obviously would result in $h_F = h_D^{-1}$ which means a complete deconvolution or inversion of h_D. If as the other limit $\| x \| \leq \| n \|$ the obvious way of data processing

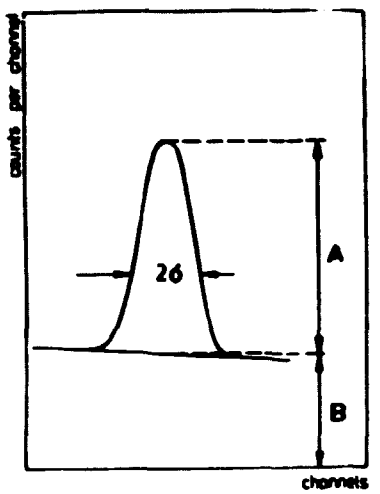

Fig. 2: Model of a typical situation arising in measured spectra: a Gaussian peak and linear background.

is an averaging in order to smooth the noise fluctuations, and hence one obtaines from the equ. (4) a concept of optimal smoothing of the measured data, where optimal means a minimal damping of the interesting structures. In this way stochastic filters are valid for the whole scale of possible situations between n and x. According to numerical experience one can define the following "criterion of fidelity": no wrong interpretation of statistical fluctuations!

$$r^2 = \chi \frac{A\sigma}{1\ SB/A} \qquad \chi = 0.2, \ldots, 1$$

The value χ depends on the complexity of the spectrum and of the sampling. If the sampling is poor, that means if there are only few channels over a peak there is more danger of a wrong interpretation, because the noise and the signal cannot be well seperated in the frequency space.

In practical calculations the measured spectrum is divided into several part with different signal to noise-ratios. In this way one overcomes the difficulties with a solution of the Wiener-Hopf integral equation and has a possibility to examine critically the measured data. Fig. 3 illustrates this method. In this figure are shown the measured data and filter outputs with different values r^2 which are meaningful by the structure of the measured spectrum. As one can see from this example the concept of optimal filtering is a powerful tool to estimate the "true" signal x.

However, there are also difficulties with this method. A serious problem for example are the spurious oscillations. They are produced by the structure of the filter response function (fig. 4). The amplitude of these oscillations increase with increasing r or increasing degree of deconvolution. In particular in cases of drastic improvement of the resolution one has to be careful to remove these oscillations. From numerical experience the following summary of the main features of optimal filters can be concluded:

optimal filters: frequency separation between signal and noise, partial deconvolution or correlation analysis

applications: signal processing in space research picture processing, sound analysis parameter etimation in control systems only few results in spectra evaluation [3]

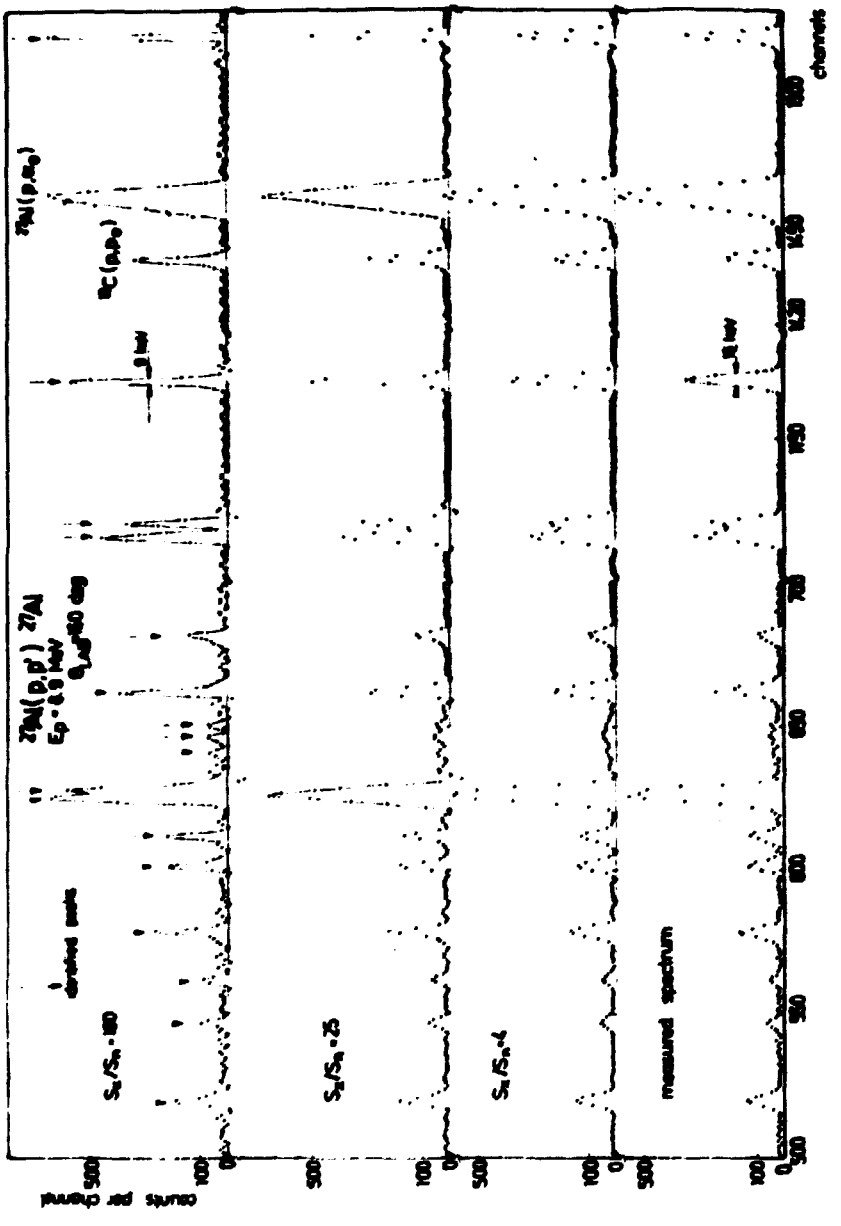

Fig. 3: Particle spectrum from inelastic proton scattering and filter outputs at different signal to noiserations.

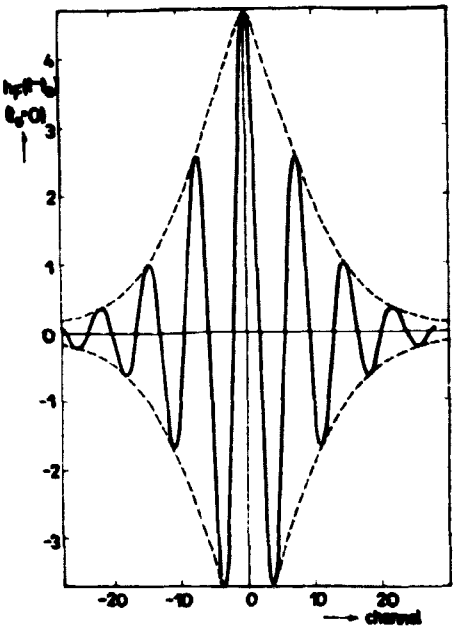

Fig. 4: Structure of the filter response function derived from a Gaussian detector response function and a signal to noise ratio $S_x/S_n \approx 10^4$.

advantages: the noise is included explicitely High speed (FFT), reasonable accuracy less detailed input information is necessary good results at large noise (optimal smoothing)

drawbacks: spurious oscillations "integral" error treatment difficulty to include further knowledge about more accuracy.

The combination of stochastic filters with fit procedures seem to be the most effective way of data processing.

References:

[1] B.R. Hunt, Proceed. IEEE 63 (April 1975), 693
[2] M. Sondhi, Proceed. IEEE 60 (July 1972), 842
[3] T. Inouye, T. Harper and N.C. Rasmussen, Nucl. Instr. Meth. (1969) 123
E. Hentschel, H. Förtsch and G. Zschornack, ZfK-262 (1973) 254

RESULTS AND PLANS ON THE DEVELOPMENT OF A PULSED NEUTRON GENERATOR

T. Sztaricskai, L. Vasváry and G. Pető
Institute of Experimental Physics, Kossuth University 4001 Debrecen, POB 105, Hungary

In the last years a good cooperation was founded on the field of neutron physics by regular meetings among the institutes in Dresden, Bratislava, Obninsk, Kiev and Debrecen. In addition to the angular meetings, there are more possibilities to make this cooperation stronger for common developments and utilizations of the experimental technique based on the common peculiarity the use of neutron generators [1]. The study of neutron emitting reactions on the basis of the neutron time of flight analysis is well developed in Dresden, Kiev and Obninsk [2, 3, 4]. An other method, is used to study this reactions on the basis of activation technique since long times in Debrecen [1].

Measuring the prompt gamma rays, the time of flight technique gives a good possibility to decrease the background in the gamma ray spectrum.

In our former experiment it is pointed out, that the use of Ge(Li)-detector in an APM arrangement gives not so good results as expected [5]. The possibility of the practical help of Salnikov's group from Obninsk in the construction of a pulsed neutron generator in Debrecen coincide with our plans to investigate the (n,n') and (n,2n) reactions on the basis of prompt gamma ray analysis.

We handed over our old open-air Van de Graaff machine to the Technical Museum and we began to plan the pulsed neutron generator in the 7x7 m^2 area, 8,5 m high accelerator hall. Only a small part of the earlier vacuum system is used from the old Van de Graaff machine which was placed on the ceiling of the lower/ earlier target-/ ha l. The general plan of the new generator is shown in fig. 1 and fig. 2. The accelerator tube was placed in the center of the upper hall and so we have to use a negative high voltage on the target.

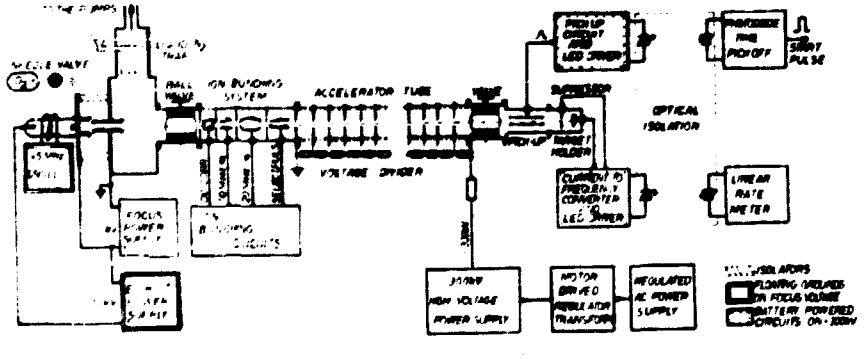

Fig. 1: The block diagram of the pulsed neutron generator

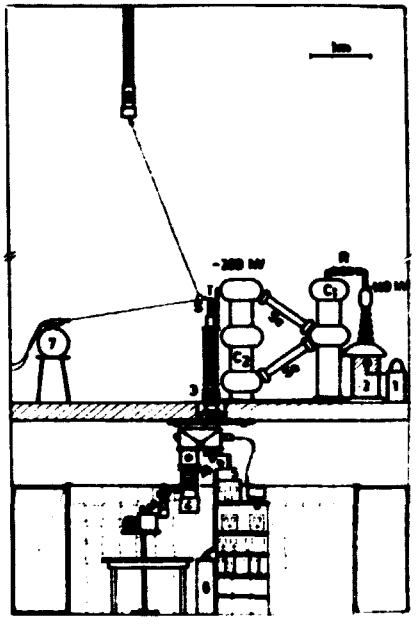

Fig. 2: The scheme of the neutron generators arrangement

The ion bunching system is placed between the vacuum system opening and the accelarator tube [6]. The ion source and the focussing electrodes are connected to the vacuum system in the lower hall. While the focus electrode is on the ground potential, so the ion source is on the focusing 30 kV. This set up has an advantage: the ion bunching system is on ground potential, and a disadvantage: the target is on the accelerating high voltage.

To supply the accelerators tube we use a 300 kV high voltage power supply. This high voltage is controlled by a motor driven variable autotransformer. The input of the variable transformer is driven by 5 kW regulated AC power supply. The rectifiers are two 5 mA 180 kV selenium rectifiers.

In the vacuum system a 20 m^3/h roughing pump and a 1000 l/s oil diffusion pump with booster stage is used. Near to the diffusion pump a 5 l volume liquid nitrogen vacuum trap is placed. In front of the bunching system is used a 60 mm diameter ball vacuum valve. The target can be separated by a similar, but smaller diameter ball vacuum valve. To measure the vacuum in the system some Pirani and Penning vacuum gauges were used.

In the radiofrequence ion source we use a 45 Mc/s, 200 W power push-pull oscillator where two GI 6 B power tube with ceramic to metal seals are used to generate the oscillations. The ion extraction electrodes [7] are placed on the opposite side of the quartz balloon. To regulate the D_2 flow a mechanical needle valve is used.

In consequence of the vertical arrangement it was necessary to develop a special form quartz cap to the negative extraction electrode. The ion source deliver about mA D^+ currents. In order to focus the deuterium ion beam a simple electrostatic cylindrical ion lens was used. Since the focussing electrode is on the ground potential the base plate voltage of the ion source is floating between 0-30 kV relative to the ground.

The accelerator tube is a homogenous field accelerator tube with 16 electrodes. The diaphragms of the tube are supplied from a voltage divider of about 300 Mohm full resistance.

To measure the ion current of the target and to pick up the start signal an optical isolation method was developed. At the target current measurements we use a current to frequency converter - based on the application of a programable

unijunction transistor - to convert the target current to the frequency of light pulse produced by a light emitting diode. The converter is linear in an $1 : 10^4$ input current range. The target current measurements will be taken on the earth potential by a ratemeter with photodiode detector in the range of 0,01 - 100 /uA target currents.

To get the start signal on the ground potential a similar LED-PIN photodiode optoisolation was developed. By 5 ns length light pulses on the fast LED, smaller as 90 ps time jitter was arrived at the use of PIN fast photodiode on a distance of 2 m. To drive the LED at the target in the leading edge time pick off and to recive the light pulses on the zero potential Schottky clamped analog and digital integrated circuits was used.

Florov's ion bunching system is practically the same as the one used in Obninsk. The ion beam is deflected by 10 Mc/s frequency, and the bunching is on 20 Mc/s.

In the up today state, the bunching electrode system and the 10 and 20 Mc/s stages are ready on workshop level. The quartz controlled base oscillator and the phase shifter stage will be placed in the control pult of the generator, the output stages will be built around the bunching vacuum system on the ground in the upper accelerator hall. In our system more integrated circuits and vacuum tubes were used. After the set of the full bunching system on the accelerator - with the help of the collaborators of the Salnikov's group from Obninsk - we shall develope the electronics for the selector deflection plates. The help from Obninsk is for us very valuable, while on the field of ion bunching we have not experiences. Fig. 3 shows the arrangement of the bunching system and the wave forms of the individual electrodes.

We hope that the generator shall be finished as soon as possible and so we can investigate the final states populated by the (n,n') and (n,2n) reactions. Through these investigations we hope to get more information on the (N-Z) dependence of these reactions. Parallel with the development of the pulsed neutron generator, the timing system for Ge(Li) measurements and a neutron detector system [8], has been developed. This experimental technique and the experiences can be used also for the prompt radiation investigations at the IBR-2 reactor in Dubna.

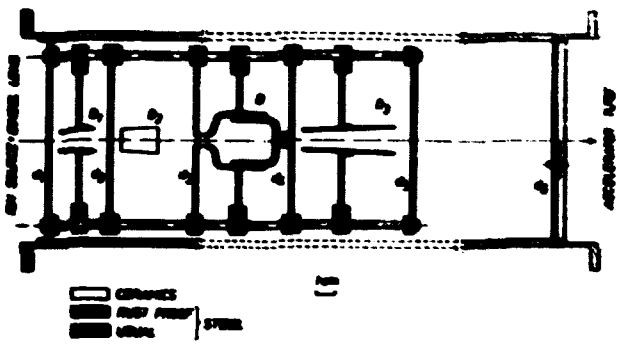

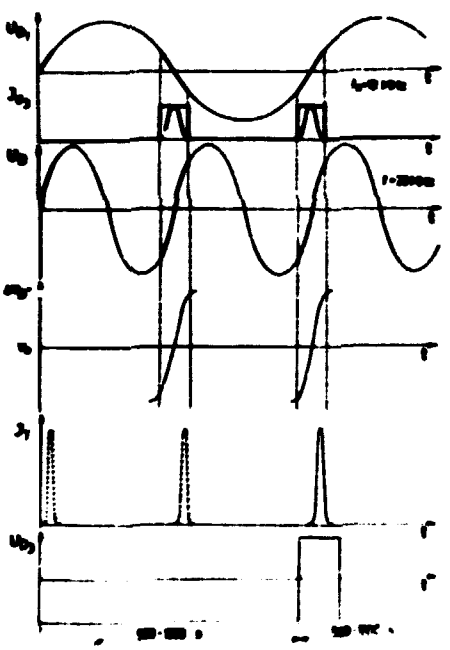

Fig. 3: The electrode system of the ion bunching parts and the wave forms on the electrodes

REFERENCES

[1] J. Csikai: Atomic Energy Review 11 (1973) 415

[2] D. Hermsdorf, S. Sassonov, D. Seeliger, K. Seidel: Kernenergie 17 (1974) 176, 259

[3] M.E. Gurtowoj, V.I. Strizak, B.E. Leschenko: Voprosi fisiki büstrich neutronov (Problems of fast neutrons) University of Kiev (1973)

[4] O.A. Salnikov, G.V. Lovchikova, G.N. Kotelnikova, N.I. Petisov, A.N.Trufjanov: Proc. 2nd. Conf. Nucl. Data for Reactors Helsinki 1970, T.2, 359

[5] T. Sztericzki, E. Barutcugil, T. Scharbert, G. Petö: Wiss. Zeitschrift TU Dresden 21 (1972) 697

[6] V.B. Anufrienko, N.V. Baulin, B.V. Devkin, V.I. Sabolotiskij, J.S. Kalabuchov, L.A. Matalin, V.N. Matveev, V.I. Maroka, O.A. Salnikov, L.A. Timochin: Impulsnüj istochnik s pseudosluchajnoj modulaciej (Ion source with semiaccident modulation) PEI-307, Obninsk, 1971

[7] J. Nagy, P. Gombos: ATOMKI Közl.: 4 (1962) 4

[8] T. Sztaricskai: ATOMKI Közl. 17 (1975) 31

О ВОЗМОЖНОСТИ ПРИМЕНЕНИЯ СПЕКТРОСКОПИЧЕСКИХ МЕТОДОВ ДЛЯ ИССЛЕДОВАНИЯ ВРЕМЕННОГО ПРОЦЕССА ИОНИЗАЦИИ АТОМОВ В ЭЛЕКТРОННОМ СГУСТКЕ УСКОРИТЕЛЯ ТЯЖЕЛЫХ ИОНОВ

Х.-У. Зиберт, Д. Лемани, Г. Музиоль, Г. Норман

Объединенный Институт Ядерных Исследований, ОИЯИ, Дубна, (СССР)

В Отделе Новых Методов Ускорения Объединенного Института Ядерных Исследований ведутся работы по запуску ускорителя тяжелых ионов на основе нового принципа коллективного ускорения. Основная идея коллективного метода состоит в том, что поле, ускоряющее частицу, создается не только внешними источниками, но и возникает как результат взаимодействия группы ускоряемых частиц с другой группой зарядов [1]. На коллективном ускорителе тяжелых ионов (УТИ) ускоряющее ионы поле создается электронным сгустком с числом частиц $\sim 5 \cdot 10^{13}$, что приводит к значительному выигрышу в величине ускоряющего поля по сравнению с обычным линейным ускорителем. Суть метода состоит в том, что небольшое число ионов, захваченных электронным сгустком, ускоряется при некоторых условиях его собственным полем. В свою очередь, сам электронный сгусток может быть ускорен внешними полями

$$\mathcal{E} = \mathcal{E}_K \cdot \frac{m}{M}$$

где: m - эффективная масса электрона, M - масса иона и $\mathcal{E}_K$ - напряженность поля, действующего на ион со стороны электронов. В силу большего различия масс ионов и электронов, конечная энергия ионов значительно, а именно в M/m раз, превосходит энергию электронов. Дубненский ускоритель тяжелых ионов [2] состоит из сильточного импульсного линейного ускорителя электронов в качестве инжектора с энергией электронов в пучке до $E_e = 3$ Мэв, максимальном токе в импульсе $I_e \sim 1000$ А и длительностью импульса $\tau = 10 \div 15$ нсек. В АДиабатическом ГЕнераторе ЗАряженных ТОРов (Адгезатор) формируется электронный сгусток на орбите $R = 40$ см. Под действием сильных магнитных полей электронный сгусток сжимается до $R = 4$ см при уменьшении его размеров и увеличении энергий электронов в нем примерно на $10 \cdot E_e$. На орбите $R = 4$ см электронный сгусток загружается ионами, т.е. запущенные в адгезатор атомы пересекают орбиты электронного сгустка, ионизируются и захватываются полем электронов

$$E_K = \frac{1}{4\pi\varepsilon_0} \cdot \frac{e\,Ne}{\gamma\, Ra}$$

где R - радиус кольца, a - радиус сечения тора. Ускорение кольца осуществляется в спадающем вдоль оси магнитном поле засчет перехода части вращательной энергии электронов в энергию движения по оси магнитного поля.

Ожидаются параметры такого ускорителя:
энергия ионов E; ≤ 10 Мэв/нуклон
количество ионов в импульсе $Ni \approx 5 \cdot 10^{10}$ при $Ne \approx 5 \cdot 10^{13}$
частота посылок $1 \div 5$ Гц

Нами подготавливается эксперимент для исследования одного из важнейших параметров пучка тяжелых ионов - степень их ионизации в зависимости от времени [3].

Очевидно, что градиент поля не должен превосходить значение, которое определяется значением сила удерживания ионов в электронном сгустке, которое является функцией степени ионизации. Процесс ионизации нейтральных атомов в электронном сгустке определяется в основном, временем их пребывания в сгустке, т.е. несколько сотен мксек. Добавочной ионизацией во время ускорения значительно меньше (~ 10 мсек), чем время формирования ионно-электронного кольца. При столкновении между электронами и атомами образуется вследствие ионизации в континуум или эффекта Оже дырки в электронных оболочках. При этом отношение сечений многократной и однократной ионизаций составляет ~ 1 : 10. Заполнение дырок с электронами из более высокорасположенных оболочек сопровождается рентгеновским излучением атома или приводит к испусканию электрона вследствие эффекта Оже. Каждое образование дырок в электронной конфигурации связано с изменением эффективного потенциала, в котором находятся электроны. Изменение потенциала приводит к сдвигу относительных положений электронных оболочек и таким образом, к изменению энергии рентгеновских переходов.

Принципом эксперимента является экспериментальное наблюдение сдвигов энергий рентгеновских лучей при использовании расчетных данных. Изменения орбитальных энергий атома в зависимости от конфигураций электронных состояний вычисляются с помощью релятивистской мультиконфигурационной программы типа Дирака-Фока. Значения сдвигов энергий рентгеновских лучей получаются при сравнении рентгеновских энергий иона с определенной конфигурацией электронных состояний с рентгеновскими энергиями атома с одной дыркой в К-оболочке и заполненными внешними оболочками.

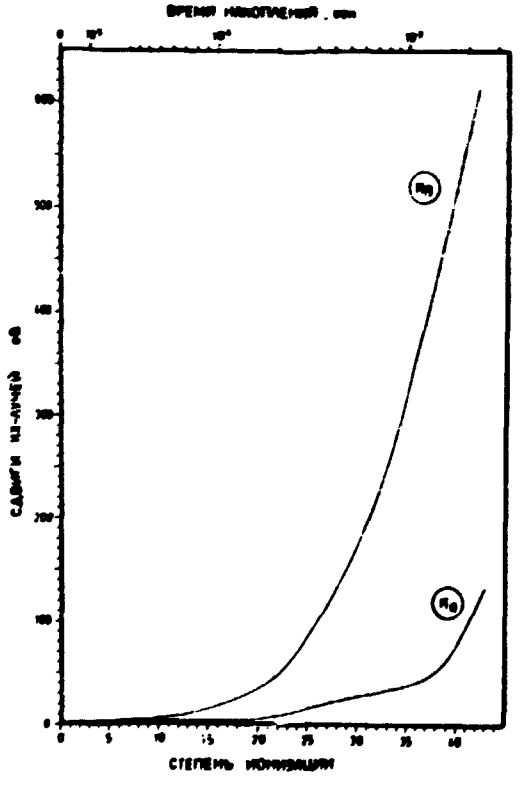

Рис. I

На рис. I изображены в качестве предварительной оценки значения энергетических сдвигов рентгеновских лучей для разных степеней ионизации в случае ксенона. Энергетические сдвигу были получены при помощи менее сложной программы по методу Хартри-Фок-Слетера. На верхней абсциссе отложены накопительные времена соответственных степеней ионизации с помощью программы, которая при известных параметрах кольца использует литературные данные о сечениях ионизации атомов. Видно, что более заметные сдвиги наблюдаются для K_β - лучей и, что со степени I ~ 15 сдвиги достигают такие величины, которые можно в ходе обработки регистрировать.

Вблизи адгезатора УТИ ожидаются следующие компоненты электро-магнитного излучения:

I. Рентгеновское излучение, возникающее вследствие ионизации атомов электронами.

2. Тормозное излучение
   а) возникающее при попадании электронов на стенку адгезаторного кольца
   б) возникающее на ионах, находящихся в адгезаторе во время накопительного процесса.

Время исследования процесса ионизации атомов ограничивается накопительным временем, в котором наблюдается рентгеновское и тормозное излучение электронов на ионах. Мы оценивали число РХ-лучей в течение накопительного времени, составляющее 200 мксек, на линии ускорения примерно $6 \cdot 10^8$ и число квантов тормозного излучения примерно $1{,}5 \cdot 10^8$ (при $R = 4$ см, $a = 0{,}2$ см и $N_e = 5 \cdot 10^{13}$).

Из относительно малого значения сдвига рентгеновских лучей, условий излучения вблизи адгезатора и числа регистрируемых импульсов и временного режима измерения вытекает ряд требований к используемому спектрометру. Для получения наилучшего энергетического разрешения при высокой эффективности регистрации предлагается применение сверхчистого Ge – детектора с энергетическим разрешением ~180 эв на линию 5,9 кэв. Появление мощных вспышек электромагнитного излучения перед и после накопительного времени, возникающих вследствие тормозного излучения при инжекции и сброса кольца требует надежного экранирования детектора и строгого коллимирования телесного угла детектора. Можно выбрать такую геометрию, при которой детектор увидит светом кольцо или часть его, которая позволяет измерение с разумной точки зрения мертвого времени амплитудно-цифрового преобразователя и наложения импульсов (нагрузкой ~$3 \cdot 10^4$ имп/сек). Как видно из рис. 2, на котором представлены результаты расчета временного развития ионизации степень ионизации меняется во время с различной скоростью. Для получения информации о средней степени ионизации в разные моменты времени требуется измерение РХ -лучей по временным окнам, причем длина временного окна должна быть меньше времени изменения средней степени ионизации. Из этого вытекают длины временного диапазона в случае ксенона:

~ 10 мксек при $I \leq 25$
~ 100 мксек при $I \leq 25$

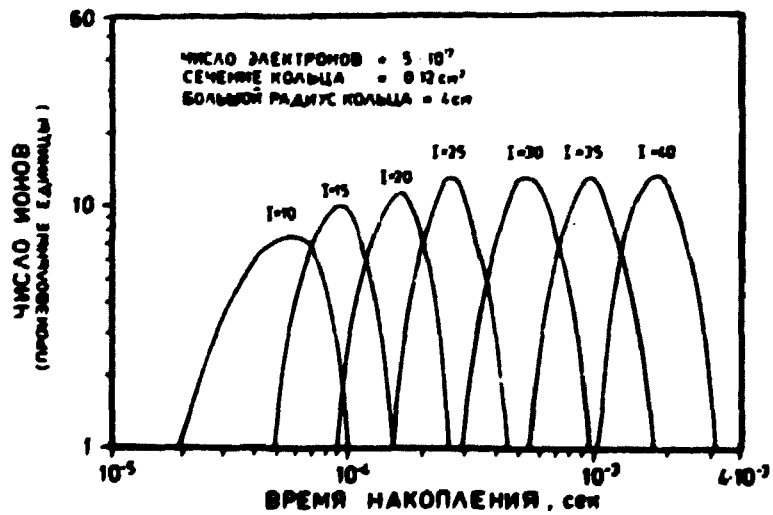

Рис. 2

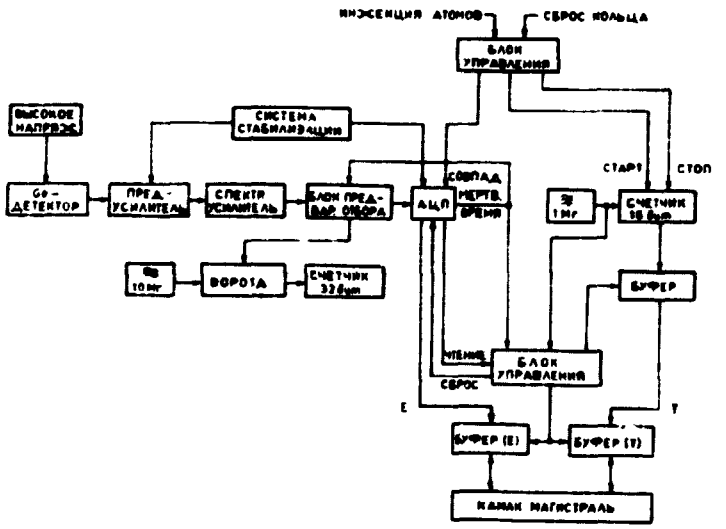

Рис. 3

Принципальная схема аналоговой и цифровой электроники предложенного эксперимента представлена на рис. 3. В спектроскопической ветви схемы образуется энергетический сигнал, в то же время цифровой счетчик представляет соответствующий сигнал, который позволит приписать временную отметку к каждому зарегистрированному энергетическому импульса. Блок управления согласует одновременную запись энергетической и временной информаций в буферы E и T. После сброса кольца до до начала нового цикла информация буферов E и T читается в память ЭВМ М-6000. Этот способ дает возможность рассортирования энергетической информации по временным окнам различной ширины. Пики рентгеновского излучения будут сложными, так как в каждом временном окне складывается пики, соответствующие разным степеням ионизации. Энергия, на которую будут отнесены все энергетические сдвиги пиков $K\beta_1$-лучей, является энергия пика $K\beta_1$-лучей, например изотопа, распадающего вследствие электронного захвата. С помощью расчетов энергии КХ-лучей при разных степенях ионизации по релятивистикой мультиконфигурационной программе типа Дирака-Фока можно заранее точно сказать, что в каком канале спектра появляется пик $K\beta_1$-лучей определенной степени ионизации. Это значит, что при заданных положениях всех возможных компонент суммарного пика и, требуя для всех компонент пика одинаковую полуширину, можно с помощью подгоночных процедур разделить все отдельные пика, из которых состоит суммарный пик одного определенного временного окна. Решение такой задачи требует знания полуширины одиночного пика в рассматриваемой области энергии. Такое значение может быть получена при обработке суммарного пика $K\alpha_1$-лучей первого временного окна ширины $\sim$ 100 мксек как одиночной.

Исходя из разрешающей способности спектрометра и того, что точность определения положения пиков с помощью подгоночных процедур составляет примерно одну сотую полуширины пиков, можно оценить точность определения средней степени ионизации в разные времена.

$I \lesssim 25$	Δt = 10 мксек	$\Delta I \lesssim 3$
$I \gtrsim 25$	Δt = 100 мксек	$\Delta I \lesssim 2$

При этом следует учесть, что точность определения средней степени ионизации значительно зависит от ширины выбранного временного окна.

В заключении заметим, что данное предложение эксперимента представляет интересное применение спектроскопических методов для исследования степени ионизации пучка УТИ. Важно, что этот эксперимент позволяет такие исследования без вмешательства в процесс формирования ионно-электронного кольца.

Литература

[1] И.Н. Иванов и др. ЭЧАЯ том I, выпуск 2, Москва, Атомиздат 1971 г.
[2] Л.С. Барабаш и др. Сообщение ОИЯИ, Р9-7697, Дубна, 1974.
[3] Х. Зиберт и др. Сообщение ОИЯИ, Р9-9366, Дубна, 1975.

РАЗРАБОТКА МОДУЛЕЙ В СТАНДАРТЕ КАМАК И ИХ ПРИМЕНЕНИЕ В СВЯЗИ С МАЛОЙ ЭВМ

KRS 4200 **Robotron**

В. Майлинг, Ф. Вайдхазе

Технический Университет Дрезден, (ГДР)

I. Введение

Система КАМАК [1, 2] представляет собой систему электронных блоков для обработка и передачи данных между ЭВМ и экспериментальным устройством. Система КАМАК хорошо выполняет требования физиков, имеющих в своем распоряжении современную и мощную электронную аппаратуру.

Стандарт КАМАК обеспечивает связь многих внешних приборов с ЭВМ в реальном времени. Как и прежние стандарты, КАМАК основан на модульном принципе, в нем нормализованы механические конструкции, разъемы, напряжения питания и параметры входных и выходных сигналов. Каждый модуль состоит из двух частей устройства связи с магистралью и устройства для осуществления конкретных операций совместно с внешним прибором. Нумерация станций в крейте ведется слева направо, если смотреть на крейт спереди. Первые 24 станции называются нормальными, а 25-я управляющей.

Наиболее простой способ создания многокрейтной системы - это непосредственное подсоединение каждого крейта к система ввода-вывода ЭВМ (рис. I).

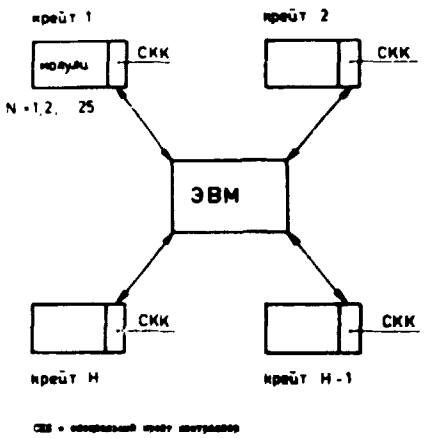

Рис. I Радиальный метод связи с ЭВМ
СКК - специальный крейт контроллер

Наибольшее распространение получила многокрейтная система типа ветви. Система допускает объединение в одну ветвь до 7 крейтов (рис. 2). Контроллеры системы также стандартизованы, они не зависят от применяемой ЭВМ. Эти контроллеры получили название "А-I". Через контроллеры всех крейтов проходит так называемая вертикальная магистраль, которая соединяет их с общим драйвером ветви. Он обеспечивает связь всех крейтов с ЭВМ и является единственным блоком, зависящим от нее.

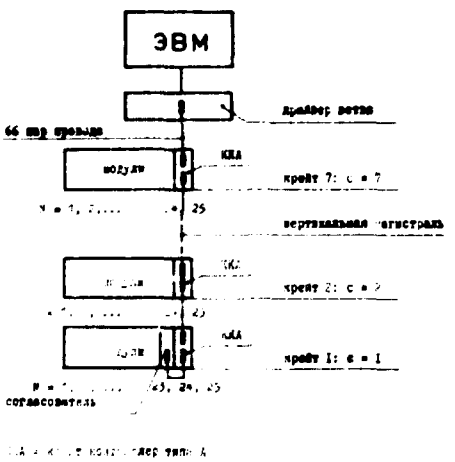

Рис. 2 Ветвевой метод связи с ЭВМ

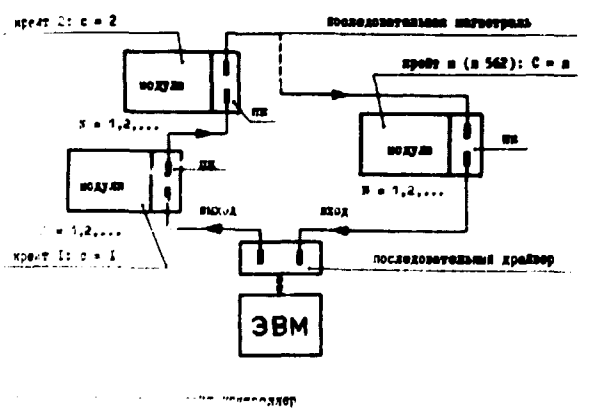

Рис. 3 Последовательная многокрейтная система

Имеется и третья возможность соединения с ЭВМ, так называемой последовательной магистрали, связывающей все крейты системы, число которых может доходить до 62 (рис. 3)

Описаны модули в стандарте КАМАК, предназначенные для обработки данных и для управления ядерными экспериментами. Предусмотрено использование этих модулей в экспериментах с быстрыми нейтронами.

II. Разработаны модули

Следующие модули были разработаны:

I. Крейт-контроллер типа А [3]
2. Дисплей магистрали крейта (3321) [4]
3. Двойчный счетник импульсов (1110) [5, 6]
4. Параллельные входные ворота (1211) [7]

5. Параллельный входной регистр (I220) [8]
6. Параллельный выходной регистр (I420) [9]
7. Сдвоенный таймер (I3II) [IO]

Эти модули были представлены в 1975 г. на VIII -ом Международном Симпозиуме по Ядерной Электронике в г. Дубне. Для интересующихся имеется в распоряжении литература. [II]

Обсуждаются ещё два новых модуля этой системы. Такие блоки пока без примера за счет последовательного использования управляющих действий и возможности контроля с помощью ЭВМ.

8. Модуль-блок для общих задач управления (номер характеристики I520 по номенклатуре [I2]

Разработанный блок может осуществить множество отдельных действий управления. Он применяется, например, для управления временного режима "старт - стоп" или при управлении приборов вне системы "КАМАК".

Блок состоит из четырех идентичных каналов, как показано на рис. 4. Не входя в подробности, здесь только указан принцип работы одного канала. С помощью электронного переключателя *ES1* инвертируются входные сигналы. Электронным переключателем *ES2* можно пропустить входные сигналы, а также создать на выходе высокий или низкий потенциал.

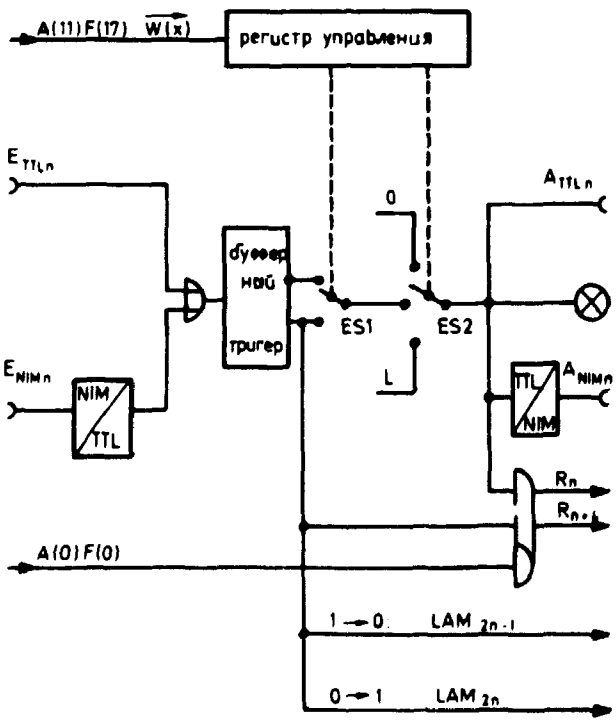

Рис. 4 Построение одного канала в блоке для общих задач управления I520

Каждый канал выполняет следующие задания:

- Вход для запроса: т.е. контроль логического сигнала на переход от *L* до нуля или наоборот. Каждый переход вызывает другой запрос.
- Вход и выход сигнала выполнены как по уровню "*NIM*" так и по уровню "*TTL*".
- Вход для ввода сигнала от клавиши.
- Преобразование сигнальных стандартов *TTL* в *NIM*, *NIM* в *TTL*, *TTL* в *NIM* отрицание, *NIM* в *NIM* отрицание и т.д.
- Переключение регулирующих контуров: т.е. ЭВМ с помощью этого блока может включать или выключать автоматическое управление, причем она получит информацию о состоянии контура.

В отличие от различных специальных блоков этот прибор соединяет основные их свойства, причем блок занимает только одиночную ширину.

9. Реверсивный счетчик (может работать как установленный счетчик, номер характеристики II70) [I3]

Модуль-блок предназначен, прежде всего, для задач управления, зависящих от числа импульсов (как, например, управление потоком частиц или локализации приборов). Возможность снятия сигнала, который зависит от знака содержания счетчика (больше или меньше нуля), позволяет использовать его в автономных регулирующих контурах.

Блок имеет защитные схемы, которые не допускают ошибок при чтении содержания во время счета. Также не допускаются ошибки в случае, когда на соответствующие входы для считывания вперед и назад одновременно поступают импульсы.
Благодаря его универсальному построению блок может быть использован для решения многих задач счета импульсов.
Режим работы блока определяется содержанием регистра управления с подадресом A(II). ЭВМ может установить в счетчике три главных режима.

а) Вход E_1 считает вперед.
Вход E_2 считает назад.

б) Вход E_1 считает импульсы, а уровень сигнала на входе E_2 определяет считывание вперед или назад.

в) ЭВМ определяет, считаются ли импульсы, поступающие на вход E_1 вперед или назад.

Запрос на ЭВМ исполняется так, как указано в таблице первой. Блок имеет пять возможных источников запросочного сигнала. Все они могут быть маскированы и обработаны в отдельности.

номер запроса	значение
I	счётчик переполнен при счете вперед
2	счётчик переполнен при счете назад
3	при счёте назад содержание достигло нуля
4	то же при счёте вперед
5	Уровень внешнего управляющего сигнала перешел из высокого состояния в низкое

Таблица I: Запрос на ЭВМ от счетчика II70

Важные технические данные:

- стандарт входных сигналов *NIM* или *TTL*, по желанию потребителя
- выход по *TTL*

- максимальная скорость счета: I8 Мгц и при работе на совпадение: 6 Мгц
- максимальное содержание счетчика: 24 двойных разрядов, включая знак

III. Рекомендация для конструкции

При разработке блоков в стандарте КАМАК мы старались повторять удачные схемные комплексы в разных приборах. Разработана рекомендация с указанием для конструкции, применяемая в ГДР [I4].

Ширина блоков I7,2 мм, ширина крейт-контроллера и таймера 34,4 мм. Все блоки кроме крейт-контроллера обладают показателем модуля [I2]. Чтение показателя производится с командой A(I5)F(1). В модулях используется единая структура обработки запросов L. Исходя из предложений для многих источников запросов [I, I4] мы предпочитаем в модулях следующие команды:

чтение запросов без маски
выборочный сброс регистра запросов
чтение регистра маски
запись регистра маски
чтение маскированных запросов
проверка всех маскированных запросов

Для декодирования сигналов и подадресов A используется дешифратор на основе интегральных схем 7442 (рис. 5).

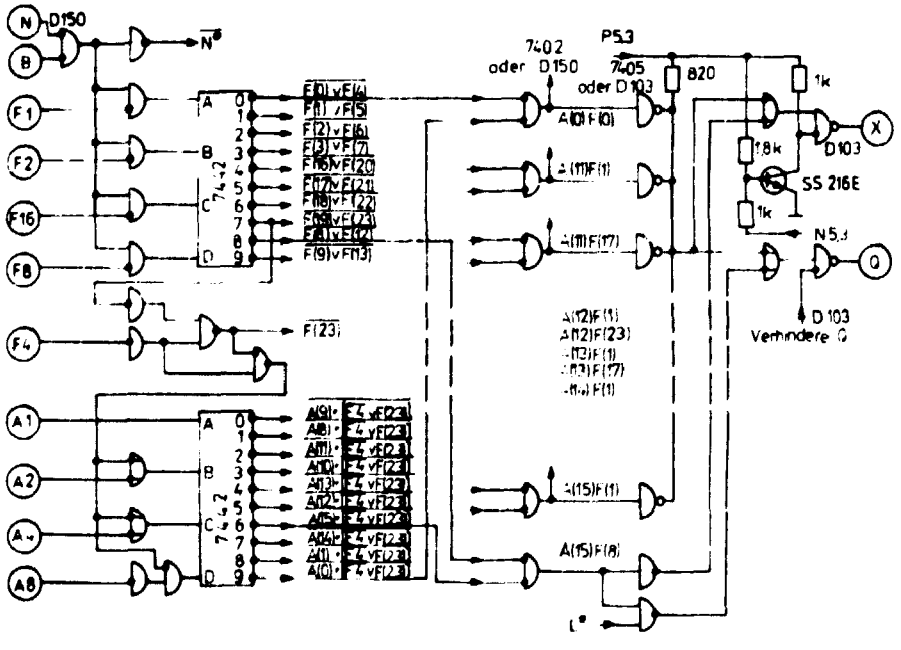

Рис. 5 Дешифратор сигналов N, A, F и B

I. Эксперименты

Выше указанные блоки в стандарте КАМАК вместе с блоками, разработанными в ОИЯИ Дубне (ЛЯП), планируется использовать по концепции [I5]. Для этого созданы блок-схемы для экспериментов, которые проводятся в ядерной секции Технического Университета Дрездена:

I. (n,f), эксперимент двухмерного анализа параметров энергии и времени, как указано в рис. 6.

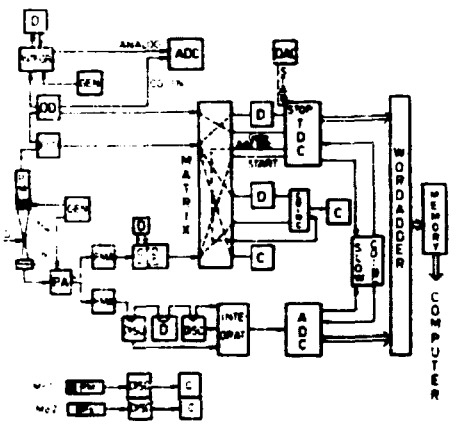

Рис. 6 Блок-схема эксперимента (n,f)

2. $(n,2n)$, эксперимент, использующий время-пролетную технику, как указано в рис. 7.

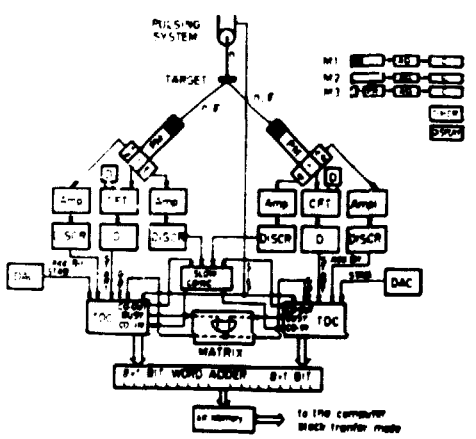

Рис. 7 Блок-схема эксперимента $(n,2n)$

3. (n,Z), эксперимент с многомерным анализом сигналов от кремниевых E и E детекторов, как указано в рис. 8

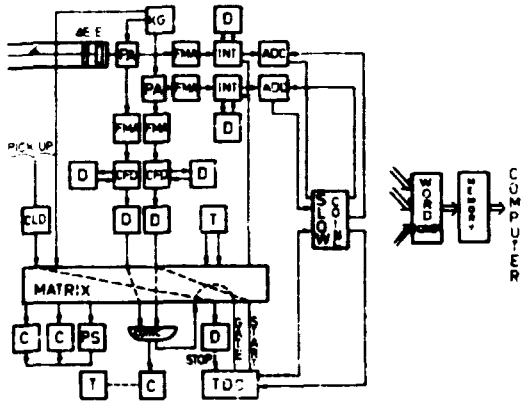

Рис. 8 Блок-схема эксперимента (n,Z)

Все эти эксперименты подключаются "*on-line* " на типичную малую ЭВМ KRS 4200 комбината Robotron, имеющую длину слов в I6 бит и емкость памяти в I6 К. При этом ЭВМ управляет КАМАК крейтами содержащими электронику эксперимента и выполняет роль памяти для экспериментальных данных. Кроме того, используются различные блоки в стандарте КАМАК для ввода данных и вывода накопленных спектров на дисплей, на рисующее устройство и цифропечать. Реализация первого управляемого ЭВМ эксперимента находится в подготовительной фазе.

Эти три схемы были разработаны совместно с экспериментаторами К. Андерт, Р. Арльт, К. Зейдель, В. Вагнер и С. Сассонов.

Легенда

PA	: Предусилитель	D	: Линия задержки
T	: Таймер	C	: Счетчик
INT	: Интегратор	Amp	: Усилитель
Discr	: Дискриминатор	AD	: Порочовой усилитель
FMA	: Быстрый усилитель	PS	: Управляющий счетчик
PM	: Фотоэлектронный умножитель	CLD	: Интегральный дискриминатор
KG	: Калибровочный генератор	ADC	: Амплитудный преобразователь
CFD	: Дискриминатор с временной привязки	DD	: Дискриминатор длительности
TDC	: Конвертор "время-двоичное слово"		

Литература

[1] ESONE-Committee: CAMAC-A Modular Instrumentation System for Data Handling, EUR 4100, 1972

[2] ESONE-Commitee: CAMAC-Organisation of Multi-Crate System, EUR 4600, 1972

[3] W. Hirsch, K. Andert, W. Meiling, I. Churin: CAMAC-Crate Controller Typ A TU Dresden Informationen Nr. 05-18-74

[4] S. Glöser, W. Hirsch, W. Meiling, F. Weidhase: CAMAC-Modul "Datenweganzeige", TU Dresden, Informationen Nr. 05-19-74

[5] F. Heinrich, F. Weidhase, W. Meiling, W. Hirsch: CAMAC-Modul "2x16 bit Binärzähler", TU Dresden Informationen Nr. 05-21-74

[6] F. Weidhase, J. Rommel, Ch. Kluge: CAMAC-Moduln "2 x 24 bit-Zähler 1111" und "24 bit Parallel-Datenausgaberegister mit SI 1.2-Anschlußmöglichkeit 1421", Gemeinsamer Jahresbericht 1975, ZfK-295

[7] W. Rahn, W. Hirsch, W. Meiling, F. Weidhase: CAMAC-Modul "24 bit Dateneingabetor mit SI 1.2 Eingangsstufe", TU Dresden Informationen Nr. 05-20-74

[8] F. Weidhase, W. Meiling, R. Foth, D. Horstmann, A. Rink, J. Schubert, G. Stemmler: CAMAC-Moduln für Daten- und Steuersignalübertragung, Gemeinsamer Jahresbericht 1975, ZfK

[9] W. Ullrich, F. Weidhase, W. Hirsch, W. Meiling: CAMAC-Modul "24 bit-Parallel-Ausgaberegister mit SI 1.2-Anschlußmöglichkeit, TU Dresden Informationen Nr. 05-22-74

[10] R. Krause, W. Meiling: CAMAC-Modul "Zweikanal-Zeitsteuerung", TU Dresden Informationen Nr. 05-15-75

[11] З. Майлинг, Ф. Вайдхазе, В. Хирш, Р. Краузе
Модули САМАС, разработанные в Техническом Университете г. Дрезден
TU Dresden Informationen Nr. 05-16-75

[12] O.P. Nicolaysen, CAMAC-Bulletin Nr. 9, 26

[13] U. Meyer, F. Weidhase: CAMAC-Modul "Voreinstellbarer Vor-Rückwärts-Zähler 1170", Gemeinsamer Jahresbericht 1975, ZfK-295

[14] W. Meiling, F. Weidhase: Einige Empfehlungen und Konstruktionshinweise für CAMAC-Moduln, Проэкт комиссии КАМАК академии наук ГДР